Summer 7-17-2023

PROTEOMIC APPROACHES TO IDENTIFY UNIQUE AND SHARED SUBSTRATES AMONG KINASE FAMILY MEMBERS

Charles Lincoln Howarth
Dartmouth College, charles.l.howarth.gr@dartmouth.edu

PROTEOMIC APPROACHES TO IDENTIFY UNIQUE AND SHARED SUBSTRATES AMONG KINASE FAMILY MEMBERS

A Thesis
Submitted to the Faculty
in partial fulfillment of the requirements for the degree of
Doctor of Philosophy
in
Biochemistry and Cell Biology
by Charles Lincoln Howarth

Guarini School of Graduate and Advanced Studies
Dartmouth College
Hanover, New Hampshire
July 2023

Examining Committee:

_____
(Chair)Scott Gerber, PhD

_____
James Moseley, PhD

_____
Duane Compton, PhD

_____
W. Andy Tao, PhD

_____
F. Jon Kull, PhD
Dean of the Guarini School of Graduate and Advanced Studies

Abstract

Protein phosphorylation is a reversible post-translational modification that is a critical component of almost all signaling pathways. Kinases regulate substrate proteins through phosphorylation, and nearly all proteins are phosphorylated to some extent. Crucially, breakdown in phosphorylation signaling is an underlying factor in many diseases, including cancer. Understanding how phosphorylation signaling mediates cellular pathways is crucial for understanding cell biology and human disease.

Targeted protein degradation (TPD) is a strategy to rapidly deplete a protein of interest (POI) and is applicable to any gene that is amenable to CRISPR-Cas9 editing. One TPD approach is the auxin-inducible degron (AID) system, which relies on the expression of an AID fusion protein and the F-box protein Tir1. Addition of auxin drives binding of the AID-POI and Tir1, resulting in rapid ubiquitination and degradation. Recently, we demonstrated that this approach can be used to study kinase-substrate relationships in a manner analogous to small-molecule inhibition using the kinase Plk1 as a proof-of-concept. Based on the results of this study, we applied AID-Tir1 protein degradation to interrogate kinase-substrate relationships for the Polo-like kinase (Plk), p21-activated kinase (PAK), and Aurora kinase families. Additionally, we made significant improvements to the CRISPR-Cas9 workflow and improved efficiency of AID-Tir1 cell line generation for kinases of interest.

Targeted degradation of PAK1 revealed low PAK1 activity in HEK293 cells. Follow-up experiments showed that, while many phosphorylation sites are regulated by the group 1 PAKs, PAK1 does not regulate these pathways alone and likely has overlapping functions with the closely related kinase, PAK2. We applied AID-Tir1 to Aurora B and observed high correlation between Aurora B degradation and inhibition by the Aurora B inhibitor AZD1152, demonstrating that protein degradation is a selective approach to identify direct Aurora B substrates. We identified an uncharacterized truncated Aurora B isoform that is sufficient for Aurora B signaling in the absence of full-length Aurora B. Finally, we used fluorescent reporter proteins and Fluorescence Activated Cell Sorting (FACS) to greatly improve the efficiency of AID-Tir1 cell line generation for kinases of interest. These improvements make strides towards widespread implementation of targeted degradation as a tool to study kinase-substrate relationships.

Dedication

This work is dedicated to my parents, Maeryta and Chuck, my sister Sophie, my aunt and uncle, Rich and Kari, and my partner Adrianna.

Acknowledgements

I would like to thank my advisor, Dr. Scott Gerber, for his mentorship and patience over the years. He was always supportive of me pursuing new approaches and techniques even when we didn't know how they would play out, and he was always there to help me get them working. I would also like to thank professors Arminja Kettenbach, Jamie Moseley, and Duane Compton for all of their guidance and support throughout these projects. Additionally, I would like to thank my peers, particularly past and current members of the Gerber lab Juan Mercado del Valle, Rufus Kards, Kate Carango, Andrew Grassetti, Katelyn Cassidy, and Mark Adamo. Finally, I would like to thank my earliest scientific mentors Dr. Jennifer Brakeman and Dr. Dzwokai Zach Ma for inspiring me and encouraging me to pursue a career in life science research.

Table of Contents

List of Figures

Chapter 1

Introduction

Protein phosphorylation mediates signaling by transiently altering protein-protein interactions and affecting protein activity via conformational changes. Understanding phosphorylation signaling is crucial for comprehending cellular biology as it plays a fundamental role in nearly all cellular processes (Cohen, 1992, 2002a; Humphrey et al., 2015). These pathways are governed by kinases, protein enzymes that catalyze the transfer of phosphate to a substrate protein, as well as phosphatases that catalyze its removal, imparting multiple layers of regulation to target proteins and the pathways in which they function. Frequently, the breakdown of phosphoregulation can trigger the onset of various disorders, including metabolic, neurological, or infectious diseases, as well as cancer (Zhang et al., 2009). A robust understanding of phosphorylation signaling is essential for the development of new therapeutics that seek to silence or enhance certain pathways to treat disease.

The fields of proteomics and phosphoproteomics are well situated to analyze protein signaling pathways from the level of the whole proteome. In particular, a myriad of phosphoproteomic-centric methods have been developed to identify and study kinase and

phosphatase substrates and determine how members of these important enzyme families factor into key pathways. We recently demonstrated the use of targeted protein degradation coupled with mass spectrometry-based phosphoproteomics to study signaling for the kinase Plk1 and showed that this approach was analogous to the study of phosphorylation signaling using small molecule inhibitors (Hards et al., 2021). The central focus of this thesis was to apply targeted protein degradation to precisely interrogate the substrates for closely related kinases. As described in later chapters, we focused on the Polo-like kinase (Plk), p21-activated kinase (PAK), and Aurora kinase families to assess redundancy and substrate overlap for members of these kinase families. Another key focus, detailed in Chapter 3, is the development and optimization of fluorescent reporter-based methods to increase the efficiency of CRISPR-Cas9 tagging strategies and thereby increase the throughput of cell line generation.

Phosphorylation signaling

Protein phosphorylation is one of the most common post-translational modifications (PTMs) with estimations suggesting that 75% or more of the human proteome is phosphorylated to some extent (Sharma et al., 2014). In eukaryotic cells, phosphorylation almost exclusively occurs on serine, threonine, or tyrosine residues and there are nearly 700,000 potential phosphorylation sites in the human proteome (Ubersax & Ferrell, 2007). Phosphorylation occurs when a phosphate group is transferred from an ATP molecule to a substrate protein, a reaction catalyzed by protein kinases. This is an ideal strategy for rapid signal transduction given that phosphorylation is a chemically stable post-translational modification at physiological conditions that is easily reversible (Schwartz & Murray, 2011). Phosphorylation can alter protein behavior in almost every way, by changing PPIs, activity, localization, or marking the protein for degradation (Cohen, 2002a). For example, phosphorylation at binding interfaces may affect complex formation and localization, either by stabilizing or destabilizing protein-protein interactions (Davis, 2011; Nishi et al., 2011). To date, 90,000 serine and threonine phosphosites have been identified, but the vast majority have not been attributed to any particular kinase (Hornbeck et al., 2019; Johnson et al., 2023) and the functional relevance is unknown (Ochoa et al., 2020).

Protein phosphorylation is achieved by a class of enzymes called kinases that catalyze the transfer of phosphate from ATP to a specific sequence on a target protein, or substrate. In total, there are 518 protein kinases in the human proteome (Manning, Whyte, et al., 2002) with all major kinase groups and most kinase families conserved among metazoans and yeast (Manning, Plowman, et al., 2002). Of these, 106 have been characterized as pseudokinases that lack catalytic function but may regulate the function of other protein kinases (Manning, Whyte, et al., 2002; Rajakulendran & Sicheri, 2010) and another 90 specifically phosphorylate tyrosine residues (Schwartz & Murray, 2011). The remaining 322 are serine/threonine-specific kinases and are responsible for 99% of phosphorylation events (Ubersax & Ferrell, 2007). Considering the small number of protein kinases relative to the massive number of reported phosphorylation sites, substrate recognition must be a key regulatory mechanism for kinases to find and phosphorylate their targets without rampant off-target phosphorylation (de Oliveira et al., 2016). Substrate specificity is achieved through several mechanisms including peptide sequence at the target site (Kemp et al., 1975; Songyang et al., 1994), binding to docking sites (Biondi & Nebreda, 2003), complex formation (Pawson & Scott, 1997), or localization (Draviam et al., 2001). In addition, many kinases are themselves regulated by phosphorylation signaling, and modification of specific sites is sometimes required for full activity (Schwartz & Murray, 2011). The activity of kinases is opposed by protein phosphatases, which have their own set of intricate methods of regulation. While there are 189 identified phosphatase catalytic subunits, 90% of dephosphorylation is thought to be carried out by only 13 members of the phosphoprotein phosphatase (PPP) family (Nguyen & Kettenbach, 2023). Phosphatases, as opposed to kinases, primarily achieve specificity through interaction with regulatory components and binding to short linear motifs (SLiMs) (Brautigan & Shenolikar, 2018; Heroes et al., 2013). The integration of both of these enzyme classes into a common signaling network provides opportunities for incredibly rapid, precise, and reversible signaling in response to intracellular or extracellular cues.

Protein kinases and their opposing phosphatases coordinate to regulate substrate phosphorylation in complex pathways like response to stress, growth factors, and mitosis (Cohen, 1992, 2000; Deribe et al., 2010; Hunter, 2000). For example, epidermal growth factor receptor (EGFR), a receptor tyrosine kinase (RTK), dimerizes and autophosphorylates in response to stimulation by an activating ligand, EGF, leading to downstream signal transduction through the Ras-Raf-mitogen-activated-kinase (MAPK)

pathway (Lemmon & Schlessinger, 2010; Pinilla-Macua et al., 2017). EGFR signaling results in the dynamic phosphorylation of thousands of phosphosites (Olsen et al., 2006) and the change in expression of hundreds of proteins (Waters et al., 2012; Wee & Wang, 2017). While a large proportion of proteins are phosphorylated after EGF stimulation, only a subset of sites is differentially regulated, allowing for a precise signal integration (Olsen et al., 2006). Mitosis is another key example of how kinase and phosphatase activity drive large-scale morphological changes in the cell. Master mitotic kinases, including CDK1, Plk1, Aurora A, and Aurora B, all participate in the phosphorylation of thousands of phosphosites to bring about chromatin alignment and faithful segregation into two identical daughter cells (Joukov & De Nicolo, 2018; Nigg, 2001). Cdk1/Cyclin B activity is precisely regulated by various feedback loops to ensure mitotic entry once the commitment to mitosis has been made (Lindqvist et al., 2009). At the onset of anaphase, Cdk1 activity is silenced, allowing the full activation of counteracting phosphatases PP1 and PP2A-B55, which drive progression through mitosis (Holder et al., 2020). It has also been demonstrated that the occupancy of certain sites can vary dramatically depending on inputs like cell cycle stage (Olsen et al., 2010). The choreography between mitotic kinases and phosphatases brings about massive morphological changes to the cell but the accuracy of these phosphorylation signaling networks is essential to ensure that cell division occurs with sufficient fidelity to build a complex organism.

It has been known for at least 2 decades that abnormal protein phosphorylation is at the root of many diseases, including cancer (Cohen, 2002a). Because kinases and phosphatases are at the heart of key pathways that control growth and cell division, aberrant phosphorylation signaling is a common driver of disease (Ardito et al., 2017). Furthermore, nearly half of all kinase genes map to disease loci or amplicons that are common in cancer (Manning, Whyte, et al., 2002). For this reason, an enormous amount of money and effort has been spent over the last 20 years to develop specific inhibitors against kinases implicated in cancer (Attwood et al., 2021; Cohen, 2002b; Cohen et al., 2021; Rix & Superti-Furga, 2009; Zhang et al., 2009). One of the primary concerns in the development of kinase inhibitors is the development of drug-resistance mechanisms, which presents a major challenge to overcome (Cohen et al., 2021). Since signaling pathways governed by kinases and phosphatases are exceptionally complicated, a detailed understanding of these networks, particularly with how they are dysregulated in disease states, will provide fuel for the rational development of secondary therapeutic

modalities that act on specific network branches, thus providing alternative strategies to combat disease.

Because phosphorylation signaling is so essential in both fundamental cell biology and human health and disease, a myriad of techniques have been developed to study how kinases and phosphatases recognize their specific set of substrates. Nearly 50 years ago, it was shown that kinases bind to and phosphorylate specific amino acid sequences, called motifs, which imparts substrate specificity to each kinase (Bylund & Krebs, 1975; Daile et al., 1975; Kemp et al., 1975). While it was previously assumed that kinases recognize their substrates primarily through tertiary complex formation, structural evidence emerged demonstrating that the specific sequence of a linear peptide played an important role in the interaction between the kinase active site and the substrate (Brown et al., 1999; Lowe et al., 1997). Since then, there has been extensive interest in developing methods to determine motifs for kinases of interest, typically using degenerate peptide libraries and purified kinases, in order to attribute substrates to specific kinases (Songyang et al., 1994; Songyang et al., 1996). Along these lines, positional scanning peptide libraries were developed which use a randomized library of peptides with a centered phosphoacceptor and an amino acid fixed at one other position in the sequence (Hutti et al., 2004; Sugiyama & Ishihama, 2016). An *in vitro* kinase assay carried out on the peptide library either in solution or on a microarray, reveals motif preferences for queried kinase, providing important insights into the regulation of phosphorylation signaling networks (Alexander et al., 2011). However, kinase assays performed *in vitro* using linearized peptides as substrates remove many layers of regulation of kinase substrate recognition, such as temporal and spatial localization, and may lead to results that are not completely representative of the regulation *in vivo*. Advancements in mass spectrometry and proteomics techniques have facilitated the identification of phosphorylated peptides derived from cell lysates, enabling the study of kinase signaling using *in vivo* assays (Johnson, 2011). To uncover motif preferences and potential substrates, researchers have employed kinase inhibition by small molecule inhibitors in various cell models (Grosstessner-Hain et al., 2011; Kettenbach et al., 2011; Koch et al., 2011). However, this approach relies heavily on the availability of a selective inhibitor for the kinase of interest, which is lacking for the majority of kinases (Roskoski, 2019, 2020). Interestingly, numerous understudied kinases are seen to be dysregulated in various cancers (Moret et al., 2020). In addition, even the most selective inhibitors may have off-target effects, which can

complicate experimental interpretation. An early chemical genetics approach that was developed to be broadly applicable is the use of analog-sensitive kinase (as-kinase) alleles along with a bulky ATP analog that cannot be used by non-engineered kinases (Bishop et al., 2000). This method utilizes mutations to the ATP binding pocket, allowing the binding of an ATP analog, which specifically inhibits the as-kinase when bound (Shah & Shokat, 2003). This method has also been adapted as a strategy to label substrates of the as-kinase (Blethrow et al., 2008) and when coupled to mass-spectrometry, can be used to identify changes in phosphosite abundance with acute inhibition (Carlson et al., 2011). However, a major drawback of the as-kinase approach is that many kinases do not tolerate the mutation necessary for binding of the ATP analog and may become inactive or have severely compromised activity, as is the case for human Plk1 (Hards et al., 2021). Therefore, there is a pressing need for the development of broadly applicable and easy-to-implement techniques to identify kinase substrates and motifs and gain deeper insight into a broader range of the kinome.

Mass spectrometry-based proteomics approaches

Mass spectrometers for biological research emerged in the 1990s, providing a powerful tool with which to study large numbers of proteins at once (Pandey & Mann, 2000). In the intervening years, mass spectrometry has become the tool of choice for proteomics research (Zhang et al., 2013). In the case of bottom-up, or shotgun, proteomics, protein samples are digested to peptides with sequence-specific proteases and then analyzed by mass spectrometry (Aebersold & Mann, 2003; Zhang et al., 2013). Within an instrument, individual peptides are fragmented and the resulting spectrum is matched against a database based on the genome from the organism of interest (Patterson & Aebersold, 2003; Steen & Mann, 2004), an approach that is dependent on previous successes of the genomics field (Tyers & Mann, 2003). Proteomics is a rapidly expanding field with techniques and instrumentation that are constantly evolving, making it possible to study the proteome with less and less sample input and at greater and greater depths (Aebersold et al., 2018; Yates, 2019).

One of the major advantages of mass spectrometry-based proteomics is the ability to preserve and analyze PTMs, providing insight into the dynamics of cellular signaling (Mann & Jensen, 2003). By searching against a database for a modified peptide, a

phosphopeptide for example, it is possible to identify previously unknown PTMs, localize them, and quantify them with high accuracy (Choudhary & Mann, 2010). However, the analysis of PTMs is technically more challenging than standard proteome analysis (Olsen & Mann, 2013). In part, this is because only a small fraction of a given protein might be modified, resulting in lower abundance and thus a lower chance of identification (Jensen, 2006). Additionally, each modified site may only be represented by a single peptide, making it more difficult to identify with high confidence (Olsen & Mann, 2013). This is in contrast to protein identification and quantification which is typically based on the identification of more than one peptide.

Abundance is a challenge for phosphoproteomics in particular, as typically only 1%-2% of digested peptides exist as phosphopeptides, making it difficult to precisely analyze phosphosites among the background of the full proteome. To address this issue, a wealth of methods have been developed allowing researchers to specifically enrich for phosphorylated peptides, increasing the depth of coverage of the phosphoproteome (Bodenmiller et al., 2007; Ficarro et al., 2002; Villen & Gygi, 2008; Zhou et al., 2001). For example, tyrosine phosphosites make up about 1% of all phosphopeptides, and since only 1% of peptides are phosphopeptides, it can be difficult to quantify a meaningful number of phospho-tyrosines in a given experiment. Enrichment strategies using α-pTyr antibodies allow for specific enrichment of this species and analysis by mass spectrometry (Boersema et al., 2010; Kettenbach & Gerber, 2011; Rush et al., 2005) greatly improving the ability to study signaling pathways that are dependent on tyrosine phosphorylation. For general phosphoproteomics, metal affinity strategies have been developed to enrich phosphopeptides with high selectivity (McLachlin & Chait, 2001; Porath et al., 1975; Reinders & Sickmann, 2005). Techniques such as immobilized metal affinity chromatography (IMAC) and metal oxide affinity chromatography (MOAC) provide a means to enrich samples for phosphopeptides up to 99% (Qiu et al., 2020; Riley & Coon, 2016; Urban, 2022). When combined with downstream labeling and fractionation methods, these techniques allow for deep coverage of the phosphoproteome with tens of thousands of identified phosphosites, greatly improving our ability to study phosphorylation signaling pathways.

Another advancement that has greatly impacted throughput and quantitative accuracy is the use of chemical labels, allowing direct comparison of multiple peptide species within the same sample. One example of this is stable isotope labeling by amino

acids in cell culture (SILAC) in which cells are grown in isotopically labeled media (Ong et al., 2002; Ong & Mann, 2006), giving the advantage that harvested cells can be mixed immediately following treatment and limiting the effect of sample processing errors. Dimethyl labeling is another strategy that allows for a direct quantitative comparison between samples (Boersema et al., 2009; Hsu et al., 2003) by chemically labeling peptides with isotopically distinct modifications, allowing for sample mixing and side-by-side comparison. Both of these approaches apply distinct mass labels, which, when analyzed by mass spectrometry, can be used to directly compare abundances of the peptide analytes, providing a means to confidently assess quantitative differences between samples.

More recently, tandem-mass tag (TMT) labeling has become the tool of choice for sample multiplexing (Rauniyar & Yates, 2014), with the ability to combine up to 18 samples into a single multiplex (Li et al., 2021; Li et al., 2020; Thompson et al., 2019). Similar to dimethyl labeling, TMT utilizes a chemical tag to quantify peptides between samples within the same multiplex. This is possible because each isobaric TMT reagent has the same number of light and heavy carbon and nitrogen atoms distributed between a balancer and reporter region (Thompson et al., 2003; Werner et al., 2012). Thus, the mass of the reagent is the same for each channel while the reporter has a unique mass that can be identified and quantified by mass spectrometry (McAlister et al., 2012). In a proteomics experiment, these reagents can be used to give peptides from each treatment condition a unique flavor, allowing for direct quantification between treatment conditions and a quantitative assessment of differences between samples.

The combination of the techniques outlined above (i.e., phosphopeptide enrichment, TMT multiplexing, peptide fractionation) allows us to directly compare the effects of perturbations, for example, the addition of a kinase inhibitor, on the proteome and phosphoproteome with exceptional depth and quantitative accuracy. The ability to multiplex up to 18 samples also provides an opportunity to compare multiple conditions within a single experiment with enough biological replicates for statistical analysis. The application of these methodologies is an incredibly powerful tool to study phosphorylation signaling and allows us to dig deeper into pathways governed by kinases and phosphatases than has previously been possible.

Inducible protein degradation techniques

Knockdown by RNAi and knockout by CRISPR-Cas9 are common methods to deplete a protein of interest and study the effects of its loss on cellular physiology. These approaches have the advantage of being relatively fast, cheap, and easily customizable to target any gene of interest. Because of the endless customizability of CRISPR guide RNAs and RNAi oligos, these techniques have been shown to be powerful for genome-wide studies (Olivieri & Durocher, 2021; Tsherniak et al., 2017; Vit et al., 2022). However, both approaches are known to suffer from off-target effects (Buehler et al., 2012; Jackson et al., 2006) and a slow mechanism of action that allows time for cellular adaptations to adjust for the loss of the targeted protein. Another consideration is that, for proteins that are essential for the continuous growth and viability of the cell, knockdown and knockout approaches are not the best option as they would likely compromise cell survival. Gene knockdown or knockout studies have many useful applications, in particular for genome-wide experiments that identify or exploit cancer dependencies (Ghandi et al., 2019; Vazquez & Sellers, 2021), but since these technologies function at the pre-translational level, the time required to reduce protein level is problematic when studying dynamic processes such as phosphorylation signaling (Natsume & Kanemaki, 2017).

Conditional protein degradation techniques are a family of approaches that are used to acutely control the expression of a protein of interest upon the addition or removal of a small molecule to induce degradation (Natsume & Kanemaki, 2017). Targeted protein degradation (TPD) has a distinct advantage over genetic approaches, which take days to weeks to properly deplete a gene of interest, while degron-mediated degradation can completely deplete a protein of interest 2 hours or less (Nabet et al., 2018). Furthermore, the longer timescale required for gene knockdown or knockout may allow cells time to reconfigure signaling networks (Holland et al., 2012; Nagashima et al., 2019). While there are a number of TPD strategies, most make use of native proteasomal degradation machinery to degrade the target protein (Verma et al., 2020). Ubiquitin ligases bind to target proteins and covalently attach ubiquitin to lysine side chains, marking them for destruction by the proteasome (Bard et al., 2018). The majority of TPD strategies work by encouraging an association between the protein of interest and an E3 ligase, thereby promoting ubiquitination and proteasomal degradation (Aisha Yesbolatova et al., 2019). This can be accomplished through the use of a chemical modality that binds to both the protein of interest and an E3 ligase to promote ternary complex formation, as is the case

for proteolysis targeting chimeras (PROTACs) and molecular glues, or by using CRISPR-Cas9 to genetically engineer a protein degradation tag to the gene of interest (Wu et al., 2020).

The original genetically encoded, conditional degradation approach used a temperature-sensitive degron fused to the protein of interest (Dohmen & Varshavsky, 2005; Dohmen et al., 1994). With this strategy, a temperature-sensitive dihydrofolate reductase (ts-DHFR) with an exposed N-terminal arginine is fused to the N-terminus of a protein of interest. When cultured at 24C, the protein function is unaffected, but raising the temperature to 37C results in rapid destabilization and unfolding of ts-DHFR, causing ubiquitination and degradation. While protein depletion is extremely rapid, with a half-life of less than 30 minutes, it can only be applied in contexts where growing cells at 24C and 37C is possible. Temperature-sensitive methods have been applied in yeast for over 70 years (Horowitz, 1950), but this is unfortunately not possible in mammalian cells.

The HaloTag, a versatile protein tag derived from bacterial dehalogenase, can also function as a degron (Kanemaki, 2022; Aisha Yesbolatova et al., 2019). Originally, it was found that the HaloTag could be bound with a synthetic hydrophobic ligand, HyT13 or HyT36, to mimic protein unfolding and degradation (Neklesa et al., 2011; Tae et al., 2012). This was further improved upon by the development of a heterobifunctional ligand that induced an association between the HaloTag and the E3 ligase VHL, called HaloPROTAC (Buckley et al., 2015), which was able to degrade the HaloTag fusion protein to a much greater extent. Another similar approach uses a mutant of the FK596-binding protein ($FKBP12^{F36V}$) as a conditional degron tag, along with a heterobifunctional degrader, called dTag (Nabet et al., 2020; Nabet et al., 2018; Yesbolatova & Kanemaki, 2018). The dTag approach is a modification of a previously discovered PROTAC that promotes binding between endogenous FKBP12 and the E3 ligase Cereblon, leading to ubiquitination and degradation. By applying a bump-and-hole approach, mutant FKBP12 was modified to work as a degron tag and the PROTAC was adapted to specifically bind to mutant $FKBP12^{F36V}$, making this inducible degradation strategy broadly applicable. Both the HaloPROTAC and dTag approaches are broadly applicable and effective targeted protein degradation strategies. However, one concern is that, even though tagged proteins can be fully depleted within a few hours, the kinetics are slower than other comparable technologies, which could pose problems when applied to study phosphorylation

signaling, where broad changes to the phosphoproteome can occur within minutes of kinase or phosphatase depletion.

Of the commonly used conditional protein depletion methods, the auxin-inducible degron (AID) approach uses the smallest degron and typically has the fastest degradation kinetics (Natsume et al., 2016; Aisha Yesbolatova et al., 2019). This technique was developed by adapting protein components of the auxin signaling network in *Arabidopsis thaliana.* In plants, auxin-responsive factors (ARFs) are transcriptional elements that activate or repress target genes, but they are kept inactivated by the binding of Aux/IAA proteins that prevent ARFs from binding their target genes. However, auxin stimulates the binding of Aux/IAA proteins to F-box proteins like Tir1, degrading the Aux/IAA protein and activating the ARF (Dharmasiri et al., 2005; Kepinski, 2007; Kepinski & Leyser, 2004, 2005; Tan et al., 2007). The Kanemaki group adapted this signaling network to yeast and mammalian cells by ectopic expression of Tir1 and using Aux/IAA proteins as auxin-inducible degron (AID) tags on proteins of interest (Nishimura et al., 2009) and it can be applied to a wide variety of mammalian cell lines and animal models (Yesbolatova, Saito, & Kanemaki, 2020). The kinetics afforded by AID make it an attractive option for studying rapid processes, with some studies reporting protein half-lives of less than 20 minutes (Holland et al., 2012), and it has been applied to study mechanisms like DNA replication and chromatin dynamics (Kubota et al., 2013; Nagashima et al., 2019; Takagi et al., 2016). With such a short timescale, it is possible to identify direct kinase substrates with similar results to using small-molecule inhibitors (Hards et al., 2021). Furthermore, as Tir1 is a plant protein derived from *Oryza sativa,* there are no natural targets for it in animal cells and auxin does not cause identifiable changes to the proteome or phosphoproteome, suggesting that there is a minimal risk for off-target effects. In short, AID is an ideal system for studying rapid processes like protein phosphorylation, especially for kinases without inhibitors.

One concern with the AID-Tir1 system is degradation that occurs in the absence of auxin, called auxin-independent degradation. When auxin binds to Tir1, it satisfies a hydrophobic pocket in Tir1, allowing AID to bind efficiently for degradation (Tan et al., 2007). However, Tir1 can degrade AID-tagged proteins to a certain extent in the absence of auxin, leading to a basal level of degradation that may confound experimental results or make it difficult to create knock-in cell lines. This has been recognized as a substantial issue in AID-Tir1-based degradation and alternative F-box/degron pairs have been

identified and implemented (Li et al., 2019; Saito & Kanemaki, 2021; Yesbolatova, Saito, Kitamoto, et al., 2020). AFB2, a Tir1 analog from *Arabidopsis thaliana*, does not exhibit auxin-independent degradation when used with the degron miniIAA7 (Li et al., 2019). However, in our hands, the degradation kinetics are considerably slower and AFB2 does not degrade highly abundant proteins as efficiently as Tir1. More recently, a bump-and-hole strategy was employed to develop the $Tir1^{F74G}$ mutant with the intent of creating an orthogonal Tir1-IAA pair that could be used to more precisely study auxin signaling in plants (Uchida et al., 2018). $Tir1^{F74G}$, when used with the corresponding auxin analog 5-Ph-IAA, does not exhibit auxin-independent degradation and has similar degradation kinetics to $Tir1^{WT}$ (Nishimura et al., 2020; Yesbolatova, Saito, Kitamoto, et al., 2020), addressing some of the more prominent concerns with the AID-Tir1 approach. Furthermore, AID2 uses a much lower auxin concentration (1μM 5-Ph-IAA) compared to AID (1mM IAA), which has allowed this strategy to be employed to specifically deplete proteins in adult mouse models (Macdonald et al., 2022).

As with any genetically encoded protein degradation system, AID-Tir1 is dependent on gene editing, typically by CRISPR-Cas9, to introduce the necessary components. This is a challenge because degron tags must be incorporated into every allele of a target gene for degradation to remove the protein of interest completely and have the intended effect. It can take multiple rounds of CRISPR-Cas9 transfection, selection, and screening to identify clones that are homozygous knock-ins with fast degradation kinetics. Typically, selection is accomplished by introducing antibiotic resistance cassettes within a CRISPR targeting vector, allowing for the use of antibiotics to select for in-frame insertion of the degron tag (Lambrus et al., 2018; Natsume et al., 2016). However, antibiotic resistance can be acquired by other mechanisms, and it is necessary to screen many genomic clones to identify homozygous knock-ins. With the AID-Tir1 approach, there is an additional step compared to other genetically encoded TPD systems, like dTAG and HaloPROTAC, because Tir1 must also be introduced to AID-tagged cells. There are multiple strategies to do this, such as CRISPR-Cas9 or lentiviral transduction, but an extra selection and screening step is necessary to identify clones with Tir1 expression and AID degradation. Screening individual clones for auxin-induced degradation is a time-consuming process but it is a necessary step to create AID-Tir1 cell lines. Although genetically encoded TPD systems are arduous to implement, it is a

relatively straightforward strategy that is faster and cheaper than it would be to design a novel PROTAC molecule for every protein of interest.

In parallel to the rise of genetically encoded TPD methodologies, there has been a surge in the development and implementation of small molecule degraders as therapeutics, typically in the form of proteolysis targeting chimeras (PROTACs) and molecular glues (Burslem & Crews, 2020; Burslem et al., 2019; Xiao et al., 2022). Both of these technologies rely on a small molecule to bind to a protein of interest on one end, and an E3 ligase on the other, promoting dimerization and degradation of the target (Hanzl & Winter, 2020). PROTAC molecules are typically made up of three modular components and include a warhead to bind the target protein, a known E3 ligase ligand, and a linker region connecting the two (Cromm & Crews, 2017). Because the warhead only needs to bind the target protein and does not need to cause inhibition by itself, this opens up the potential to use previously discarded small molecules that are known to bind but not inhibit a target protein. This also presents an opportunity to target previously “undruggable” protein targets, as they do not need to have enzymatic activity to be degraded (Xiao et al., 2022). The PROTAC molecule also typically includes a known E3 ligand, meaning that the E3 ligase to be recruited for ubiquitination can be chosen *a priori*. This imparts an added layer of specificity to PROTAC design (Bondeson et al., 2018) and in theory, multiple PROTACs with different E3 ligands could be developed against the same protein to overcome resistance mechanisms, or even allow for tissue-specific protein degradation. The linker is also an essential component of the PROTAC molecule, and it is known that the length and composition of this module influence binding between an E3 ligase and the target protein (Burslem et al., 2018). It has been shown that the ability of a PROTAC to induce ternary complex formation between its target and the E3 ligase is an essential mechanism for whether or not the protein of interest will be degraded (Li & Crews, 2022; Pettersson & Crews, 2019). Since there are three different components to PROTAC molecules, all of which influence binding, target engagement, and degradation, these therapeutic modalities can be designed with much higher specificity than traditional inhibitors (Müller & Rauh, 2018). In fact, it has been demonstrated that promiscuous kinase inhibitors can be adapted into PROTACs that have high selectivity for a single kinase (Huang et al., 2018). However, the trade-off is that there is a considerable investment needed to design and construct a functional PROTAC and many labs do not have the synthetic or medicinal chemistry knowledge necessary to create bespoke

PROTACs (Burslem & Crews, 2020). While this will certainly be an influential drug modality in the clinical space in the near future, it is difficult to implement for independent projects to induce the degradation of one or multiple proteins of interest.

Kinases in cell cycle control and mitotic progression

In order for the continuous inheritance of genetic material to occur, cells must constantly replicate their DNA and divide into new daughter cells. The bulk of the cell cycle is a stage called interphase, during which cellular material is synthesized in preparation for division into two cells (McIntosh, 2016). The process by which this occurs, mitosis, was discovered in the early 19th century and is itself broken in distinct phases (Paweletz, 2001; Yanagida, 2014). In the early stages of prophase, duplicated chromosomes are condensed into chromatin, highly dense and organized structures of DNA and protein before being aligned in the central plane of the cell during metaphase. After satisfaction of the spindle assembly checkpoint, sister chromatids are pulled to opposite poles of the cell where each is organized into a new nucleus in telophase. Finally, the cell is pinched apart along the central axis in cytokinesis to form two new daughter cells. This process is an intricate dance that requires the formation of supramolecular structures and gross changes to cell morphology. Each step in the process is regulated by phosphorylation signaling through kinases and phosphatases, the activity of which is essential for faithful DNA segregation.

Cyclin-dependent kinase 1 (Cdk1) is the most prominent driver of mitosis and, when bound to cyclin, phosphorylates a host of substrates to promote mitotic entry (Nigg, 2001). At the G2/M transition, the transition point between interphase and mitosis, Cdk1 is suppressed by inhibitory phosphorylation by the kinases Wee1 and Myt1. This is reversed by the counteracting phosphatase Cdc25C, which, by dephosphorylating Cdk1 at the same residues, promotes Cdk1 activation. When Cdc2525C outweighs Wee1 and Myt1, Cdk1-cyclin is fully activated and promotes entry into mitosis by phosphorylating numerous substrates, leading to a breakdown of the nuclear envelope, centrosomal separation, chromosome condensation, and spindle assembly (Nigg, 1995, 2001).

Polo-like kinases (PLKs)

Along with Cdk1, the Polo-like kinase (Plk) and Aurora kinase families play major roles in the orchestration of mitosis (Joukov & De Nicolo, 2018). Polo kinase is an essential driver of mitosis and is conserved from yeast to humans (Archambault & Glover, 2009; Archambault et al., 2015). The Plks, of which there are five in humans, all have a Polo-box domain (PBD) that has been shown to bind phosphorylated serines and threonines to mediate localization and promote substrate interaction (Elia, Cantley, et al., 2003; Elia, Rellos, et al., 2003). Together, the Plks maintain key cell cycle checkpoints and coordinate mitotic progression.

Plk1, the founding member of the Plk family, plays a number of important roles throughout mitosis. Plk1 helps to drive entry into mitosis at the G2/M transition by phosphorylating Wee1 to generate a phosphodegron and induce degradation (Watanabe et al., 2004), and by phosphorylating and inhibiting Myt1 (Inoue & Sagata, 2005). In response to the G2 DNA damage checkpoint, Plk1 is dephosphorylated and inactivated to prevent mitotic entry (Smits et al., 2000), and its reactivation is necessary for mitotic entry after resolution of the checkpoint (van Vugt et al., 2004). During mitosis, Plk1 localizes to centrosomes where it influences centrosome maturation by recruiting proteins to the pericentriolar matrix (PCM), including Aurora A, and Nek9 (De Luca et al., 2006; Santamaria et al., 2011; Sdelci et al., 2012). At kinetochores, Plk1 phosphorylates and activates the kinase Haspin, which in turn phosphorylates histone H3 to promote centromere binding of the chromosomal passenger complex (CPC), the key complex regulating kinetochore-microtubule (k-MT) attachments (Ghenoiu et al., 2013; Zhou et al., 2014). Recruitment of CPC to centromeres creates a positive feedback loop since Aurora B phosphorylates Plk1, which functions to stabilize k-MT attachments (Archambault & Carmena, 2012; Carmena, Pinson, et al., 2012; Liu et al., 2012). Following anaphase, Plk1 is partially degraded through the activity of the anaphase promoting complex/cyclosome (APC/C), but the remainder is localized to the central spindle and midbody where it recruits proteins required for cytokinesis and thereby drives formation of the cleavage furrow (van Vugt & Medema, 2005; Zitouni et al., 2014). Overall, Plk1 is a dynamic regulator of mitosis that coordinates with other master mitotic kinases to ensure the fidelity of chromatin separation and cytokinesis.

Significantly less is known about the related kinase, Plk3. While Plk1 and Plk3 have very similar structures, particularly with respect to the catalytic domains, it's thought that they have largely opposing functions throughout the cell cycle (Zitouni et al., 2014). Plk3 was originally characterized as an immediate early gene and was suspected to regulate the cell cycle because its mRNA expression is rapidly increased with growth factors in human and mouse cell lines, but its expression is limited to certain tissues in both mice and humans (Donohue et al., 1995; Li et al., 1996). In addition, Plk3 mRNA expression is cell cycle regulated and limited to G1 but Plk3 protein is stable and consistent throughout the cell cycle (Winkles & Alberts, 2005). It has been suggested that Plk3 is required for entry into S phase by acting on Cdc25 phosphatases to indirectly regulate Cdk activity (Bahassi el et al., 2004; Myer et al., 2005). In addition, Plk3 is implicated in regulating Cyclin E activity through Cdc25A and thereby controls the transition from G1 to S in interphase (Zimmerman & Erikson, 2007b). While Plk1 is inhibited upon genotoxic stress, Plk3 is primarily thought to play roles mediating the DNA damage response. Plk3 is increased after DNA damage (van de Weerdt & Medema, 2006) and activated as part of a positive feedback loop with Chk2 in order to phosphorylate and stabilize p53 (Bahassi el et al., 2002; Xie, Wang, et al., 2001; Xie, Wu, et al., 2001; Xie et al., 2002). Consistent with this likely stress response function, the predominant localization of Plk3 is in the nucleolus (Zimmerman & Erikson, 2007a). However, a more recent study challenged the validity of Plk3 antibodies used in previous studies and failed to replicate a response to Hif1a (Aquino Perez et al., 2020; de Cárcer, 2019). In addition to studies defining the role of Plk3 in the cell cycle and stress response, there have been numerous studies investigating the effects of Plk3 on tumor formation. While Plk1 is frequently considered an oncogene and is upregulated in various cancers, it has been reported that Plk3 is downregulated in certain tumors (Ando et al., 2004; Dai et al., 2000) and Plk3 deficient mice are larger and prone to develop large tumors with advanced angiogenesis, consistent with a role for Plk3 as a tumor suppressor (Yang et al., 2008). This is an important consideration for the development of Plk1 inhibitors for therapeutic use, as inhibition of Plk3 would be an undesirable side-effect, and currently, the most selective Plk1 inhibitors also inhibit Plk3 with high affinity because of their structural similarity (Rudolph et al., 2009; Steegmaier et al., 2007). Although Plk3 is implicated in a number of key signaling pathways and disease states, it is still unclear how it achieves those functions. For this reason, the development and implementation of Plk3-centric

phosphoproteomics experiments would be ideal to determine the exact signaling pathways in which Plk3 is a main component.

Aurora kinases

The Aurora kinases work in coordination with Plk1 and Cdk1 as key drivers of mitosis and orchestrate a host of processes ranging from centrosome maturation to k-MT attachments (Joukov & De Nicolo, 2018; Nigg, 2001). In mitosis, Aurora A is localized to centrosomes by the scaffolding protein CEP192, where it drives recruitment and activation of Cdk1-Cyclin B1, as well as Plk1, generating a positive feedback loop and accelerating mitotic entry (Barr & Gergely, 2007; Hirota et al., 2003; Joukov et al., 2014; Macurek et al., 2008). In addition, the feedback loop with Plk1 is a key requirement of centrosome maturation and activity, and active Plk1 helps to drive the localization of both Aurora A and TPX2 (Asteriti et al., 2015; De Luca et al., 2006). At centrosomes, Aurora A promotes centrosome maturation by phosphorylating and recruiting proteins, such as TACC3, that stabilize microtubules (MTs) at the microtubule organizing center (MTOC) (Burgess et al., 2015; Willems et al., 2018). Aurora A also has key roles along spindle microtubules, where it is recruited and activated by TPX2 (Bird & Hyman, 2008). TPX2, a prominent component of the spindle apparatus, directly binds and is phosphorylated by Aurora A at microtubule spindles (Kufer et al., 2002), which in turn promotes Aurora A autophosphorylation on Thr288 and protects it from dephosphorylation by PP6 (Bayliss et al., 2003; Eyers et al., 2003; K. Zeng et al., 2010). By phosphorylating key microtubule-associated proteins, Aurora A has been implicated in the regulation of spindle microtubule dynamics (Hochegger et al., 2013). Finally, Aurora A is also involved in the development of the bipolar spindle by phosphorylating the kinesin Eg5 to promote centrosome separation (Giet et al., 1999).

Aurora B is structurally similar and closely related to Aurora A and regulates multiple complementary pathways in mitosis and cell division. In particular, Aurora B functions as a core component of the error correction (EC) and spindle assembly checkpoints (SAC) (Willems et al., 2018). Aurora B functions as the catalytic component of the chromosomal passenger complex (CPC), which is targeted to the outer centromere and includes the proteins Incenp, Survivin, and Borealin (Hochegger et al., 2013). The CPC is targeted to centromeres through the activity of Haspin, which phosphorylates

Histone 3 on Thr3, creating a binding site for Survivin and recruiting the CPC to centromeres (Kelly et al., 2010; Wang et al., 2010). As a second mechanism for enriching the CPC at centromeres, the mitotic kinase Bub1, by phosphorylating Histone H2A on Thr210, creates a binding site for Shugoshin proteins, which in turn recruit the CPC through Incenp or Borealin (Musacchio, 2010; Yamagishi et al., 2010). Aurora B itself binds directly to Incenp and its localization to centromeres triggers its activation by autophosphorylation of Thr232 (Ma & Poon, 2011; Samejima et al., 2015). One of the key functions of Aurora B at centromeres is the phosphorylation of kinetochore proteins to correct k-MT attachments and promote bipolar spindle attachments (Ditchfield et al., 2003; Hauf et al., 2003). Spindle microtubules emanating from the poles attach to kinetochores via the KNL-1/Mis12 complex/Ndc80 complex (KMN) network in a stochastic process that leads to improper attachments, but by phosphorylating kinetochore proteins in the absence of tension, Aurora B destabilizes the attachment and promotes error correction (Cheeseman et al., 2006; Nicklas, 1997). The tension generated by bioriented attachment creates a spatial separation between the centromere and kinetochore, preventing Aurora B from reaching and phosphorylating its kinetochore substrates, and stabilizing the attachment point (Liu et al., 2009). Aurora B also prevents premature mitotic exit by regulating the spindle assembly checkpoint (SAC) in the absence of k-MT tension (Willems et al., 2018). When both chromosomes are attached to the same spindle pole (i.e. monotelic attachments), components of the mitotic checkpoint complex (MCC), including MAD2, BUBR1, BUB3, and Cdc20, accumulate at kinetochores where they form a complex and coordinate to inhibit the APC/C (Musacchio & Salmon, 2007; Nezi & Musacchio, 2009). When k-MT tension is low, continuous Aurora B activity results in the recruitment of MCC proteins, in particular Mps1, an upstream activator of the SAC, sending a diffusible inhibitory signal to the APC/C and delaying anaphase (Carmena, Wheelock, et al., 2012; Roy et al., 2022). Bi-oriented chromosome attachment and establishment of tension reduce Aurora B activity, silencing the SAC and resulting in activation of APC/C, degradation of Cyclin B1, and progression into anaphase (Ma & Poon, 2011).

At the onset of anaphase, Aurora B, along with Incenp, localizes to the central spindle, a structure comprised of bundled, anti-parallel microtubule plus ends at the central plane of the dividing cell (Hadders & Lens, 2022). Here, it establishes an activity gradient, maintaining kinetochore stability during anaphase and establishing the eventual

positioning of the cleavage furrow (Fuller et al., 2008; Papini et al., 2021). Once at the central spindle, Aurora B phosphorylates the centralspindlin complex to promote its microtubule bundling activity and stabilize spindle microtubules (Carmena et al., 2009; Mishima et al., 2002). Additionally, this promotes the downstream activation of RhoA, assembling the contractile ring and driving cytokinesis (Minoshima et al., 2003; Wadsworth, 2005). In the final stages of cell division, persistent Aurora B activity is required at the midbody to regulate the abscission checkpoint, which delays the resolution of cytokinesis in response to chromatin trapped in the intracellular canal (Petsalaki & Zachos, 2019). It is through these mechanisms that Aurora B acts as one of the key gatekeepers of mitosis, delaying progression until all checkpoints are satisfied and preventing chromosome segregation errors, which would have disastrous consequences for the cell.

An interesting aspect of Aurora biology is to what extent Aurora A and Aurora B have overlapping substrates. They have both been implicated in positive feedback loops to activate Plk1, which is targeted to both centrosomes and centromeres in mitosis, suggesting that they could share substrates that localize to both of these structures. Aurora A is thought to localize along spindle microtubules in mitosis and although it does not colocalize with Aurora B at centromeres, it is possible that Aurora A and B come into contact with shared substrates from opposite ends at k-MT attachment points. In fact, shared substrates for Aurora A and B primarily localize to spindles (Hochegger et al., 2013; Kettenbach et al., 2011) and there is evidence that Hec1, a component of the NDC80 complex in the KMN network that is bound by microtubules, can be phosphorylated by both Aurora A and Aurora B at different sites (DeLuca et al., 2018). However, up to this point, many studies analyzing the effects of Aurora A and Aurora B inhibition have utilized small-molecule inhibitors, and it is therefore not possible to rule out the potential for off-target effects. Therefore, to definitively address the extent of Aurora A and B substrate overlap, a more selective approach, such as targeted protein degradation, is required.

p21-activated kinases (PAKs)

The p21-activated kinase (PAK) family consists of six kinases that regulate a myriad of proliferation pathways including ERK, AKT, and WNT (Kumar et al., 2006; Radu et al., 2014). The PAKs are categorized into group 1 (PAK1-3) and group 2 (PAK4-6), with

distinct structural features for each group. All six PAKs function as effectors of the Cdc42 and RAC GTPases, owing to their GTPase binding domain (GBD). PAKs typically exist in an autoinhibited state with the GBD bound to the kinase domain, inhibiting kinase activity. Binding of a small GTPase to the GBD causes a conformational shift, releasing the GBD and allowing for autophosphorylation and activation (Bokoch, 2003). The PAK family is best understood for its roles in regulating actin dynamics and through these functions, they are thought to contribute to invasion and metastasis, particularly in breast cancer (Best et al., 2022). In addition to roles regulating the actin cytoskeleton, there is evidence that the PAKs are cell cycle regulators that promote the G1/S and G2/M transitions (Maroto et al., 2008; Nekrasova & Minden, 2011; Radu et al., 2014; Z.-s. Zhao et al., 2005). All of the PAKs are seen to be upregulated in various cancers, with PAK1 and PAK4 the most frequently upregulated and typically correlated with poorer prognosis (Kumar & Li, 2016; Rane & Minden, 2019). As a result, there has been extensive interest in understanding signaling networks regulated by the PAK family and how these kinases contribute to cancer and metastasis.

PAK1 is the best-studied member of this kinase family and has multiple roles in promoting proliferation, mitotic entry, and regulation of cytoskeletal dynamics (Kumar et al., 2017). It has been shown that PAK1 is targeted to centrosomes by GIT1 where it influences mitotic entry by phosphorylating and activating both Aurora A and Plk1 (Maroto et al., 2008; Z. S. Zhao et al., 2005), both of which are frequently upregulated in various cancers. In growth factor signaling pathways, PAK1 connects ERK and AKT to KRAS and is essential for driving this pathway. PAK1-deficient mice with KRAS drive tumor formation were observed to have reduced AKT and ERK activation, delayed tumor onset, and overall better survival suggesting that PAK1 signaling plays a key part in KRAS driven tumorigenesis (Chow et al., 2012). The best-characterized functions for PAK1 are in regulating the actin cytoskeleton. Activation by master cytoskeletal coordinators such as Cdc42 promotes cellular motility by phosphorylating F-actin regulators at the leading edge (Kumar et al., 2017). PAK1 phosphorylates Ser 273 of Paxillin, a cytoskeletal protein involved in connecting the actin cytoskeleton to the extracellular matrix at focal adhesions, increasing cellular motility (Nayal et al., 2006). PAK1 also functions in the turnover of invadopodia, which is thought to be related to its roles in cancer and metastasis (Williams et al., 2019). While there are multiple substrates and pathways in which PAK1 has been implicated, a complete picture of PAK1 signaling has not been resolved. Furthermore,

PAK1 and PAK2 are highly similar kinases, with nearly 95% sequence similarity in the catalytic domain between the two kinases (Semenova & Chernoff, 2017). This has complicated the development of PAK1-specific inhibitors as small molecules that bind to the active site of PAK1 are likely to bind to the active site of PAK2, and vice versa. The high sequence similarity and the similarity in substrate motif preference between PAK1 and PAK2 suggest that these two kinases could have redundant functions within the cell (Rennefahrt et al., 2007). However, up to this point, the bulk of the research into the group 1 PAKs has centered around PAK1 with most functions for this group of kinases being attributed to PAK1 specifically. Probing the PAK-dependent signaling network using selective PAK inhibitors, protein degradation, and phosphoproteomics approaches will be an essential step forward in determining key pathways regulated by group 1 PAKs and the extent of redundancy and substrate overlap between PAK1 and PAK2.

Chapter 2

Characterizing Plk family substrate overlap and elucidating novel Plk3 substrates with AID-Tir1 protein degradation

Author Contributions:

C. Lincoln Howarth: Wrote text and designed figures for chapter 2. Designed, executed, and analyzed experiments.

Scott A. Gerber: Conceptualized, designed, and analyzed experiments. Provided feedback and edits on text.

Introduction

The polo-like kinase family (Plk1-5) is involved in a diverse range of cellular processes. There is a wealth of information on Plk1, an essential driver of mitosis that is conserved in yeast (Cdc5), *Drosophila* (Polo), and *Xenopus* (Plx1). Plk1 is part of the feedback loop that activates Cdk1 and is necessary for re-entry into mitosis after the completion of DNA repair (Zitouni et al., 2014). Plk1 inactivates Wee1, an inhibitory kinase of Cdk1, and activates Cdc25, a CDK activating phosphatase and mitotic driver (Archambault & Glover, 2009). Plk1 also plays a key role in centriole maturation, and its inhibition causes cells to form a monopolar spindle and arrest in G1 (Zitouni et al., 2014). As a key driver of progression through mitosis, Plk1 is frequently upregulated in many types of cancer (Eckerdt et al., 2005). Efforts have been made to develop small molecule inhibitors specific to Plk1 as a therapeutic strategy in cancers where Plk1 is upregulated (Goroshchuk et al., 2019). In contrast, however, little is known about how Plk3, an important kinase thought to have roles in DNA damage response and as a tumor suppressor protein, achieves its functions.

Many of the inhibitors that have been developed thus far, such as the FDA approved drug volasertib and GSK461364, were developed as ATP-competitive inhibitors of Plk1 but target multiple members of the Plk family (Strebhardt, 2010). The kinase domain is highly conserved between Plk family members, and it has been shown that the ATP-binding site of Plk1 matches those of Plk2 and Plk3 with 90% and 86% identity, respectively (Johnson et al., 2007). Therefore, it is not surprising that ATP-competitive inhibitors of Plk1, including volasertib, are able to inhibit Plk2 and Plk3 with high affinity (Rudolph et al., 2009). Although not much is known about the regulation of Plk2 and Plk3 or their downstream targets, it has been suggested that both kinases function as tumor suppressors because their expression has been shown to be downregulated in certain cancers. Furthermore, it is thought that both Plk2 and Plk3 play roles in mediating a response to DNA damage and may link the response to DNA damage to p53-mediated apoptosis (Li et al., 2005; Zitouni et al., 2014), strongly indicating that both of these kinases may function as tumor suppressor proteins.

Plk3 was originally characterized as an immediate early gene that is upregulated upon the addition of growth factor (Donohue et al., 1995) and it is thought to play a role in

cell cycle regulation by mediating cyclin E1 accumulation and Cdc25A activation (Zimmerman & Erikson, 2007b). However, it was later demonstrated that Plk3-deficient mice are viable (Yang et al., 2008), casting some doubt on the importance of Plk3 in cell cycle regulation. This study also found that Plk3-deficient mice displayed increased weight and developed large and highly vascularized tumors later in life (Yang et al., 2008). A follow-up study concluded that Plk3 phosphorylates and destabilizes Hif-1α in order to regulate the response to hypoxia and to prevent angiogenesis (Xu et al., 2010), which may explain how Plk3 functions as a tumor suppressor and why Plk3-null mice develop larger tumors. Furthermore, it was shown that Plk3 expression may be regulated by NF-κB in order to induce an apoptotic response through phosphorylation and activation of p53, and that overexpression of Plk3 in a $p53^{+/+}$ background can induce apoptosis (Li et al., 2005). Therefore, the possibility exists that tumors exposed to anti-Plk1 therapeutics also experience a reduction in Plk3 activity and signaling, leading to a resistance to apoptosis, which is one of the 6 hallmarks of cancer progression (Hanahan & Weinberg, 2011). From this perspective, a full understanding of Plk3 signaling is necessary for tailoring the development of Plk1-specific inhibitors and informing pharmaceutical innovation.

Over the last 2 decades, there has been considerable effort to understand how Plk3 fits into the DNA damage response pathway and what downstream proteins may be effector molecules of Plk3 kinase activity. This includes work suggesting that Plk3 phosphorylates and regulates p53 (Xie, Wu, et al., 2001), Chk2 (Bahassi et al., 2006), and Hif1α (Xu et al., 2010). However, more research is needed to validate known Plk3 substrates and identify novel substrates (Helmke et al., 2016). Understanding how Plk3 fits into the DNA damage response pathway is essential for determining how Plk3 dysregulation can play a role in tumorigenesis, and it may illuminate potentially new therapeutic strategies. Considering that Plk1 inhibition is a frequently used strategy in some cancer therapies, determining similarities and differences with Plk3 substrates will help inform more sophisticated strategies for clinical use of Plk1 inhibitors.

Taking a mass spectrometry-based approach to investigate Plk3-dependent phosphorylation events will allow us to identify novel Plk3 substrates and explore Plk3-regulated signaling pathways in an unbiased way. Here, we applied an auxin-inducible degron (AID)-Tir1 targeted protein degradation approach to Plk3 to specifically and selectively uncover the Plk3-dependent phosphoproteome. Plk3 also presents an exciting test case for this technology due to the lack of available tools to study Plk3 biology.

Development of an AID-Plk3 cell line would allow for rapid and precise control of Plk3 expression, providing a means to directly interrogate how acute loss of Plk3 activity affects cell signaling.

Methods

Cell culture and cell lines

HeLa, HEK293, and DLD1 cells were grown in Dulbecco's Modification of Eagle's Medium (DMEM, Corning) supplemented with 8% fetal bovine serum (FBS, Hyclone) and 1% penicillin-streptomycin (100IU/mL penicillin and 100µg/mL streptomycin, Corning). Cells were incubated at 37C with 5% CO_2.

HeLa cells are used as a model system because they are amenable to CRISPR-Cas9 gene editing and cell cycle arrest. DLD1 cells are diploid, requiring fewer CRISPR-Cas9 transfections to create endogenous knock-in clones, and were used for AID-Plk3 tagging experiments for increased tagging efficiency. HEK293 cells, similar to HeLa cells, are amenable to CRISPR-Cas9 gene editing and are an ideal system for expression of transfected vectors.

CRISPR-Cas9 homologous recombination clone generation

AID-Plk3 targeting constructs were designed around the start or stop codon based on the Plk3 genomic sequence in UCSC genome browser. 500bp homology arms, as well as the inserts, were ordered as g blocks (IDT) and assembled in pBluescript (see **Figure 2.1** and **Figure 2.2** for a diagram of the completed targeting vectors). sgRNAs were designed based on scoring from CRISPOR.tefor.net and were cloned into the U6 site of the Cas9 expressing vector pX330. The homology arms of the Plk3 targeting vector were designed to be resistant to all sgRNAs used in these experiments.

For Plk3 knockout and replace, 3xFlag-AID-Plk3 was introduced to the AAVS1 safe-harbor locus as previously described (Mali et al., 2013). Briefly, 3xFlag-AID and the Plk3 protein coding sequence were amplified by PCR separately and cloned into an AAVS1 CRISPR targeting vector and sgRNAs were cloned into the U6 promoter of the Cas9 expressing vector pX330.

For transfection, cells were plated to 6-well dishes at ~50% confluency in media free of penicillin/streptomycin. 1.4µg of targeting vector was linearized *in vitro* with

restriction enzymes external to the homology arms. The digested targeting vector was mixed with 0.4µg of pX330 in Jetprime and Jetprime transfection buffer (Polyplus) and incubated at room temperature for 10 minutes as per manufacturer protocol. The transfection mix was added dropwise to each well and incubated overnight. After 16hrs of incubation, the media was washed off and exchanged for media containing penicillin/streptomycin and the cells were left to grow for another day. On day three, transfected cells were expanded to 10cm dishes and treated with blasticidin (10µg/mL), hygromycin (100µg/mL), Zeocin (100µg/mL), or puromycin (10µg/mL). Media was exchanged for fresh media containing antibiotic every two days for two weeks or until colonies visible to the naked eye had formed. Individual colonies were isolated by incubation in trypsin diluted 1:40 in PBS and then manually harvested under a 10x screening microscope and transferred to a 96-well plate. Colonies were expanded to the 24-well stage and then harvested for analysis by genomic PCR and western blotting.

Genomic PCR

To harvest DNA for genomic PCR, 20% of cells from a 96 well were pelleted and lysed in 40uL of QuickExtract (Lucigen). The lysates were heated at 65C for 8 minutes, vortexed, heated at 98C for 3 minutes, and vortexed again. PCR was performed with primers recognizing the genomic locus exterior to the homology arms and primers internal to each resistance cassette.

siRNA Plk3 knockdown

WT HeLa, 293, and RPE1 cells were plated to 20% confluency in 12-wells and were transfected with 20nM-40nM of a mixed pool of 4 siRNA targeting Plk3 (Dharmacon) using INTERFERin (PolyPlus) and following the manufacturer protocol. Media was exchanged the day after transfection and cells were collected 48hrs after transfection, lysed, and analyzed by western blot.

Western Blotting

Cells to be analyzed by western blot were collected, washed once in PBS, and lysed in 2x Lamelli. Poly-acrylamide gels were poured in house from a 30% acrylamide solution (Protogel, National Diagnostics). Gels were run at 140V for 80 minutes in running buffer containing 25mM Tris, 200mM glycine, and 1% SDS. The gels were then transferred to nitrocellulose blotting membrane (Amersham Protran) at 100V for 60 minutes in a transfer buffer containing 25mM Tris, 200mM glycine, and 20% MeOH. To account for loading, blots were briefly stained with ponceau (0.01% ponceau, 0.5% acetic acid) and imaged. Blots were washed in TBST (50mM Tris, 150mM NaCl, 0.2% Tween-20) before blocking for 30 minutes in a solution of 4% milk in TBST and overnight incubation with primary antibody in 4% milk in TBST. Finally, blots were incubated with an HRP-conjugated secondary antibody for 1hr at room temperature, treated with Clarity ECL substrate (BioRad) and imaged.

Results

N-terminal AID tagging Plk3

In previous work, our lab demonstrated the use of AID-Tir1 targeted protein degradation as an approach to study kinase-substrate relationships, for deployment ultimately in cases where kinase inhibitors are not available. This project centered on Plk1 as a proof-of-concept because of the availability of a potent and broadly selective small-molecule inhibitor, BI2536 for comparison and validation purposes. In that work, we were able to demonstrate that targeted protein degradation can approximate inhibition by a small molecule (Hards et al., 2021). We were also interested in applying this approach to the related kinases Plk2 and Plk3 as relatively little is known about the roles that these two kinases play, and selective inhibitors are not available. Therefore, extending AID-Tir1 as a methodology to elucidate novel substrates to the remainder of the Plk family would highlight the power and modularity of this approach as well as uncover novel substrates and pathways that are regulated by Plk2 and Plk3.

To extend the AID-Tir1 approach to Plk3, we generated CRISPR-Cas9 targeting vectors to introduce a 3xFlag-AID tag to the N-terminus of Plk3, along with guide RNAs targeting the Plk3 endogenous locus. The targeting vector includes 500bp arms that are homologous to the Plk3 endogenous locus immediately upstream and downstream of the start ATG, to promote homologous recombination after Cas9-induced double strand breaks (DSBs) (**Figure 2.1A**). We incorporated a 3xFlag-AID tag between the homology arms to append this tag to the N-terminus of Plk3, along with one of three antibiotic resistance cassettes which are separated from 3xFlag-AID by a P2A ribosomal skip site. This design allows for selection of in-frame insertion after CRISPR-Cas9 transfections using an antibiotic selection agent. The targeting vector was linearized *in vitro* and, along with a pX330 plasmid expressing Cas9 and a guide RNA against Plk3, transfected into HeLa and DLD1 cells. After transfection, cells were selected for 1-2 weeks with an antibiotic and collected as a pool to be used in the next round of transfections. The transfection and selection process was repeated three times in HeLa cells and twice in DLD1 cells, each time using a unique gRNA/selection cassette in combination with the corresponding antibiotic, before individual clones were selected and screened by genomic PCR and western blot for 3xFlag-AID tag incorporation. After screening, we were unable

to identify a knock-in of the 3xFlag-AID tag for antibiotic resistant clones in either HeLas (data not shown) or DLD1s (**Figure 2.1B**). We verified that the antibody used against Plk3 was able to detect Plk3 by spiking exogenous Plk3 previously purified from Sf9 insect cells into wild-type DLD1 cell lysate (**Figure 2.1B**). We hypothesized that the N-terminus of Plk3 was inaccessible for CRISPR-Cas9 gene editing, possibly due to the GC rich nature at this locus, and that the antibiotic resistance cassettes were incorporated elsewhere in the genome and conferring antibiotic resistance to these clones non-selectively.

C-terminal AID tagging Plk3

To address this, we created new targeting vectors and guide RNAs to target the C-terminus of Plk3. While the overall targeting strategy was largely the same, we inverted the order of the tags and used homology arms that were homologous to genomic sequences directly upstream and downstream of the Plk3 stop codon. As with the N-terminal targeting approach, three versions of the targeting vector were constructed, each with a different antibiotic resistance cassette, along with four guide RNAs targeting the C-terminus of Plk3 (**Figure 2.2A**).

To endogenously tag Plk3, the targeting vector conveying blasticidin resistance was linearized *in vitro* and transfected into HeLa cells along with a pX330 plasmid expressing Cas9 and one of three guide RNAs (sgRNA1a, sgRNA1b, sgRNA2). After allowing two days for recovery, the transfected cells were expanded and treated with blasticidin to select for cells with in-frame insertion of the targeting vector at the endogenous locus. Cells were grown into visible colonies at which point they were collected and maintained as a pool. To verify incorporation of the targeting vector, genomic DNA was harvested for each of the three transfection conditions and a locus-specific genomic PCR was performed using a forward primer recognizing the Plk3 endogenous locus upstream from the LHR of the targeting vector, and a reverse primer recognizing the blasticidin resistance cassette. A positive band in this assay demonstrated that in each of the three transfection conditions, the targeting vector was incorporated into the Plk3 endogenous locus in all three transfection conditions (**Figure 2.2B**). However, western blotting of the pool did not show a mass-shifted Plk3 product, as anticipated when appending an AID-3xFlag tag to the C-terminus of Plk3 (**Figure 2.2C**). We reasoned that these contradicting results could be due to the higher sensitivity in the genomic PCR

assay, which would be able to detect incorporation of the targeting vector even if it existed only in a small population of cells, while western blotting required expression of the fusion protein at levels comparable to WT. The Plk3-AID-3xFlag fusion protein is expected to have a molecular weight of 82.3kDa. However, no signal was observed at this expected molecular weight when the pools were blotted with a Flag antibody (**Figure 2.2C**). While these experiments to assess the degree of AID-tagging for Plk3 were ongoing, we transfected the pool of single-hit cells originally transfected with sgRNA1a a second time with a targeting vector containing a hygromycin resistance cassette and pX330 expressing sgRNA2. Similar to the first round of transfection, these cells were expanded and were treated with hygromycin to select for in-frame insertion of the targeting vector. After selection, the second-hit pools were harvested and screened for tag incorporation by western blot. We were unable to observe a mass-shifted Plk3-AID-3xFlag using either Plk3 (**Figure 2.2D**) or Flag antibodies (data not shown), and we were unable to properly assess tag incorporation to the endogenous Plk3 locus by genomic PCR (data not shown). Taken together, these results suggested that while the targeting vector was likely being incorporated, at the Plk3 endogenous locus but possibly also elsewhere in the genome, Plk3-AID-3xFlag was not being expressed at detectable levels by western blot relative to wild-type Plk3. As Plk3 has a highly GC rich gene structure, we hypothesized that it is largely inaccessible to Cas9, making gene editing difficult. Since expression of the antibiotic resistance gene is dependent on the transcriptional activity of the target gene, and Plk3 is thought to have low transcriptional activity, it is also possible that clones with in-frame incorporation of the targeting vectors did not produce enough antibiotic resistance and were screened out during the selection step. We reasoned, therefore, that ectopic expression of 3xFlag-AID-Plk3 and knockout of endogenous Plk3 would be an effective strategy to overcome both of these complications.

3xFlag-AID-Plk3 knockout and replace

Given that attempts to incorporate an AID tag to either the N or C terminus of the Plk3 endogenous locus in HeLa or DLD1 cells were unsuccessful, we pursued a knock-out and replace strategy to express 3xFlag-AID-Plk3. This approach relies on expressing an AID-tagged version of the protein of interest, followed by CRISPR-Cas9 mediated knockout of the endogenous gene. While this is an efficient strategy to quickly introduce

high levels of a gene of interest for AID targeted protein degradation experiments, ectopic expression removes native transcriptional regulation of the target protein. In the case of Plk3, this would likely result in cell lines with much higher than physiological expression levels of Plk3 that was no longer under the control of the cell cycle. On the other hand, increasing the expression of a low abundant kinase would likely increase the phosphorylation signaling of Plk3, potentially facilitating the detection and attribution of phosphosites to this kinase.

To ectopically express 3xFlag-AID-Plk3, we created an AAVS1-AID-Plk3 targeting vector to introduce 3xFlag-AID-Plk3 to the AAVS1 safe-harbor locus. Genes of interest can be integrated into safe harbor loci, which are sites in the genome with highly active transcriptional machinery but that do not cause adverse effects to the cell when disrupted (Sadelain et al., 2012). This approach utilizes a CRISPR-Cas9 targeting vector with homology arms designed to integrate a construct into the first intron of AAVS1 flanking a multiple cloning site (MCS) to facilitate insertion of a gene of interest (GOI) for expression (**Figure 2.3A**). The GOI to be expressed is introduced between the homology arms along with a puromycin resistance cassette to select for in-frame insertion. Recombination of the targeting vector ensures that 3xFlag-AID-Plk3 is inserted into the first intron of the AAVS1 locus. A splice acceptor site in the construct ensures that 3xFlag-AID-Plk3 is spliced into the nascent mRNA, while two 2A ribosomal skip sites force cleavage events that result in 3xFlag-AID-Plk3 and a puromycin resistance gene to be expressed as independent proteins (Mali et al., 2013).

After transfection and selection with puromycin, 24 individual clones were isolated and screened for expression of 3xFlag-AID-Plk3 by western blot. When analyzed with an antibody against Plk3, we did not observe the expression of 3xFlag-AID-Plk3 at the expected molecular weight (**Figure 2.3B**). Furthermore, even clones that appeared to have higher expression of Plk3 compared to WT HeLa cells, such as clone 6, did not have a flag positive band that corresponded to the observed Plk3 positive band (**Figure 2.3C**). Although this experiment was repeated, we were ultimately unable to identify clones expressing 3xFlag-AID-Plk3 despite having resistance to puromycin. This could suggest that the construct was integrated into the genome at random and that the clones that were recovered were able to express the puromycin resistance gene but did not have the 3xFlag-AID-Plk3 construct inserted in frame to the AAVS1 locus. It is also possible that the construct was integrated at the correct site and that post-translational mechanisms

maintained a low level of Plk3 in the cell, thus making it difficult to identify overexpression of the Plk3 construct. In any case, this approach was not successful in generating AID-Plk3 cells.

HSV-Thymidine kinase negative selection

A primary concern identified in previous attempts to endogenously tag Plk3, as well as with other kinases, was the propensity for cells to develop resistance to antibiotic selection agents in the absence of in-frame insertion of the targeting vector. This phenomenon was observed frequently in this project and in other projects in the lab, in that it was common to identify clones that were resistant to multiple antibiotics without evidence of incorporation of the targeting vector by western blot. We hypothesized that this was the result of random integration into the genome, most likely through non-homologous end joining (NHEJ), conferring the antibiotic resistance genes to a small percentage of transfected cells. To combat this problem, we designed a strategy to create negative selection pressure for targeting vector incorporation via NHEJ.

This approach utilized a modified CRISPR-Cas9 targeting vector that included *Herpes simplex* virus thymidine kinase (HSV-TK) driven by a CMV promoter on the outside of the homology arms for the target gene (**Figure 2.4**), as well as the antiviral ganciclovir that is normally nontoxic but can be converted to a toxin when phosphorylated by HSV-TK. Incorporation of the targeting vector via HDR would result in loss of the CMV-HSV-TK sequence as it sits downstream of the Plk3 right homology arm. However, integration via NHEJ to a random site in the genome would result in incorporation of the entire targeting vector and CMV-driven expression of HSV-TK, providing a direct method to distinguish between incorporation via HDR and NHEJ. Treatment with ganciclovir should not affect cells with in-frame insertion to the target locus (**Figure 2.4A**), while expression of HSV-TK would result in cell death in cells with off-target NHEJ targeting vector incorporation in the presence of ganciclovir (**Figure 2.4B**).

We modified the N-terminal Plk3 targeting construct to include CMV-HSV-TK transfected this construct into HeLa cells. After allowing time for recovery, cells were treated with blasticidin to select for clones that had incorporated the Plk3 targeting vector. This population of cells were treated with ganciclovir to eliminate colonies that had

incorporated the targeting vector via NHEJ. Finally, individual clones were isolated and screened for expression of 3xFlag-AID-Plk3 by western blot. However, we were unable to identify the expression of tagged Plk3 in any of the 24 clones tested (**Figure 2.4C**). This suggested that the targeting vector was not being integrated to the Plk3 locus, while some clones were still able to acquire resistance to blasticidin, possibly by expressing the blasticidin resistance gene through other means.

Validating Plk3 antibody

After many attempts to endogenously tag Plk3 with an AID tag and to ectopically express 3xFlag-AID-Plk3, an article was published demonstrating that most commercial antibodies raised against Plk3 either do not recognize endogenous Plk3 or recognize an abundant contaminating band at roughly the same molecular weight as Plk3 (Aquino Perez et al., 2020). The authors were able to demonstrate that while the Cell Signaling Technologies (CST) antibody we used in our experiments does recognize Plk3, as confirmed via CRISPR/Cas9 to knock-out endogenous Plk3 and siRNA to knock down of Plk3 in both HeLa and RPE1 cells, this siRNA- and CRISPR/Cas9-responsive band was very faint, and that the primary band at a slightly higher molecular weight detected by the authors was not responsive to Plk3 knockdown.

Based on this report, we tested the specificity of the CST Plk3 antibody in our cell lines using siRNA to knock down Plk3. An siRNA pool from Dharmacon that includes a mix of 4 individual siRNAs was transfected into WT HeLas, 293s, and RPE1s. In all three cell lines, we were unable to identify a Plk3-positive band that decreased to any appreciable extent with RNAi depletion (**Figure 2.5A**). This confirmed that the major Plk3 positive band that we had been ascribing to Plk3 abundance was likely not Plk3 and provided an explanation for our prior challenges in identifying AID-tagged variants of Plk3. This was repeated for two other antibodies, including one raised in-house, with similar results (data not shown). Furthermore, our review of data from an exhaustive proteomic study that relied on massive subfractionation of cell lysates to deeply profile the HeLa proteome and phosphoproteome also failed to detect even a single peptide from Plk3 (Sharma et al., 2014), raising the possibility that it is either not expressed in this context, or that it is expressed at below the limit of detection for the CST Plk3 antibody.

Discussion

The Polo-like kinase family plays diverse roles throughout the cell cycle, ranging from regulating mitotic entry to sensing DNA damage and promoting cell cycle arrest and apoptosis. While the body of literature surrounding Plk1 is extensive, there is relatively little known about Plk2 and Plk3. In large part this is due to a limited availability of tools to study these kinases. For Plk3, there is a growing body of literature over the past 20 years demonstrating the roles of Plk3 in various stress response pathways and in cell cycle regulation, albeit mostly by genetic manipulation or loss-of-function studies. However, recently it was demonstrated that most commercial Plk3 antibodies are unreliable and may recognize epitopes on proteins other than Plk3 (Aquino Perez et al., 2020). This study also directly contradicted most of the literature surrounding the role of Plk3 in responding to cellular stress, and suggested that Plk3 is not necessary for cell stress response pathways as was previously thought (Aquino Perez et al., 2020). To address the confusion surrounding the Plk3 literature, it would be greatly beneficial to develop nonbiased, proteomics-based tools to study the substrates of Plk3 and to determine the major cellular roles and signaling pathways that it regulates.

In this project we aimed to generate 3xFlag-AID-Plk3 cell lines in order to more directly study the Plk3-dependent phosphoproteome. Despite attempting multiple gene editing- and ectopic expression-based approaches, our efforts to create AID-tagged Plk3 cell lines were not successful. It is possible that this is at least in part due to the gene structure of Plk3, which may be less accessible and less amenable to CRISPR-Cas9 gene editing than other genes. Another possibility is that the CRISPR-Cas9 targeting strategy using antibiotic resistance as the mechanism for selection was not the most efficient method. We have since developed other workflows for CRISPR-Cas9 mediated gene editing (described in Chapter 3), through which we have observed that our earlier methods using serial CRISPR-Cas9 transfections and antibiotic selections at the pool level may actually hinder the generation of AID knock-in clones. The CRISPR-Cas9 gene editing workflows presented in this chapter depend on multiple guide RNAs to efficiently cut the target locus and promote HDR with the targeting construct. However, we now have evidence that the efficacy of individual guide RNAs to promote DSBs and HDR is highly

variable, making the reliance on serial transfections with multiple guide RNAs more likely to inhibit homozygous incorporation of the targeting vector rather than promote it.

Another limitation from this study was the availability of Plk3-specific tools. We were unable to validate the ability of the Plk3 antibodies at our disposal to recognize endogenous Plk3 in HeLa cells, although we did observe that it was able to detect purified Plk3 spiked into a WT cell lysate. This greatly complicated the interpretation of results when screening for 3xFlag-AID-Plk3 clones because it was never possible to observe a shift in the molecular weight of Plk3 that would correspond to a knock-in of the targeting vector. However, the fact that we were also unable to observe knock-in of the 3xFlag-AID tag or even expression of 3xFlag-AID-Plk3 from an ectopic locus using a highly sensitive Flag antibody suggests that our inability to generate 3xFlag-AID-Plk3 clones was not due to the lack of specificity of the Plk3 antibody alone and could be related to Plk3 translational or post-translational regulation maintaining low levels of Plk3.

Knowing the potential pitfalls in the Plk3 targeting workflows, it would be interesting to apply more recent CRISPR-Cas9 targeting strategies to create targeted protein degradation cell lines for Plk3. We have found that the workflows outlined in the following chapter of this thesis have been effective to append tags to genes of interest in cases where previous methods were not. It may therefore be possible to redesign the CRISPR-Cas9 targeting strategy to take advantage of these new approaches and endogenously tag Plk3. However, this is ultimately dependent on the extent of Plk3 expression in cultured cells as expression of the selection marker is required to isolate tagged clones.

Moving forward, it would be interesting to apply overexpression studies to interrogate the potential substrates of Plk3. Since Plk3 does not appear to be expressed in our cell lines, it should be possible to generate CMV-driven 3xFlag-AID-Plk3 stable cell lines in a Tir1 background. This could also be coupled with stable proximity labeling Plk3 cell lines to identify the Plk3 interactome. Comparing all of the potential Plk3 interactors to potential Plk3 substrates would be an efficient strategy to shine light onto signaling pathways in which Plk3 is a regulatory component. This does come with the obvious caveat that Plk3 expression seems to be low in HeLa and 293 cells, and over-expressed Plk3 may therefore be orders of magnitude more abundant than physiological expression. Nevertheless, this would provide a comprehensive, non-biased set of substrates and interacting partners that could be used as a starting point for other Plk3 focused studies.

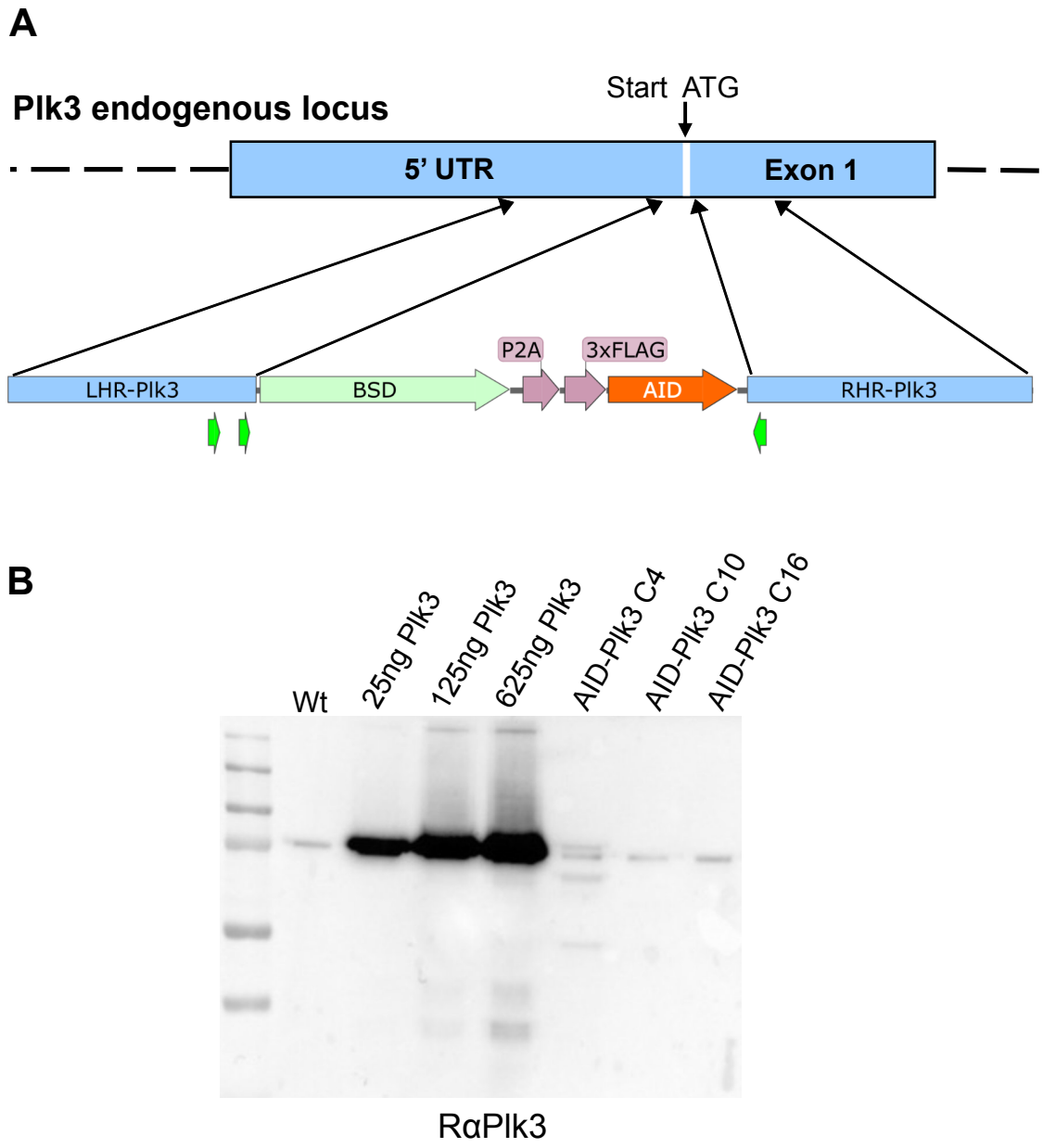

Figure 2.1. CRISPR-Cas9 targeting strategy for Plk3 N-terminus. **A)** The Plk3 N-terminal targeting vector includes 500bp homology regions (LHR and RHR) that are homologous to the Plk3 endogenous locus directly upstream and downstream of the start ATG and can be used as a repair template after induction of DSBs by Cas9. Included in the targeting vector is an antibiotic resistance cassette, conferring resistance to blasticidin in this example, followed by a P2A ribosomal skip site to separate the resistance conferring protein from the rest of Plk3 during translation, and the 3xFlag-AID tag, which are fused to the N-terminus of Plk3. The sequences targeted by guide RNA, which the targeting

vector itself is mutated so that it they will not bind, are depicted as light green arrows. **B)** After two rounds of CRISPR-Cas9 transfection and antibiotic selection, 3 clones were collected and analyzed for knock-in by western blot. To validate that the Plk3 antibody was able to recognize Plk3 and not an off-target protein, we added purified Plk3 to DLD1 cell lysate (25ng, 125ng, or 625ng). While the band in WT DLD1 cells and all three 3xFlag-AID-Plk3 clones runs at the expected molecular weight for Plk3, we did not observe a shifted Plk3 band, indicating that the 3xFlag-AID tag was not incorporated into the Plk3 locus.

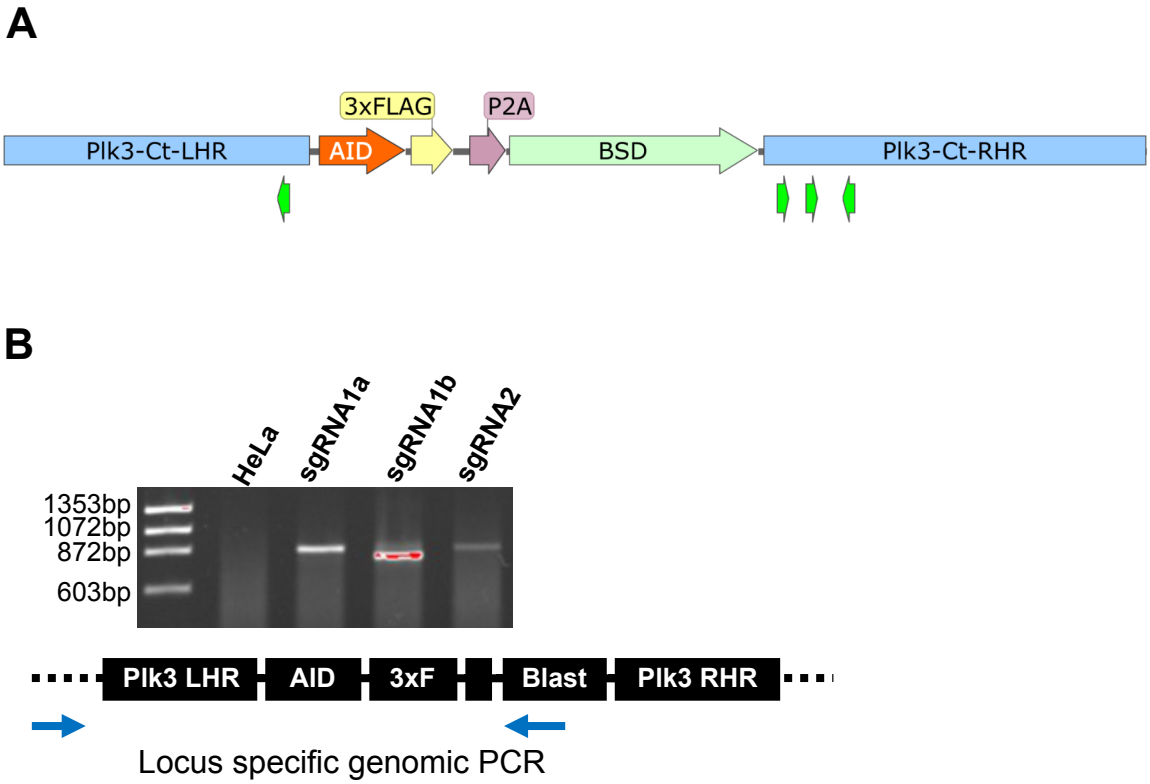

Figure 2.2. Plk3-AID-3xFlag C-terminal CRISPR-Cas9 targeting strategy. **A)** As with the N-terminal CRISPR targeting vector, the C-terminal vector includes the AID-3xFlag tag and an antibiotic resistance cassette, flanked by 500bp sequences homologous to the Plk3 endogenous locus upstream and downstream of the stop codon. The sequences

bound by sgRNAs are highlighted with light green arrows. **B)** After a single round of CRISPR-Cas9 transfection and antibiotic selection, pools were analyzed by genomic PCR to verify incorporation of the targeting vector using a primer pair that recognizes the Plk3 endogenous locus on one end and the targeting vector on the other, ensuring that a PCR product is only produced if the targeting vector is incorporated at the Plk3 locus. This assay was performed on WT HeLas as well as HeLas transfected with the targeting vector and one of three guide RNAs (sgRNA1a, sgRNA1b, sgRNA2). **C)** Pools of single-hit cells were harvested and blotted for Plk3 and Flag to identify a potential Plk3-AID-3xFlag fusion protein. **D)** After a second round of transfection and selection, the second-hit pool of cells were harvested and analyzed for AID-3xFlag incorporation by western blot using an antibody against Plk3.

A

B

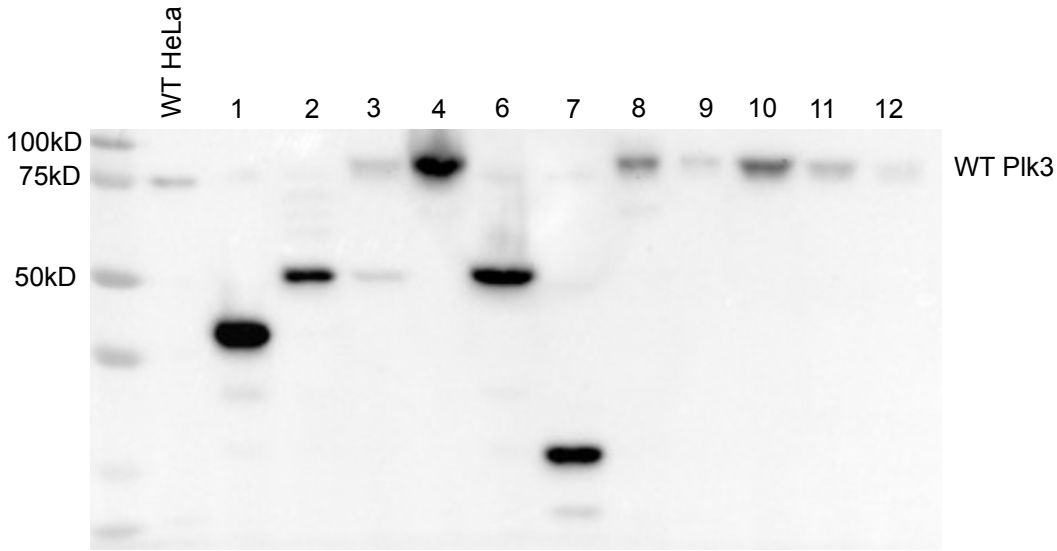

αPlk3

C

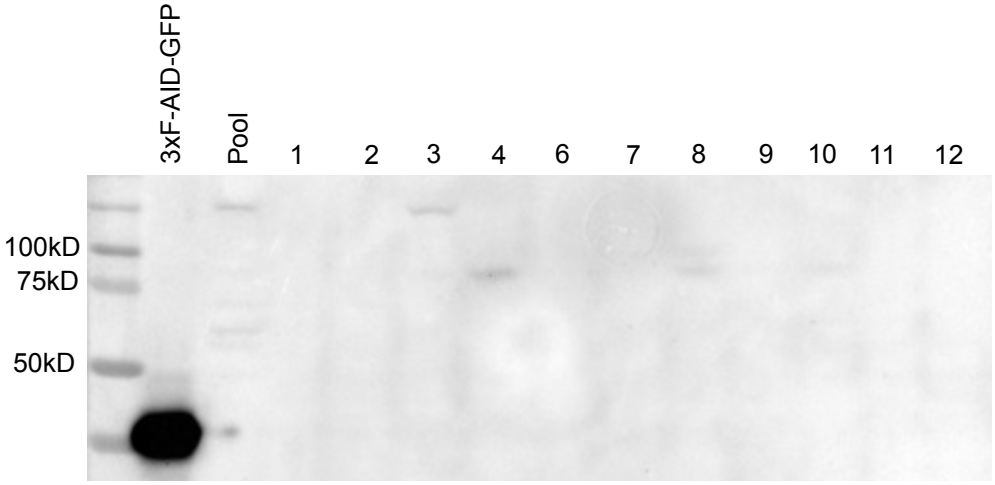

αFlag

Figure 2.3. Knockout and replace strategy to engineer 3xFlag-AID-Plk3 cell lines. **A)** A CRISPR targeting vector was created to introduce 3xFlag-AID-Plk3 to the AAVS1 safe-harbor locus. The homology arms (HA-L and HA-R) are homologous to the endogenous locus and promote homology directed repair after Cas9 induced DSBs. A splice acceptor (SA) sequence ensures that 3xFlag-AID-Plk3 and the puromycin resistance gene (PuroR) are expressed on the same transcript as the first exon of the native AAVS1 locus protein, while the ribosomal skip sites (P2A and T2A) cause cleavage during translation ensuring that all 3 components and translated as separate proteins. HeLa cells were transfected with this targeting construct, selected with puromycin, and isolated for screening by western blot. Clones were blotted for Plk3 (**B**) or Flag (**C**) to identify expression of the 3xFlag-AID-Plk3 protein.

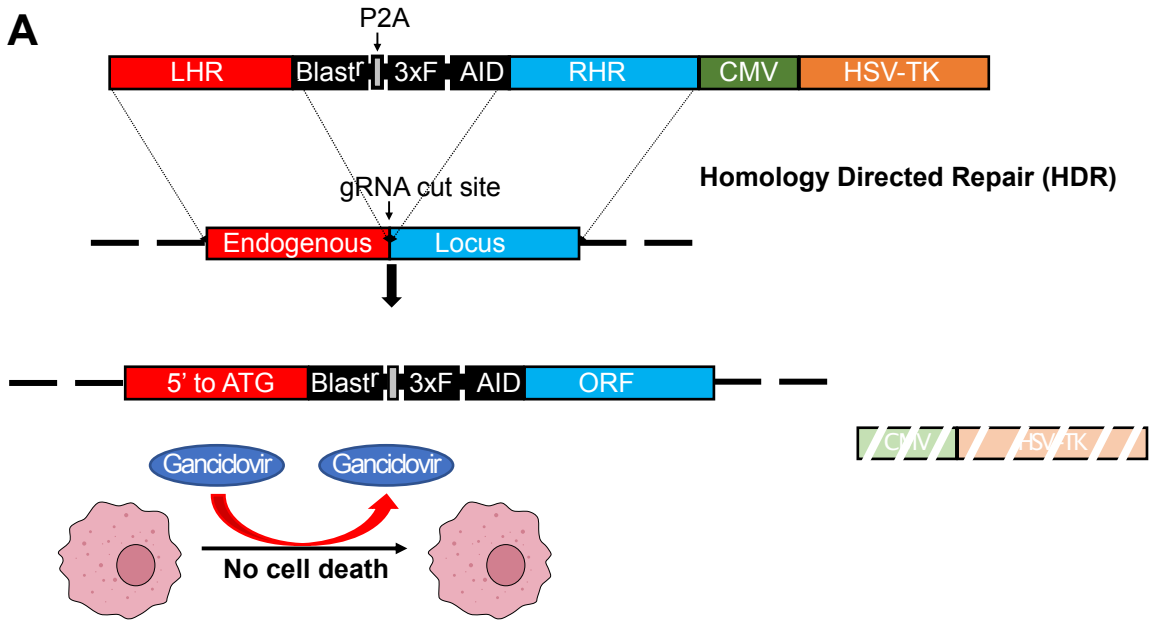
A
P2A
LHR
Blastr
3xF
AID
RHR
CMV
HSV-TK
gRNA cut site
Homology Directed Repair (HDR)
Endogenous
Locus
5' to ATG
Blastr
3xF
AID
ORF
CMV
HSV-TK
Ganciclovir
Ganciclovir
No cell death

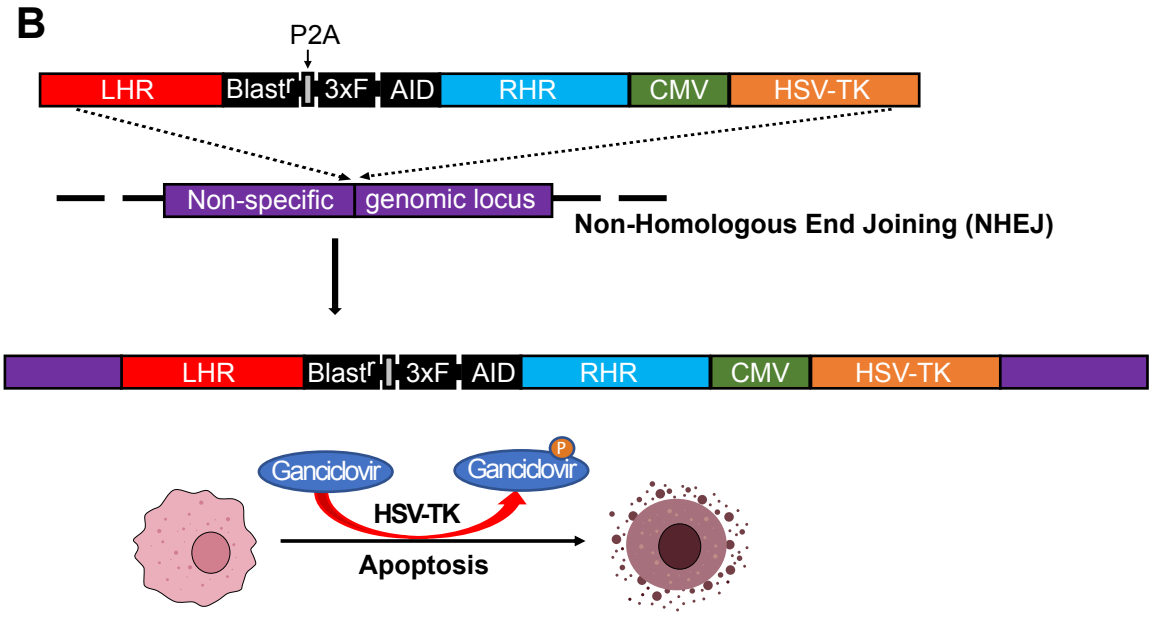
B
P2A
LHR
Blastr
3xF
AID
RHR
CMV
HSV-TK
Non-specific
genomic locus
Non-Homologous End Joining (NHEJ)
LHR
Blastr
3xF
AID
RHR
CMV
HSV-TK
Ganciclovir
Ganciclovir
P
HSV-TK
Apoptosis

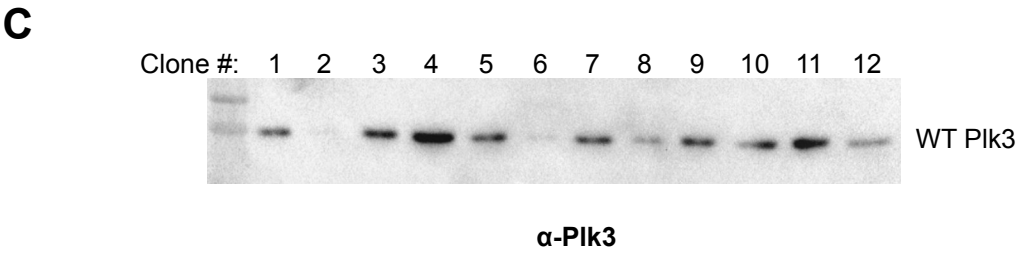
C
Clone #: 1 2 3 4 5 6 7 8 9 10 11 12
WT Plk3
α-Plk3

Figure 2.4. Negative selection of CRISPR targeting vector by NHEJ using CMV-HSV-TK and ganciclovir. **A)** The Plk3 N-terminal targeting vector (outlined in Figure 2.1) was modified to include a CMV promoter followed by *Herpes simplex* virus thymidine kinase (HSV-TK). When the targeting vector is incorporated to the Plk3 locus via HDR, the CMV-HSV-TK sequence is lost as it is downstream of the homology arms that are needed for recombination. Ganciclovir treatment of cells that have incorporated the targeting vector via HDR will not affect cell health as it is natively non-toxic. **B)** Incorporation of the targeting vector via NHEJ results in integration of CMV-HSV-TK along with the rest of the targeting vector, allowing for expression of HSV-TK. Ganciclovir is phosphorylated by HSV-TK and converted into a toxic form, resulting in apoptosis. **C)** Individual clones were isolated, expanded, and screened by western blot using an antibody detecting Plk3 to identify expression of 3xFlag-AID-Plk3.

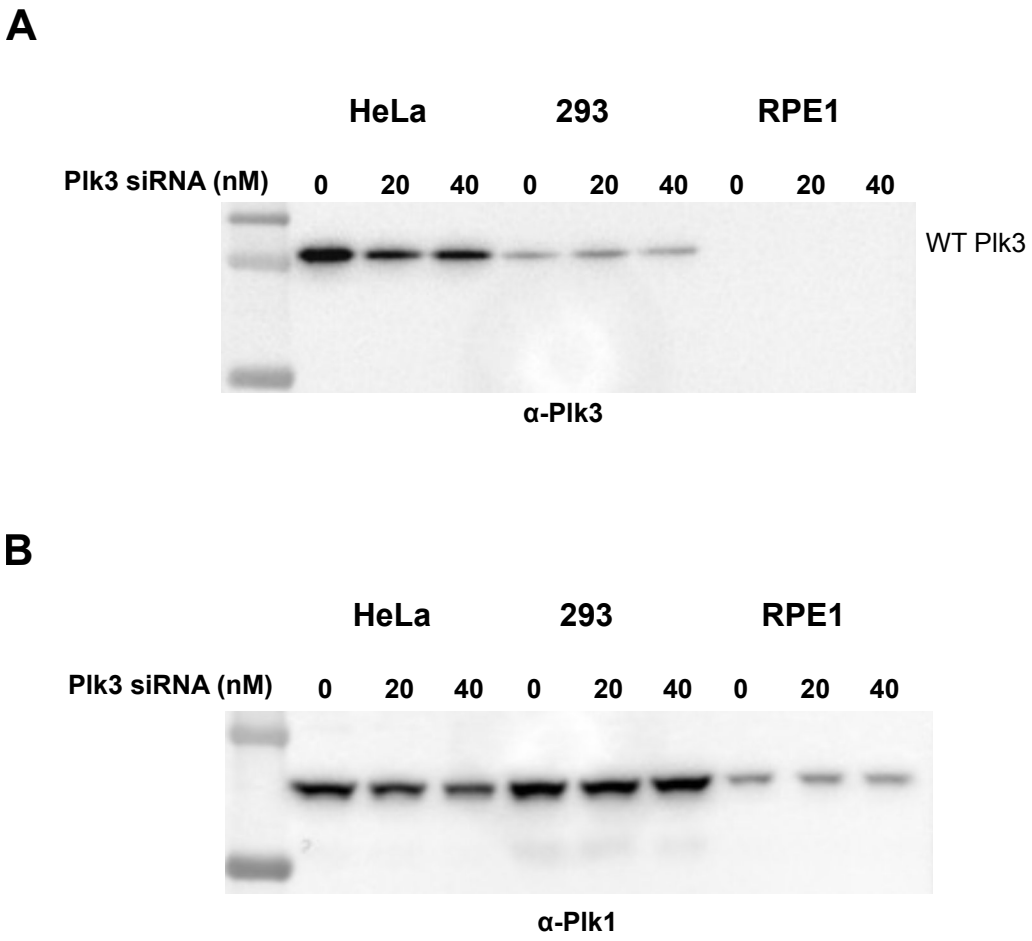

Figure 2.5. Validation of Plk3 antibody using siRNA knockdown. **A)** HeLa, 293, and RPE1 cells were transfected with a mix of 4 siRNA at the indicated concentrations for 48hrs before harvesting and western blotting for Plk3 using the cell signaling technologies (CST) antibody at a 1:500 dilution. **B)** A CST antibody against Plk1 was used as a loading control.

Chapter 3

Improving efficiency of AID-Tir1 CRISPR cell line generation with fluorescent reporter proteins and FACS

Author Contributions:

C. Lincoln Howarth: Wrote text and designed figures for chapter 3. Designed, executed, and analyzed experiments.

Scott A. Gerber: Conceptualized, designed, and analyzed experiments. Provided feedback and edits on text.

Introduction

Targeted protein degradation (TPD) refers to a family of technologies that aim to acutely deplete a protein of interest (POI), typically by encouraging an interaction between the POI and an E3 ubiquitin ligase (Prozzillo et al., 2020; Wu et al., 2020; Aisha Yesbolatova et al., 2019). There are a number of technologies available for this approach including small molecule proteolysis targeting chimeras (PROTACs), the degradation tag (dTAG) system, or Halo-PROTAC (Natsume & Kanemaki, 2017), to name a few, but the one that balances small tag size with rapid kinetics and general applicability is the Auxin-Inducible Degron (AID)-Tir1 system (Aisha Yesbolatova et al., 2019).

AID-Tir1 is a technology that uses proteins or protein sequences adapted from the auxin-responsive machinery in plants (Natsume et al., 2016; Nishimura et al., 2009). In certain plant species, such as the rice *Oryza sativa*, auxin facilitates the interaction between an IAA/Aux protein and the F-box protein Tir1, leading to ubiquitination and degradation of the IAA/Aux protein (Dharmasiri et al., 2005; Kepinski & Leyser, 2005; Tan et al., 2007). Typically, degradation of the IAA/Aux protein activates one or more auxin response factors (ARF), a family of transcription factors that are inhibited by the IAA/Aux protein; this mechanism defines how auxin signaling is translated into a change in a transcriptional program in plant cells (Kepinski, 2007; Leyser, 2018; Tan et al., 2007).

The AID-Tir1 system has been adapted to work in mammalian cells via the ectopic expression of Tir1, which can interface with mammalian Skp1-Cullin-F-box (SCF) E3 ligase machinery, as well as the introduction of an AID tag, a minimal fragment of an IAA/Aux protein that contains the degron sequence, to a gene of interest at its endogenous locus using modern genome editing techniques (Natsume et al., 2016). We previously demonstrated that, when applied to kinases and coupled with quantitative proteomics methods, this approach can be analogous to the use of a kinase inhibitor to uncover novel substrates (Hards et al., 2021), but with the added benefit of ideal chemogenetic selectivity and specificity. In this scheme, protein kinases marked with the AID-tag are selectively degraded to turn off kinase activity upon addition of auxin, resulting in a decrease in the phospho-occupancy of their phosphorylated substrates which can be monitored by mass spectrometry-based proteomics.

One key observation stemming from the development of targeted protein degradation as a means to identify kinase-substrate relationships was the importance of degradation kinetics in order to mimic acute drug inhibition. We found that for a fast-degrading clone (**Figure 3.1A**, $T_{1/2}$= 8mins), significantly downregulated phosphopeptides exhibited a strong correlation with inhibition using the selective Plk1 inhibitor BI2536. However, a slow-degrading clone (**Figure 3.1B**, $T_{1/2}$= 31mins) demonstrated a poorer correlation with chemical inhibition, with lower overall reduction in phosphosite occupancies and reduced capacity to distinguish candidate substrates from technical and biological noise. This highlights the need for fast degradation kinetics in order to accurately identify candidate substrates of a kinase of interest. Interestingly, cycloheximide chase experiments determined that the fast-degrading clone exhibited much faster overall rates of protein turnover, suggesting that degradation kinetics and the total extent of degradation may be intrinsic to specific clones or sub-populations of cells.

While AID-Tir1 is a viable option for studying kinase-substrate relationships by selectively depleting a kinase of interest, its heavy reliance on genome editing to generate endogenous AID-tagged kinases presented a number of issues that we identified in our initial experiments. First, it takes a considerable amount of time to generate AID-Tir1 knock-in cell lines. Typically, multiple rounds of CRISPR-Cas9 gene editing and antibiotic selection were required before screening out clones for knock-in by genomic PCR and western blotting, a work-intensive approach that could sometimes take multiple months to isolate homozygously tagged AID-Tir1 clones. Second, even after ectopically expressing Tir1 in homozygous AID clones, many cells were unable to degrade the AID-kinase at all, while others did not fully degrade or were too slow to be comparable to chemical inhibition. Finally, an issue known to affect the AID-Tir1 system, called auxin-independent degradation, in which some cells are able to degrade an AID-tagged protein in the absence of auxin, can contribute to knock-in failure by premature loss of essential kinases during Tir1 introduction.

Several recent publications have provided additional strategies to alleviate one or more of these problems. For example, an alternative degron/F-box protein combination with AFB2/atIAA7 has been proposed (Li et al., 2019), as well as a bump-in-hole strategy for AID-Tir1 termed “AID2” (Yesbolatova, Saito, Kitamoto, et al., 2020), which exploits a mutant Tir1 protein (Tir1 F74G, hereafter referred to as $Tir1^{Mut}$) and a synthetically altered auxin molecule (5-phenyl-indole-3-acetic acid). Both of these strategies have been

reported to eliminate auxin-independent degradation. Because the kinetics and dynamic range are slightly different for all three degron/F-box pairs, we incorporated and tested all of them to determine which was the most consistently efficient system in our hands. Improvements in all of these areas would greatly decrease the workload associated with making AID-Tir1 cell lines, improve the likelihood of recovering homozygous and degrading clones, and in turn allow us to expand our repertoire of targeted kinases.

To address these gaps in capability and throughput, we hypothesized that we could use fluorescent reporter proteins, along with fluorescence-activated cell sorting (FACS), to create a population of degrading cells to use as a starting point for CRISPR-Cas9 experiments and improve the rate and quality of AID knock-in cells.

Methods

Cell culture and cell lines

HeLa and HEK293 cells were grown in Dulbecco's Modification of Eagle's Medium (DMEM, Corning) supplemented with 8% fetal bovine serum (FBS, Hyclone) and 1% penicillin-streptomycin (100IU/mL penicillin and 100µg/mL streptomycin, Corning). Cells were incubated at 37C with 5% CO_2.

HeLa and HEK293 cells were used as a model system because they are amenable to CRISPR-Cas9 gene editing and protein expression by transient transfection of expression vectors. In addition, they are amenable to analysis and sorting by FACS.

Fluorescence-activated cell sorting

Cells to be analyzed were collected by trypsinization, washed once with PBS (Corning), and resuspended in 2mL PBS in 15mL conical tubes where they were kept on ice until sorting. Analysis and collection were performed on a Sony SH800S cell sorter using a 100µm microfluidic sorting chip. Cells were initially gated on forward scatter (FSC) and back scatter (BSC) to ensure a homogenous population of cells. Untransfected controls were used to establish baseline fluorescence and set up gates for collection. Cells were collected to using the ultra-purity collection mode.

CRISPR-Cas9 homologous recombination clone generation

AID-Plk1 CRISPR targeting constructs were described previously (Hards et al., 2021). Briefly, Plk1 homology arms were designed based on the genomic sequence from UCSC genome browser upstream and downstream of the start codon. Targeting vector components were designed and ordered as g-blocks (IDT) and assembled into pBluescript. Fluorescent reporter versions of the Plk1 CRISPR targeting construct were designed by excising the antibiotic resistance cassette and swapping in EGFP.

For transfection, cells were plated to 6-well dishes at ~50% confluency in media free of penicillin/streptomycin. 1.4µg of targeting vector was linearized *in vitro* with restriction enzymes external to the homology arms. The digested targeting vector was mixed with 0.4µg of pX330 in Jetprime and Jetprime transfection buffer (Polyplus) and incubated at room temperature for 10 minutes as per manufacturer protocol. The transfection mix was added dropwise to each well and incubated overnight. After 16hrs of incubation, the media was washed off and exchanged for media containing penicillin/streptomycin and the cells were left to grow for another day. Cells were expanded to 10cm dishes on the third day and either selected with blasticidin (10µg/mL) or collected for FACS analysis. For antibiotic selected cells, media was exchanged for fresh media containing antibiotic every two days for two weeks or until colonies visible to the naked eye had formed. Individual colonies were isolated by incubation in trypsin diluted 1:40 in PBS and then manually harvested under a 10x screening microscope and transferred to a 96-well plate. Colonies were expanded to the 24-well stage and then harvested for analysis by western blotting.

Cells transfected with fluorescent reporter CRISPR targeting constructs were harvested and analyzed by FACS. Collection gates were determined by comparing GFP intensity in transfected to untransfected controls and cells with the highest GFP intensity were collected to 96-well dishes. Clones were given time to grow into colonies (~2 weeks) before expansion up to the 24-well stage and harvesting for analysis of tag knock-in rate by western blot.

Generating AAVS1-Tir1-BFP degrading cells

The AAVS1-Tir1 CRISPR targeting construct to introduce ectopic Tir1 to the AAVS1 safe harbor locus has been described previously (Hards et al., 2021). This targeting construct was modified to include a mTagBFP2 sequence (AddGene) fused to the C-terminal end of Tir1. 1.4µg of the AAVS1 targeting vector was linearized *in vitro* and was transfected along with 0.4µg of pX330 containing an sgRNA targeting the AAVS1 locus into HeLa cells as described above. After recovery from transfection, cells were expanded to 10cm dishes and treated with 10µg/mL puromycin until colonies visible to the naked eye formed (up to 2 weeks) with fresh media containing puromycin exchanged

every 2 days. Selected cells were harvested and collected for analysis by FACS (described below) and collected based on BFP expression (Tir1-BFP cells herein).

To generate the degradation reporter construct, 3xFlag-AID-EGFP-P2A-mCherry was ordered as a g-block (IDT) and cloned into a CMV-driven promoter. Tir1-BFP cells were plated to 50% confluency in 6-well dishes and transfected with 1µg of the 3xF-AID-GFP-P2A-mCherry reporter using JetPrime (Polyplus) as described above. The day after transfection (day 2) cells were expanded to 10cm dishes and on the third day, they treated +/- auxin for 1hr and harvested for analysis and collection by FACS. Untransfected Tir1-BFP cells were used to establish baseline GFP and mCherry signal intensities. Cells were gated on FSC and BSC to ensure a homogenous population in terms of size and health and then on BFP to ensure Tir1-BFP expression. Finally, gates for collection were determined by comparing the GFP:mCherry ratio in +auxin to -auxin, drawing gates around populations of interest (i.e. cells that did or did not respond to auxin treatment) and sorting into 6 well dishes.

Western Blotting

Cells to be analyzed by western blot were collected, washed once in PBS, and lysed in 2x Lamelli. Poly-acrylamide gels were poured in house from a 30% acrylamide solution (Protogel, National Diagnostics). Gels were run at 140V for 80 minutes in running buffer containing 25mM Tris, 200mM glycine, and 1% SDS. The gels were then transferred to nitrocellulose blotting membrane (Amersham Protran) at 100V for 60 minutes in a transfer buffer containing 25mM Tris, 200mM glycine, and 20% MeOH. To account for loading, blots were briefly stained with ponceau (0.01% ponceau, 0.5% acetic acid) and imaged. Blots were washed in TBST (50mM Tris, 150mM NaCl, 0.2% Tween-20) before blocking for 30 minutes in a solution of 4% milk in TBST and overnight incubation with primary antibody in 4% milk in TBST. Finally, blots were incubated with an HRP-conjugated secondary antibody for 1hr at room temperature, treated with Clarity ECL substrate (BioRad) and imaged.

Results

Creating a parental population of fast-degrading, Tir1-expressing cells for subsequent POI-specific AID-tagging

Our initial workflow for generating AID-Tir1 degrading clones relied on first identifying a homozygous knock-in AID-kinase clone and then using CRISPR-Cas9 to introduce Tir1 to the AAVS1 safe-harbor locus for ectopic expression. Through many iterations of this process, we observed that the kinetics of auxin-induced degradation were largely dependent on the specific AID-kinase knock-in clone, and all degraders from one genomic background appeared to degrade the kinase with similar kinetics and efficiency upon addition of auxin. Therefore, we sought to generate a pool of Tir1 cells that were previously verified for optimal degradation performance prior to CRISPR-Cas9 knock-in of the AID tag, thereby saving time and alleviating the issue of having a limited number of genomic backgrounds.

To create a homozygous population of Tir1-expressing cells, we used CRISPR-Cas9 to introduce Tir1-BFP fusion gene, separated from a puromycin resistance cassette with a ribosomal skip sequence (T2A), to the AAVS1 safe-harbor locus for high, ectopic expression (**Figure 3.2A**). Previously, we used puromycin as the primary selection agent for Tir1 incorporation and expression, but we observed that about 50% of clones recovered from this process did not express Tir1 despite having the antibiotic resistance marker (data not shown). Adding an mTagBFP2 tag (BFP for simplicity) to Tir1 enabled the dual isolation of Tir1-expressing cells via antibiotic selection followed by FACS. With this approach, we collected homogenous populations of cells that were verified to express high levels of Tir1.

To monitor degradation at the level of individual cells, we created a dual-fluorescent reporter. This construct includes a 3xF-AID-GFP sequence, followed by a ribosomal skip site (P2A), and finally the red fluorescent protein mCherry (**Figure 3.2B**). Separating GFP from mCherry by P2A ensures that they would be expressed from the same mRNA transcript and thus at similar levels within a cell. As GFP is linked to an AID tag while mCherry is not, the extent of degradation on an individual cell basis can be monitored by screening the ratio of GFP to mCherry using flow cytometry. This construct can be transfected into the parental population of Tir1-BFP cells, followed by treatment

with auxin for various lengths of time to select for increasingly fast degraders (**Figure 3.2C**). Finally, cells could be sorted into populations of degraders or non-degraders based on the depletion of GFP with respect to mCherry in each cell.

This approach was applied to a population of cells expressing $Tir1^{WT}$-BFP, as well as to $Tir1^{Mut}$-BFP, the F-box protein for the AID2 system (Yesbolatova, Saito, Kitamoto, et al., 2020). Cells expressing 3xF-AID-GFP-P2A-mCherry mostly displayed a GFP and mCherry signal on a linear axis in the absence of auxin (**Figure 3.3A**, top left panel). However, there are many $Tir1^{WT}$-BFP cells that have a decreased GFP signal with respect to mCherry prior to addition of auxin, which is indicative of the auxin-independent phenomenon. In the $Tir1^{Mut}$-BFP pool, all cells express GFP and mCherry along the one-to-one axis and there is no noticeable auxin-independent degradation (**Figure 3.3A**, bottom left panel). The addition of auxin for one hour to these populations of cells resulted in a clear decrease in the GFP:mCherry ratio, which is indicative of GFP degradation (**Figure 3.3A**, middle panels, gates 1A). In both cases, however, there is a still a large population of cells that is not able to appreciably degrade GFP despite having been previously puromycin selected and flow sorted for Tir1-BFP (**Figure 3.3A**, middle panels, gates 1B). From this experiment, we collected the populations of degraders (1A) and non-degraders (1B) for further studies.

The population of Tir1-BFP degraders (1A) were further gated into groups of “fast degraders” (2A) or “slow degraders” (2B) based on the extent to which they were able to degrade GFP in the one-hour treatment (**Figure 3.3A**, right panels, 2A and 2B, respectively). The fast-degrader populations were then taken as the starting point for AID tagging experiments. Both degrading populations of cells were cultured for sufficient time to allow for loss of the transiently transfected 3xF-AID-GFP-P2A-mCherry vector before being re-transfected and re-analyzed for auxin dependent turnover rates as was done before. When the experiment was repeated on these groups of cells, we observed that the population of previously sorted “fast degraders” were able to deplete GFP to a greater extent than the population of previously sorted “slow degraders” (**Figure 3.3B**). This can be seen by the percentage of cells that fall within the degraders gate in the respective populations. Furthermore, a histogram of the GFP signal for cells within the degrader gate demonstrates the lower average GFP signal for the fast degrader population compared to the slow degrader population (**Figure 3.3C**). Finally, it was found that when non-degrader cells collected in the previous experiment were re-transfected and tested for ability to

degrade, they were unable to deplete GFP signal (data not shown). Overall, these sets of experiments demonstrate that there is something intrinsic to these populations of Tir1-BFP cells that determines whether or not they are able to degrade AID-tagged proteins and, if so, the rate and/or extent to which that occurs.

Improving the rate of homozygous AID tag insertion

Many cell lines used in cell biology labs are derived from cancer cells which are known to be aneuploid (Nicholson & Cimini, 2013). This has been demonstrated for HeLa (Landry et al., 2013) and HEK293 cells (Lin et al., 2014), both of which are frequently used in biochemistry and cell biology labs, and are our cell lines of choice for AID-Tir1 experiments. Unfortunately, these cell lines are pseudotriploid with 3 or more copies of many chromosomes and/or chromosomal regions, necessitating the use of more than two rounds of CRISPR-Cas9 transfection to introduce tags to each locus. In our previous AID-Tir1 tagging workflow, we employed three rounds of CRISPR-Cas9 transfection with gRNAs and antibiotic selection markers unique to each round of genome editing (**Figure 3.4A**), working on the assumption that homologous recombination events leading to single tag insertion were rare, much less achieving homozygous insertion at three or more individual chromosomes. This was supported by empirical observations that ~99.9% of cells died during antibiotic selection, suggesting that the rate of tag incorporation was low. However, it turns out that it is possible for recombination to occur at all targeted loci within a single cell, yielding a homozygous knock-in after one round of CRISPR-Cas9 transfection (**Figure 3.4B**, lane 7). In this experiment, clones were screened out after a single round of CRISPR-Cas9 transfection and antibiotic selection and, while half of the isolated clones show little to no tag insertion, demonstrating the problem of using antibiotic selection, clone 7 was a homozygous AID knock-in, challenging our previous assumptions about the frequency of tag insertion.

Based on these experimental results, we hypothesized that an alternative selection method might improve the rate of recovering homozygous AID clones. Fluorescent reporter proteins are an attractive option because they provide a means to more quantitatively assess the extent of tag insertion, as cells with greater fluorescence intensity would be more likely to be homozygous knock-ins. Furthermore, this approach also allows for immediate cell sorting to 96-well plates within days of the CRISPR-Cas9 transfection,

eliminating the need to grow individual colonies on a dish and hand-pick them (**Figure 3.5A**).

As a proof of concept, we adapted existing N-terminal Plk1 targeting vectors by swapping out the antibiotic resistance cassette for EGFP (**Figure 3.5A**). HeLa and 293 cells were transfected with this targeting vector, along with a plasmid expressing Cas9 and a guide RNA targeting the Plk1 endogenous locus. After allowing cells to remain in transfection reagents for 24 hours prior to wash out, the cells were allowed an additional day to recover before expansion to a 10cm dish. After an additional 24 hours of recovery time, cells were then sorted and analyzed (**Figure 3.5B**). In this experiment, a small but quantifiable increase in GFP fluorescence was observed for cells transfected with the EGFP targeting vector, demonstrating the ability to use the fluorescent reporter as a marker for homologous recombination. Gates were set using the control samples to establish baseline GFP signal and the cells with the highest GFP signal were sorted into 96-well dishes, expanded to 24-well dish stage, and screened by western blot (**Figure 3.5C**). Remarkably, of the 24 HeLa clones screened, 12 were apparently homozygous knock-ins based on western blot from this single round of genome editing (**Figure 3.5C**). Although most of the homozygous knock-ins appear to have a small amount of signal at the WT Plk1 molecular weight, based on subsequent experiments it is likely that this was a result of inadvertent cleavage of the 3x-FLAG-AID tag, and not an untagged allele. These initial results were encouraging evidence that we could use fluorescent reporters as our selection marker of choice for all future AID tagging experiments.

Discussion

AID-Tir1 targeted protein degradation is an effective strategy to acutely deplete proteins of interest and assess corresponding changes to the proteome and phosphoproteome. However, an important caveat with this approach is that generating homozygous knock-in AID-Tir1 cell lines for proteins of interest is not trivial and requires a considerable time investment for a given target. Here, we established new methods to generate a parental line of degrading Tir1 cells to be used as a starting point for AID tagging and to rapidly identify homozygous AID knock-ins after a single round of CRISPR-Cas9 transfection. These two approaches can be combined, allowing for the generation of degrading AID-Tir1 clones in as little as 1 month. This workflow has greatly improved the speed at which we are able to create AID-Tir1 clones for kinases of interest and allowed us to expand the number of kinases to survey in our experiments.

Since developing this workflow, we have applied it to endogenously tag multiple kinases of interest, including Plk2, Nek6, Nek7, Nek9, PAK1, Aurora A and Aurora B, as well as some phosphatases. Reducing the number of rounds CRISPR-Cas9 transfection and selection from 3 to 1 and sorting directly into 96-well dishes has demonstrable benefits to the rate of cell line generation as well as the bandwidth for targeting multiple genes. Importantly, this has also allowed us to execute experiments more quickly and to rapidly test various aspects of AID tagging, such as different versions of the AID tag, different linkers in the targeting vector, and the effects of guide RNAs on homology directed repair and tag insertion. Interestingly, we have routinely found that the choice of guide RNA makes a big impact in the efficiency of tag incorporation, as some guides lead to a high rate of homozygous knock-ins and others do not, despite targeting regions that are within or very close to protein coding regions of the target gene, and thus very close to one another. Despite this, our success rate when targeting genes of interest remains high and finding guide RNAs that efficiently promote homology-directed repair has not been a limiting factor. Because the fluorescent reporter-based sorting approach outlined in this chapter only needs a single guide RNA to work efficiently, as compared to at least three for the antibiotic selection method used previously, it increases the chances of finding guides that promote homology directed repair and tag insertion. Antibiotic selection, on the other hand, requires that all guides work to some extent and if a single guide is not

efficient, it greatly diminishes the chances of identifying homozygous AID knock-in clones. This observation is slightly paradoxical in that we would expect multiple rounds of CRISPR-Cas9 to be better for creating homozygous knock-ins than only a single round because there are more selection pressures for tag insertion with multiple rounds. In practice, relying on tagging experiments using a single guide RNA and 1 round of CRISPR-Cas9 transfection is not only a more time efficient strategy to create homozygous knock-ins, but a more faithful one.

One of the main problems that we have come across in the implementation of this workflow is spectral bleed-through from one fluorescence channel to another. Tir1-BFP, for example, is expressed at high enough levels that BFP is detectable in the GFP channel, making it difficult to use a GFP reporter on the targeting vector when inserting the AID tag into the Tir1-BFP parental line. We have found that using pairs of fluorescent proteins with excitation/emission spectra sufficiently far apart alleviates this problem and we routinely use red-shifted fluorescent reporters, such as mRuby3, when introducing AID tags into Tir1-BFP lines. However, this requirement for spectral separation of reporter pairs makes it difficult to use multiple fluorescent reporters in a single cell line if more than one round of CRISPR-Cas9 transfection is required. Nevertheless, in all of the genes that we have targeted thus far, we have not found multiple rounds of transfection and selection to be necessary. In the future, it might be possible to adjust the use of fluorescent tags to introduce the furthest red-shifted fluorescent protein first and move up the spectrum towards green and blue wavelengths with successive rounds of transfection. This may help to prevent some of the problems with spectral bleed-through given the asymmetrical nature of emission spectra for most fluorophores.

In future projects, this workflow could be applied to implement multiple, orthogonal protein degradation strategies in the same cell. For example, it should be possible to combine AID-Tir1 with a system such as the dTAG system (Nabet et al., 2020; Nabet et al., 2018), which requires addition of a degron tag to a protein of interest but does not rely on a E3 ligase adaptor protein. Two technologies like this could be combined in a single cell line to target two closely related kinases, such as Nek6 and Nek7 for example, allowing the experimenter to observe the effects of depleting either or both proteins at the same time.

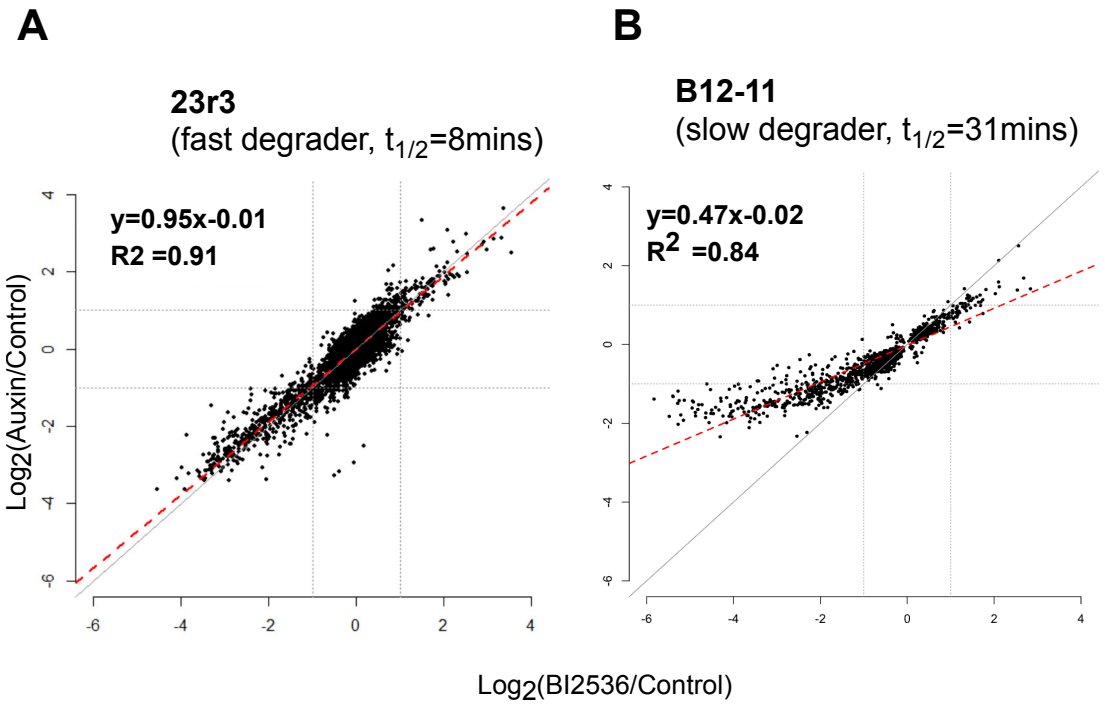

Figure 3.1. AID-Tir1 degradation kinetics are essential for mimicking small molecule inhibition. **A)** Correlation plot from a fast-degrading AID-Plk1 clone, 23R3, comparing the change in phosphopeptide abundance with Plk1 inhibition by the selective Plk1 inhibitor BI2536 (x-axis) to Plk1 degradation (y-axis) for phosphopeptides with p-value < 0.1. This plot highlights that, for an AID clone with fast kinetics ($t_{1/2}$= 8mins), the change in phosphopeptide abundance is tightly correlated for Plk1 dependent phosphopeptides with Plk1 inhibition or degradation. **B)** Correlation plot for a slow-degrading AID-Plk1 clone, B12-11, of change in abundance of phosphopeptides in degradation vs. inhibition conditions. While there is still a strong correlation between the two conditions (R^2=0.84), the slope of the regression is 0.47x, demonstrating that Plk1 regulated sites change in abundance 2x more with BI2536 vs. Plk1 degradation. Together, these plots highlight the importance of degradation kinetics in order to approximate the effects of drug inhibition. Figure adapted from Hards et al. 2021 and reprinted with permission.

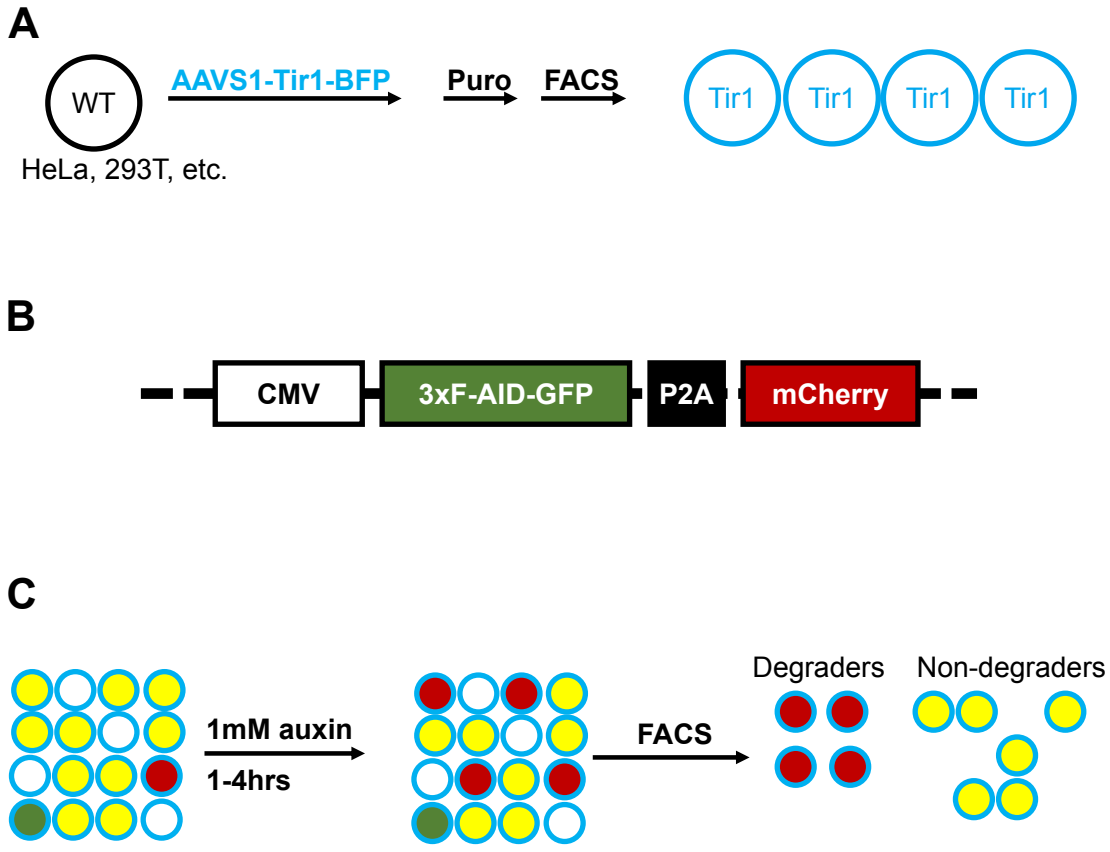

Figure 3.2: Model to generate and validate degrading a Tir1-BFP parental cell line. **A)** An AAVS1 targeting vector carrying Tir1-BFP and a puromycin resistance cassette is transfected into WT cells along with a pX330 vector expressing Cas9 and a guide RNA against the AAVS1 locus. Constructs can be inserted to the AAVS1 locus for high ectopic expression. Transfected cells are selected for in-frame insertion with puromycin selection and finally Tir1-BFP expressing cells are selected using fluorescence assisted cell sorting (FACS). The combination of puromycin selection followed by cell sorting helps to ensure a strong enrichment for Tir1 expressing cells in the collected population. **B)** We designed a construct expressing 3xF-AID-GFP and mCherry. The P2A ribosomal skip site ensures that both fluorescent proteins are expressed separately but off of the same mRNA transcript, ensuring roughly equal expression levels. The 3xF-AID-GFP can be used to assess degradation in each cell while mCherry controls for expression. The combination of the two fluorescent reporters allows for the GFP:mCherry fluorescent ratio to be analyzed in individual cells, making it possible to measure degradation efficiency on a cell-by-cell basis. **C)** The reporter construct can be transfected into Tir1-BFP cells (yellow

indicates expression of both fluorescent proteins, green is GFP only, red is mCherry only). These cells can be treated with auxin for various lengths of time to induce degradation of GFP. Cells can be gated and sorted into groups using FACS based on the change in GFP:mCherry ratio after auxin.

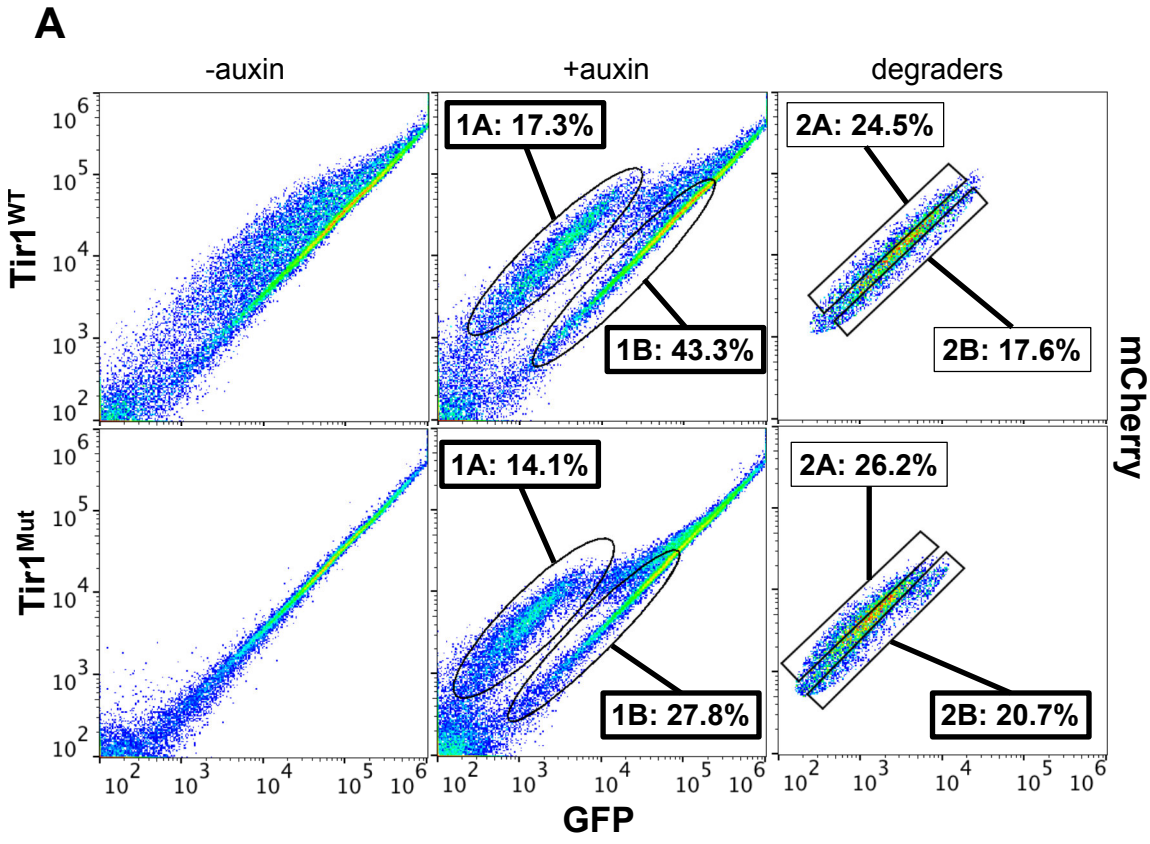
A
-auxin
+auxin
degraders
Tir1WT
Tir1Mut
1A: 17.3%
1B: 43.3%
2A: 24.5%
2B: 17.6%
1A: 14.1%
1B: 27.8%
2A: 26.2%
2B: 20.7%
mCherry
GFP

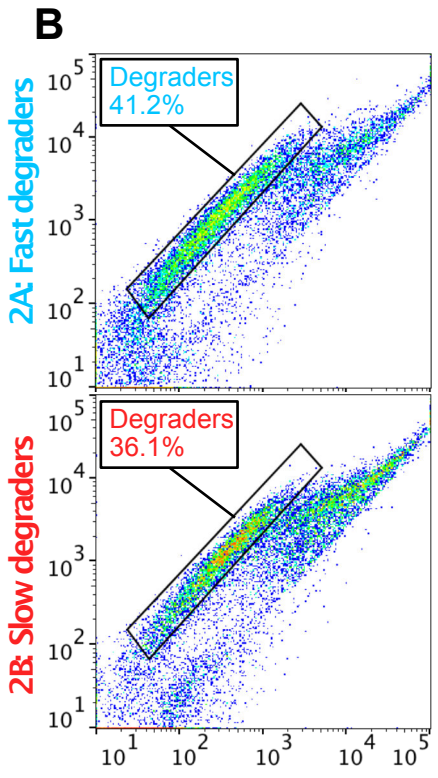
B
2A: Fast degraders
2B: Slow degraders
Degraders
41.2%
Degraders
36.1%

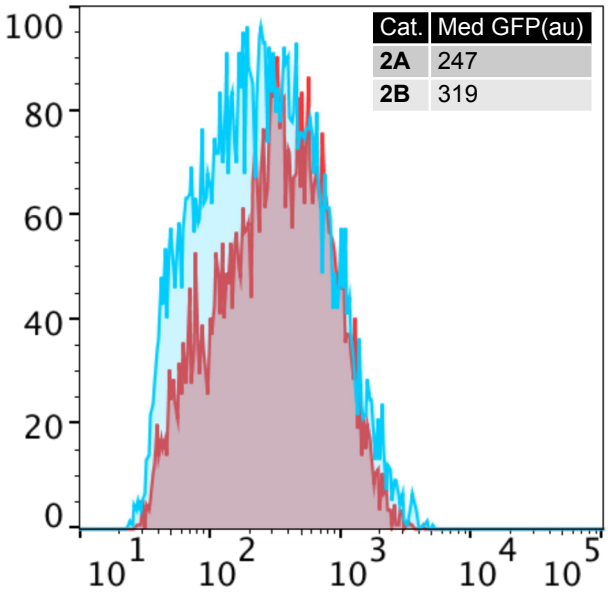
C
Cat.
Med GFP(au)
2A
247
2B
319

Figure 3.3. Sorting out degrading and non-degrading pools of Tir1-BFP cells. **A)** The 3xF-AID-GFP-P2A-mCherry targeting construct (described in **Figure 3.2**) was transiently transfected into $Tir1^{WT}$-BFP and $Tir1^{mut}$-BFP expressing HeLa cells. Cells were treated +/- 1mM Auxin for 1hr and analyzed for GFP:mCherry ratio. Control cells are shown in the left-most panels. In the $Tir1^{WT}$-BFP control cells, the cells falling to the left of the 1:1 axis are exhibiting auxin-independent degradation. The middle panels show degradation after 1hr of auxin treatment. Gates were set around the degrading (1A) and non-degrading cells (1B), which were collected as pools for further experiments. The degrading cells (1A) were sub-gated into fast (2A) and slow (2B) degraders based on the extent of GFP degradation (right panels). These cells were also collected as a pool of cells for further experiments. The 2A cells were also expanded and used as a starting point for AID endogenous tagging experiments. **B)** The fast and slow degrading cells collected in the experiment shown in **A** were expanded, retransfected, and treated with 1mM Auxin for 1hr to analyze maintenance of degradation kinetics. Gates were placed equally over the populations of degrading cells for both cell lines. Based on GFP:mCherry ratio, cells in the degrading gate in 2A are shifted slightly further left than those in the degrading gate in 2B, suggesting that the extent of degradation was maintained after expansion and re-transfection of these populations of cells. **C)** A histogram of GFP intensity for the cells in the degrading gates in **B** shows that, after degradation, the average GFP intensity is lower for the 2A cells than the 2B cells. This also demonstrates that degradation kinetics and efficiency can be maintained over many cell-doublings.

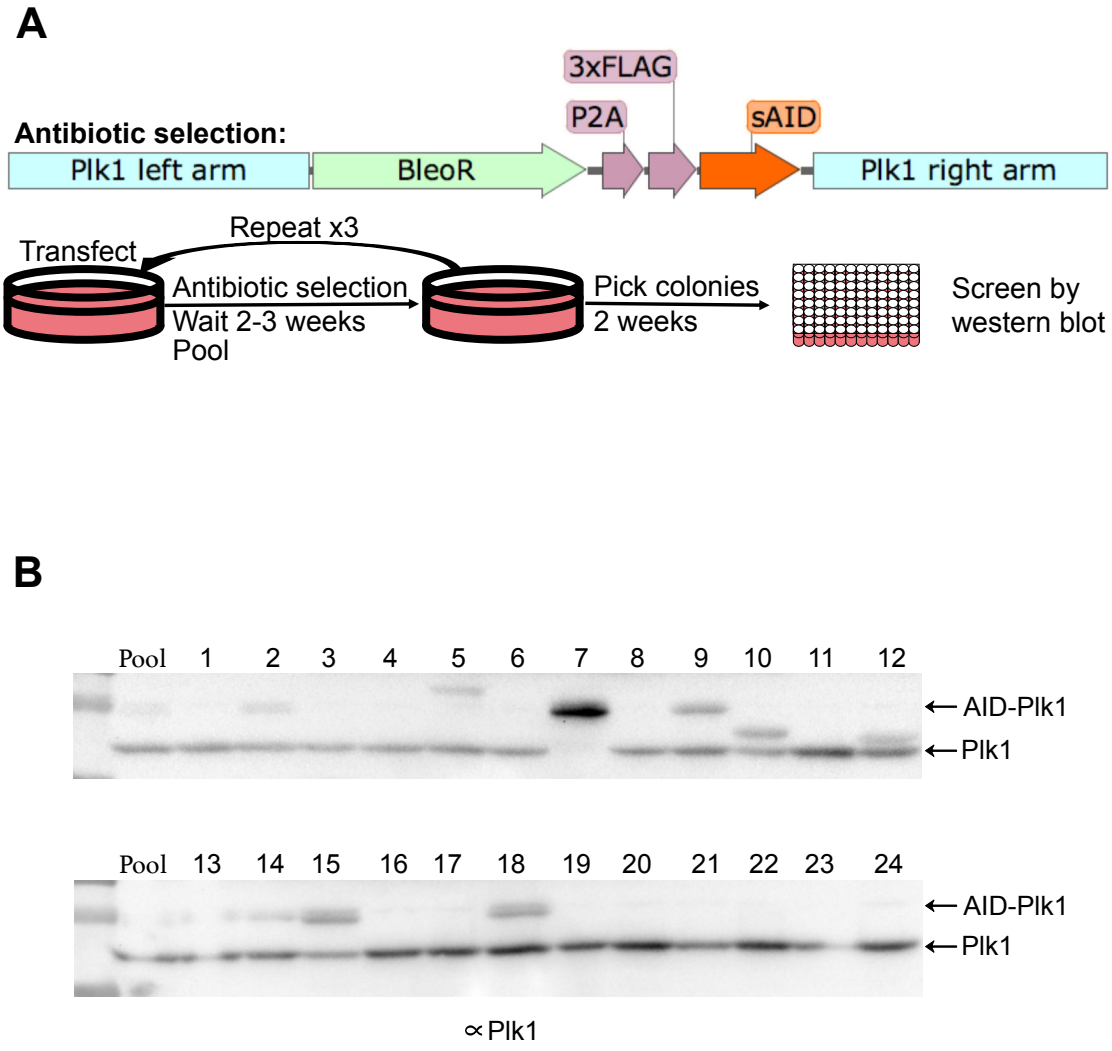

Figure 3.4. Methodology for 3xF-AID tag insertion using antibiotic selection. **A)** A targeting vector, in this case for Plk1, is designed to have 500bp arms homologous to the endogenous locus upstream and downstream of the gRNA cut site (Plk1 left arm and right arm, respectively). In between the homology arms are an antibiotic resistance cassette and the 3xF-AID tag, separate by a P2A ribosomal skip site to ensure independent expression. Cells are transfected with a pX330 plasmid expressing Cas9 and a guide RNA against the target gene, as well as the linearized targeting vector. Cas9 induces a double strand break (DSB) at the endogenous locus and the targeting vector is used as a repair template, causing an incorporation of the tags included between the left and right homology arms. After the CRISPR-Cas9 transfection, an antibiotic is added to select for cells with in-frame tag insertion. The selected cells are then allowed to grow for 2-3 weeks until they are confluent in a 10cm dish, and the pool is analyzed by western blot to check

for tag incorporation at the pool level. The transfection/selection process is carried out 2 more times with different antibiotic selection agents and resistance cassettes for a total of 3 times. Finally, individual colonies are allowed to grow on 10cm plates and are picked by hand under a microscope into 96-well dishes, then expanded to 24-well dish stage, and screened by western blot to check for tag incorporation at the level of individual clones. **B)** Individual clones were picked, expanded to 24-well stage, and screened by western blot to test the rate of tag incorporation after a single round of CRISPR-Cas9 transfection and antibiotic selection. From this experiment it was found that most clones had very little or no tag incorporation (ex. clones 19-24). However, some clones were heterozygous knock-ins (ex. Clones 2, 9, 15) and one was a homozygous knock-in (clone 7). This suggested that, while still rare events, homozygous knock-in after a single round of CRISPR-Cas9 transfection and selection is possible.

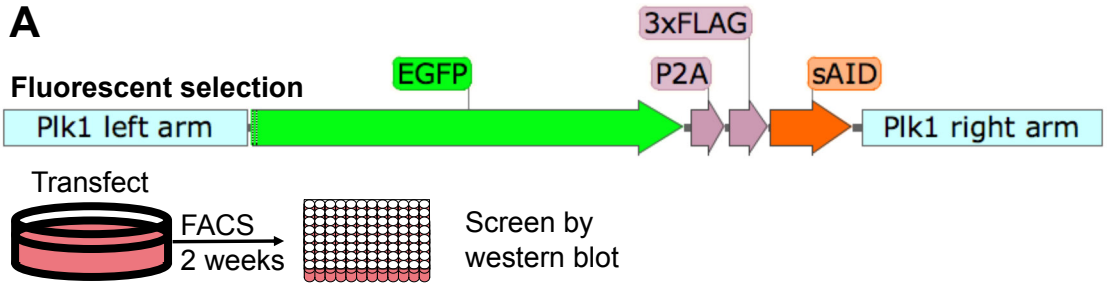
A
Fluorescent selection
Plk1 left arm
EGFP
3xFLAG
P2A
sAID
Plk1 right arm
Transfect
FACS
2 weeks
Screen by
western blot

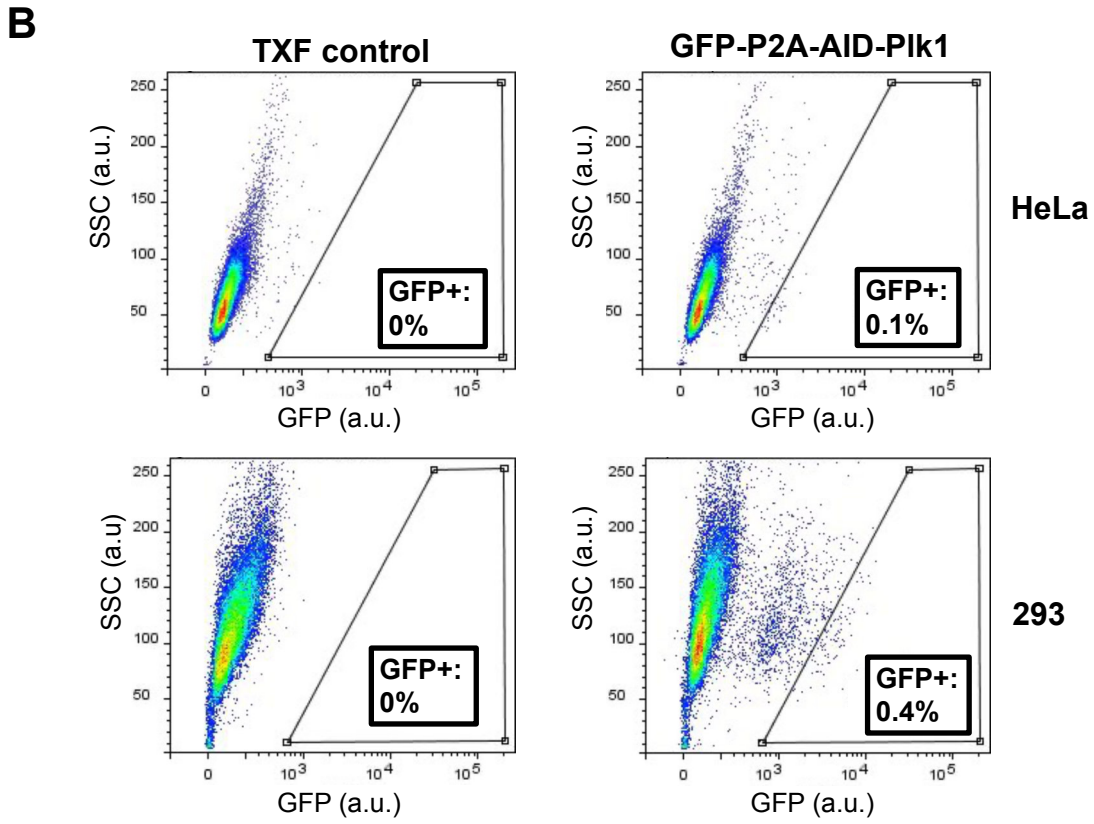
B
TXF control
GFP-P2A-AID-Plk1
SSC (a.u.)
GFP (a.u.)
GFP+:
0%
GFP+:
0.1%
HeLa
GFP+:
0%
GFP+:
0.4%
293

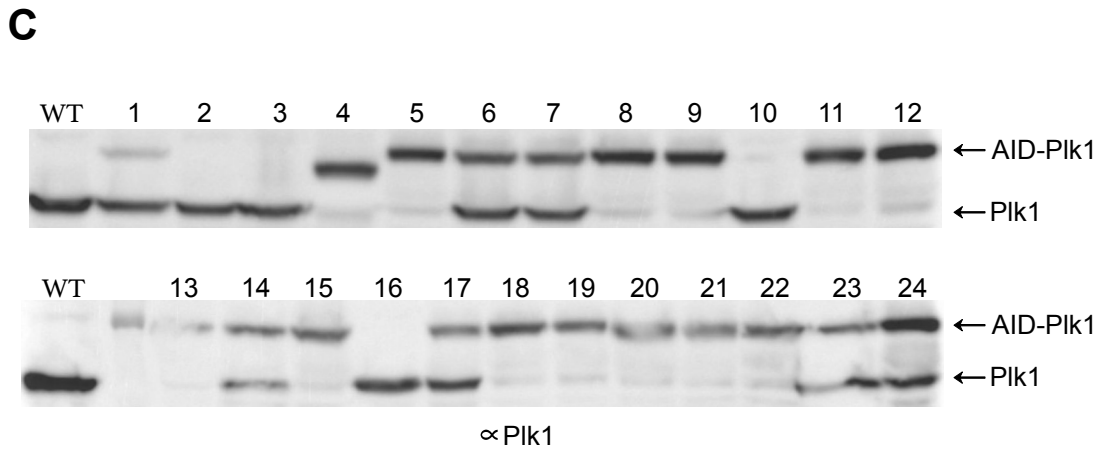
C
WT 1 2 3 4 5 6 7 8 9 10 11 12
← AID-Plk1
← Plk1
WT 13 14 15 16 17 18 19 20 21 22 23 24
← AID-Plk1
← Plk1
∝Plk1

Figure 3.5. Methodology to create homozygous knock-in AID clones using fluorescent reporters and FACS. **A)** The targeting vector is the same as described in **Figure 3.4**, with the exception that the antibiotic resistance cassette is swapped out for a GFP fluorescent reporter protein. In this system, the fluorescent reporter is separated from the start of the protein of interest with a P2A ribosomal skip site, ensuring that the fluorescent protein and AID-tagged kinase are expressed from the same mRNA but are not fused. The targeting vector is transfected into WT cells, along with a pX330 plasmid expressing Cas9 and a guide RNA targeting the Plk1 endogenous locus to induce double strand breaks (DSBs). In-frame insertion of the targeting vector allows for the expression of GFP, which can be used to sort single cells to a 96-well dish. After ~2 weeks, the clones can be expanded up to the 24-well dish stage and screened by western blot for AID tag incorporation. **B)** FACS plots comparing side scatter (y-axis) to GFP intensity (x-axis) for a transfection control (left panels) and cells transfected with pX330 and the targeting vector (right panels) into HeLas (top panels) or 293s (bottom panels). The transfection controls are used to establish baseline GFP intensity, and a gate can be set to exclude noise and only include GFP signal stemming from tag incorporation. In HeLa cells, transfection led to a subtle but quantifiable difference in GFP intensity with 0.1% of cells falling within the GFP+ gate. The effect of GFP expression after transfection is much clearer in 293s, with 0.4% of cells falling within the GFP+ gate, but many more displaying GFP expression well above baseline. By collecting only the cells at the very high end of GFP expression, it is possible to enrich for cells that are more likely to be homozygous knock-ins. **C)** Representative western blots using an antibody raised against Plk1 of individual HeLa clones after a single round of CRISPR-Cas9 transfection and flow sorting. Half of the recovered clones were likely to be homozygous knock-in (clones 5, 8, 9, 11, 12, 13, 15, 18-22) based on the amount of AID-PLK1 compared to WT Plk1. While there is a small amount of signal at the WT Plk1 molecular weight, even in the clones that are thought to be homozygous knock-in, it is likely that this is the result of proteolysis, either within the cells or during the collection and lysis and does not represent an untagged Plk1 species in these cells.

Chapter 4

Targeted degradation and small molecule inhibition to analyze group 1 PAK functional redundancy

Author Contributions:

C. Lincoln Howarth: Wrote text and designed figures for chapter 4. Designed, executed, and analyzed experiments.

Scott A. Gerber: Conceptualized, designed, and analyzed experiments. Provided feedback and edits on text.

Introduction

The p21-activated kinase (PAK) family consists of 6 kinases that positively regulate a number of pro-proliferation pathways including ERK, AKT, and WNT (Kumar et al., 2006; Radu et al., 2014). PAK1 is the best-studied member of this kinase family and has multiple roles in promoting proliferation and regulating cytoskeletal dynamics (Kumar et al., 2017). Interestingly, PAK1 is upregulated in 30-33% of breast tumor samples and cell lines (Shrestha et al., 2012), and overexpression of catalytically active PAK1 is sufficient to promote mammary tumorigenesis in mice (Wang et al., 2006). *PAK1* gene amplification correlates with poor prognosis in breast cancer, and inhibiting PAK1 with FRAX1036, an ATP-competitive inhibitor of PAK1-3, sensitizes cancer cells to docetaxel (Ong et al., 2015). Furthermore, PAK1 is frequently upregulated and hyperphosphorylated in estrogen receptor-positive (ER+) breast cancer, suggesting that PAK1 signaling promotes and maintains oncogenesis in this disease context (Mertins et al., 2016). Although targeting PAK1 could be an effective treatment strategy for breast cancer, inhibiting PAK1 systemically results in cardiovascular toxicity, possibly due to co-inhibition of PAK2 (Rudolph et al., 2016; Semenova & Chernoff, 2017). For these reasons, identifying specific PAK1 substrates that could be targeted for therapeutic intervention presents an alternative strategy for combating PAK1-driven breast cancer.

The upregulation of PAK1 in multiple cancer types relates to its roles in stimulating mitotic entry, promoting cellular proliferation, and orchestrating cytoskeletal remodeling (Ong et al., 2011). PAK1 stimulates mitotic entry by phosphorylating and activating the master mitotic regulators AURKA and PLK1 (Maroto et al., 2008; Z. S. Zhao et al., 2005), both of which are common drivers of oncogenesis. As a component of cellular proliferation, PAK1 function is thought to be required for KRAS-mediated oncogenesis by regulating the activation of AKT and ERK. In a mouse model of KRAS-driven tumor formation, $PAK1^{-/-}$ mice have delayed tumor onset, longer survival time, and decreased activation of AKT and ERK (Chow et al., 2012). As a cytoskeletal regulator, PAK1 promotes motility and invasion by phosphorylating F-actin regulators at the leading edge of cells (Kumar et al., 2017). For example, PAK1 phosphorylation of Paxillin at Ser273 increases cellular motility (Nayal et al., 2006), overexpression of kinase-dead PAK1 decreases cellular motility (Adam et al., 2000), and PAK1 indirectly inactivates F-actin regulator Cofilin by phosphorylating and

activating LIM domain kinase 1 (LIMK1) (Edwards et al., 1999; Yang et al., 1998). Moreover, PAK1 increases the rate of extravasation and metastasis by regulating invadopodia turnover (Williams et al., 2019). However, in spite of these observations, there is a need for a comprehensive, unbiased assessment of PAK activity to uncover novel substrates and assign known, relevant substrates to individual PAKs (Radu et al., 2014). By probing the PAK1 signaling network with a specific, selective, and unbiased approach, we will identify novel PAK1 substrates and provide a deeper understanding of the role of PAK1 in tumorigenesis.

One approach for studying the human kinome to uncover candidate mechanisms of function is the use of selective inhibitors to rapidly inactivate targeted kinases, coupled with mass spectrometry-based quantitative phosphoproteomics (Kettenbach et al., 2011). This approach connects a kinase of interest with its downstream phosphorylation sites by quantitatively measuring phosphorylation site abundance during acute kinase inhibition. This has a distinct advantage over knockdown or knockout methods, which are slow and may result in adaptation or alterations in cell physiology or state, complicating the assignment of direct substrates. Unfortunately, the best available PAK1 inhibitors are not ideally selective for PAK1 (Ndubaku et al., 2015; Singhal & Kandel, 2012). Thus, using an inhibitor to determine PAK1 substrates would result in the identification of off-target substrates for other kinases. An alternative strategy is the use of targeted degradation approaches, which rely on genetic engineering and the introduction of a small molecule to stabilize or degrade the protein of interest (Natsume & Kanemaki, 2017; Aisha Yesbolatova et al., 2019). One such approach exploits an auxin-inducible degron (AID) appended to the protein of interest, as well as the plant F-box protein Tir1, which can bind to mammalian components of the SKP1, Cullin, F-box (SCF) complex. Tir1 promotes rapid degradation of AID proteins, only in the presence of auxin. By tagging a protein of interest with the AID degron and expressing Tir1 in mammalian cells, this system can be used to rapidly and specifically degrade the tagged protein upon the addition of auxin (Natsume et al., 2016; Nishimura et al., 2009; A. Yesbolatova et al., 2019). We recently demonstrated that this approach can be applied to study kinase-substrate relationships in a manner analogous to the use of kinase inhibitors (Hards et al., 2021). In the present work, we apply that approach to identify novel PAK1 substrates and deepen our understanding of PAK1-dependent signaling networks.

Materials and Methods

Cell culture and cell lines

HeLa and HEK293 cells were grown in Dulbecco's Modification of Eagle's Medium (DMEM, Corning) supplemented with 8% fetal bovine serum (FBS, Hyclone) and 1% penicillin-streptomycin (100IU/mL penicillin and 100µg/mL streptomycin, Corning). SU.86.86 cells were a gift from Dr. Steve Leach and were grown in RPMI 1640 (Corning) supplemented with 8% FBS and 1% penicillin-streptomycin. Cells were incubated at 37C with 5% CO_2.

HEK293 cells were used as model cell lines for AID-PAK1 experiments because they have high PAK1 expression and are amenable to CRISPR-Cas9 gene editing. SU.86.86 cells were used for PAK inhibition experiments with NVS-PAK1-1 because they have high expression and activity of PAK1 and PAK2, as previously shown (Karpov et al., 2015). In addition, HeLa cells were used in EGF experiments because they express EGFR and have an active EGF response pathway.

Fluorescence-activated cell sorting

Cells to be analyzed were collected by trypsinization, washed once with PBS (Corning), and resuspended in 2mL PBS in 15mL conical tubes where they were kept on ice until sorting. Analysis and collection were performed on a Sony SH800S cell sorter using a 100µm microfluidic sorting chip. Cells were initially gated on forward scatter (FSC) and back scatter (BSC) to ensure a homogenous population of cells. Untransfected controls were used to establish baseline fluorescence and set up gates for collection. Cells were collected to using the ultra-purity collection mode.

CRISPR-Cas9 3xFlag-AID-PAK1 homologous recombination clone generation

AID-PAK1 targeting constructs were designed using the genomic sequence for PAK1 in UCSC genome browser. An sgRNA overlapping the PAK1 start codon was

designed based on scoring from CRISPOR.tefor.net (PAK1 PITCh sgRNA Forward – 5' GTGGTGACAATGTCAAA 3') and was cloned into pX330-Bbs1-PITCh (Addgene plasmid #127875) (Lin et al., 2019). To make a version of pBluescript with PITCh sgRNA recognition sequences (pBS-PITCh, (Sakuma et al., 2016), DNA oligos were ordered (IDT, 5' GGTACCGCATCGTACGCGTACGTGTTTGGGGTACCGACATGGAGCTCCCAAACAC GTACGCGTACGATGCGAGCTC 3'), annealed, and inserted into pBluescript via Gibson assembly. 20bp homology arms were designed immediately upstream and downstream of the sgRNA cut site and were ordered along with internal tagging components as a g-block (IDT) and cloned into pBS-PITCh.

For transfection, cells were plated to 6-well dishes at ~50% confluency in media free of penicillin/streptomycin. 1.4µg of pBS-PITCh-AID-PAK1 targeting vector was mixed with 0.4µg of pX330-PAK1-PITCh in Jetprime and Jetprime transfection buffer (Polyplus) and incubated at room temperature for 10 minutes as per manufacturer protocol. The transfection mix was added dropwise to each well and incubated overnight. After 16hrs of incubation, the media was washed off and exchanged for media containing penicillin/streptomycin and the cells were left to grow for another day. On day three, transfected cells were expanded to 10cm dishes and treated with blasticidin (10µg/mL). Media was exchanged for fresh media containing antibiotic every two days for two weeks or until colonies visible to the naked eye had formed. Individual colonies were isolated by incubation in trypsin diluted 1:40 in PBS and then manually harvested under a 10x screening microscope and transferred to a 96-well plate. Colonies were expanded to the 24-well stage and then harvested for analysis by western blotting.

The AAVS1-Tir1 CRISPR targeting construct to introduce ectopic Tir1 to the AAVS1 safe harbor locus has been described previously (Hards et al., 2021). 1.4µg of the AAVS1 targeting vector was linearized *in vitro* and was transfected along with 0.4µg of pX330 containing an sgRNA targeting the AAVS1 locus into HeLa cells as described above. After recovery from transfection, cells were expanded to 10cm dishes and treated with 1µg/mL puromycin until colonies visible to the naked eye formed (up to 2 weeks) with fresh media containing puromycin exchanged every 2 days. Colonies were isolated by hand to a 96-well dish, expanded to the 24-well dish stage, and screened for Tir1 expression and auxin-induced degradation by western blot.

Cdc42^{G12V} cloning and lentiviral production

YFP-Cdc42^{G12V} was ordered as a plasmid (Addgene #11399)(Hoppe & Swanson, 2004) and the pCW57.1 lentiviral vector was received as a gift from the Kettenbach lab. YFP-Cdc42G^{G12V} was amplified using the following primers (Forward: 5' TCAGATCGCCTGGAGAATTGGCTAGCATGGTGAGCAAGGGCG 3', Reverse: 5' TGGTGGTGGTGGTGGACCGGTTTAGAATATACAGCACTTCCTTTTGGG 3') and cloned into pCW57.1 via Gibson assembly. To produce lentivirus, pCW57.1-YFP-Cdc42^{G12V}, CMV-VSVG, and psPAX2 plasmids were mixed with polyethylenimine (PEI) transfection reagent in DMEM (penicillin/streptomycin and FBS-free), which was added to 10cm dishes of 293 cells cultured at 50% confluency in DMEM and incubated overnight at 37C. Media was exchanged for fresh media (+FBS) on day 2. Virus-containing media was collected every day for three days, centrifuged at 1000g to remove cellular debris, split to 2mL aliquots, and snap-frozen in liquid nitrogen. For viral transduction, 3xFlag-AID-PAK1 cells (clone S48) were plated at 50% confluency to 6-well dishes and incubated in pCW57.1-YFP-Cdc42^{G12V} lentivirus media with 4µg/µL polybrene. Transduced cells were incubated overnight, washed 5x with PBS, and given time to recover. On day three, doxycycline (1µg/mL) was added overnight to induce YFP-Cdc^{G12V} expression and transduction efficiency was assessed under an epifluorescent screening microscope.

Since transduction efficiency as assessed by YFP signal under a fluorescent microscope appeared low (< 10%), cells were enriched for YFP-Cdc42^{G12V} induction via FACS as described above. Briefly, doxycycline induced cells were collected and resuspended in PBS. To establish YFP gates, a non-transduced AID-PAK1 cell line was used as a control for baseline YFP intensity and the top 1% of YFP-expressing cells were collected to 6-well dishes.

EGF activation experiments

EGF was received as a gift from the Miller Lab. Cells were cultured at 90% confluency in 12-well dishes and 1ng/mL EGF was added to media for the indicated times. In the case of serum starvation experiments, media was exchanged for FBS-free media and the cells were cultured overnight and treated with 1ng/mL EGF. Samples were collected for

analysis by western blot by aspirating the media and adding 2x Lamelli lysis buffer directly to the well and pipetting up and down to collect lysate.

PAK1 and PAK2 CRISPR knockout clones

PAK1 and PAK2 knockout sgRNAs were designed using the CRISPick tool (Doench et al., 2016; Sanson et al., 2018) and were cloned into pX330. HeLa cells were plated at 50% confluency in a 6-well dish and 1µg each sgRNA was transfected into a single well following the JetPrime transfection protocol (Polyplus). Two days after transfection, cells were expanded to 15cm dishes and treated with 1µg/mL puromycin, exchanging for fresh media every 2 days until visible colonies had formed. Clones were isolated by hand on a 10x screening microscope to 96-well dishes, expanded to the 24-well dish stage, and assessed for PAK1 or PAK2 knockout by western blotting.

Western Blotting

Cells to be analyzed by western blot were collected, washed once in PBS, and lysed in 2x Lamelli. Poly-acrylamide gels were poured in house from a 30% acrylamide solution (Protogel, National Diagnostics). Gels were run at 140V for 80 minutes in running buffer containing 25mM Tris, 200mM glycine, and 1% SDS. The gels were then transferred to nitrocellulose blotting membrane (Amersham Protran) at 100V for 60 minutes in a transfer buffer containing 25mM Tris, 200mM glycine, and 20% MeOH. To account for loading, blots were briefly stained with ponceau (0.01% ponceau, 0.5% acetic acid) and imaged. Blots were washed in TBST (50mM Tris, 150mM NaCl, 0.2% Tween-20), blocked for 30 minutes and incubated overnight with primary antibody at 4C. Finally, blots were incubated with an HRP-conjugated secondary antibody for 1hr at room temperature, treated with Clarity ECL substrate (BioRad) and imaged. A solution of 4% milk in TBST was used for blocking, and incubation in primary and secondary antibodies. For phospho-specific antibodies, the phosphatase inhibitors β-glycerophosphate (5mM), sodium fluoride (5mM), and sodium molybdate (5mM) were added.

Phosphoproteomic TMT experiments

Cells were grown to ~90% confluency in 10cm dishes in triplicates and were treated +/- 1mM 1-napthaleneacetic acid (NAA/Auxin) or NVS-PAK1-1 (Tocris). In the case of hyper-activated AID-PAK1 cells, the expression of YFP-Cdc42^{G12V} was induced by the addition of doxycycline 16hrs before drug treatmet. After treatment, cells were trypsinized for collection, pelleted, washed with PBS, snap-frozen in liquid nitrogen, and stored at -80C until processing. Cell pellets were partially thawed on ice and resuspended with 1.6mL of a lysis buffer containing urea (8M, AMRESCO), NaCl (100mM, Fisher), Tris pH 8.1 (50mM, Alfa Aesar), protease inhibitor (RPI protease inhibitor cocktail III, mammalian), and phosphatase inhibitors β-glycerophosphate (2mM, Sigma), sodium fluoride (2mM, Fluka), and sodium molybdate (2mM, Sigma). Lysates were sonicated 3x10 seconds at 15% power on a Branson sonicator equipped with a microtip. Protein concentration was determined with a protein BCA assay kit (ThermoFisher). Samples were centrifuged at max speed at 4C for 10 minutes and the supernatant was collected. Lysates were reduced with dithioretitol (DTT, 5mM, Sigma) for 20 minutes at 55C, cooled to room temperature, and alkylated with iodoacetamide (15mM, Sigma) in the dark for 1hr. The alkylation was quenched with DTT (5mM) for 15 minutes at room temperature in the dark. Finally, lysates were diluted to 10mL total with a buffer containing 25mM Tris pH 8.1, 100mM NaCl, and 20µg sequencing grade trypsin (Promega) and incubated overnight at 37C. Digested peptides were acidified to pH< 3 with 125µl 20% trifluoroacetic acid (TFA, Honeywell). 600µl of MeOH was added and samples were incubated at room temperature for 10 minutes and centrifuged at 5,000g for 5 minutes to pellet insoluble material. The peptide digest solutions were desalted on a 60mg Oasis desalting plate (Waters). 40µg of desalted peptides were saved for proteomic analysis and the remainder of the peptide solutions were partially dried in a vacuum centrifuge at 35C for 30 minutes, frozen at -80C, and lyophilized overnight. Dried peptides were resuspended in 50% acetonitrile/0.1%TFA and enriched for phosphopeptides with the High-Select Fe-NTA phosphopeptide enrichment kit (ThermoFisher). Eluted phosphopeptides were dried in a vacuum centrifuge and desalted on a 2mg Oasis µElution plate (Waters) and vacuum centrifuged to dryness.

Dried phosphopeptides were resuspended in 166mM EPPS pH 8.5 and 70µg of the corresponding TMT channel was added to each sample, which were incubated at room

temperature for 1 hour. The reactions were quenched with hydroxylamine for 15 minutes, acidified with 1% TFA, mixed into a single sample tube, and desalted on a 10mg Oasis plate (Waters). The eluted, labeled phosphopeptides were dried in a vacuum centrifuge and separated to 48 fractions by HPLC using a pentafluorophenyl (PFP) column as previously reported (Grassetti et al., 2017). The separated fractions were concatenated into either 16 or 24 fractions, depending on peptide abundance as determined by HPLC and were analyzed by mass spectrometry as described below.

LC-MS/MS analyses

LC-MS/MS analysis was performed as previously described (Hards et al., 2021) on an Orbitrap Fusion Lumos Tribrid mass spectrometer (ThermoFisher) equipped with an EASY-nLC 1000 ultra-high pressure liquid chromatograph (ThermoFisher). Samples were dissolved in loading buffer (5% methanol/1.5 % formic acid) and injected directly onto an in-house pulled, polymer coated, fritless, fused silica analytical resolving column (35 cm length, 100µm inner diameter; PolyMicro) packed with ReproSil, C18 AQ 1.9 µm 120 Å pore stationary phase particles (Dr. Maisch). Phosphopeptides were loaded at 450 bar by chasing on to the column with 8µl loading buffer. Samples were separated with a 120-minute gradient of 4 to 33% LC-MS buffer B (LC-MS buffer A: 0.125% formic acid, 3% ACN; LC-MS buffer B: 0.125% formic acid, 95% ACN) at a flow rate of 330 nl/minute. The instruments were operated with an Orbitrap MS1 scan at 120K resolution and an AGC target value of 500K. The maximum injection time was 100 milliseconds, the scan range was 350 to 1500 m/z and the dynamic exclusion window was 15 seconds (+/- 15 ppm from precursor ion m/z). Precursor ions were selected for MS2 using quadrupole isolation (0.7 m/z isolation width) in a “top speed” (2 second duty cycle), data-dependent manner. MS2 scans were generated through collision-induced dissociation (CID) fragmentation (35% CID energy) and either linear ion trap analysis (Rapid setting) for peptides or Orbitrap analysis at 30K resolution for phosphopeptides. Ion charge states of +2 through +4 were selected for HCD MS2. The MS2 scan maximum injection time was 60 milliseconds and AGC target value was 60K. For TMT runs, top 8 MS2 peaks were dynamically isolated and further fragmented by higher-collision energy (HCD) at 55% via SPS-MS3 for quantification of liberated reporter ions (110 – 500 m/z).

Peptide spectral matching and bioinformatics

Peptide spectral matching was performed as previously reported (Hards et al., 2021). Raw data were searched using COMET against a target-decoy version of the human (*Homo sapiens*) proteome sequence database (UniProt; downloaded 2018; 20,241 total proteins) with a precursor mass tolerance of +/- 1.00 Da (Hsieh et al., 2010) and requiring fully tryptic peptides with up to 3 missed cleavages, carbamidomethyl cysteine as a fixed modification and oxidized methionine as a variable modification. For phosphopeptide data, searches were expanded to include the dynamic addition of phosphate to serine, threonine, and tyrosine residues. For TMT-labeled samples, the mass of the TMT reagent (229.162932 Da for TMT11, 304.2071 Da for TMTPro ragents) was added as a static modification to all peptide N-termini and lysine residues. Phosphorylation of serine, threonine and tyrosine were searched with up to 3 variable modifications per peptide, and were localized using the phosphoRS algorithm (Taus et al., 2011). The resulting peptide spectral matches were filtered to ≤1% false discovery rate (FDR) by defining thresholds of decoy hit frequencies at particular mass measurement accuracy (measured in parts per million from theoretical), XCorr and delta- XCorr (dCn) values. Statistical analyses and data visualization were performed in excel, GraphPad Prism, and R.

Results

Generation of endogenously tagged AID-PAK1 cells

We first sought to develop a homozygous, endogenously tagged 3xFlag-AID-PAK1 HEK293FT cell line, which could be used to measure the effects of rapid, specific, and selective PAK1 depletion on the phosphoproteome. To endogenously tag PAK1, we engineered DNA constructs with a 3xFlag-AID tag flanked by short sequences of DNA homologous to the N-terminus of PAK1 (**Figure 4.1A**). These targeting constructs follow a CRISPR gene editing system called Precision Integration into Target Chromosome (CRIS-PITCh) (Lin et al., 2019; Nakade et al., 2014; Sakuma et al., 2016). This method relies on co-transfection of two vectors: a targeting vector with 20bp homology arms flanking the start codon at the *PAK1* endogenous locus, and a Cas9 / dual gRNA expression vector to both cut the *PAK1* locus as well as linearize the targeting vector *in cellulo* (**Figure 4.1A**). The *PAK1* locus is subsequently repaired through Microhomology-Mediated End Joining (MMEJ), a high-fidelity DNA repair process that makes use of short, microhomology sequences and is an active pathway for a greater duration of the cell cycle than homology-directed repair (HDR) (Sfeir & Symington, 2015). We deployed this strategy in HEK293FT cells, selected for in-frame insertion using blasticidin, and generated homozygously tagged 3xFlag-AID-PAK1 clones, as confirmed by western blot (**Figure 4.1C**). HEK293FT cells were chosen for this experiment because they have shown to be amenable to CRISPR-Cas9 gene editing in our hands for other AID-kinases.

After establishing a homozygous 3xFlag-AID-PAK1 cell line, the plant F-box protein Tir1, which induces degradation of AID-tagged proteins in the presence of auxin, was introduced ectopically into the AAVS1 safe-harbor locus (**Figure 4.1B)**. Single colonies were picked by hand, expanded, and tested for Tir1 expression and PAK1 degradation by addition of auxin (1-naphthaleneacetic acid; NAA) for 4h by western blot (**Figure 4.1D)**. These efforts yielded the 3xFlag-AID-PAK1/Tir1 clone 22-5 used in subsequent phosphoproteomic experiments. While there is a small proportion of apparently wild-type PAK1 in this cell line, it is likely that this is the result of a tag cleavage event since the level of untagged PAK1 is greatly reduced upon NAA addition, suggesting that it is still degradable. Furthermore, we confirmed that AID-PAK1 clone 22-5 does not have significantly different expression of PAK1 compared to WT HEK293FTs (data not

shown). Time-course experiments revealed that the majority of PAK1 is degraded within 2h, but PAK1 is degraded to the maximum extent within 4h (**Figures 4.1D and 4.1E**).

To validate the efficacy of the 3xFlag-AID-PAK1 cell line and identify novel PAK1 substrates, cells were treated in triplicate with either 1 mM NAA, 5 μM of the allosteric PAK1 inhibitor NVS-PAK1-1 (NVS) (Karpov et al., 2015), or left untreated for 4 hours and analyzed by western blot to assess degradation (**Figure 4.1E**), as diagrammed in **Figure 4.2A**. Briefly, asynchronous cells were treated, collected, and lysed. Protein lysates were digested to peptides, enriched for phosphopeptides, and labeled with isobaric tandem-mass tag (TMT) reagents (Rauniyar & Yates, 2014). To identify phosphopeptides that are positively or negatively regulated by PAK1, we plotted the $\log_2$ fold change in abundance by the p-value (Student's t-test; **Figure 4.2B and 4.2C**). Phosphopeptides that are statistically (p-value < 0.05) and biologically significant (> 2-fold change in treated vs. control) represent potential PAK1 substrates (**Figure 4.2B and 4.2C,** red circles). A correlation plot was generated for all phosphopeptides with a p-value of <0.1 between drug and auxin treatments (**Figure 4.2D**). This plot highlights a clear correlation between phosphosites that are decreased upon PAK1 degradation (NAA/Cont) and PAK1 inhibition (NVS/Cont), demonstrating the efficacy of the 3xFlag-AID-PAK1 cell line to deplete PAK1-dependent signaling. This experiment also revealed that degrading PAK1 is more selective for PAK1 substrates than the inhibitor, as phosphosites on PAK2, including pS141, the main activating phosphorylation site on PAK2, were observed to be significantly decreased upon NVS-PAK1-1 inhibition, but not with PAK1 degradation (**Figure 4.2D**, red circles).

Although the canonical activation site, S144, on PAK1 was observed to be significantly downregulated in both the degradation and inhibition conditions, only 28 phosphosites decreased in abundance when PAK1 was degraded (**Figure 4.2C**), of which 16 were phosphosites on PAK1 itself. The PAK1 phosphorylation motif has been previously characterized, and it was found that PAK1 has a preference for basic residues and a strong disfavoring of acidic residues upstream of the phosphorylation site (Rennefahrt et al., 2007). Of the remaining 12 phosphopeptides, 4 had acidic residues directly upstream of the phosphosite, 2 were Tyr phosphopeptides, and none were enriched for basic residues in the upstream positions. Furthermore, none of these 12 phosphosites have been previously attributed to PAK1 activity or were on proteins that are known substrates or interactors of PAK1. This suggested to us that, while the AID-PAK1 system was working to reduce PAK1 activity in this context, PAK1-dependent pathways

may not have been particularly active before degradation or inhibition, resulting in a small number of regulated phosphosites. We therefore hypothesized that hyperactivation of PAK1 prior to degradation or inhibition would potentially yield more PAK1-dependent phosphosites.

Hyperactivation of PAK1 with Cdc42 and EGF pathways

Group 1 PAKs, including PAK1 and PAK2, are canonically thought to be activated by the binding of a GTPase, such as Cdc42 or RAC1, to the GTPase binding domain (GBD) (Radu et al., 2014). This interaction relives autoinhibition of the PAK kinase, allowing for autophosphorylation of a key activation site (S144 on PAK1 or S141 on PAK2), and full activation (**Figure 4.3A**). Given our assumption that the activity of PAK1 in our AID-PAK1 cell line could be a limiting factor for the discovery of novel PAK1 substrates, we sought to exploit PAK1 activation via Cdc42 to create a hyperactivated PAK1, potentially allowing for larger changes to PAK1-dependent phosphosites upon degradation and easier identification of PAK1 substrates.

To do this, we used lentivirus to introduce constitutively active YFP-Cdc42^{G12V} under the control of a doxycycline inducible promoter to the AID-PAK1 HEK293FT cell lines 22-5 and S48 (S48 was subcloned from 22-5 and degrades to a slightly greater extent with better kinetics). Because initial experiments showed a low penetrance of the lentivirus, we used FACS to sort these cells into pools based on high YFP expression in the presence of doxycycline (data not shown). We further validated that doxycycline treatment was able to induce expression of YFP-Cdc42^{G12V} and that this expression resulted in a hyperphosphorylated PAK1 and phosphorylation of STMN1 and GEFH1, substrates that have been previously attributed to PAK1 (**Figure 4.3B**). Furthermore, the phosphorylation of PAK1, STMN1, and GEFH1 was diminished when cells were treated with the group 1 PAK inhibitors G5555 or NVS-PAK1-1, demonstrating that this effect was mediated through group 1 PAK activation. As the activation mechanism of PAK2 is thought to be similar to that of PAK1 and both G5555 and NVS-PAK1-1 inhibit PAK1 and PAK2, it was still not possible to determine if the phosphorylation of these substrates was occurring through PAK1 or PAK2, although these experiments were sufficient to demonstrate activation of PAK1 and PAK2 pathways.

Using our AID-PAK1 cell line with doxycycline-inducible YFP-Cdc42^{G12V}, we performed a phosphoproteomics experiment comparing the effects of PAK1 degradation to group 1 PAK inhibition with 5uM NVS-PAK1-1 after an overnight induction of YFP-Cdc42^{G12V}, following the same workflow as previously described. Importantly, complete inhibition with NVS-PAK1-1 could be observed in one hour, but four hours of auxin treatment were required to effectively deplete PAK1 (data not shown). Although we identified a similar number of downregulated phosphosites in the inhibition condition as compared to the earlier experiment without hyperactivation (**Figure 4.4A,** 0.59% for fig. 2 vs. 0.63% for fig. 4), we observed 2.03% of phosphosites to be significantly downregulated with PAK1 degradation with hyperactivation compared to 0.07% after degradation without hyperactivation (**Figure 4.4B**). The fact that many more sites were identified with PAK1 degradation vs. PAK1/PAK2 inhibition suggested that PAK1 could also be functioning as a scaffold protein and that its degradation resulted in disruption of pathways regulated in ways other than through its kinase activity. We also considered the possibility that the difference in significantly downregulated phosphosites (0.63% for inhibition vs. 2.03% for degradation) is due to the difference in treatment time since counteracting phosphatases would have more time to turn over PAK1-dependent phosphosites in the four hour degradation than the one hour inhibition. An analysis of the phosphorylated motifs shows an enrichment for basic residues directly upstream of the phosphorylated residue in both the inhibited and degraded conditions (**Figure 4.4A and 4.4B**), which is consistent with the previously established PAK1 motif. In particular, phosphosites that are significantly downregulated with PAK inhibition show a strong preference for arginine in the -2 and -3 positions, as well as a preference for leucine in the -1 position, which are characteristics shared with the characterized PAK1 motif. However, we do not observe a strong preference for hydrophobic residues in the downstream positions as was previously reported. PAK1 degradation similarly demonstrates an enrichment for basic residues, particularly upstream of the phosphosite. However, there is a slight enrichment for acidic residues as well, which contradicts the previously reported disfavoring of acidic residues by PAK1 and is not entirely consistent with phosphosites observed with PAK inhibition. Taken together, the results of this experiment suggest that, while some phosphosites significantly downregulated with PAK1 degradation conform to the characterized PAK1 motif, there are many significantly downregulated phosphosites that cannot be explained by the reduction in PAK1 activity alone.

To ensure that the increase in observed PAK1-dependent phosphosites was the direct result of YFP-Cdc42^{G12V} induction, we performed a follow-up phosphoproteomics experiment to analyze the changes to the phosphoproteome upon YFP-Cdc42^{G12V} induction. We also compared the lentivirally transduced AID-PAK1 S48 cell line to the parental S48 line to analyze the effects of lentiviral transduction. While we did find that 844 phosphosites (2.93% of total phosphosites) are significantly different in the transduced S48 cells compared to the parental (**Figure 4.5A**), we only observed 32 significantly different phosphosites (0.11% of total phosphosites) with doxycycline induction of YFP-Cdc42^{G12V} (**Figure 4.5B**). This includes phosphorylation sites on proteins that are known effectors of Cdc42, such as MRCKA, BORG4, and PAK2, as well as the cytoskeletal organizing proteins KTNA1 and WIPF2. The remainder of significantly upregulated phosphosites are on proteins such as BRCA2 and TP53BP1 that play roles in the DNA damage response, apoptosis, or membrane trafficking. Therefore, we can conclude that doxycycline induction of YFP-Cdc42^{G12V} did cause changes to the phosphoproteome in ways that are consistent with known Cdc42 biology. However, the main autoactivation sites on PAK1 and PAK2 were only modestly upregulated (~50% increase) and we did not observe a statistically significant increase in the phosphorylation of known PAK substrates. Taken together, these observations demonstrate that induction of YFP-Cdc42^{G12V} has an effect on the global phosphoproteome, but that it was not a successful strategy for hyperactivating PAK signaling.

When analyzed by western blot it was also seen that perhaps the extent of YFP-Cdc42^{G12V} induction was diminished over time, as cells kept in culture for a longer time (**Figure 4.5C**, December freeze) had a reduced response to doxycycline when compared to cells kept in culture for a shorter amount of time (**Figure 4.5C**, June freeze). We considered that this limitation could be overcome by using cells from an earlier/younger frozen stock and rapidly stepping them up for phosphoproteomics, reducing the amount of time for the loss of doxycycline responsiveness to occur, but we were unable to achieve a robust and consistent activation of PAK1 and its target substrates, making it difficult to accurately and reliably repeat experiments in this system.

It has been previously shown that PAK1 and PAK2 are downstream of EGFR and can be activated by stimulating cells with 1ng/mL EGF (Liu & Burridge, 2000; Schiller, 2006; Tu et al., 2003), which presents an interesting and alternative method to activate PAK1 signaling. To test this approach, we added EGF to WT HeLas and a pancreatic

ductal carcinoma cell line SU.86.86, the growth of which is thought to be dependent on PAK1/PAK2 activity (Karpov et al., 2015). When HeLa cells were treated with 1ng/mL EGF, a rapid response in EGFR signaling was observed based on the EGFR hyperphosphorylation within 2.5 minutes and subsequent internalization and degradation of EGFR by 30 minutes (**Figure 4.6A**). In contrast to literature reports (Kim et al., 2015; Nuche-Berenguer & Jensen, 2015; Schiller, 2006; Yang et al., 2011), PAK1 was not observed to be hyperphosphorylated with EGFR induction based on either the PAK1 antibody or an antibody against pS144/pS141, the main activating sites on PAK1 and PAK2, respectively (**Figure 4.6A**). In Su.86.86 cells, activation of the EGF pathway was observed to be much less robust via addition of EGF (**Figure 4.6B**). Consistent with HeLa cells, however, there was no obvious change to pS144 on PAK1. These experiments were repeated several times in various cell lines including the AID-PAK1 cell line and WT 293T cells, but in all cases, while EGF treatment was shown to activate EGFR, activation of PAK1 was not observed (data not shown). Thus, we were not able to achieve a robust and consistent activation of PAK1 via the EGF/EGFR pathway, either because PAK1 is not involved in this signaling pathway, or because of variables that we were unable to account for.

Chemical inhibition of PAK1 and PAK2 in Su.86.86 cells

As previously mentioned, the pancreatic ductal carcinoma cell line SU.86.86 has high PAK1 and PAK2 activity and the proliferation of this cell line is reportedly dependent on the activity of both of these kinases (Karpov et al., 2015). This same study used the SU.86.86 cell line to demonstrate moderate selectivity for PAK1 over PAK2 for the allosteric inhibitor that they developed, NVS-PAK1-1. Based on this finding, we hypothesized that we could identify a dosage of NVS-PAK1-1 that would exhibit greater selectivity of PAK1 versus PAK2 inhibition in Su.86.86 cells and that this intermediate concentration could be used in large-scale phosphoproteomics experiments to enrich for substrates of PAK1 versus PAK2. We additionally screened the dosage response of PAK1 and PAK2 to the group 1 PAK competitive inhibitor G5555, which is not known to be selective for either of the two kinases. Using serial dilutions of either kinase inhibitor, we observed maximal inhibition of PAK1 without significantly affecting the activation state of

PAK2 with 250nM NVS-PAK1-1 (**Figure 4.7A**), while G5555 was observed to inhibit both kinases at similar concentrations (**Figure 4.7B**).

Based on the results of the dosage response experiments, we compared a low dose of NVS-PAK1-1 (250nM) to a high dose that would inhibit both PAK1 and PAK2 (5uM) in a large-scale phosphoproteomics experiment (**Figure 4.7C, 4.7D**). The 250nM NVS-PAK1-1 condition yielded 5 sites that were significantly downregulated (**Figure 4.7C**). Interestingly, the 3 sites with the greatest downregulation were all phosphorylation sites on PAK1 itself, including the canonical activating site S144, demonstrating clear inhibition of PAK1 activity. The only other two sites that were downregulated were on PAK2, highlighting that even at this lower concentration of NVS-PAK1-1, we were impacting the activity of both kinases. However, it is likely that, despite the reduction in PAK2 activation, there was still an active pool of PAK2 that was available to phosphorylate substrates. The 5uM NVS-PAK1-1 condition yielded 89 total phosphopeptides that were significantly downregulated (**Figure 4.7D**). Of these, 10 were phosphopeptides derived from PAK1 or PAK2, including the autoactivation sites S144 (PAK1) and S141 (PAK2), indicating a strong deactivation of both of these kinases. We also identified phosphosites on cytoskeletal regulators including S16 on Stathmin, a phosphosite previously attributed to PAK1 that is reported to inhibit Stathmin activity and stabilize microtubules (Daub et al., 2001; Wittmann et al., 2004). We also observed a decrease in phosphorylation on proteins involved in the cytoskeleton and attachment including TB182, Afadin, and Septin 9, as well as proteins involved in Cdc42/RAC signaling and cell adhesion/spreading such as DOCK5. Taken together, these results are consistent with PAK1 and PAK2 being key effector kinases of Cdc42 and functioning in regulation of the actin cytoskeleton but suggest that it is necessary to strongly inhibit both PAK1 and PAK2 to observe a robust response in the Group 1 PAK-dependent phosphoproteome. We further considered the possibility that most sites in this subset could be phosphorylated by either PAK1 or PAK2.

Another interpretation of this experiment was that a one-hour timepoint was long enough for a turnover in PAK2 sites, but not long enough for a turnover in PAK1 sites, which could explain why sites were only observed when PAK2 was maximally inhibited but not when PAK1 alone was inhibited. To address this hypothesis, we repeated the experiment using 250nM NVS-PAK1-1 for either two or four hours (**Figure 4.7E, 4.7F**), in order to allow counteracting phosphatases sufficient time to dephosphorylate PAK1-dependent sites. Once again, the only sites that were identified to be significantly

downregulated in either context were phosphorylation sites on PAK1 itself. This suggested to us that the time component was not a dominant factor in these experiments and that more likely than not, there is a high level of redundancy between PAK1 and PAK2. It is also possible that the small amount of active PAK1 that was still present was sufficient to continue phosphorylating PAK1 substrates. Unfortunately, increasing the dose of NVS-PAK1-1 would have also affected the activity of PAK2 and it would not have been possible to separate out substrates for these two kinases.

Discussion

In this work, we attempted to identify PAK1 kinase substrate sites via an array of concerted, orthogonal approaches that included chemical inhibition and selective, targeted degradation and mass spectrometry-based phosphoproteomics. In addition, we sought to augment PAK1 signaling through the use of two reported signaling agonists, constitutively active Cdc42 and epidermal growth factor. However, we consistently observed that blocking the activity of PAK1, either by chemical inhibition or by degradation, does not seem to significantly impact the phosphoproteome. One interpretation of these results is that PAK1 is not the dominant group 1 PAK kinase in the cell lines that were examined, and that PAK2 is responsible for phosphorylating most, if not all, group 1 PAK substrates. These experiments were mostly PAK1-centric and focused specifically on the effect of depleting PAK1 activity while leaving PAK2 activity unaffected, with the exception of our experiments using high dose (5μM) NVS in Su.86.86 cells. Generating an AID-PAK2 cell line would help to determine the exact role of PAK2, at least in HeLa or HEK293 cells. It is possible that acute depletion of PAK2 would result in the same set of identified substrates as inhibition of both PAK1 and PAK2 with higher concentrations (i.e. 5uM) of the allosteric group 1 PAK inhibitor NVS-PAK1-1, which would tell us that PAK2 is the more dominant of the two kinases in this context. However, it is also possible that selective depletion of PAK2 would also not result in significant downregulation in a large number of phosphopeptides, which would support substrate redundancy between PAK1 and PAK2.

A parallel approach to assess the degree of substrate redundancy between PAK1 and PAK2 would be to create CRISPR knockout cell lines for PAK1 and PAK2 separately, and to then test the effects of inhibition on each of them. By comparing PAK inhibition in a PAK1 knockout and a PAK2 knockout to PAK inhibition in wild-type cells, it should be possible to determine the extent of redundancy between the two kinases. For example, knocking out PAK2 might sensitize cells to PAK inhibition with NVS-PAK1-1, in which a 250nM treatment might be sufficient to cause a significant reduction in group 1 PAK-dependent phosphosites. This approach would have the advantage of isolating PAK1 or PAK2, allowing us to identify substrates of one in the absence of the other. However, the biggest caveat to this approach is that generating CRISPR knockouts affords time for cellular adaptation, which could conceivably alter the proteome or phosphoproteome of

PAK1 or PAK2 knockout cells, making them unrepresentative of the “baseline” proteome or phosphoproteome in the parental HeLa line. While this approach has drawbacks, generating CRISPR knockout lines for PAK1 and PAK2 is relatively straightforward and may be an effective way to compare PAK1 and PAK2 activity in many different cell lines to an extent that would be more difficult using AID-Tir1 approaches.

Another interesting approach would be combining proximity labeling tags, such as TurboID, with PAK inhibitors. A similar strategy was recently used in which the proximity labeling tag Apex2 was fused to a kinase of interest, making it possible to track changes in localization and activity of the kinase when activated by certain cellular pathways (Zhang et al., 2022). A similar approach could be applied to study the PAK kinases wherein a TurboID version of either kinase would be expressed, and cells could be treated with or without NVS-PAK1-1. This would have the added advantage of simultaneously elaborating the interactomes of both PAK1 and PAK2, which might help to explain observed redundancy. By enriching for proximal interactors before inhibition, it may also be possible to determine specific substrates for either of the two kinases. However, it is also possible that if the interactomes of PAK1 and PAK2 are highly similar, it would be difficult to accurately assign substrates to one kinase over the other.

One final approach that would be interesting to explore is the use of genome wide synthetic lethality screens. This approach relies on a library of CRISPR-Cas9 guide RNAs against the entire genome (Shalem et al., 2014; Wang et al., 2014), which can be used to identify genes that are required for cell survival in certain contexts. For example, this screen can be performed on cells grown in the presence of an inhibitor in order to identify genes that, when knocked out, sensitize the cells to the inhibitor being tested (Vit et al., 2022; Zimmermann et al., 2018). Although depletion of PAK1 does not cause obvious defects, either at the morphological level or the level of the phosphoproteome, a genome wide knockout screen performed with and without PAK1 depletion could identify genes of interest that are involved in pathways with PAK1. This would be an interesting approach to identify potential direct or indirect interactors of PAK1 and would help to highlight which pathways PAK1 is most active in.

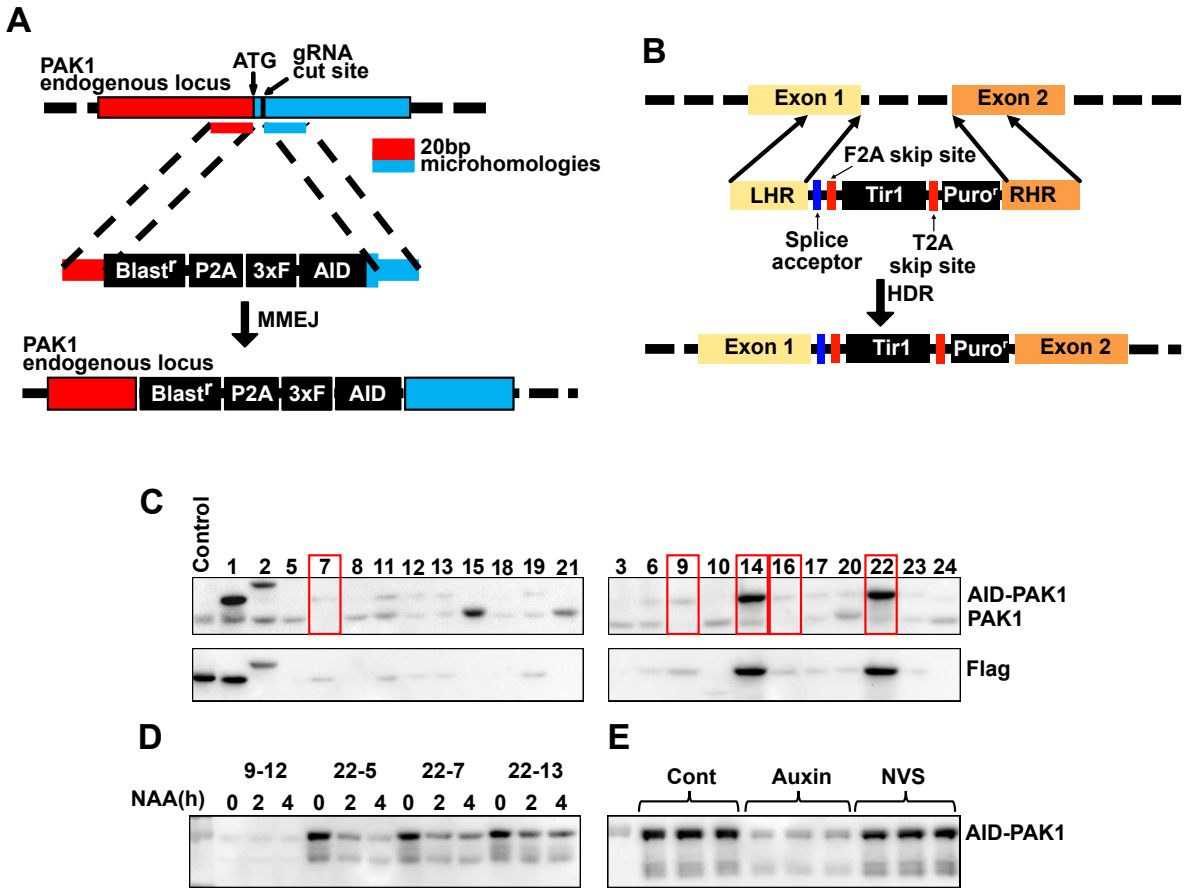

Figure 4.1: Engineering an AID-PAK1 cell line. **A)** To endogenously tag PAK1 with 3xFlag-AID, we used the CRIS-PITCh MMEJ CRISPR-Cas9 editing approach. Small, 20bp homology regions in the targeting vector promote Microhomology Mediated End Joining (MMEJ), resulting in the incorporation of a 3xFlag-AID tag to the N-terminus of PAK1, along with an antibiotic resistance cassette that allows for chemical selection of tagged clones. **B)** Tir1 is introduced to the AAVS1 safe-harbor locus using CRISPR-Cas9. This allows for relatively high and stable ectopic expression of Tir1. **C)** Clones recovered and screened by western blot after a single round of CRISPR-Cas9 and antibiotic selection in HEK293FT cells. Clones 7, 9, 14, 16, and 22 were taken as potential homozygous knock-ins. Tir1 was introduced to these clones. **D)** AID-PAK1 clones with Tir1 were screened for PAK1 degradation by western blot. Clone 22-5 was determined to have the best degradation kinetics and was taken for future experiments. **E)** Clone 22-5 was treated with 1mM auxin or 5uM NVS-PAK1-1 for 4hrs and blotted with an anti-PAK1 antibody.

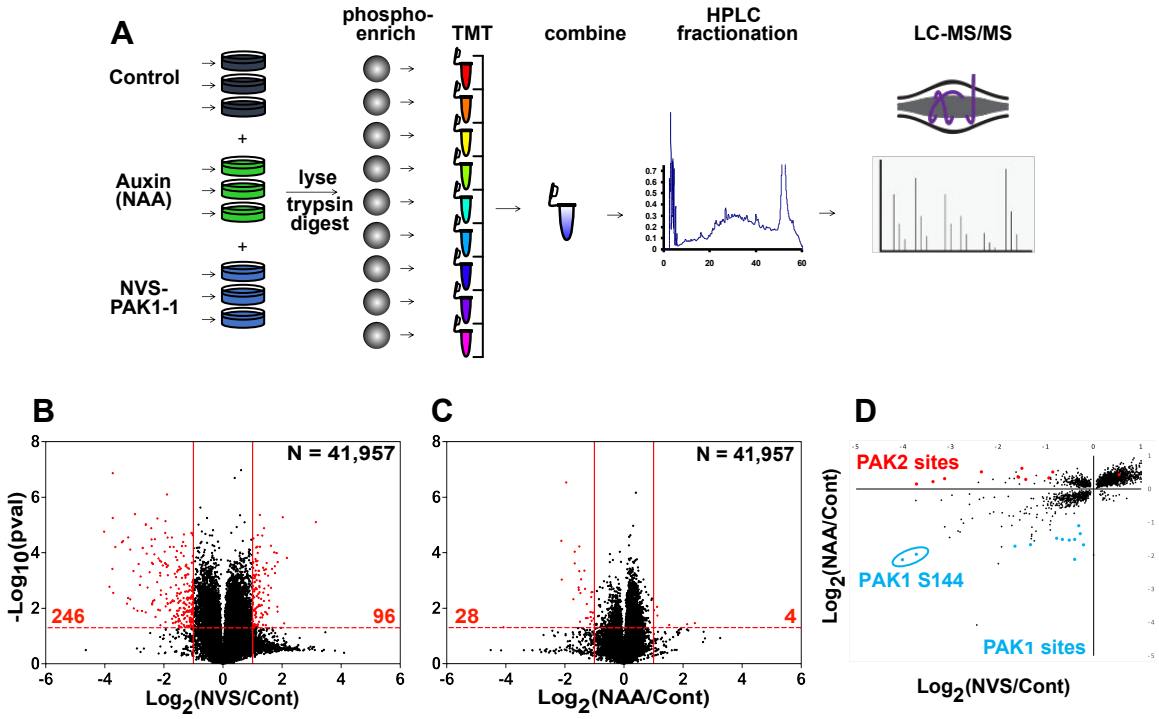

Figure 4.2: Phosphopeptides identified in PAK1 degraded (NAA) vs. PAK1 inhibited (NVS). **A)** Workflow for phosphoproteomics. 10cm dishes are treated with 1mM auxin or 5uM NVS-PAK1-1, an allosteric inhibitor of PAK1 and PAK2. The cells are collected and lysed, and the proteins are digested with trypsin. Peptide samples are enriched for phosphopeptides using Fe-NTA resin. Phosphopeptides are labeled with TMT reagent, combined, fractionated on a PFP column by HPLC, and analyzed on an Orbitrap Fusion Lumos. **B+C)** Volcano plots depicting change in phosphopeptide abundance after PAK1 inhibition (**B**) or PAK1 degradation (**C**). The $\log_2$ change in abundance is plotted against the $-\log_{10}$ of the p-value. Phosphopeptides with either $\log_2$(fold change)>1 or $\log_2$(fold change)<1 and a $-\log_{10}$(p-value)>1.3 are colored in red and are considered to be phosphopeptides that are potentially regulated by PAK1 activity. **D)** Correlation of phosphopeptides identified in PAK1 inhibited vs. PAK1 degraded with p-value<0.1. Phosphosites on PAK1 and PAK2 are highlighted in light blue and red, respectively. Phosphopeptides with the main activation site on PAK1, S144, are also circled in light blue. The low number of phosphopeptides identified upon PAK1 degradation suggested that PAK1 is not highly active in HEK293FT cells.

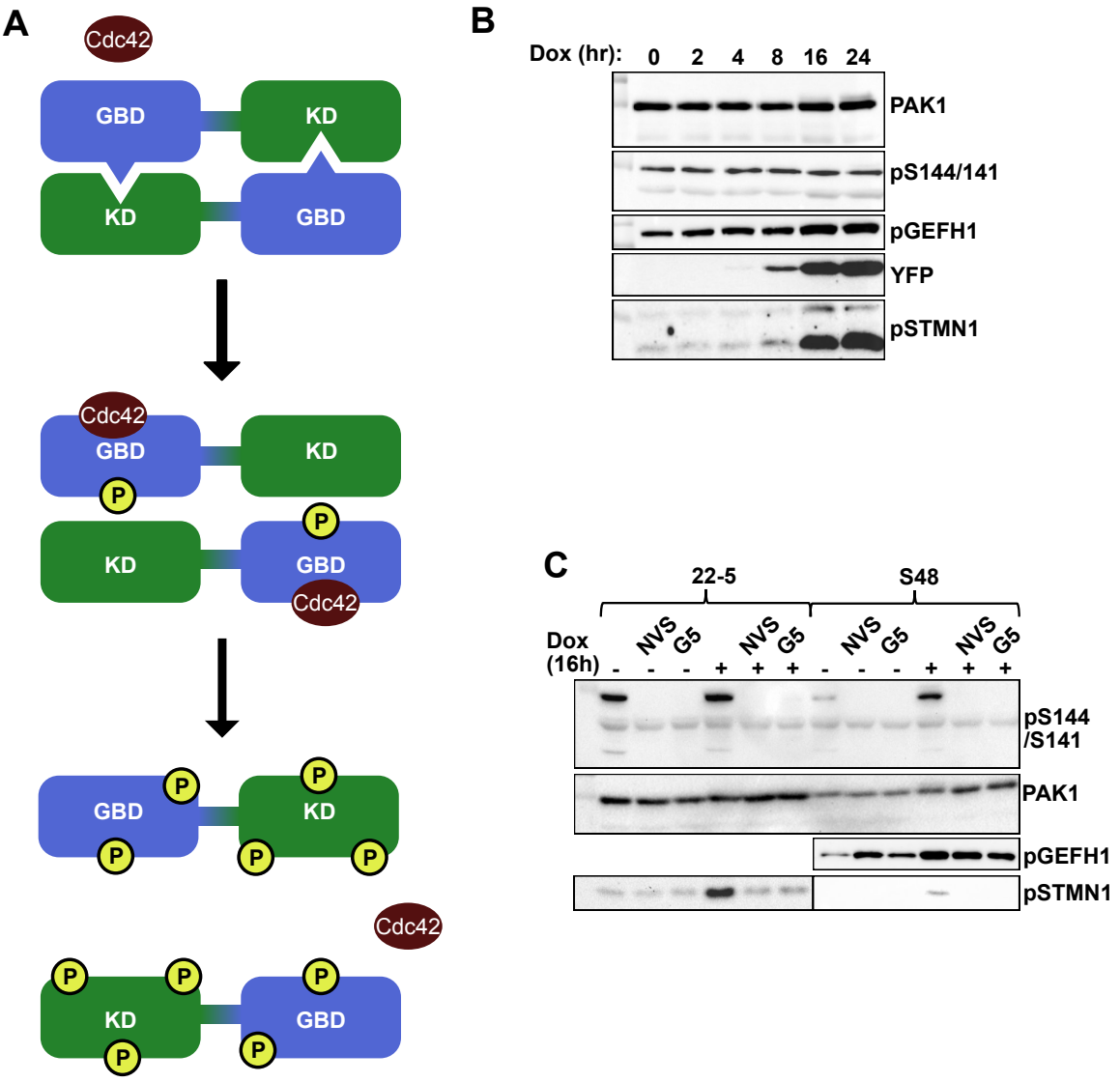

Figure 4.3: Hyper-activating PAK1 with inducible Cdc42. **A)** Cdc42 is one of the main activators of PAK1 activity. When inactive, PAK1 exists as a homodimer with the GTPase binding domain (**GBD**) of one PAK1 molecule inhibiting the kinase domain (**KD**) of the second. Cdc42 binds to GBD, releasing inhibition of the KD, and promoting autophosphorylation on the main activation site, S144. After this initial phosphorylation, PAK1 autophosphorylates on multiple sites and is stabilized as a fully active monomer, at which point Cdc42 dissociates from PAK1. **B)** We introduced constitutively active, doxycycline (Dox) inducible Cdc42 via a lentivirus. A 24hr time-course of doxycycline induction revealed a strong induction of Cdc42 expression by 16hrs, which coincided with increased phosphorylation of pSTMN1, a known PAK1 substrate, as well as a modest

increase in pGEFH1, another reported PAK1 substrate. **C)** A 16h induction of Cdc42 greatly increased pS144 PAK1 in clone S48, a subclone of the original AID-PAK1 clone 22-5. Dox induction also increased pSTMN1 and pGEFH1. Importantly, phosphorylation of these sites was decreased with a 1hr, 5uM treatment with the allosteric PAK1 inhibitor NVS-PAK1-1 (**NVS**) and the competitive inhibitor G5555 (**G5**), indicating that induced Cdc42 is able to stimulate PAK1 activity.

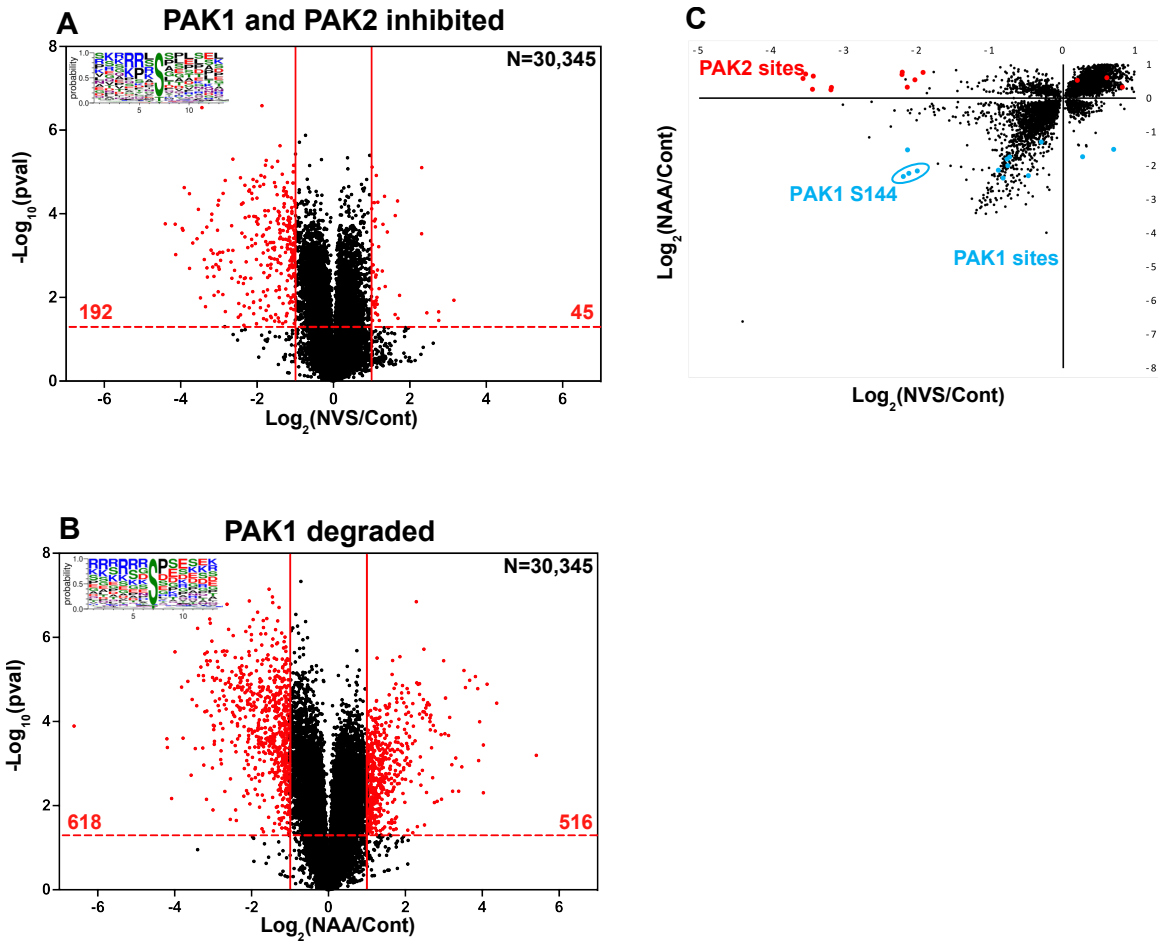

Figure 4.4: Phosphoproteomics of inhibited and degraded PAK1 in a hyper-activated PAK1 system. AID-PAK1 cells were treated with doxycycline for 16hrs to induce Cdc42 and stimulate PAK1 activity. Cells were then subjected to the same workflow outlined in figure 4.2. **A+B)** Volcano plots depicting change in phosphopeptide abundance after PAK1 inhibition (**A**, 1hr, 5uM NVS-PAK1-1) or PAK1 degradation (**B**, 4hr, 1mM NAA). As in figure 4.2, the $\log_2$(fold-change) was plotted against the $-\log_{10}$(pval). Phosphopeptides that met the significance cutoff ($\log_2$(fold-change)>1 or <1 and $-\log_{10}$(pval)>1.3) are plotted in red. Significantly decreased phosphopeptides were used to generate consensus motifs for PAK1, which are presented in the top left corner of each volcano plot and indicate an upstream, basophilic preference, consistent with previous reports. **C)** Correlation plot of

phosphopeptides identified in PAK1 inhibited (NVS) and PAK1 degraded (NAA) with a p-value<0.1. Phosphosites on PAK1 and PAK2 are highlighted in blue and red, respectively, and the main activation site on PAK1, pS144, is circled in blue.

A

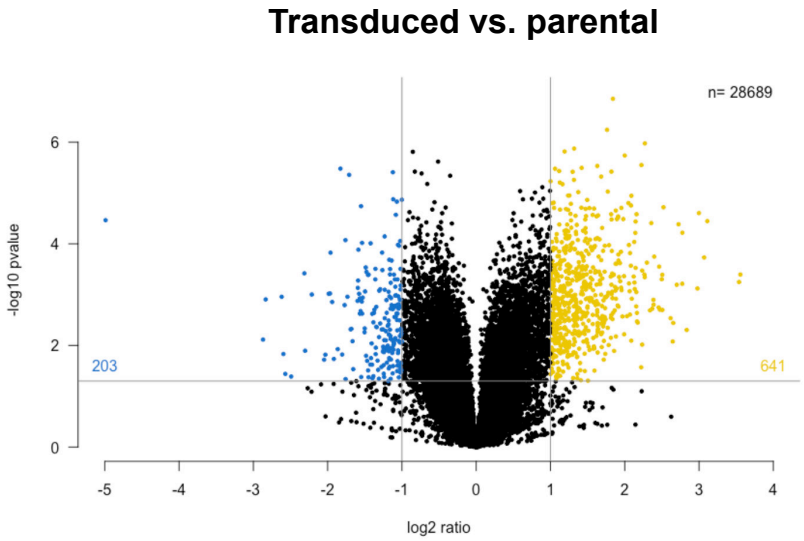
Transduced vs. parental
n= 28689
-log10 pvalue
log2 ratio
203
641

B

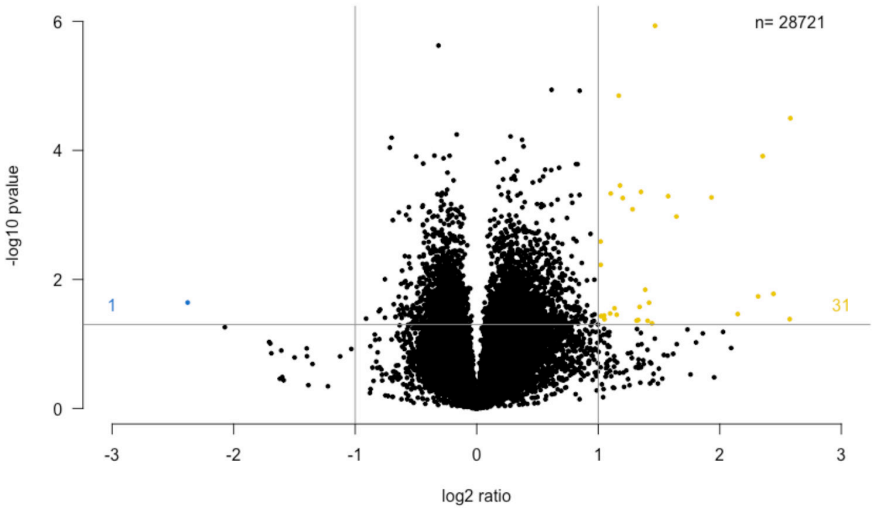
16hr Dox induction
n= 28721
-log10 pvalue
log2 ratio
1
31

C

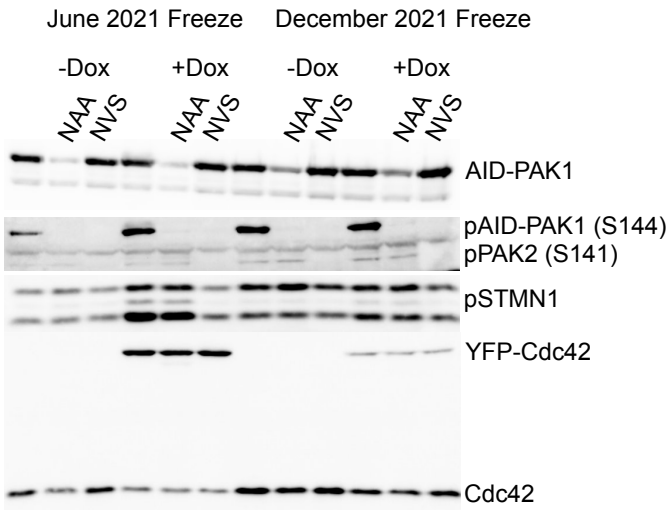
June 2021 Freeze
December 2021 Freeze
-Dox
+Dox
-Dox
+Dox
NAA
NVS
AID-PAK1
pAID-PAK1 (S144)
pPAK2 (S141)
pSTMN1
YFP-Cdc42
Cdc42

Figure 4.5: Phosphoproteomics demonstrating effects of lentiviral transduction and doxycycline induction on AID-PAK1 cells. **A)** Volcano plot depicting difference in phosphopeptide abundance in AID-PAK1 cells transduced with pCW57.1 Cdc42 lentivirus compared to parental AID-PAK1 cells. Phosphosites in blue or yellow are considered to be significantly differentially regulated between the two populations of cells. **B)** Overnight (16h) doxycycline induction of pCW57.1 Cdc42 lentivirally transduced AID-PAK1 cells shows limited change in phosphopeptide abundance despite Cdc42 induction. **C)** AID-PAK1 cells transduced with pCW57.1 Cdc42 lentivirus maintain doxycycline responsiveness but corresponding changes to phosphorylation status of canonical PAK substrates (i.e. PAK1(S144), PAK2(S141), and STMN1(S10)) have reduced response in cells maintained in culture for a longer time period.

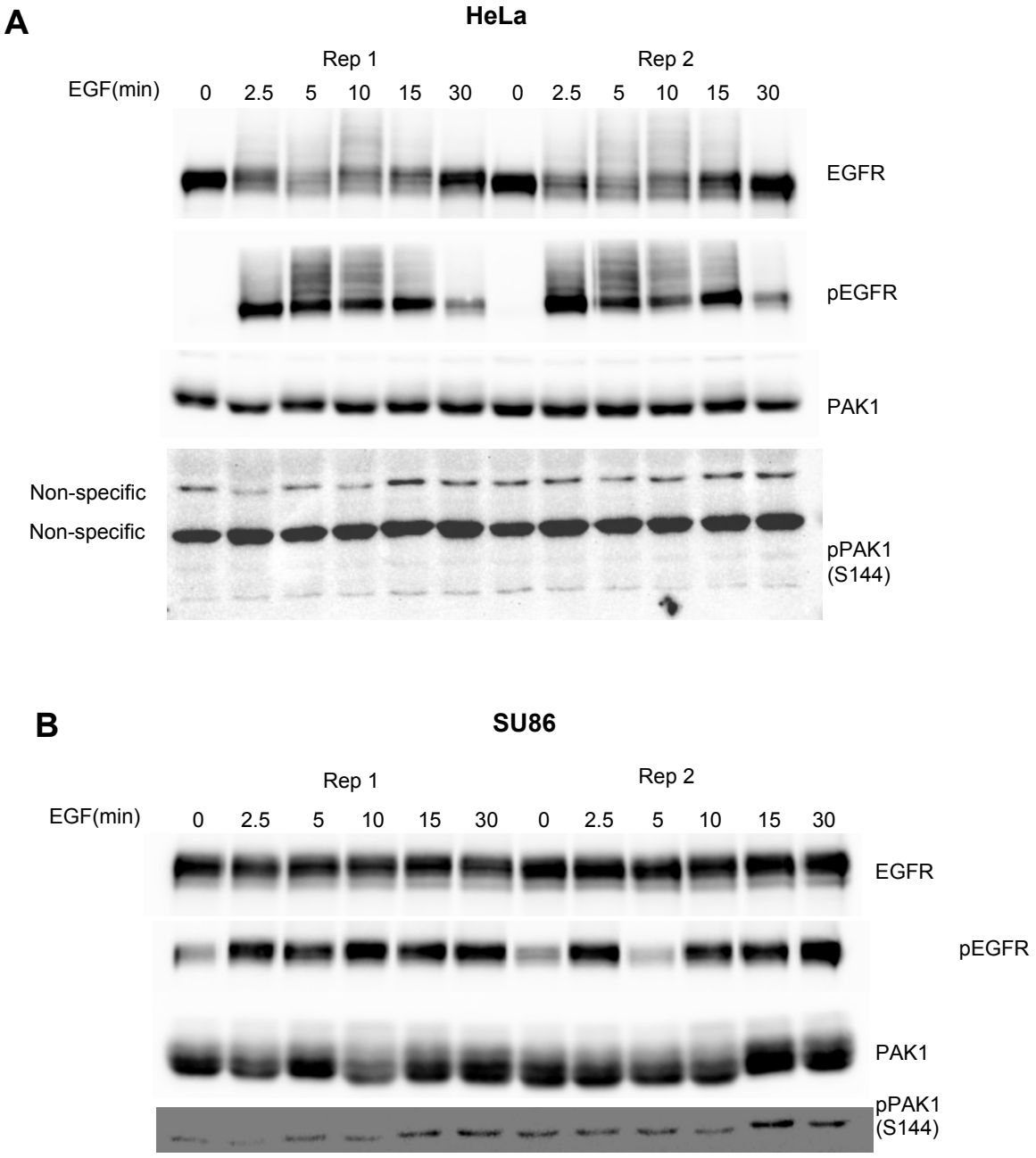

Figure 4.6: EGF stimulation of PAK1/PAK2. **A)** Western blots showing activation status of PAK1/PAK2 in HeLa cells based on S144/S141 autophosphorylation site. WT HeLa cells were treated with 1ng/mL EGF for the indicated times, lysed in place, collected, and analyzed by western blot. The rapid increase in pEGFR coupled with hyperphosphorylation and degradation of EGFR demonstrates EGF signaling cascade while no detectable increase in PAK1 pS144 was observed. **B)** The same experiment

repeated in SU.86.86 cells shows a more modest EGF response based on pEGFR and no appreciable increase in PAK1 pS144.

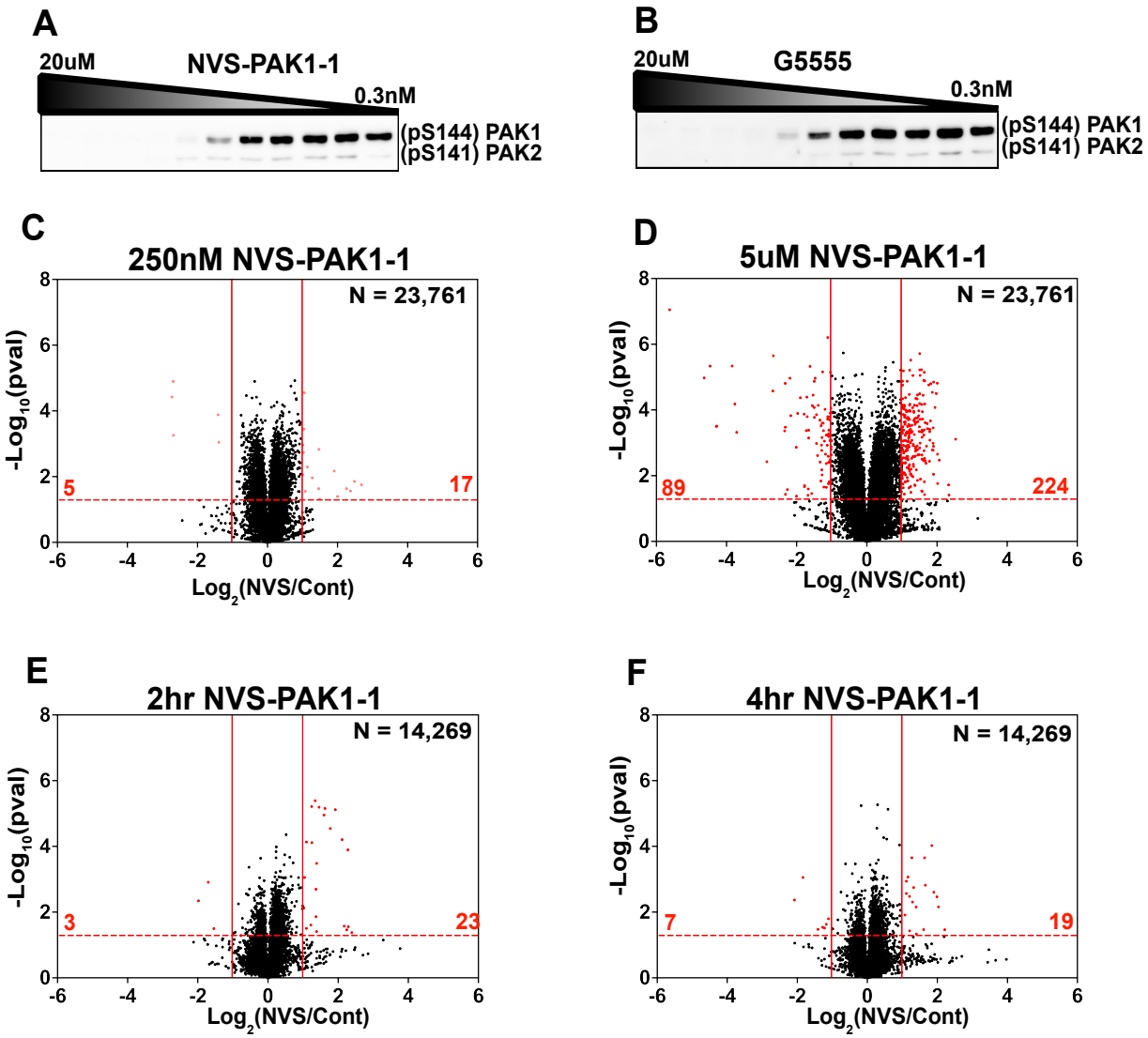

Figure 4.7: Phosphoproteomics of PAK1 inhibition in SU.86.86. **A+B)** Cells were treated for 1hr with 3-fold dilutions of PAK inhibitors G5555 (**A**) or NVS-PAK1-1 (**B**) to identify a concentration of NVS-PAK1-1 capable of inhibiting PAK1 without affecting PAK2 activity, as assessed by western blot using an antibody against pS144(PAK1)/pS141(PAK2). It was determined that 250nM NVS-PAK1-1 was the most effective intermediate concentration. **C+D)** Cells were treated for 1hr with 250nM NVS-PAK1-1 to inhibit only PAK1 (**C**) or 5uM NVS-PAK1-1 to inhibit PAK1 and PAK2 (**D**) and processed for phosphoproteomics, the results of which are shown on volcano plots. PAK1 appears to be 90% inhibited as indicated by phosphorylation status of S144, but very few phosphosites beyond PAK1 change significantly in abundance with PAK1-specific inhibition. **E+F)** PAK1 was

specifically inhibited with 250nM NVS-PAK1-1 for 2h (**E**) or 4h (**F**), processed for phosphoproteomics, and visualized in volcano plots. Longer exposure to PAK1-specific concentrations of NVS-PAK1-1 did not increase the number of identified PAK1-regulated phosphosites, suggesting that the lack of identified PAK1-regulated phosphosites is not due to slow turnover of counteracting phosphatases.

Chapter 5

Uncovering Aurora A and Aurora B substrate overlap with targeted protein degradation

Author Contributions:

C. Lincoln Howarth: Wrote text and designed figures for chapter 5. Designed, executed, and analyzed experiments.

Kate W. Carango: Assisted in execution and analysis of experiments

Scott A. Gerber: Conceptualized, designed, and analyzed experiments. Provided feedback and edits on text.

Introduction

The Aurora kinases are a family of master mitotic regulators that control fundamental processes such as mitotic spindle formation and kinetochore-microtubule (k-MT) attachments (Joukov & De Nicolo, 2018). Along with Cdk1 and Plk1, Aurora A and B coordinate major mitotic checkpoints and are among the most important drivers of mitosis. Aurora A localizes to centrosomes and spindle microtubules, where it is activated by its binding partners CEP192 and TPX2 and regulates centrosome maturation, as well as spindle microtubule formation and dynamics (Willems et al., 2018). In addition, recruitment of Aurora A to centrosomes creates a positive feedback loop with Plk1, which is essential for full activation of Cdk1/cyclin B and mitotic entry (Barr & Gergely, 2007). Aurora B, while structurally similar to Aurora A, localizes to centromeres at the center of condensed chromosomes as the catalytic component of the chromosomal passenger complex (CPC), which also includes the proteins Incenp, Survivin, and Borealin (Hochegger et al., 2013). The CPC is targeted to centromeres via the activity of Haspin, and it functions as a critical component in the spindle assembly checkpoint (SAC), phosphorylating components of the mitotic checkpoint complex (MCC) to inhibit activity of the anaphase promoting complex/cyclosome (APC/C) and prevent premature mitotic exit (Musacchio & Salmon, 2007; Willems et al., 2018). In addition, Aurora B regulates k-MT attachments by phosphorylating kinetochore proteins at improper attachments, destabilizing binding and ensuring error correction (Cheeseman et al., 2006). In anaphase, the CPC translocates to the central spindle to control resolution of cell division (Hadders & Lens, 2022). Aurora A and Aurora B are thought to have distinct localizations and regulate separate but complimentary pathways in mitosis. However, some evidence exists that Aurora A and Aurora B may have some shared substrates, despite their reported localizations.

Our lab demonstrated the use of small molecule inhibitors to study kinase-substrate relationships and to uncover novel substrates for Aurora A and B in mitosis (Kettenbach et al., 2011). This project highlighted how specific inhibitors could be used to uncover novel kinase substrates. However, this study also identified a cluster of Aurora substrates that could not be specifically attributed to either Aurora A or Aurora B activity. This raised several interesting possibilities that could not be fully addressed with small molecule inhibition: the potential for substrates that can be phosphorylated by both Aurora

A and Aurora B, or the result of off-target inhibition of the cognate Aurora kinase. More recently, we pioneered the use of AID-Tir1 targeted protein degradation as a strategy to investigate kinase-substrate relationships (Hards et al., 2021). This approach relies on CRISPR-Cas9 gene editing to fuse an auxin-inducible degron (AID) to a protein of interest and ectopic expression of the F-box protein Tir1. The addition of auxin to this system results in rapid ubiquitination and degradation of the fusion protein. This strategy can be used to precisely control the activity of a kinase of interest in a manner analogous to inhibition with small molecules. To address the questions surrounding potential Aurora A and Aurora B substrate overlap, we hypothesized that AID-Tir1 targeted protein degradation could be used to acutely deplete Aurora A or B in a genetically selective manner and reassess the Aurora-dependent phosphoproteome.

We recently developed an experimental workflow to rapidly generate AID-kinase cell lines with fast degradation kinetics using a combination of fluorescent reporter proteins and fluorescence-activated cell sorting (FACS), described in detail in chapter 4 of this thesis. In prior efforts, we sought to generate AID-Aurora A cell lines to study Aurora A signaling, but we were unable to create these cell lines using our previous antibiotic selection CRISPR-Cas9 methods. These challenges provided an ideal opportunity to demonstrate the speed and utility of this FACS-based workflow, and to simultaneously gain insight into Aurora biology. We therefore applied our improved gene editing workflow to make AID-Tir1 cell lines for Aurora A and Aurora B in order to interrogate the Aurora-dependent phosphoproteome. In addition, the availability of selective Aurora inhibitors presented an opportunity to compare targeted protein degradation to previously used methods and to reassess the extent of previously reported Aurora substrate overlap.

Methods

Cell culture and cell lines

HeLa cells were grown in Dulbecco's Modification of Eagle's Medium (DMEM, Corning) supplemented with 8% fetal bovine serum (FBS, Hyclone) and 1% penicillin-streptomycin (100IU/mL penicillin and 100µg/mL streptomycin, Corning) and incubated at 37C with 5% CO_2.

HeLa cells are used as a model organism because they are amenable to CRISPR-Cas9 cloning, as well as selection and sorting by FACS. In addition, HeLa cells can be efficiently arrested in mitosis with a variety of reagents, including taxol, nocodazole, and STLC.

Cell cycle synchronization and mitotic arrest

Cells were plated to 50% confluency and were treated with thymidine for 20hrs (2mM, Sigma). Thymidine-containing media was washed out, cells were washed once with PBS, and fresh media was added for 4hrs. Cells were arrested with taxol (100nM), nocodazole (250nM-500nM), or S-Trityl-L-cysteine (STLC, 10µM) for 16hrs. Arrested cells were then subjected to auxin-induced degradation or kinase inhibitor treatment, collected by mitotic shake-off, washed, snap-frozen in liquid nitrogen.

Fluorescence-activated cell sorting

Cells to be analyzed were collected by trypsinization, washed once with PBS (Corning), and resuspended in 2mL PBS in 15mL conical tubes where they were kept on ice until sorting. Analysis and collection were performed on a Sony SH800S cell sorter using a 100µm microfluidic sorting chip. Cells were initially gated on forward scatter (FSC) and back scatter (BSC) to ensure a homogenous population of cells. Untransfected controls were used to establish baseline fluorescence and set up gates for collection. Cells were collected to using the ultra-purity collection mode.

CRISPR-Cas9 AID-Aurora B homologous recombination clone generation

3xFlag-AID-AurKB and AurKB-3xFlag-AID targeting constructs were designed around the start or stop codon based on the Aurora B genomic sequence from UCSC genome browser. 500bp homology arms, as well as the inserts, were ordered as g blocks (IDT) and assembled in pBluescript (see **Figure 5.1** and **Figure 5.5** diagrams of the completed targeting vectors). sgRNAs were designed based on scoring from CRISPOR.tefor.net and were cloned into the U6 site of the Cas9 expressing vector pX330. The homology arms of the Aurora B targeting vector were designed to be resistant to all sgRNAs used in these experiments.

For transfection, WT HeLa and degrading Tir1-BFP cells (described in chapter 4) were plated to 6-well dishes at ~50% confluency in media free of penicillin/streptomycin. 1.4µg of CRISPR targeting vector was mixed with 0.4µg of pX330 sgRNA in Jetprime and Jetprime transfection buffer (Polyplus) and incubated at room temperature for 10 minutes as per manufacturer protocol. The transfection mix was added dropwise to each well and incubated overnight. After 16hrs of incubation, the media was washed off and exchanged for media containing penicillin/streptomycin. Cells were expanded to 10cm dishes on the third day and harvested for analysis and sorting by FACS on the fourth day. Collection gates were determined by comparing mRuby3 intensity in transfected to untransfected controls and cells with the highest mRuby3 intensity were collected to 96-well dishes. Clones were cultured for 2 weeks until confluent in 96-well dishes, expanded to 24-well dishes, harvested, and analyzed for AID-tag knock-in by western blotting.

N-terminally tagged AID-Aurora B cells, which were generated starting from WT HeLa, had $Tir1^{Mut}$-BFP introduced to the AAVS1 safe-harbor locus as described in chapter 4. Briefly, AID-Aurora B cells were transfected with the AAVS1-Tir1-BFP targeting vector, selected with 1µg/mL puromycin, collected as a pool, sorted based on BFP intensity to 96-well dishes, and screened for auxin-induced degradation by western blot.

Auxin degradation time-course experiments

3xFlag-AID-AurKB cells were treated with 1µM 5-Phenyl-indole-3-acetic acid (5phIAA, MedChem Express) (Yesbolatova, Saito, Kitamoto, et al., 2020) for the indicated

time points. AurKB-AID-3xFlag cells were treated with 1mM naphthalene-acetic-acid (NAA, Sigma). After treatment, cells were collected, washed in PBS, lysed in 2x Lamelli, and analyzed by western blot.

Western Blotting

Cells to be analyzed by western blot were collected, washed once in PBS, and lysed in 2x Lamelli. Poly-acrylamide gels were poured in house from a 30% acrylamide solution (Protogel, National Diagnostics). Gels were run at 140V for 80 minutes in running buffer containing 25mM Tris, 200mM glycine, and 1% SDS. The gels were then transferred to nitrocellulose blotting membrane (Amersham Protran) at 100V for 60 minutes in a transfer buffer containing 25mM Tris, 200mM glycine, and 20% MeOH. To account for loading, blots were briefly stained with ponceau (0.01% ponceau, 0.5% acetic acid) and imaged. Blots were washed in TBST (50mM Tris, 150mM NaCl, 0.2% Tween-20), blocked for 30 minutes and incubated overnight with primary antibody at 4C. Finally, blots were incubated with an HRP-conjugated secondary antibody for 1hr at room temperature, treated with Clarity ECL substrate (BioRad) and imaged. A solution of 4% milk in TBST was used for blocking, and incubation in primary and secondary antibodies. For phospho-specific antibodies, the phosphatase inhibitors β-glycerophosphate (5mM), sodium fluoride (5mM), and sodium molybdate (5mM) were added.

AurKB isoform-specific flag IP

Full-length and Δ41 AurKB were amplified by PCR using the following primers (Full-length forward: 5' AATAAACTAATCGAATTCATGGCCCAGAAGGAGAAC 3'; Δ41 forward 5' AATAAACTAATCGAATTCATGAGCCGCTCCAATG 3'; AurKB reverse: 5' TGATTTCATATGGTACCGGCGACAGATTGAAGGGC 3') and ligated into a C-terminal tagged pCMV expression vector. 1μg of vector was transfected into HeLa and 293 cells following the JetPrime transfection protocol (Polyplus). Two days after transfection, cells were expanded to 10cm dishes and selected with G418 400μg/mL for 2 weeks to generate stable cell lines.

For Flag immunoprecipitation (IP) interactomic experiments, triplicates of Full-length and Δ41 AurKB stable HeLa and 293 cells were cultured in 15cm dishes, synchronized in thymidine, and arrested with taxol as described above. Cells were collected by mitotic shake-off, washed, and lysed on ice with 1mL IP lysis buffer (50mM Tris pH 7.5, 200μM DTT, 400mM NaCl, 1% Triton X-100, 5mM β-glycerophosphate, 2mM sodium fluoride, 2mM sodium molybdate, 5mM $MgCl_2$, and a protease inhibitor cocktail) by sonicating 3x10 seconds at 15% power on a Branson sonicator equipped with microtip. Lysates were cleared by rotating at 4C for 1hr, the centrifugation at 21,000g for 10 minutes at 4C. Lysates were incubated with anti-Flag agarose beads (Sigma) for 3hrs at 4C. Beads were pelleted, washed 3x in wash buffer (20mM Hepes pH 7.7, 250mM KCl, 1mg/mL Chaps, 5mM $MgCl_2$, 200μM DTT, 5mM β-glycerophosphate, and a protease inhibitor cocktail), and eluted in elution buffer (20mM Hepes pH 7.7, 100mM NaCl, 1mg/mL Chaps, 5mM $MgCl_2$, 5mM β-glycerophosphate, and a protease inhibitor cocktail) containing flag peptide by shaking in a thermomixer at 24C, 1500rpm, for 20 minutes. Eluted proteins were purified by SP3 isolation as described previously (Hughes et al., 2019), digested to peptides in 50mM ammonium bicarbonate with sequencing grade trypsin (Promega), and desalted by the stop-and-go-extraction (STAGE-tip) method (Rappsilber et al., 2003). LC-MS/MS analysis was performed using a 120-minute gradient on an Orbitrap Fusion Lumos as described below.

ndCyclinB cloning and lentiviral production

Wild-Type Cyclin B2 (WTCyclinB) and non-degradable Cyclin B2 (R42A+L45A double-mutant, ndCyclinB) sequences were ordered from Twist Biosciences and cloned into pCW57.1. To generate lentivirus, 293 cells were cultured in 10cm dishes at 50% confluency and transfected with pCW57.1-ndCyclinB or pCW57.1-WTCyclinB, along with CMV-VSVG and psPAX2 plasmids, using the JetPrime transfection protocol (Polyplus). The media was exchanged for fresh media on day 2 and lentiviral media was harvested on days 3-5. Lentivirus media was centrifuged to remove cellular debris, aliquoted, and snap-frozen in liquid nitrogen.

For viral transduction, AurKB-AID-3xFlag Tir1-BFP cells were cultured in 10cm dishes at 50% confluency and were incubated with ndCyclinB or WTCyclinB lentivirus media containing 4μg/mL polybrene. The following day, cells were washed 4x with PBS

and fresh media was added. On the third day, 30µg/mL puromycin was added to select for viral transduction (a higher-than-normal concentration of puromycin was necessary as these cells already had a puromycin resistance cassette from insertion of Tir1-BFP) and selection was continued for 2 weeks until colonies had formed, and cell death had stopped. Doxycycline (1µg/mL) was added overnight to test for induction efficiency, which was assessed by noting the percentage of cells that were arrested in mitosis.

Phosphoproteomic TMT experiments

For the AID-AurKB experiments shown in Figure 5.3 and AurKB-AID experiment shown in Figure 5.5 and Figure 5.6, cells were cultured in 10cm plates at 50% confluency, synchronized with thymidine, and mitotically arrested with taxol as described above. Cells were treated in triplicate with DMSO or 1µM 5phIAA for 1hr (3xFlag-AID-AurKB), or were treated with 1mM NAA, 5µM MLN8054 (Millennium) or left untreated (control) for 2hrs (AurKB-AID-3xFlag). Cells were harvested by mitotic shake-off, washed with PBS, and snap-frozen in liquid nitrogen.

For the AurKB-AID experiment shown in Figure 5.11 and on, cells were plated on 15cm dishes at 50% confluency, synchronized with thymidine, and arrested overnight with STLC (Sigma-Aldrich). In triplicates, plates were treated with 1mM NAA for 1 hour, 2µM AZD1152 (AZD1152-HQPA, Selleckchem), 1µM MLN8054, or 5µM MLN8054 for 45 minutes. Cells were collected by mitotic shake-off, washed with PBS, and snap-frozen in liquid nitrogen. Additionally, 5% of the cell suspensions were collected separately for analysis by western blot.

Cell pellets were partially thawed on ice and resuspended with 1.6mL of a lysis buffer containing urea (8M, AMRESCO), NaCl (100mM, Fisher), Tris pH 8.1 (50mM, Alfa Aesar), protease inhibitor (RPI protease inhibitor cocktail III, mammalian), and phosphatase inhibitors β-glycerophosphate (2mM, Sigma), sodium fluoride (2mM, Fluka), and sodium molybdate (2mM, Sigma). Lysates were sonicated 3x10 seconds at 15% power on a Branson sonicator equipped with a microtip. Protein concentration was determined with a protein BCA assay kit (ThermoFisher). Samples were centrifuged at max speed at 4C for 10 minutes and the supernatant was collected. Lysates were reduced with dithioretitol (DTT, 5mM, Sigma) for 20 minutes at 55C, cooled to room temperature,

and alkylated with iodoacetamide (15mM, Sigma) in the dark for 1hr. The alkylation was quenched with DTT (5mM) for 15 minutes at room temperature in the dark. Finally, lysates were diluted to 10mL total with a buffer containing 25mM Tris pH 8.1, 100mM NaCl, and 20µg sequencing grade trypsin (Promega) and incubated overnight at 37C. Digested peptides were acidified to pH< 3 with 125µl 20% trifluoroacetic acid (TFA, Honeywell). 600µl of MeOH was added and samples were incubated at room temperature for 10 minutes and centrifuged at 5,000g for 5 minutes to pellet insoluble material. The peptide digest solutions were desalted on a 60mg Oasis desalting plate (Waters). 40µg of desalted peptides were saved for proteomic analysis and the remainder of the peptide solutions were partially dried in a vacuum centrifuge at 35C for 30 minutes, frozen at -80C, and lyophilized overnight. Dried peptides were resuspended in 50% acetonitrile/0.1%TFA and enriched for phosphopeptides with the High-Select Fe-NTA phosphopeptide enrichment kit (ThermoFisher). Eluted phosphopeptides were dried in a vacuum centrifuge and desalted on a 2mg Oasis µElution plate (Waters) and vacuum centrifuged to dryness.

Dried phosphopeptides were resuspended in 166mM EPPS pH 8.5 and 70µg of the corresponding TMT channel was added to each sample, which were incubated at room temperature for 1 hour. The reactions were quenched with hydroxylamine for 15 minutes, acidified with 1% TFA, mixed into a single sample tube, and desalted on a 10mg Oasis plate (Waters). The eluted, labeled phosphopeptides were dried in a vacuum centrifuge and separated to 48 fractions by HPLC using a pentafluorophenyl (PFP) column as previously reported (Grassetti et al., 2017). The separated fractions were concatenated into either 16 or 24 fractions, depending on peptide abundance as determined by HPLC and were analyzed by mass spectrometry as described below.

LC-MS/MS analyses

LC-MS/MS analysis was performed as previously described (Hards et al., 2021) on an Orbitrap Fusion Lumos Tribrid mass spectrometer (ThermoFisher) equipped with an EASY-nLC 1000 ultra-high pressure liquid chromatograph (ThermoFisher). Samples were dissolved in loading buffer (5% methanol/1.5 % formic acid) and injected directly onto an in-house pulled, polymer coated, fritless, fused silica analytical resolving column (35 cm length, 100µm inner diameter; PolyMicro) packed with ReproSil, C18 AQ 1.9 µm 120 Å pore stationary phase particles (Dr. Maisch). Peptides and phosphopeptides were

loaded at 450 bar by chasing on to the column with 8µl loading buffer. Samples were separated with a 120-minute gradient of 4 to 33% LC-MS buffer B (LC-MS buffer A: 0.125% formic acid, 3% ACN; LC-MS buffer B: 0.125% formic acid, 95% ACN) at a flow rate of 330 nl/minute. The instruments were operated with an Orbitrap MS1 scan at 120K resolution and an AGC target value of 500K. The maximum injection time was 100 milliseconds, the scan range was 350 to 1500 m/z and the dynamic exclusion window was 15 seconds (+/- 15 ppm from precursor ion m/z). Precursor ions were selected for MS2 using quadrupole isolation (0.7 m/z isolation width) in a “top speed” (2 second duty cycle), data-dependent manner. MS2 scans were generated through collision-induced dissociation (CID) fragmentation (35% CID energy) and either linear ion trap analysis (Rapid setting) for peptides or Orbitrap analysis at 30K resolution for phosphopeptides. Ion charge states of +2 through +4 were selected for HCD MS2. The MS2 scan maximum injection time was 60 milliseconds and AGC target value was 60K. For TMT runs, top 8 MS2 peaks were dynamically isolated and further fragmented by higher-collision energy (HCD) at 55% via SPS-MS3 for quantification of liberated reporter ions (110 – 500 m/z).

Peptide spectral matching and bioinformatics

Peptide spectral matching was performed as previously reported (Hards et al., 2021). Raw data were searched using COMET against a target-decoy version of the human (*Homo sapiens*) proteome sequence database (UniProt; downloaded 2018; 20,241 total proteins) with a precursor mass tolerance of +/- 1.00 Da (Hsieh et al., 2010) and requiring fully tryptic peptides with up to 3 missed cleavages, carbamidomethyl cysteine as a fixed modification and oxidized methionine as a variable modification. For phosphopeptide data, searches were expanded to include the dynamic addition of phosphate to serine, threonine, and tyrosine residues. For TMT-labeled samples, the mass of the TMT reagent (229.162932 Da for TMT11, 304.2071 Da for TMTPro ragents) was added as a static modification to all peptide N-termini and lysine residues. Phosphorylation of serine, threonine and tyrosine were searched with up to 3 variable modifications per peptide, and were localized using the phosphoRS algorithm (Taus et al., 2011). The resulting peptide spectral matches were filtered to ≤1% false discovery rate (FDR) by defining thresholds of decoy hit frequencies at particular mass measurement accuracy (measured in parts per million from theoretical), XCorr and delta- XCorr (dCn)

values. Statistical analyses and data visualization were performed in excel, GraphPad Prism, and R.

Results

N-Terminal endogenous tagging of Aurora B

We designed and generated an N-terminal Aurora B CRISPR-Cas9 targeting vector to endogenously append a 3xF-AID tag to Aurora B (**Figure 5.1A**) using the fluorescent reporter approach described in chapter 3. This construct was transfected into WT HeLa cells, as well as pools of degrading $Tir1^{WT}$-BFP and $Tir1^{F74G}$-BFP HeLa cells created in chapter 3. Using Fluorescence Activated Cell Sorting (FACS), single cells were collected in 96-well dishes based on mRuby3 intensity, expanded to 24-well dishes, and screened for AID tag insertion by western blot. Although we were unable to recover homozygous knock-in clones in Tir1-BFP cells, we did identify homozygous knock-in clones in WT HeLa cells (data not shown). These clones were expanded and transfected with the AAVS1-Tir1-BFP targeting vector, selected with puromycin, and sorted to single cells based on BFP intensity. Clones were expanded to the 24-well stage and screened for degradation by treating +/- Auxin for two hours. Clones that degraded the most Aurora B within the two-hour timepoint were expanded and subjected to a time-course experiment to better analyze degradation efficiency and kinetics (**Figure 5.1B**). Remarkably, the clones tested in this time-course experiment were able to degrade Aurora B to >95% within 60 minutes.

We sought to determine if acute Aurora B depletion resulted in noticeable cell cycle-related defects. Typically, Aurora B inhibition results in an override of the SAC, leading to DNA segregation defects after one or two cell doublings, eventually resulting in polyploidy and abnormally large nuclei and cells (Hauf et al., 2003). To monitor for this in cells with degraded Aurora B, we performed live-cell imaging and tracked cells for up to 48 hours by DIC in the presence and absence of auxin (data not shown). However, AID-Aurora B depletion did not result in mitotic arrest, cell death, or any observable change in cellular morphology. To ensure that this was not due to the stress caused from the live-cell imaging experiment itself, we also maintained a culture of cells in auxin in the incubator and tracked changes to morphology on a phase-contrast screening microscope daily over a two day time course. Again, as before, cells appeared to divide normally and no noticeable changes in morphology or growth rate were observed. After AID-Aurora B cells were maintained in auxin either under the microscope or in the incubator for 48 hours,

they were collected for analysis by western blot (**Figure 5.2A**). We were able to verify that Aurora B remained completely degraded at this timepoint, suggesting that the results were not due to a lack of Aurora B degradation. Finally, to ensure that this was not the effect of the specific clone we were working with, we maintained 12 different AID-Aurora B clones in auxin in the incubator. None of the clones tested showed a growth defect, morphological change, or cell cycle arrest during culture in the presence of auxin. We also analyzed the effect of Aurora B depletion on a well characterized Aurora B substrate, H3S10, and found that Aurora B degradation did not cause a reduction in H3S10 phosphorylation as is typically observed (**Figure 5.2B**). We did, however, observe a slight reduction in phosphorylation with Aurora B inhibition by AZD1152.

Despite the lack of changes to cell morphology or ploidy, we decided to perform a phosphoproteomics experiment to determine the effects of AID-Aurora B degradation with higher precision. Briefly, AID-Aurora B cells were synchronized with thymidine, arrested with Taxol, and treated with auxin for one hour, resulting in nearly complete degradation as assessed by western blot (**Figure 5.3A**). Cell pellets were lysed, trypsin digested to peptides, enriched for phosphorylated peptides, TMT labeled, fractionated, and analyzed by LC-MS/MS. The results of this phosphoproteomics experiment showed that depletion of AID-Aurora B caused almost no notable effects to the phosphoproteome (**Figure 5.3B**), and we were unable to detect any potential Aurora B substrates. Notably, the only site on Aurora B itself that was significantly downregulated was T35 in the N-terminus of Aurora B. Given that Aurora B is being degraded, we would expect almost all phosphopeptides on Aurora B to decrease in abundance. However, other phosphopeptides on Aurora B were not observed to change significantly. This includes the main auto-catalytic phosphorylation site on Aurora B, T232. This is strong evidence that, despite the fact that we could see Aurora B degrade by western blot, there was still an active population of Aurora B in these cells that was confounding the experiment.

Given that Aurora B Thr232 was not changed significantly based on phosphoproteomics, we hypothesized that a population of Aurora B that is resistant to auxin-induced degradation could be present in these cells. To address this, we performed a proteomics experiment on the same samples in order to analyze change in the abundance of proteins, rather than phosphorylation sites. Despite an exceptionally deep dataset with nearly 80,000 peptides identified, the only two Aurora B peptides that were detected were in the middle region of Aurora B (125-147 and 200-215), neither of which

was observed to change significantly (**Figure 5.3C**). A peptide in the N-terminus that could corroborate the significant downregulation of T35 observed in the phosphoproteomics experiment was not observed. Importantly, the western blot results and the results of the proteomics and phosphoproteomics experiments were all derived from samples from the same experiment. Thus, the results of our proteomics experiments and western blotting were not in agreement.

One explanation for the lack of changes to the phosphoproteome with Aurora B degradation in mitotically arrested cells is the presence of an alternative Aurora B isoform that is not recognized by western blotting. While full-length Aurora B is generally thought to be the only form of Aurora B, we were surprised to discover a previously annotated Aurora B cDNA that is missing the first 41 amino acids, which is thought to be the result of an alternative translational start site (Ota et al., 2004). However, aside from this one publication describing the large-scale annotation of ~15,000 cDNAs in the human genome, there are no studies specifically describing or characterizing an N-terminal truncation of Aurora B. Upon further review of the manufacturer's information, we note that the antibody used to assess Aurora B degradation by western blot was raised against the first 20 amino acids of Aurora B, and thus the short Aurora B isoform is not detectable by this antibody. We therefore reasoned that because the shorter isoform is missing the first exon of Aurora B, it would be expressed without the AID tag and would not be degradable. Experiments conducted with an antibody raised against the C-terminus of Aurora B (Bethyl) detect a second, truncated Aurora B isoform (**Figure 5.3D**), thus confirming our hypothesis that a second Aurora B isoform was compensating for Aurora B degradation in N-terminally tagged AID-Aurora B cells. Furthermore, in later CRISPR-cas9 tagging experiments targeting the C-terminus of Aurora B, this lower band increased in mass along with full-length Aurora B, indicating that it is a true Aurora B isoform.

Following up on the identification of a truncated Aurora B, we sought to determine if there were functional differences between the two isoforms. One hypothesis is that the two Aurora B isoforms could localize differently or interact with members of the CPC with different affinities. To address these questions, we generated 3xF-Aurora B constructs for both the long (full-length) and short (Δ41) isoforms and used them to generate HeLa and 293T cells stably expressing Flag-tagged variants of either isoform of Aurora B. When anti-Flag immunoprecipitations were performed with lysates from mitotically arrested cells from these cell lines, we were unable to detect significant differences in binding between

the two isoforms (**Figure 5.4A**) in HeLa cells. Most notably, the key protein components of the chromosomal passenger complex were pulled down in roughly equal amounts for both isoforms. This suggests that, in HeLa cells, the loss of the Aurora B N-terminus does not affect the interactome, and that localization is not likely to be different as Aurora B is targeted to centromeres as part of the CPC. On the other hand, Flag IP experiments performed in stable cell lines in 293Ts showed variable binding between the long and short Aurora B isoforms, particularly for members of the CPC (**Figure 5.4B**). Interactome experiments using full-length Aurora B identified almost twice as much INCENP and 5-10x more survivin and borealin as when done using Δ41 Aurora B. One key difference between the experiments performed in HeLa and 293 cells was the extent of Aurora B overexpression (**Figure 5.4C**). In HeLa cells, Aurora B-3xFlag was downregulated below the level of endogenous Aurora B, while in 293Ts both isoforms were expressed well above the level of endogenous Aurora B, which could account for the differences in Aurora B interactions seen in these two cell lines. However, it is possible that the results from 293T cells suggest that the N-terminal domain of Aurora B is able to promote more stable interactions with other components of the CPC and that full-length Aurora B may be preferentially recruited to centromeres, while Δ41 Aurora B is part of a more soluble, cytoplasmic population of Aurora B. It is also possible that, while the long and short isoforms do not appear to play separate roles in HeLa cells, the differences in the Aurora B isoform interactomes could be related to pathways that are active or inactive in HeLa cells compared to 293Ts.

C-Terminal tagging of both Aurora B isoforms

Regardless of the potential for differential functions of the two Aurora B isoforms, identification of Aurora B substrates by inducible degradation requires homozygous knock-in of an AID tag for all forms of the kinase. In order to fully tag Aurora B, it was necessary to target the C-terminus to append the AID tag to both isoforms. To adapt our targeting strategy for C-terminal tagging, we designed a new targeting vector with homology arms recognizing regions 500bp upstream and downstream of the Aurora B stop codon to promote homology directed repair after Cas9-induced DSBs (**Figure 5.5A**). The internal tagging components, AID-3xF-P2A-mRuby3, were cloned in between the homology arms to ensure incorporation to the endogenous locus after HDR. This approach is analogous

to the N-terminal targeting strategy described earlier and makes use of mRuby3 as a fluorescent reporter to sort out single cells by FACS.

We introduced this targeting vector, along with pX330 to express Cas9 and an sgRNA, into degrading Tir1^{WT}-BFP HeLa cells collected previously (see chapter 4) and wild-type HeLas. Five sgRNAs were designed, cloned into pX330, and tested for their ability to promote HDR through CRISPR tagging experiments. The efficiency of these C-terminally targeting sgRNAs was lower than N-terminal sgRNAs, suggesting a difference in locus accessibility or amenability to CRISPR-Cas9 editing. In total, we screened 350 Tir1-BFP colonies by western blot to check for tag incorporation and identified 2 clones, 1-17 and 2-77, that appeared to be homozygous knock-ins (**Figure 5.5B**). Importantly, it appears that the amount of Aurora B in these clones is reduced compared to WT HeLa cells. This could be the result of two different mechanisms. It's possible that recombination occurred at a single allele, while indels resulted in knockouts at the other alleles, resulting in a lower copy number of Aurora B. Another explanation is that Aurora B is reduced by auxin-independent degradation, maintaining Aurora B expression at lower than physiological levels in Aurora B-AID cells. To validate degradation efficiency, we performed auxin time-course experiments which revealed that that clone 2-77 degrades to 90% within 60mins while clone 1-17 is not able to degrade Aurora B (**Figure 5.5C**).

After developing and validating a degrading Aurora B-AID clone, we performed a phosphoproteomics experiment to analyze the effects of acute Aurora B depletion. For this experiment, cells were synchronized with thymidine, arrested in mitosis with overnight Taxol treatment, and treated for 2 hours with either auxin or 5μM MLN8054, a concentration high enough to inhibit Aurora A and B. After treatment, cells were collected, lysed, and processed for proteomics and phosphoproteomics. Aurora B depletion resulted in a significant decrease of 3362 phosphopeptides (**Figure 5.6A**), exhibiting a strong enrichment for SP and TP phosphorylation sites (**Figure 5.6B**), the known phosphorylation motif for CDK1/Cyclin B in mitosis. The rapid and extensive turnover of CDK1 phosphorylation sites indicates an activation of the phosphatases PP1 and PP2A that drive mitotic exit (Holder et al., 2020). This result was to be expected considering that Aurora B kinase activity is required to maintain the SAC and that loss of Aurora B signaling coincides with depletion of cyclin B, activation of PP1 and PP2A, and entry into anaphase (Hindriksen et al., 2017; Joukov & De Nicolo, 2018). A similar result, albeit to a greater extent, was observed when both Aurora kinases were inhibited with MLN8054, which

caused significant downregulation of 8734 phosphopeptides (**Figure 5.6C**) with a strong enrichment for SP and TP phosphosites (**Figure 5.6D**), again demonstrating inactivation of CDK1/cyclin B signaling and release from Taxol arrest. The mitotic release phenotype was further supported by analyzing the change in protein abundance after Aurora B degradation by proteomics. As cells progress through mitosis and are released from metaphase and into anaphase, CDK1 activity is reduced via APC/C-mediated degradation of cyclin B, allowing for full activation of PP1 and PP2A. Analysis of the proteome revealed that, along with Aurora B, cyclin B1 and cyclin B2 were significantly depleted (**Figure 5.7**). Taken together, these experiments demonstrate that Aurora B degradation results in an almost immediate override of the SAC, promoting an escape from Taxol arrest conditions. This was strong evidence that depletion of Aurora B results in similar physiological changes to drug inhibition and could be an effective strategy to study Aurora B kinase signaling. However, it was necessary to determine ideal mitotic arrest conditions where Aurora B degradation would not result in escape from arrest.

Alternative mitotic arrest conditions to uncover Aurora B substrates

We demonstrated previously that degradation of Aurora B causes escape from Taxol-induced mitotic arrest. This is most likely because Aurora B phosphorylates substrates as part of the SAC, and silencing of this checkpoint is known to activate APC/C. Since escape from arrest is primarily driven by the degradation of cyclin B, one way to overcome this phenomenon is through the use of the proteasomal inhibitor MG132, preventing protein degradation and maintaining CDK1/cyclin B activity (Kettenbach et al., 2011). This approach, however, is not possible with the AID-Tir1 system as proteasomal activity must remain intact for the AID-tagged protein to be degraded. Therefore, it was necessary to identify optimal mitotic arrest conditions where Aurora B could be degraded without causing an escape.

We tested mitotic arrest with high concentrations of nocodazole, which destabilizes microtubules and does not allow for the formation of microtubule spindles, arresting cells in a prometaphase state. Taxol- and nocodazole-arrested cells were treated with auxin in a time-course experiment to determine the effects of Aurora B degradation on escape from these arrest conditions (**Figure 5.8A**). We observed that in Taxol-arrested cells, Aurora B degradation led to a decrease in cyclin B levels by 45 minutes; after 90 minutes, cyclin B

was almost entirely reduced. The activity of Aurora was also compromised as marked by a decrease in Aurora A T288 phosphorylation by 30 minutes and a decrease in phosphorylated Tacc3 by 90 minutes. While nocodazole arrest appeared to stabilize cyclin B abundance, the reduction in Aurora A activity was even more rapid, with a noticeable decrease in Aurora A T288 phosphorylation at 15 minutes. We therefore reasoned that the effect of Aurora B degradation on Aurora A activity was due to an escape from mitotic arrest through an alternative mechanism not involving cyclin B degradation, but where CDK1 counteracting phosphatases PP1 and PP2A are fully activated. We surmised that the rapid decrease in Aurora B activity would compromise the specificity of the AurKB-AID system and it would be comparable to using an inhibitor, such as AZD1152, that affects both Aurora A and Aurora B. Therefore, we decided not to pursue this arrest condition for large-scale phosphoproteomics experiments. These experiments were repeated multiple times with consistent results, suggesting that high dose nocodazole is not optimal for uncovering Aurora B substrates.

As escape from mitotic arrest is driven by the degradation of cyclin B by APC/C, one way to prevent escape is through the use of inhibitors of APC/C (Sackton et al., 2014; Verma et al., 2004; Zeng & King, 2012; X. Zeng et al., 2010). There are currently two inhibitors available that work through similar but distinct mechanisms to block APC/C-Cdc20 activity. One of them, Apcin, competitively binds to Cdc20 to prevent substrate recognition while the second, TAME, prevents loading of Cdc20 onto APC/C (Sackton et al., 2014). When combined, these two inhibitors can promote mitotic arrest by preventing the degradation of cyclin B and thus maintaining a state of high Cdk1/cyclin B activity. To test the feasibility of using these inhibitors for mitotic arrest, we treated Aurora B-AID cells overnight with a combination of Taxol, 20uM proTAME (a prodrug version of TAME), and 50uM Apcin. While Apcin and proTAME together can induce mitotic arrest, we reasoned that including Taxol would help to keep the SAC, and therefore Aurora B, activity high, thus allowing us to identify potential Aurora B substrates. After overnight arrest in these conditions, cells were treated with auxin for 90 minutes to deplete Aurora B. The combination of Apcin and proTAME prevented the degradation of cyclin B, suggesting that cells were not able to escape mitotic arrest (**Figure 5.8B**). However, we still observed that degradation of Aurora B caused a corresponding decrease in the activity of Aurora A as marked by decreased Aurora A pT288 and Tacc3 phosphorylation. Together, these results

suggested that Apcin and proTAME were able to stabilize cyclin B expression, but that cells were possibly escaping mitotic arrest through some other mechanism.

Another strategy that we designed to prevent escape from mitotic arrest was the introduction of doxycycline-inducible, non-degradable cyclin B (ndCyclin B) to maintain cells in a state of high CDK1/cyclin B activity and prevent mitotic exit. To accomplish this, we designed a pCW57.1 lentiviral vector to contain non-degradable cyclin B under control of doxycycline, used it to generate lentivirus, and transduced our Aurora B-AID cell line. After antibiotic selection to ensure incorporation of the construct, we tested the ability of ndCyclin B induction to promote mitotic arrest. We observed that expression of ndCyclin B was sufficient to induce a cell-cycle arrest, similar to a Taxol-induced arrest, and that Taxol and ndCyclin B induction could be combined (**Figure 5.9**). This would be an interesting system to investigate Aurora A and Aurora B phosphorylation signaling under different tension dynamics in mitotic arrest, as arresting cells with ndCyclin B alone should allow for K-MT attachments to be established, creating a tension-high system with low SAC signaling. Taxol, on the other hand, stabilizes microtubules, preventing proper K-MT tension and promoting high SAC signaling. This would therefore allow us to establish arrest at similar points in the progression of mitosis, but with different checkpoint signaling dynamics, providing an opportunity to study how Aurora B signaling changes through K-MT formation. Ultimately, we did not use this approach for to elucidate Aurora substrates by phosphoproteomics because of the limitation of time needed to generate the corresponding ndCyclin B AID-Aurora A cell line.

Mitotic arrest can also be induced using inhibitors of the kinesin Eg5, such as S-trityl-L-cysteine (STLC), which prevents centrosome separation and results in a monopolar spindle (Skoufias et al., 2006). This approach was recently used to study the effects of PP6 dephosphorylation on Aurora A (Sobajima et al., 2023) and to study kinase-substrate relationships at kinetochores. With a monopolar spindle, chromosomes are typically attached to spindle microtubules through at least one kinetochore, and we would therefore expect the SAC to be active in these conditions. Furthermore, the inhibition of Aurora B in STLC arrested cells did not cause mitotic exit (Sobajima et al., 2023). We therefore decided to analyze the efficacy depleting or inhibiting Aurora B in STLC arrested cells. We found that 45 minutes of auxin is sufficient to robustly deplete Aurora B and there is a corresponding decrease in the phosphorylation of the known Aurora B substrate H3S10 (**Figure 5.9**). Furthermore, after 1.5 hours of Aurora B degradation, we did not observe a

decrease in the activity of Aurora A as marked by phosphorylation of Aurora A T288 and the known Aurora A substrate Tacc3. Prolonged Aurora B degradation (3 hours) does eventually cause a decrease in phosphorylation of Aurora A T288. The stability of cyclin B is not affected by Aurora B depletion, even after 3 hours of auxin treatment or with 5μM AZD1152 or MLN8054, suggesting that Aurora inhibition is not resulting in mitotic exit. Taken together, the results of this experiment suggested that acute depletion of Aurora B in STLC arrest is an effective strategy to specifically inhibit Aurora B activity without affecting other pathways.

Large-scale phosphoproteomics to identify Aurora B substrates in STLC arrested cells

Based on the results of the previous experiment, we performed a large-scale phosphoproteomics experiment using STLC-arrested AurKB-AID cells and comparing Aurora B degradation to Aurora A and Aurora B inhibition with MLN8054 (1μM and 5μM, 45 minutes) and AZD1152 (2μM, 45 minutes). Briefly, 15cm dishes of AurKB-AID cells were synchronized with thymidine, arrested overnight with STLC, treated in triplicate with either auxin or an inhibitor, and harvested. It was necessary to culture AurKB-AID cells to 15cm dishes for the large-scale phosphoproteomics experiment because of a low penetrance of arrest in STLC. It is unclear what causes this effect, but we consistently observed arrest rates of ~75% in STLC, as compared to ~99% in other arrest conditions such as Taxol or nocodazole. From each sample, 5% of the cell suspension was saved separately and analyzed by western blot to confirm efficiency of degradation and inhibition before processing for phosphoproteomics (**Figure 5.10**). We were able observe a robust depletion of Aurora B and a concomitant reduction in phosphorylation of the Aurora B substrate H3S10. We also observed that, as expected, inhibition with 2μM AZD1152 reduced Aurora B activity as well as Aurora A activity, though to a lesser extent. Treatment with 1μM MLN8054 strongly inhibited Aurora A activity as seen by the abrogation of pTacc3 signal and reduction in Aurora A T loop phosphorylation. Aurora B T loop activation was also reduced, which was also expected based on previous experiments, but not to the extent necessary to affect H3S10 phosphorylation.

Given that Aurora B degradation and inhibition was occurring as expected, these samples were processed and analyzed by LC-MS/MS. This experiment revealed 643 phosphopeptides that were significantly downregulated with Aurora B degradation (**Figure**

5.11A) including phosphorylation sites on the components of the CPC Incenp and Borealin, which are known to be regulated by Aurora B phosphorylation. Survivin, the 4th component of the CPC, is also thought to be regulated by Aurora B, although the site on survivin that is phosphorylated by Aurora B was not identified in this experiment. A motif analysis for phosphorylation sites downregulated with Aurora B degradation revealed a strong preference for the basic residues Arginine and Lysine (**Figure 5.11B**). In particular, KXXRXpS and RXpS sequences were among the highest scoring motifs in this dataset and have been previously reported as Aurora B-specific motifs using inhibitors (Kettenbach et al., 2011). Similarly, Aurora B inhibition with AZD1152 resulted in the significant decrease of 867 phosphopeptides (**Figure 5.11C**), including sites on Aurora B, Incenp, and Borealin. A motif enrichment analysis revealed a preference for basic residues upstream of the phosphorylation site (**Figure 5.11D**) similar to what was observed for Aurora B degradation. Interestingly, the consensus motif for Aurora B degradation and inhibition are nearly identical. The highest scoring sequences found from phosphopeptides decreased with Aurora B inhibition were RRpS and KXpS, which are also motifs that have been previously reported for Aurora B using the same small molecule inhibitor (Kettenbach et al., 2011). Furthermore, a comparison of significant phosphopeptides identified in Aurora B degradation and inhibition revealed a strong correlation in the change in abundance for both conditions (**Figure 5.11E,** R^2 = 0.89). However, the fold change decrease appears to be more extensive with AZD inhibition than Aurora B degradation, especially for phosphopeptides with the greatest decrease in abundance. This effect could be due to the kinetics of degradation. Inhibition by a small molecule is extremely rapid and total inhibition can be accomplished within minutes of drug addition, whereas targeted degradation is innately slower as the protein of interest must first be engaged by an E3 ligase, ubiquitylated, and degraded for inhibition to occur. Attempts to account for this difference by degrading Aurora B for 60 minutes and treating with AZD1152 for 45 minutes appear to have been insufficient, and there could still be a difference in the time of effective Aurora B inhibition. Another possibility is incomplete degradation of Aurora B, which could still be contributing to signaling events and dampening the fold-change reduction in phosphopeptide abundance observed in this dataset. However, these experiments clearly demonstrate that, overall, Aurora B degradation is analogous to Aurora B inhibition, and we are able to identify and quantify Aurora B dependent phosphorylation sites by degrading Aurora B.

Inhibition of Aurora A with 1μM MLN8054 resulted in the significant decrease in 258 phosphopeptides (**Figure 5.12A**). Tacc3 S558, a well characterized Aurora A substrate, exhibited a $\log_2$ fold-change reduction of -2.96, indicating a strong inhibition of Aurora A activity. Within the subset of significantly decreased phosphopeptides, there is a clear preference for basic residues, particularly in the -1 position, and previously reported Aurora A phosphorylation motifs, such as RXpS and RXpSL, are identified with high scores (**Figure 5.12B**). Treatment with 5μM MLN8054 resulted in the significant decrease of 6675 phosphopeptides (**Figure 5.12C**). While we are able to identify reduction in Aurora A and Aurora B activity via the decrease in T288 and T232 phosphorylation, respectively, 56% of significantly decreased phosphorylation sites (3718/6675) are within SP or TP sequences, the motif for CDK1/cyclin B (**Figure 5.12D**). This is most likely due to an escape from mitotic arrest as was observed in Aurora B degradation after arrest in Taxol (**Figure 5.6**).

Interestingly, Aurora B inhibition and degradation result in variable effects on the activation state of Aurora A. While it does not meet the $\log_2$(fold-change) < -1 cut-off for biological significance in either condition, phosphorylation of the Aurora A T-loop is decreased more in Aurora B degradation than with inhibition by AZD1152. This is unexpected behavior because AZD is known to inhibit Aurora A to some extent while Aurora B and Aurora A are not thought to interact, and degradation would therefore not be expected to affect Aurora A activity. This result also appears to contradict the results shown by western blot, which indicated that Aurora A was decreased more with AZD inhibition than Aurora B degradation (**Figure 5.10**). This could be due to issues with quantification of the Aurora A T loop by mass spectrometry, or the lack of quantitative accuracy of western blotting. However, one possible interpretation of the dephosphorylation of the Aurora A T loop upon Aurora B degradation is that Aurora B supports Aurora A activation, either directly or indirectly in a manner independent of its kinase activity and removing the whole protein destabilizes Aurora A. Further experimentation will be necessary to follow up on this observation.

Comparison of the phosphorylation sites significantly downregulated with both inhibitors but not with auxin yields a number of interesting substrates that demonstrate the utility of applying targeted protein degradation to study phosphorylation signaling. For example, NGEF, a guanine exchange factor that activates RHOA, RAC1, and CDC42, is dephosphorylated at T464 with AZD or MLN inhibition, but to a much lesser extent with

Aurora B degradation. This phosphosite decreases in abundance with a $\log_2$(fold-change) -6.03 in 2μM AZD, -6.97 in 1μM MLN, and -1.09 in auxin, which serves as a proof of concept that phosphorylation sites identified after inhibition with AZD1152 may in reality be the result of Aurora A inhibition. Another example of this is WRN, a DNA helicase and exonuclease, that is significantly downregulated in 2μM AZD and 1μM MLN with a $\log_2$(fold-change) close to -5, but not in auxin. This is another case where, even though the phosphorylation site decreased to a large extent with both inhibitor treatments, it can reasonably be attributed to Aurora A since it is unchanged with auxin treatment. Taken together, these results are an exciting test case to demonstrate the specificity of targeted protein degradation to selectively attribute phosphorylation sites to a kinase of interest.

Previously, we identified a cluster of Aurora substrates that were not clearly attributed to Aurora A or Aurora B (Kettenbach et al., 2011). One of these phosphosites is S914 on RBM27, an RNA binding motif protein that is thought to be involved in mRNA processing. This phosphorylation site is similarly observed to decrease in abundance in our dataset with 2μM AZD and 1μM MLN, but does not change at all with auxin, suggesting that this site can be attributed to Aurora A specifically. Similarly, LUZP1 S957 is significantly decreased in both 1μM MLN and 2μM AZD treatment, but not in auxin. This is another site that was previously reported to be ambiguous but through these experiments, we can provide evidence that the reduction in phosphorylation with AZD is due to inhibition of Aurora A and not Aurora B. This behavior is also seen with S70 on ERF1, a protein involved in protein translation, and S295 on FOXJ3, which enables transcription activator activity. Both of these phosphorylation sites are significantly reduced with MLN and AZD treatment, but not with auxin, again suggesting that they are true substrates of Aurora A but not Aurora B. Identifications such as these allow for a reassessment of the ambiguous Aurora substrates and in these cases, assignment to one kinase or the other.

Side-by-side comparison of phosphosites that are significantly decreased ($\log_2$(fold-change) < -1, $-\log_{10}$(pval > 1.3) in AZD and auxin, but not 1μM MLN reveals phosphorylation sites that are likely to be Aurora B substrates. Examples of this include S1001 on KIF4A, a motor protein with roles in chromosome separation, S93 on Spastin, a microtubule severing protein with roles in mitosis and cytokinesis, and S40 on TERF2, a telomere binding protein that protects against end-to-end chromosome fusion. In total, there are 425 phosphopeptides that are significantly downregulated in both AZD and

auxin, but not 1μM MLN. Furthermore, these sites show a strong enrichment for previously reported Aurora B motifs, including KXXRXpS, RXpS, and RRpS sequences, suggesting that they are true Aurora B substrates.

Additionally, there are 88 phosphopeptides that are significantly decreased in all three conditions. For example, Incenp S106, CENPE S2647, KNL1 S584, and SKA3 S34, all phosphorylation sites on proteins with roles at the centromere or kinetochore in mitosis, are decreased by 2-fold or more in auxin, 2μM AZD, and 1μM MLN. This suggests that there is a subset of phosphorylation sites that can be regulated by both Aurora A and Aurora B, a potentially exciting finding considering that Aurora A and Aurora B are not thought to colocalize or act on the same structures during mitosis. However, this observation alone could be misleading since not all phosphopeptides in this subset are observed to change to the same extent in each treatment condition. For example, ZYX Y172:T179, WIZ S1480, NUSAP S285, KMT2A S1352, and KIF2C S111:S115 have a $\log_2$(fold-change) of ~2 in auxin, ~3 in AZD, and ~1 in 1μM MLN. One interpretation of this result is that, while they could be shared substrates of both Aurora kinases, they are preferentially phosphorylated by Aurora B. If this is the case, however, it presents an exciting possibility that some proteins could be alternately regulated by Aurora A and B to fine-tune localization and/or activity.

Discussion

Overall, the results of these experiments highlight the potential for targeted protein degradation to selectively uncover kinase substrates with high precision. Comparison of phosphopeptides significantly decreased with Aurora B degradation, Aurora B inhibition, or Aurora A inhibition allow for a direct comparison of phosphopeptide changes in all of these treatment conditions and afford an ability to more precisely assign Aurora B substrates. Importantly, we observed in these experiments phosphopeptides that are significantly decreased with both AZD1152 and MLN8054, but not auxin, and could therefore be characterized as Aurora A-specific substrates. We also observe, on the other hand, phosphopeptides that decrease in abundance in all treatment conditions, implying that Aurora A and Aurora B do have shared substrates, and calling for a re-evaluation of how these kinases function during mitosis.

Another interesting observation to come out of these experiments is the consistent observation that phosphorylation of the Aurora A T-loop (T288) was frequently downregulated after the activity of Aurora B was compromised, either with AZD1152 or by degradation. This was seen for cells arrested in Taxol, nocodazole, STLC, and APC/C inhibitors. It is not thought that Aurora A and Aurora B interact and affect each other's activation state, but that assessment has not been made using ideally selective chemogenetic inducible degradation methods until now. When Aurora A T288 is decreased with AZD1152, it is assumed that this is the off-target result of AZD binding to and inhibiting Aurora A directly. However, our Aurora B degradation experiments suggest that there could be a mechanism by which Aurora B influences the activity of Aurora A, either directly or indirectly. Furthermore, we have also observed the inverse to be true, whereby Aurora A degradation leads to a reduction in the activity of Aurora B as assessed by T232 phosphorylation (data not shown). We initially dismissed the potential cross-regulatory role by surmising that this effect is due to mitotic exit, but follow-up experiments examining the role of Aurora B in maintaining the activation state of Aurora A, and vice versa, are warranted. The reduction of Aurora A activity after Aurora B degradation was observed in our phosphoproteomics experiments, although the reduction of Aurora A T288 never met the $\log_2$(fold-change) < -1. Analysis of Aurora B-dependent phosphosites after Aurora B degradation could be complicated by the slight reduction in Aurora A activity and

is a potential pitfall of this experimental approach. On the other hand, the two phosphorylation sites on Tacc3 that are reduced with 1μM MLN8054 are not reduced with Aurora B degradation, raising the possibility that Aurora A T288 dephosphorylation occurs towards the end of the 1 hour auxin treatment and therefore is not significantly affecting Aurora A-dependent signaling pathways.

Previously, we applied AID-Tir1 targeted protein degradation to study Plk1 signaling in mitosis using a 2 hour degradation (Hards et al., 2021). While some master mitotic regulators like Plk1 can be acutely depleted without major changes to mitotic state, faster degradation times are necessary for the Aurora kinases to inhibit kinase activity without causing mitotic exit. Here, using approaches developed and validated in chapter 4 of this thesis, we demonstrated the development of an Aurora B degrader with degradation kinetics sufficient to identify Aurora B-dependent phosphosites within 1 hour without triggering mitotic exit. Because Aurora B degradation in mitotically arrested cells forces mitotic exit by silencing the SAC, rapid degradation kinetics are essential in order to quickly deplete Aurora B activity in the time that it takes for cells to degrade cyclin B and exit. Applying fluorescent reporter-based CRISPR-Cas9 targeting strategies, we were able to quickly generate AID Aurora B cell lines at both the N- and C-termini that degraded with rapid kinetics.

We performed our initial Aurora B degradation experiments with cells arrested in Taxol, since this strategy has been successfully used to study Aurora A and Aurora B signaling. However, this strategy is ineffective considering Aurora A and Aurora B degradation results in mitotic exit, and we were unable to use proteasomal inhibitors to block this effect, leading us to perform our experiments in STLC arrested cells as an alternative, which did not exhibit mitotic exit after Aurora degradation. However, it would be interesting to compare Aurora A and Aurora B substrates identified at different stages of mitosis by using different arresting agents. As part of this project, we introduced non-degradable, doxycycline-inducible cyclin B (ndCyclin B) to AurKB-AID cells, and we demonstrated that this cell line can be used with or without Taxol to induce mitotic arrest. In theory, ndCyclin B induction in the presence or absence of Taxol could be used to induce a cell state with high or low tension, respectively, providing insight into how Aurora B signaling changes as cells form stable k-MT attachments. Induction of ndCyclin B could also be coupled with arrest by nocodazole or STLC to arrest cells in prometaphase states and assess Aurora substrates in the earlier phases of mitosis. Overall, through the course

of this project we developed a toolbox to study mitotic phosphorylation signaling of the Aurora kinases, and it will be exciting to apply these tools to identify Aurora signaling with more temporal and spatial specificity than has been possible up to this point.

The ultimate proof of the AID-Tir1 approach to study substrate overlap for kinases in the same family will come by comparing phosphosites that are significantly downregulated with Aurora B degradation and Aurora A degradation. In parallel to the project presented in this chapter, we generated AID-Aurora A cell lines and are in the process of applying them to identify Aurora A specific substrates. When combined, the two datasets will be a powerful means to assess substrate overlap between Aurora A and B and to determine if or to what extent there are shared substrates. Data presented in this chapter suggests that some sites can be phosphorylated by both Aurora A and Aurora B, given that they decrease in abundance with Aurora A inhibition by MLN8054 and Aurora B degradation. However, it could still be argued that this is the result of Aurora B inhibition by MLN. For these reasons, the reciprocal Aurora A degradation experiments will provide key insights into the possibility of Aurora A and B substrate overlap.

An exciting discovery made by targeting the N-terminus of Aurora B is the existence of an uncharacterized Δ41 Aurora B isoform. While the significance of this discovery is still unclear, the ability of full-length and Δ41 to bind components of the CPC appears to be different depending on cellular context. Affinity pulldown experiments in mitotically arrested cells revealed a difference in binding between the two isoforms in 293T but not HeLa cells, particularly for survivin and borealin. A key difference between the two experimental conditions is the extent of overexpression of the Aurora B isoforms. While these isoforms were expressed below physiological levels in stable HeLa cells, they are clearly overexpressed well above physiological levels in 293Ts. One hypothesis is that, when components of the CPC are limiting, full-length Aurora B is preferentially recruited to the CPC while Δ41 remains cytoplasmic and unbound to centromeres. Another hypothesis is that the degradation of truncated Aurora B during mitosis might have different kinetics than full-length, giving the cell a more precise mechanism to control Aurora B expression via protein degradation as it progresses through mitosis. This idea is not without precedent and an article was recently published demonstrating that the relative expression of Cdc20 splice variants controls duration of mitosis (Tsang & Cheeseman, 2023). It would be exciting, therefore, to experiment with turnover rates of both Aurora B isoforms as cells progress through mitosis. This could be accomplished by synchronizing

cells and releasing them into mitosis to track the relative disappearance of both full-length and Δ41 Aurora B.

In conclusion, we applied FACS-based CRISPR-Cas9 gene editing methods described in chapter 4 to quickly create an Aurora B-AID cell line with fast degradation kinetics and used this cell line to identify candidate substrates in cells arrested with STLC. We demonstrated that Aurora B degradation closely mimics Aurora B inhibition by AZD1152, but with higher precision. We also identified and began the characterization of a previously unreported Aurora B Δ41 isoform. The tools and cell lines presented in this chapter can be expanded upon and combined with similar tools developed for Aurora A in order to create a picture of Aurora signaling in mitosis with a level of precision that has not been possible up to this point.

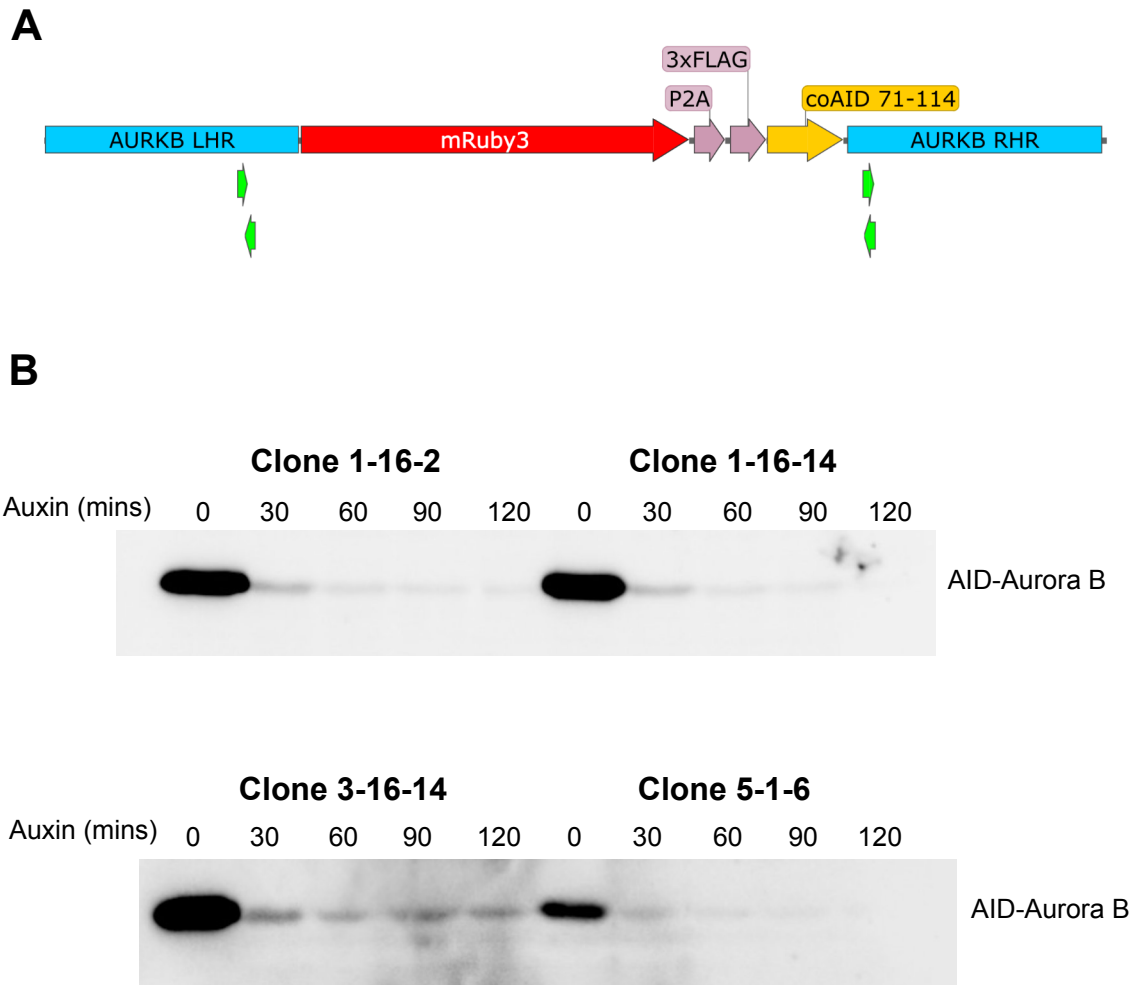

Figure 5.1. Endogenous AID tagging at the N-terminus of Aurora B using a fluorescent reporter and FACS. **A)** Schematic of the N-terminal Aurora B targeting vector. This vector includes 500bp arms homologous to the Aurora B endogenous locus directly upstream and downstream of Cas9 cut sites (LHR and RHR, respectively). mRuby3 is expressed as a fluorescent reporter, allowing for selection by FACS, and is separated from the N-terminus of Aurora B by a P2A ribosomal skip site. For these vectors, we codon optimized the sAID tag to create the coAID tag, which helped with tag stability. Finally, the green arrows represent cut sites targeted by guide RNAs. **B)** Time-course of Aurora B degradation in degrading AID-Aurora B clones. Homologous AID-Aurora B HeLa cells were recovered after a single round of transfection. Tir1-BFP was ectopically expressed

from the AAVS1 safe-harbor locus and clones were screened for their ability to degrade Aurora B. Degrading clones were then subjected to a time-course to assess the kinetics and efficiency of degradation. Clones were treated with auxin for the designated time points, collected, and analyzed by western blot using an antibody raised against Aurora B.

A

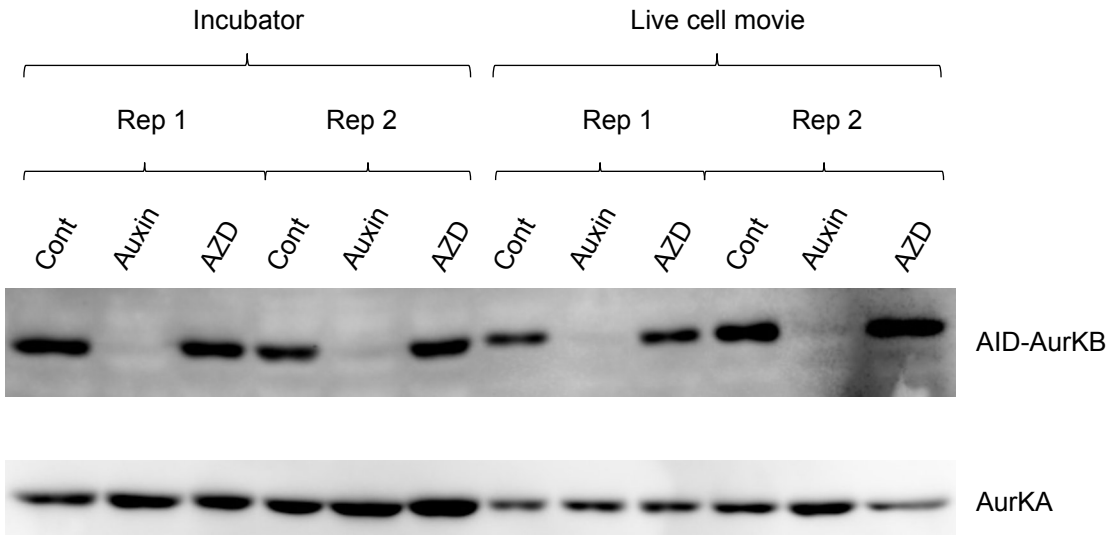
Incubator
Live cell movie
Rep 1
Rep 2
Rep 1
Rep 2
Cont
Auxin
AZD
Cont
Auxin
AZD
Cont
Auxin
AZD
Cont
Auxin
AZD
AID-AurKB
AurKA

B

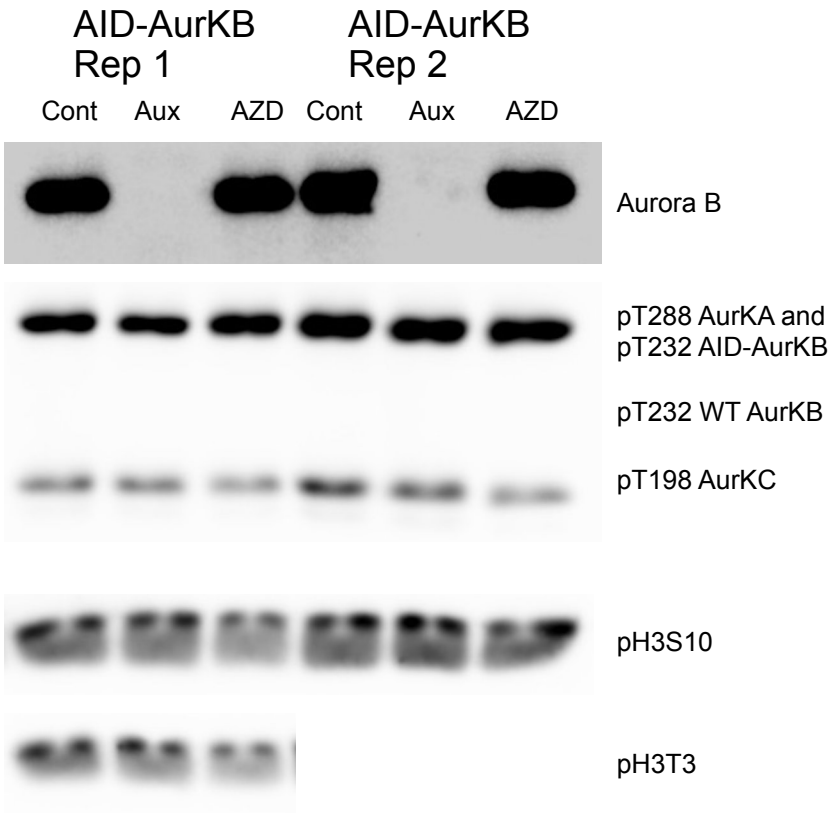
AID-AurKB
Rep 1
AID-AurKB
Rep 2
Cont
Aux
AZD
Cont
Aux
AZD
Aurora B
pT288 AurKA and
pT232 AID-AurKB
pT232 WT AurKB
pT198 AurKC
pH3S10
pH3T3

Figure 5.2. Prolonged AID-Aurora B degradation does not cause cell cycle defects. **A)** AID-Aurora B cells were grown in the presence of auxin for 48hrs, either in an incubator (left two replicates) or under the microscope (right two replicates). Blotting for Aurora B demonstrates a nearly complete degradation of AID-Aurora B. Aurora A was included as a loading control and we would not expect Aurora A expression to change with auxin. **B)** AID-Aurora B cells were arrested and treated with auxin or AZD1152 for 2 hours before being harvested for western blot. pH3S10 is a well-characterized Aurora B substrate at centromeres and its phosphorylation status does not decrease despite complete degradation of Aurora B.

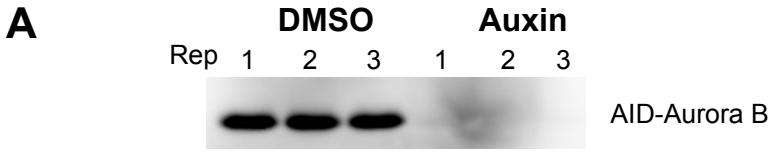
A
DMSO
Auxin
Rep 1 2 3 1 2 3
AID-Aurora B

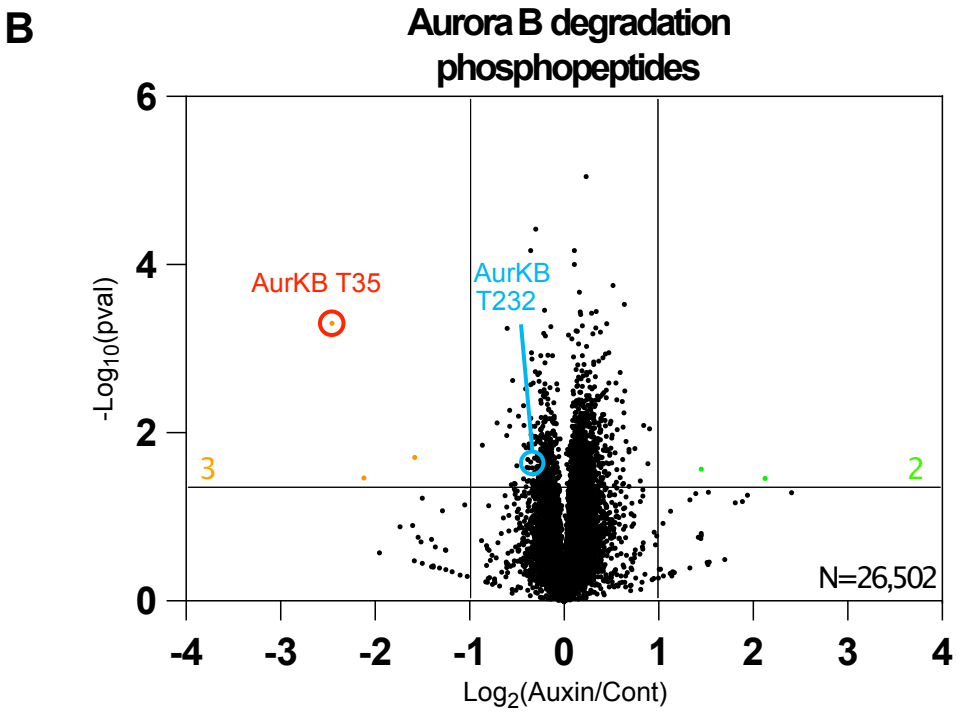
B
Aurora B degradation phosphopeptides
AurKB T35
AurKB T232
3
2
N=26,502
-Log10(pval)
Log2(Auxin/Cont)

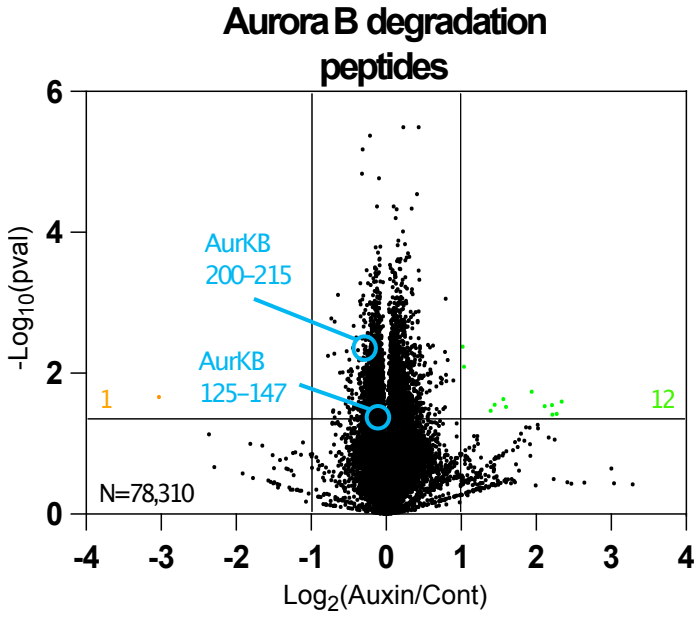
C
Aurora B degradation peptides
AurKB 200–215
AurKB 125–147
1
12
N=78,310
-Log10(pval)
Log2(Auxin/Cont)

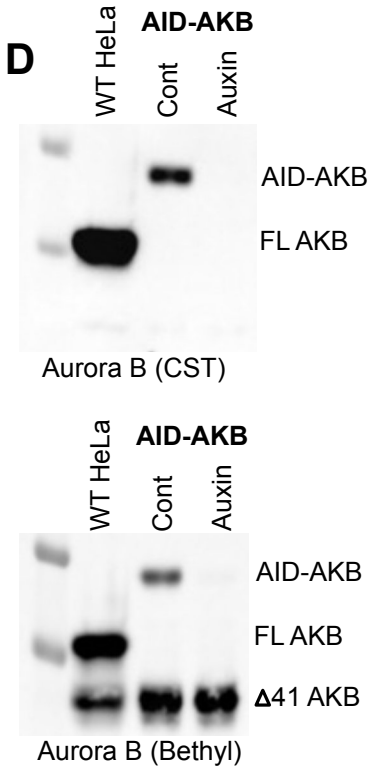
D
WT HeLa
AID-AKB
Cont
Auxin
AID-AKB
FL AKB
Aurora B (CST)
Δ41 AKB
Aurora B (Bethyl)

Figure 5.3. AID-Aurora B phosphoproteomics. AID-Aurora B cells were grown to 10cm dishes, synchronized with thymidine, arrested overnight with taxol, treated +/- auxin for 1hr, and collected by mitotic shake-off. **A)** Western blot validation of AID-Aurora B degradation demonstrates complete degradation within the 1hr treatment. **B)** Volcano plot of phosphopeptides identified in this experiment. For each phosphopeptide, the $\log_2$ fold change, showing biological significance, is plotted on the x-axis to and the $-\log_{10}$ of the p-value, showing statistical significance, is plotted on the y-axis. Phosphopeptides with values in the upper left quadrant, highlighted in yellow, are considered to be statistically significantly downregulated. Aurora B T35, one of the only phosphopeptides to be significantly downregulated, is circled in red while Aurora B T232, the main activation site on Aurora B, is circled in blue. **C)** Volcano plot of peptides identified from this experiment also comparing biological significance to statistical significance. Significantly downregulated peptides are highlighted in yellow in the upper right quadrant. The only two Aurora B peptides that were identified in this dataset (125-147 and 200-215) are highlighted in blue.

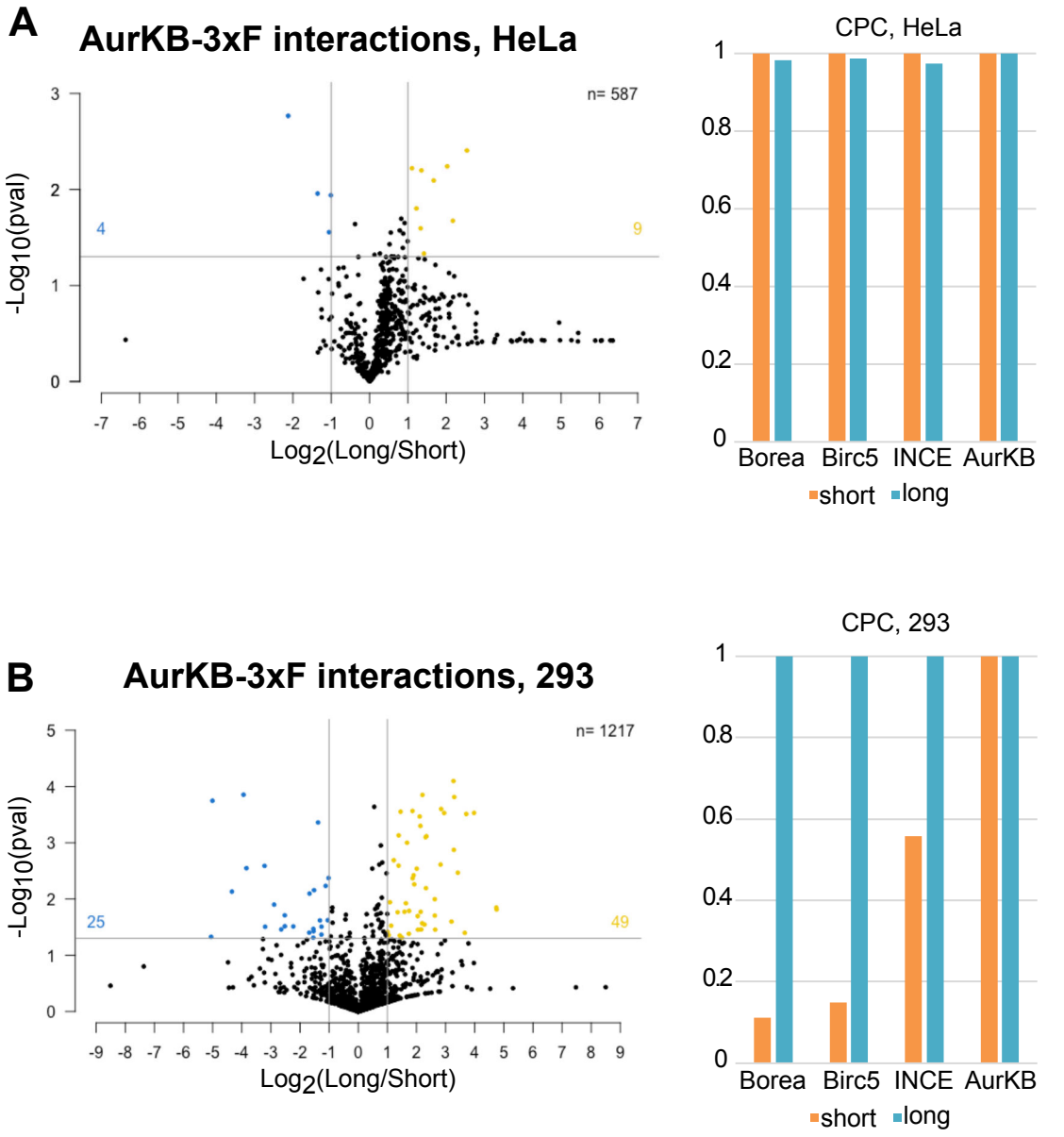
A
AurKB-3xF interactions, HeLa
n= 587
4
9
-Log10(pval)
Log2(Long/Short)
CPC, HeLa
Borea
Birc5
INCE
AurKB
short
long
B
AurKB-3xF interactions, 293
n= 1217
25
49
-Log10(pval)
Log2(Long/Short)
CPC, 293
Borea
Birc5
INCE
AurKB
short
long

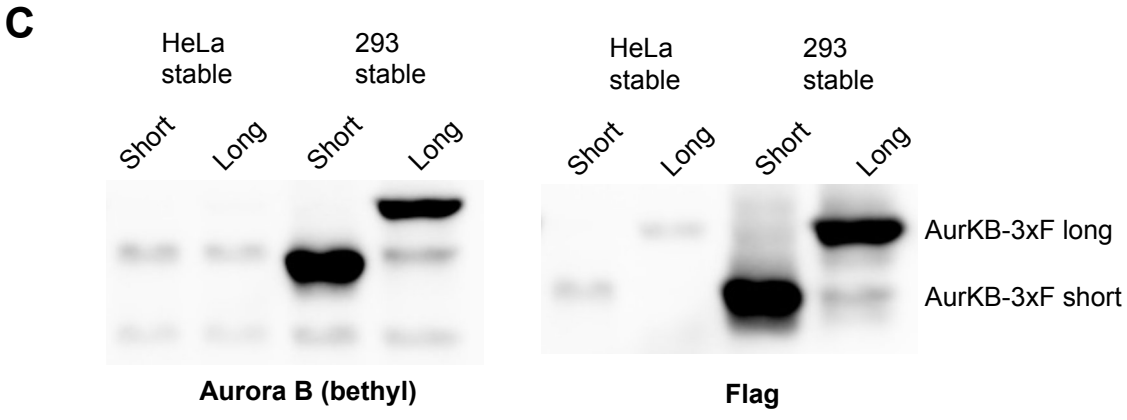
C
HeLa stable
293 stable
Short
Long
Short
Long
HeLa stable
293 stable
Short
Long
Short
Long
AurKB-3xF long
AurKB-3xF short
Aurora B (bethyl)
Flag

Figure 5.4. Full-length and Δ41 Aurora B interactomics in mitotically arrested cells. HeLa and 293 cells stably expressing 3xFlag full-length or Δ41 Aurora B were generated and used in Flag IP experiments to analyze the interactome of the two isoforms. **A)** Volcano plots comparing proteins differential protein abundance after IP with the long and short Aurora B isoforms in HeLa cells reveal similar interactomes for both isoforms. Importantly, components of the CPC, shown in the bar graphs on the right, the complex in which Aurora B is the key enzymatic component during mitosis, were pulled down in equal amounts, suggesting that Aurora B long and short isoforms have similar localization during mitosis. **B)** Differences in binding for the long and short Aurora B isoforms were observed in 293 cells. In particular, incenp, survivin (Birc5) and borealin interacted less strongly with the short isoform than the long, as highlighted by the bar graph. **C)** Western blots showing the extent of Aurora B isoform expression after stable selection in HeLas, and 293s. In particular, 293 stable cells were able to maintain a much higher expression of either Aurora B isoform that HeLa stable cells, which could account for differences in binding observed in this experiment.

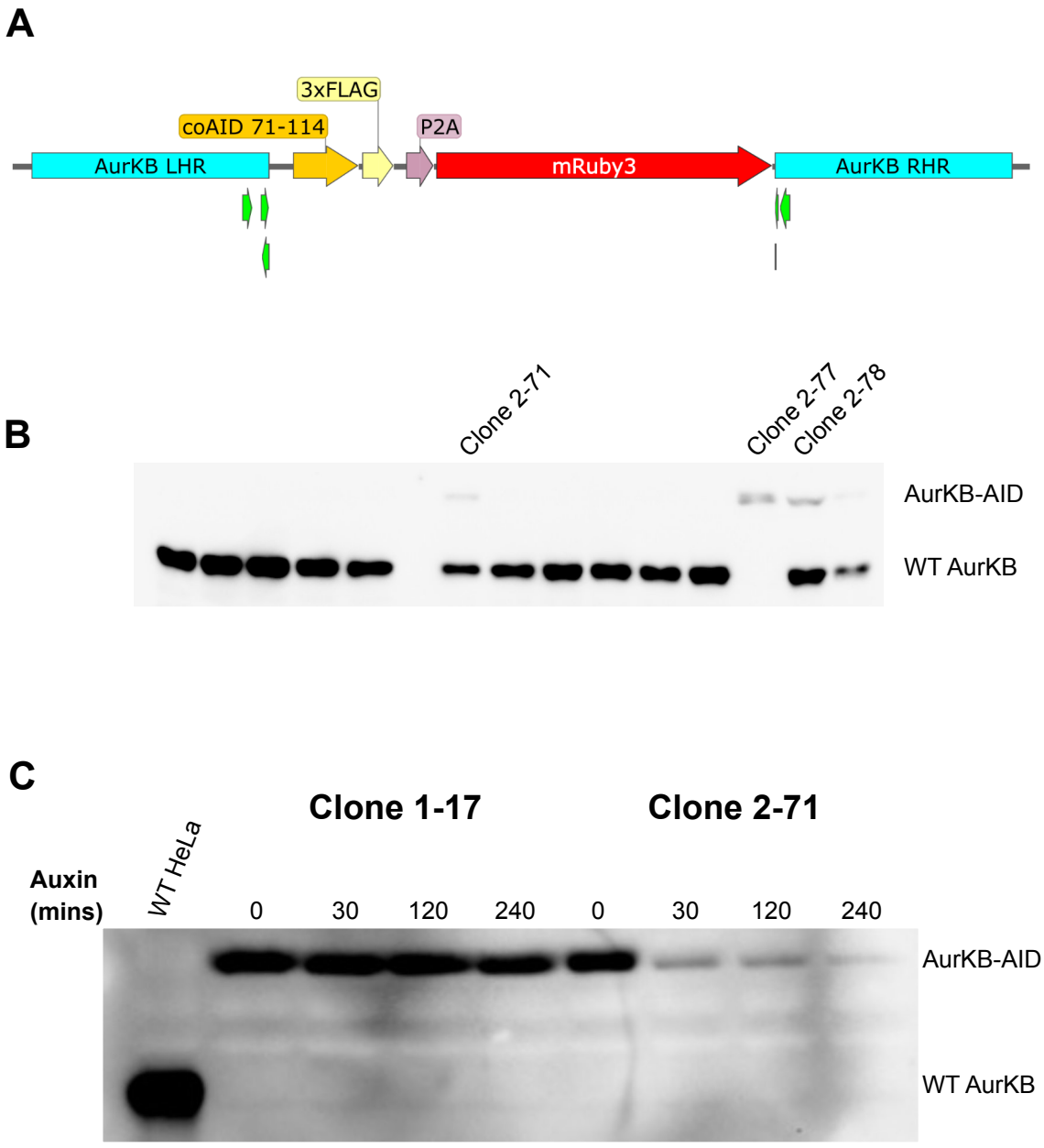

Figure 5.5. C-terminal CRISPR targeting strategy for Aurora B. **A)** The Aurora B C-terminus repair template includes 500bp homology arms flanking the stop codon to promote HDR after Cas9 induced DSBs. The AID-3xFlag tag is appended to the end of Aurora B after recombination, along with P2A-mRuby3 which is used to sort out tagged cells by FACS. Five sgRNAs targeting the C-terminus of Aurora B were designed for this approach and the sequences that they recognize in the endogenous locus are marked on

the vector map as green arrows. **B)** Representative western blot showing screening of individual clones after transfection and cell sorting. Most clones that were screened did not show signs of tag incorporation by western blot. Clones 2-71 and 2-78 appear to have had recombination for at least one allele, while clone 2-77 is a homozygous knock-in that was used for further experiments. **C)** Time-course degradation experiments were performed for both AurKB-AID homozygous knock-in clones and the extent of degradation was assessed by western blotting. Clone 1-17 appeared to be unresponsive to auxin while clone 2-77 appeared to degrade most Aurora B within 30 minutes.

A

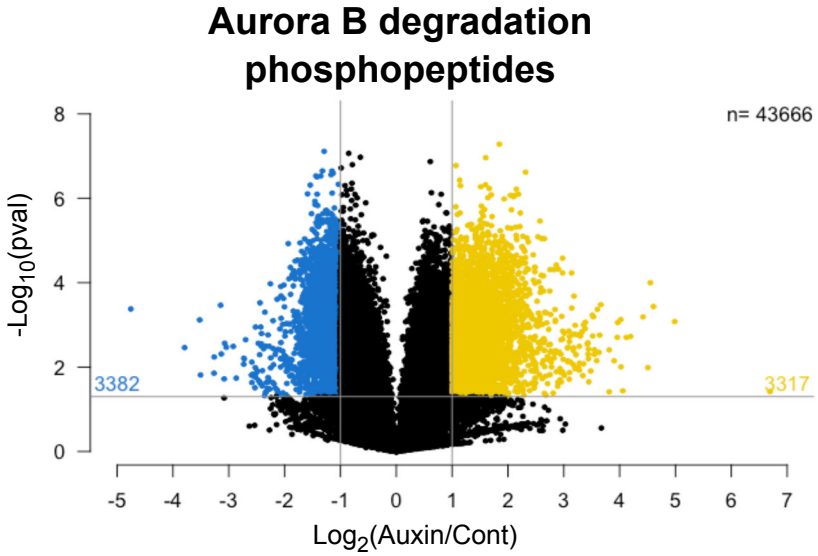
Aurora B degradation phosphopeptides
n= 43666
-Log10(pval)
3382
3317
Log2(Auxin/Cont)

B

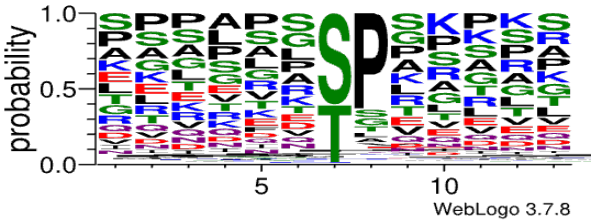
probability
WebLogo 3.7.8

C

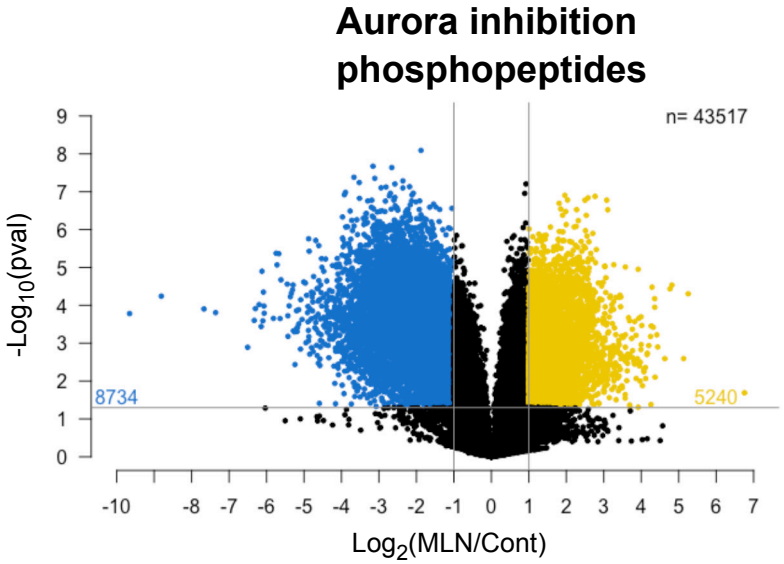
Aurora inhibition phosphopeptides
n= 43517
-Log10(pval)
8734
5240
Log2(MLN/Cont)

D

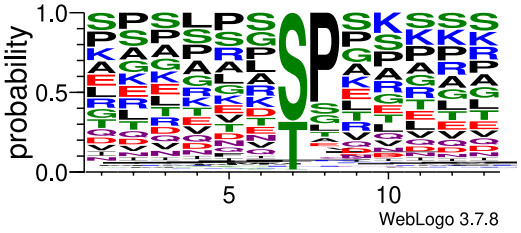
probability
WebLogo 3.7.8

Figure 5.6. Phosphoproteomics of Aurora B degradation in taxol arrested cells. **A)** Volcano plot showing change in phosphopeptide abundance after Aurora B degradation. After arrest, cells were treated with 1mM NAA for 2hrs to deplete Aurora B, resulting in a significant decrease in 3382 phosphopeptides ($\log_2$(fold-change) < -1 and -$\log_{10}$(p-value) > 1.3, which are highlighted in blue. **B)** The significantly decreased phosphopeptides were enriched for sites containing SP and TP sequences, the well characterized phosphorylation motif of CDK1/Cyclin B in mitosis, as determined by motif analysis and plotted in this WebLogo. This suggests a decline in CDK1 activity, activation of the counteracting phosphatases PP1 and PP2A which preferentially dephosphorylate SP and TP sites, and an escape from mitotic arrest. **C)** Volcano plot analyzing the effects of Aurora A and Aurora B inhibition with MLN8054 for 2hrs. As above, significantly downregulated phosphopeptides are highlighted in blue. In total, 8734 phosphopeptides were observed to decrease significantly with Aurora inhibition. **D)** Motif analysis on significantly downregulated phosphopeptides revealed a strong enrichment for SP and TP sequences, as observed with Aurora B degradation.

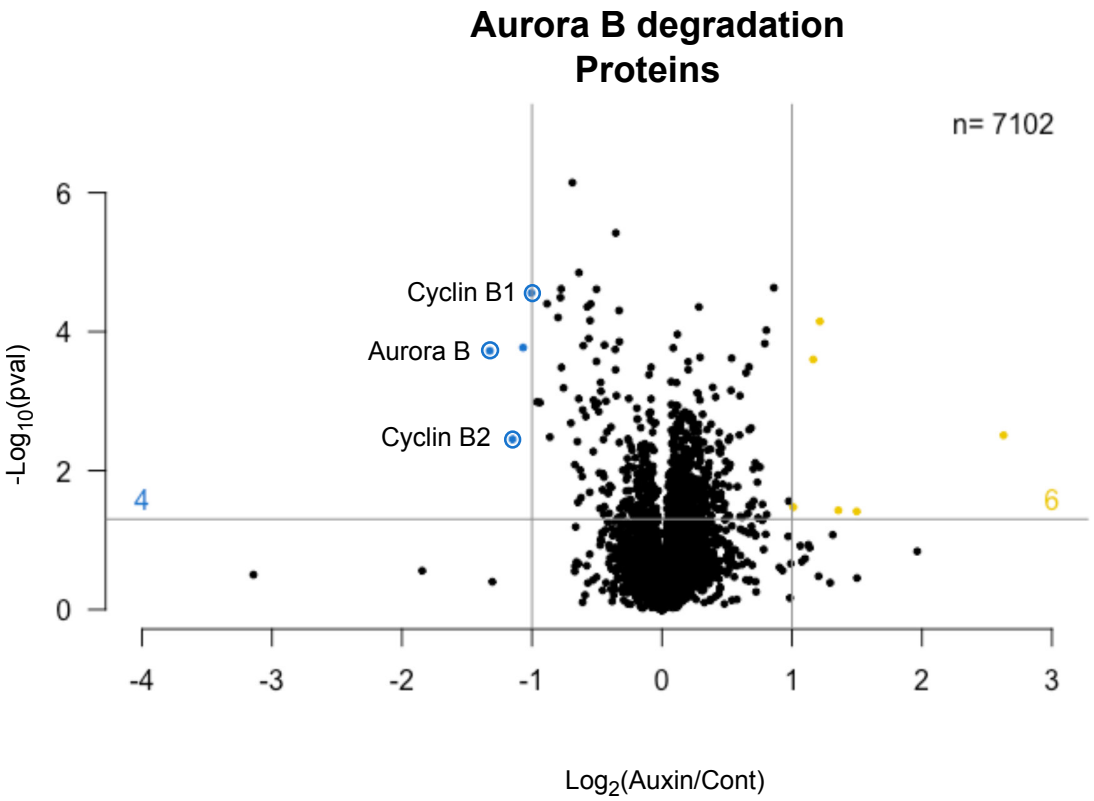

Figure 5.7. Aurora B degradation in taxol arrested cells results in depletion of Cyclin B. To complement the phosphoproteomics experiments analyzing changes to phosphorylation signaling after Aurora B degradation, we performed a proteomics analysis to both confirm the extent of Aurora B degradation and identify any other changes to the proteome. In this volcano plot, the $\log_2$ fold-change is plotted against $-\log_{10}$ of the p-value as determined by a Fisher's T-test. Proteins depleted by two-fold or more and are statistically significant ($-\log_{10}$(p-value) > 1.3) are plotted in blue in the upper right quadrant and significantly increased proteins are plotted in yellow. Three key proteins that were observed to be significantly downregulated in this experiment, Aurora B, Cyclin B1, and Cylin B2, are highlighted in blue.

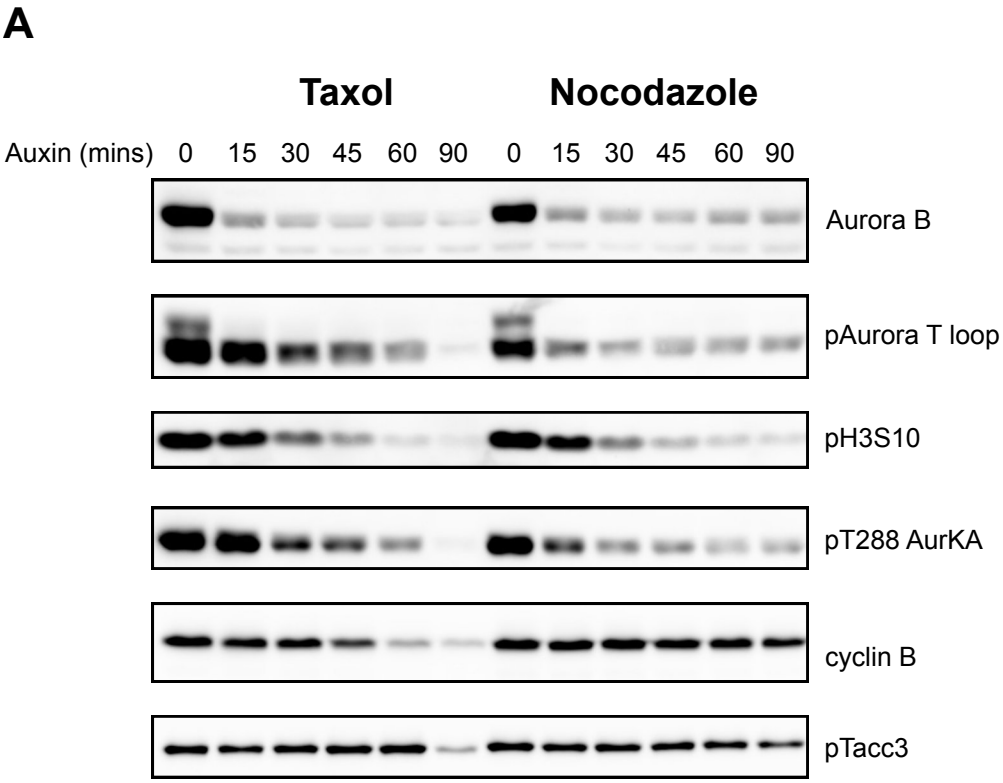
A
Taxol
Nocodazole
Auxin (mins) 0 15 30 45 60 90 0 15 30 45 60 90
Aurora B
pAurora T loop
pH3S10
pT288 AurKA
cyclin B
pTacc3
B
HeLa
AurKB-AID
Taxol+ APC/Ci
Taxol
Taxol+ APC/Ci
Cont
+AZD 2μM
Cont
+Aux
Cont
+Aux
pTacc3
cyclin B
pH3S10
pAurora T loop
C
Control
Dox
Taxol
Taxol + Dox
AurKB (bethyl)
Aurora pT loop
Aurora A pT288
Cyclin B2

Figure 5.8. Alternative mitotic arrest conditions for Aurora B-AID degradation. **A)** AurKB-AID cells were synchronized with thymidine and arrested overnight with taxol or 500nM nocodazole and with auxin for the indicated time points. Samples were blotted against Aurora B to analyze extent of degradation, Cyclin B to analyze mitotic escape, and Aurora A and Aurora B activity with antibodies against the Aurora T-loops and Aurora substrates pH3S10 and pTACC3. **B)** WT HeLa cells and AurKB-AID were synchronized with thymidine and arrested, either with taxol alone, or with a combination of taxol and the APC/C inhibitors Apcin and proTAME (APC/Ci). After arrest, HeLa cells were treated with 2μM AZD1152 for 1hr to inhibit Aurora B and Aurora B-AID cells were treated +/- auxin. The decrease in Aurora A activity is marked by a strong decrease in the lowest band of the pAurora T loop blot in AurKB-AID cells treated with auxin. **C)** Doxycycline-inducible, non-degradable Cyclin B (ndCyclin B) was introduced to AurKB-AID cells using lentiviral transduction. Cells were synchronized with thymidine and arrested with doxycycline (Dox), taxol, or both, and collected for analysis by western blot. Aurora B protein is shown in the top panel and Aurora A and B activity are assessed by antibodies against the Aurora T loops. Induction of ndCyclin B can be seen in the bottom panel as a slightly mass-shifted product, the result of a remnant P2A skip site on the C-terminus of ndCyclin B.

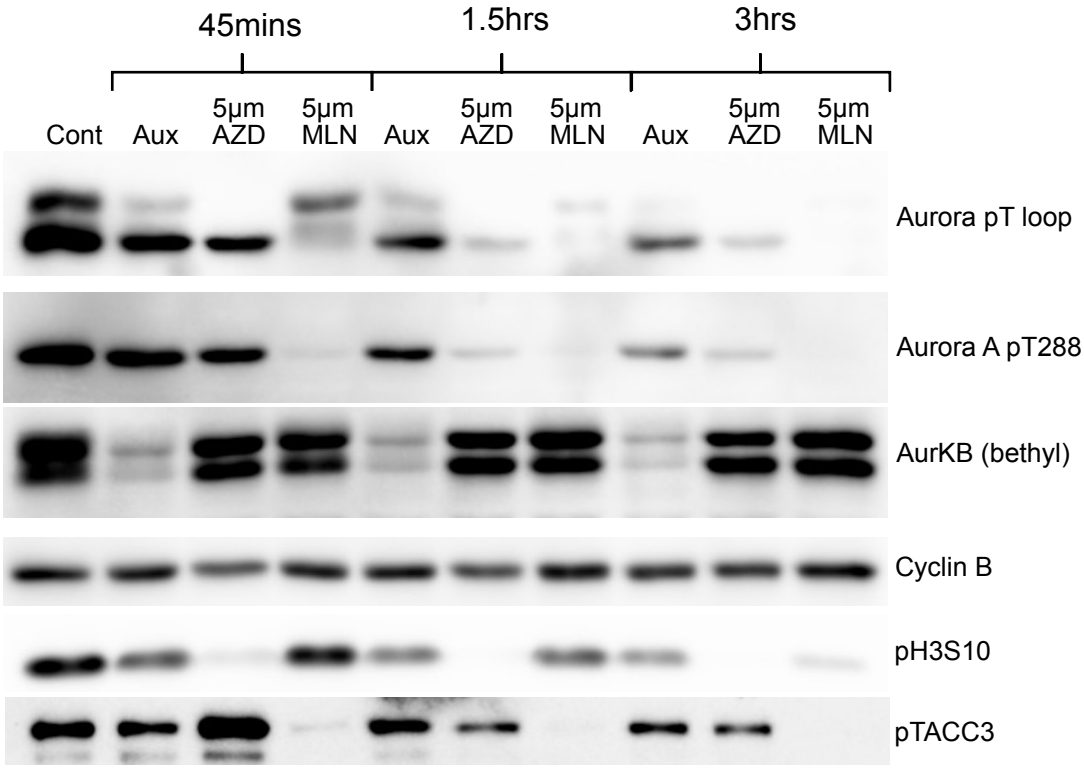

Figure 5.9. Acute Aurora B degradation does not cause exit from STLC arrested cells or affect Aurora A activity. AurKB-AID cells were synchronized with thymidine and arrested overnight with STLC, an Eg5 inhibitor that prevents centrosome separation and results in a monopolar spindle. Arrested cells were treated for the indicated times with auxin (Aux), 5μM AZD1152 (AZD), or 5μM MLN8054 (MLN) and were collected and analyzed by western blot. Note that in the Aurora T loop blot, there are 3 bands. The two upper bands are from the two Aurora B isoforms, which are shifted in mass above Aurora A because of the AID tag. The Aurora A T288 band is the lowest molecular weight and the most intense.

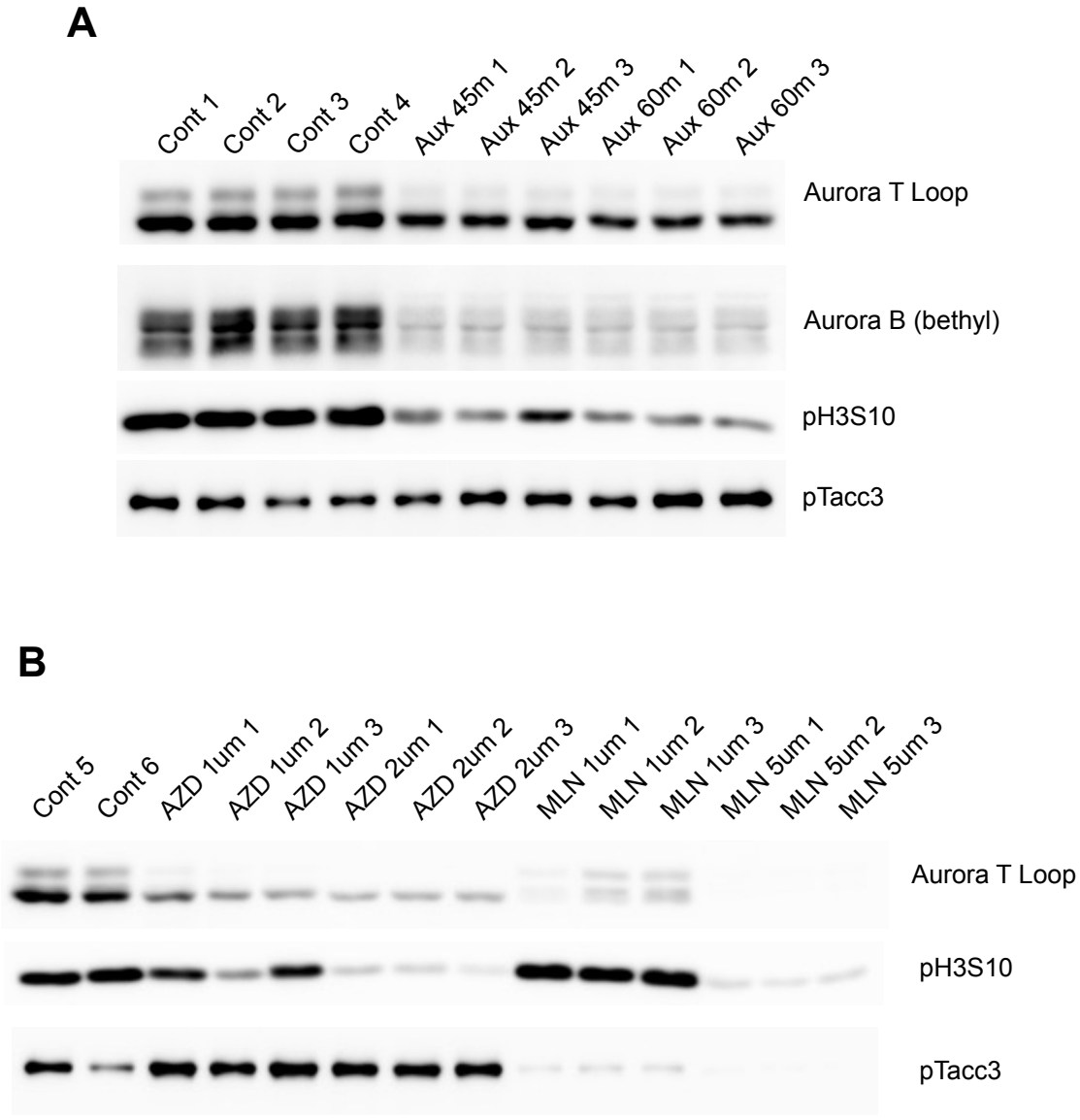

Figure 5.10. Western blot validation of Aurora B degradation and inhibition in STLC arrest. AurKB-AID cells were cultured in 15cm dishes, thymidine synchronized, and arrested overnight with STLC. In triplicates, plates of cells were treated with auxin (Aux) for 45 or 60 minutes, or with 1μM AZD1152 (AZD), 2μM AZD1152, 1μM MLN8054 (MLN), or 5μM MLN8054 for 45 minutes. Six plates of cells were left untreated as controls (Cont). A small sample was saved from the collected cells for analysis by western blot, shown here. Phosphorylation of the Aurora B T loop and H3S10 demonstrated a strong reduction in

Aurora B activity with Aurora B degradation or inhibition by AZD1152. Aurora A activity was greatly depleted in both concentrations of MLN8054.

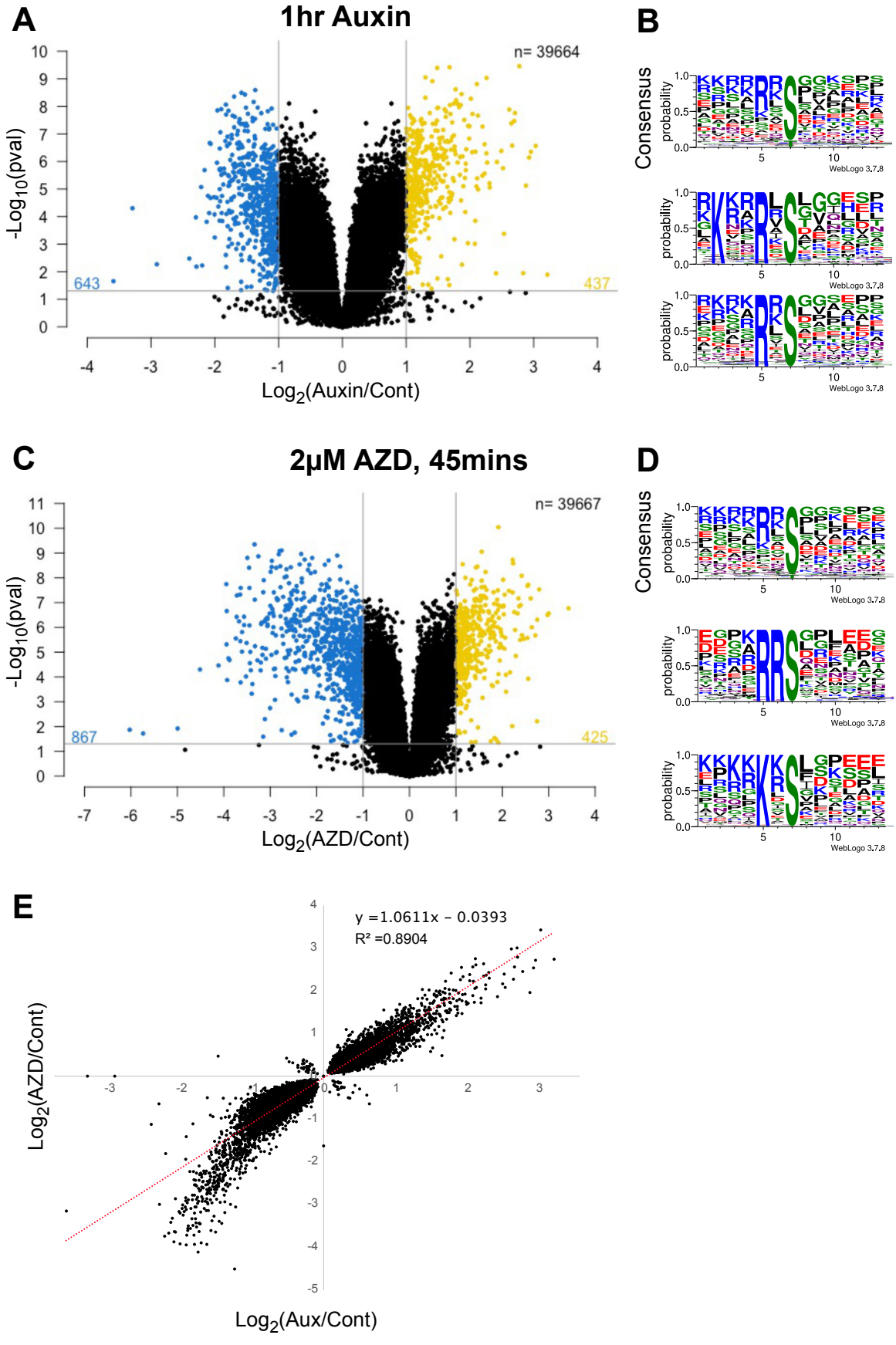
A
1hr Auxin
n= 39664
643
437
-Log10(pval)
Log2(Auxin/Cont)
B
Consensus
probability
WebLogo 3.7.8
C
2μM AZD, 45mins
n= 39667
867
425
-Log10(pval)
Log2(AZD/Cont)
D
Consensus
probability
WebLogo 3.7.8
E
y =1.0611x - 0.0393
R² =0.8904
Log2(AZD/Cont)
Log2(Aux/Cont)

Figure 5.11. Phosphoproteomics of Aurora B degradation or Aurora B inhibition in cells arrested with STLC. **A)** Volcano plot showing the $\log_2$(fold-change) in abundance vs. the -$\log_{10}$(p-value) after 1hr Aurora B degradation with auxin. Phosphopeptides that are significantly reduced ($\log_2$(fold-change) < -1) or increased ($\log_2$(fold-change) > 1) are plotted in blue and yellow, respectively. In total, 39,664 phosphopeptides were identified and quantified in degradation and control with a 643 phosphopeptides significantly reduced after Aurora B degradation. **B)** Motif analyses were performed to analyze enrichment of amino acid sequences in significantly decreased phosphopeptides and were plotted in these WebLogos. The consensus motif is shown on the top and two of the highest scoring motifs that were previously reported, KxxRxS and RxS are shown below. **C)** Volcano plots showing change in abundance of phosphopeptides after inhibition with 2μM AZD1152, an Aurora B-specific inhibitor. In total, 867 phosphopeptides were significantly decreased after inhibition and are plotted in blue. **D)** Motif analysis of phosphopeptide sequences significantly decreased after AZD1152 inhibition. The consensus motif is shown on the top and two of the highest scoring motifs that have been previously reported, RRS and KxS, are shown below. **E)** The $\log_2$(fold-change) in auxin (x-axis) plotted against $\log_2$(fold-change) in AZD1152 (y-axis) with the linear regression plotted in red for all statistically significant phosphopeptides. This plot highlights a strong correlation for reduction in abundance of phosphosites in auxin and AZD.

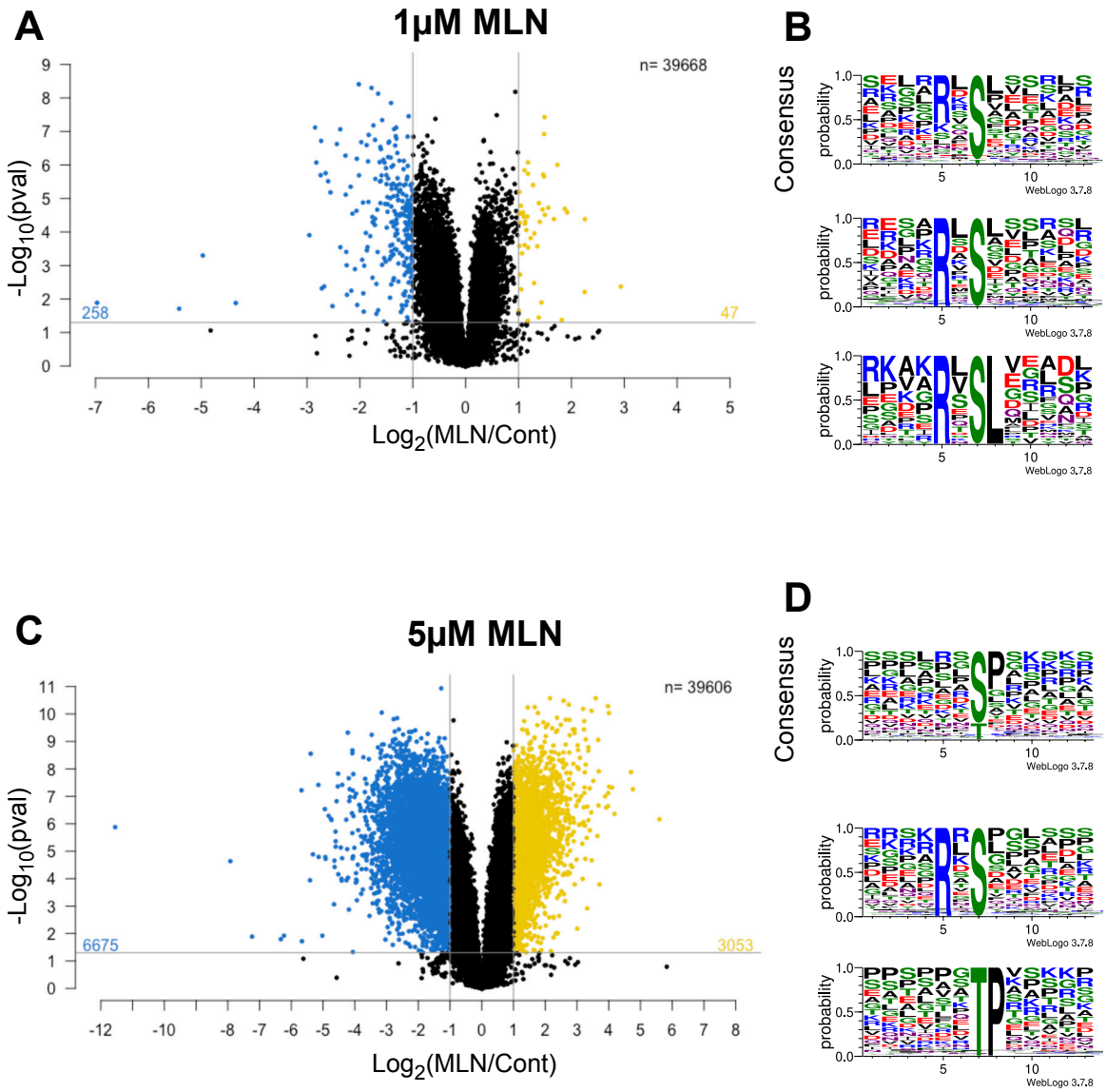

Figure 5.12. Phosphoproteomics of Aurora inhibition by MLN8054. **A)** Volcano plots showing the $\log_2$(fold change) in abundance against the $-\log_{10}$(p-value) for phosphopeptides after 45-minute treatment with 1μM MLN8054. Significantly reduced ($\log_2$(fold-change) < -1) or increased ($\log_2$(fold-change) > 1) phosphopeptides are plotted in blue and yellow, respectively. **B)** Motif analysis on significantly reduced phosphopeptides revealed an enrichment for basic residues in the upstream positions, as shown in these WebLogos. The consensus motif is shown on the top along with two highest scoring motifs, RxS and RxSL **C)** Volcano plot showing change in abundance of

phosphopeptides after treatment with 5μM MLN8054. In total, 6,675 phosphopeptides were significantly reduced after MLN treatment. **D)** Motif analysis revealed an enrichment of SP and TP sequences, suggesting that many downregulated phosphosites are CDK1/Cyclin B substrates and that cells were escaping mitotic arrest after MLN treatment. However, Aurora A motifs, such as RxS, were still identified within the downregulated phosphopeptides.

Chapter 6

Discussion and Future Directions

Summary

Over the last few decades, tremendous efforts have been made to study phosphorylation signaling networks, generate new tools and methodologies to interrogate kinases and phosphatases, and adapt what we have learned to develop novel therapeutics that combat devastating diseases like cancer. In part, this has been due to improvements in proteomics and mass spectrometry, which have allowed researchers to analyze complex samples at greater depth and with faster throughput than has been previously possible. This has, for example, enabled profiling of kinase phosphorylation motifs for the majority of serine/threonine kinases (Johnson et al., 2023), comprehensive study of stable protein-protein interactions in multiple cell lines (Huttlin et al., 2021), and deep proteomic coverage across hundreds of cancer cell lines to identify expression patterns (Nusinow et al., 2020). Our research group has been interested in developing and applying targeted protein degradation (TPD) strategies to study kinase-substrate relationships. As a proof-of-concept, we applied this workflow to Plk1, using a highly selective Plk1 inhibitor as ground truth, and found that targeted protein degradation can be used as an analogous approach to small-molecule inhibition (Hards et al., 2021). Following up on this result, we were motivated to expand this approach to other use cases for kinases of interest within the Polo-like kinase (Plk), p21-Activated kinase (PAK), and Aurora kinase families.

In the previous pages, data was presented showing the application of TPD to the study of Plk3, a kinase that is closely related to Plk1, but for which very little is known. We used a combination of targeted protein degradation and small molecule inhibitors of the group 1 PAKs to identify PAK1-dependent phosphosites and assess the extent of redundancy between PAK1 and PAK2. We greatly improved the efficiency of our cell-line generation process through the use of fluorescent reporter proteins and fluorescence-activated cell sorting (FACS). In addition, we applied fluorescent protein reporters to generate a parental Tir1 cell line to use as a starting point for auxin-inducible degron (AID) tagging CRISPR experiments. Finally, we applied this new workflow to rapidly generate cell lines for the study of Aurora A and Aurora B. Using targeted protein degradation, we are now able to assess substrate overlap between these two kinases to an extent that was not previously possible with small molecule inhibitors.

Polo-like kinase 3

Unfortunately, our attempts to create AID-Plk3 cell lines, whether through endogenous tagging or ectopic expression, were not successful. Initial tagging experiments led us to believe that the gene structure of Plk3 was impeding CRISPR-Cas9 gene editing. We observed that both the N- and C-terminus of Plk3 have a high GC content, and we hypothesized that this could hinder binding of Cas9 to the endogenous locus. Another possibility we considered is that the Plk3 locus is maintained in a more closed state in a region of more compacted chromatin. Regardless, the inability to achieve endogenous tagging of Plk3 was observed across multiple cell lines and at both termini of the Plk3 endogenous locus.

As we have progressed with AID-tagging experiments over the last few years, we have learned the importance of guide RNA choice in CRISPR-Cas9 experiments. For numerous genes of interest, we have observed high variability in the efficiency of sgRNAs to induce double-strand breaks (DSBs) and homology directed repair (HDR). Therefore, it is possible that the inability to endogenously tag Plk3 was the result of ineffective sgRNAs for both the N- and C-terminus. It would therefore be interesting to apply the fluorescent reporter-based methods outlined in chapter 3 of this thesis in attempts to endogenously tag Plk3 using a wider range of sgRNAs targeting both termini. However, another possibility is that these results were due to low transcriptional activity of Plk3. If this is the case, the reporter proteins used to select tagged clones would not be expressed, making it impossible to identify homozygous knock-in cells with either targeting method. Thus, it may be necessary to improve the fluorescent reporter system through the use of brighter fluorescent proteins or multiple fluorescent proteins in tandem to boost signal intensity.

The observation that many commonly used Plk3 antibodies may detect proteins other than Plk3 calls into question the reproducibility of previous Plk3 literature (Aquino Perez et al., 2020). Another interesting observation is that Plk3 protein is not detectable in a deep analysis of the HeLa proteome, indicating that this protein may not expressed in HeLa cells (Sharma et al., 2014). Finally, Plk3 protein data is not represented in the CCLE proteomics data set (Nusinow et al., 2020), which covers proteins from 375 cancer cell lines across the CCLE, and it is not represented in the BioPlex network, which includes proteomics data from thousands of immunoprecipitation experiments conducted in 293T and HCT116 cells (Huttlin et al., 2021). Importantly, the closely related kinase, Plk2, is

represented at the proteomics level in both of these datasets, even though Plk2 is known to be a low abundant protein. Taken together, all of these observations are strong evidence that, if Plk3 is expressed, it is likely below the limit of detection even for highly sensitive methods. The combination of low expression with a lack of tools partially explains the difficulties surrounding endogenous tagging of Plk3 and suggests that it may not be possible to study Plk3 signaling using conventional methods without overexpression.

The results of the AAVS1 ectopic expression experiments are perhaps the most difficult to reconcile, as we have had repeated success expressing proteins with this method. An inability to ectopically express Plk3 suggests that its expression is tightly controlled and is being downregulated after insertion into the AAVS1 locus. In fact, similar results have been frequently observed in Plk1 endogenous tagging. In the case of Plk1, the level of expression is controlled within a narrow range to maintain cell viability. One possibility is that higher than normal levels of Plk3 expression could result in nonviability, potentially by triggering apoptotic signaling pathways, pushing cells to downregulate Plk3. This could be the case in cells that are originally derived from tumors, as is the case for HeLas and DLD1s. A common observation in transformed cancer cells is a reduction in tumor suppressor proteins, such as p53, which typically mediate responses to stress and induce apoptosis. As a hypothesized tumor suppressor, it could be that the reduction in Plk3 protein is necessary for continued cell survival in these cell lines. This idea would fit well with the idea that Plk3 is primarily thought to function in the DNA damage and oxidative stress response pathways, which may be more toxic for transformed cancer cell lines than untransformed cells.

Moving forward, it would be interesting to explore potential Plk3 interactors and substrates using overexpression studies. This could be performed with transiently expressed 3xF-AID-Plk3 into a Tir1 background in various cell lines including HeLa, 293, and DLD1. Similar to endogenously tagged cell lines, the addition of auxin would trigger rapid depletion of Plk3 which could be used in phosphoproteomics experiments to analyze all of the candidate Plk3 substrates. In tandem, proximity labeling experiments using transiently expressed TurboID-Plk3 in the same background could be used to categorize the potential Plk3 interactome. Ideally, these experiments would result in datasets containing all of the phosphosites that can be phosphorylated by Plk3 as well as all of the proteins that can interact with Plk3 and the intersection of the two datasets may provide insight into the kinds of pathways that Plk3 is regulating at the endogenous level. The

obvious drawback with this experimental approach is that transient expression of Plk3 into almost any background would be orders of magnitude higher expression than endogenous Plk3, potentially leading to the identification of many false positives. Regardless, given the difficulties in targeting the Plk3 endogenous locus or stable integration of Plk3 into ectopic loci, alternative methods should be considered to provide insight into signaling pathways regulated by Plk3 and how the disruption of those pathways contributes to oncogenesis.

Improvements to AID-Tir1 targeted degradation

The introduction of fluorescent proteins as reporters to the AID-Tir1 system has proven to be a valuable asset in our CRISPR-Cas9 targeting toolbox. AID knock-in to an endogenous locus using fluorescent proteins as a mechanism of selection in a degrading Tir1 background has drastically reduced the time required to generate AID-kinase cell lines, and in some cases, this can be achieved in as little as one month. Moreover, this approach has greatly improved the efficiency of gene tagging, enabling routine tagging of proteins of interest even in cases where previous methods fell short. This is likely the result of reducing the number of CRISPR-Cas9 transfections from three per target to one. In our previous method, we applied multiple rounds of CRISPR-Cas9 to ensure editing at each allele and homozygous AID knock-in. However, this approach hinges on having an efficient sgRNA for each round of CRISPR transfection. We have observed significant variability in the efficiency of promoting DSBs and HDR for different sgRNAs, and it is a challenge to identify three sgRNAs that all consistently promote efficient tag incorporation. By screening clones after only a single round of CRISPR-Cas9 transfection, it is only necessary to have one sgRNA that efficiently promotes HDR and results in homozygous knock-ins, enabling us to test a greater range of sgRNAs and identify those with the highest knock-in efficiency.

The incorporation of fluorescent reporter proteins and fluorescence-activated cell sorting (FACS) into our CRISPR-Cas9 workflow has revolutionized our capabilities for generating cell lines. This approach has been successfully employed to create cell lines for various kinase and phosphatase targets within our group and has been instrumental in efficiently generating these cell lines. Improvements in this area were especially evident when tagging Aurora kinase A. We were previously unable to generate degrading AID-Aurora A cell lines using the antibiotic selection method, despite extensive screening of

clones after both the second and third round of CRISPR-Cas9 hits. Using fluorescent reporters as a selection method, we found that only one guide, sgRNA 1, efficiently promoted HDR while the other two were ineffective. The ability to perform CRISPR-Cas9 experiments with more guides and only relying on a single round of transfection has greatly improved the speed and efficiency of recovering AID-kinase cell lines. In addition, we have found that insertion of larger tags, such as a combination AID-TurboID tag that is more than seven times larger than the AID tag alone, is less efficient, and generating homozygous knock-in clones is more challenging. However, we have been able to apply fluorescent reporters as a selection method for the incorporation of bulkier tags and efficiently recover homozygous knock-in cell lines for multiple proteins of interest using this approach. As our group moves forward with the development of a combination BioID/AID approach for phosphoproteomics, the use of fluorescent reporters and FACS will continue to be a valuable asset to quickly develop cell lines for kinases of interest.

Recently, a study was performed analyzing the degradation kinetics of a variety of genetically encoded targeted protein degradation systems on a range of protein targets (Bondeson et al., 2022). The authors found that the degradation kinetics and extent of degradation are highly variable and dependent on individual protein targets. This observation fits with observations from the PROTAC field that suggest the ability of a protein to form a ternary complex with the recruited E3 ligase is crucial for degradation to occur (Li & Crews, 2022). The experiments conducted in this study demonstrated that targeted protein degradation is not a one-size-fits-all approach and underscores the importance of testing multiple degradation strategies for each protein of interest. Our GFP-P2A-mCherry degradation reporter system could be adapted and applied to evaluate a range of degradation systems before CRISPR-Cas9 targeting. For this to work, various degrons, including AID, HaloTag, and $FKBP12^{F36V}$, would be appended to the N-terminus of GFP, and the protein of interest would be appended to the C-terminus. Transient expression of the construct and subsequent treatment with a small molecule to induce degradation could be used to monitor the extent and rate of degradation in a variety of cell lines by flow cytometry. This experimental procedure would be a quick method to test multiple degradation approaches for a protein of interest before endogenous tagging by CRISPR-Cas9, aiding in the identification of the degradation strategy most likely to result in rapid and extensive depletion for the protein of interest.

The AID-GFP-P2A-mCherry reporter construct is also valuable for conducting AID tag shortening experiments to identify a minimal degron. By making truncations of the AID tag starting from either the N- or C-terminus and cloning them into the reporter construct, we can analyze their capacity for degradation when expressed in Tir1 cells. This analysis will allow us to identify a minimal AID sequence that still enables efficient auxin-induced degradation. An AID tag with a reduced footprint will be valuable for future CRISPR-Cas9 experiments by decreasing the size of the insert and thereby increasing efficiency of tag incorporation. In addition, a tandem version of this minimal AID sequence could be created to further boost degradation efficiency.

Although the improvements to the CRISPR-Cas9 AID tagging workflow greatly enhanced tagging efficiency, the process of generating AID cell lines for kinases of interest still necessitates screening hundreds of individual clones by western blot. This workload becomes a barrier to working with more than one target at a time. Ideally, our fluorescent reporter system could be adapted to minimize screening and improve throughput. One way this could be accomplished is by appending an AID tag to the fluorescent reporter of a targeting construct, providing a means to monitor degradation using fluorescent intensity. The use of an Incucyte incubator, capable of imaging multi-well plates within the incubator, could be adapted to monitor expression of the fluorescent reporter at the 96-well stage and also to detect loss of fluorescent intensity in the presence of auxin. In theory, only the clones that express the fluorescent protein and exhibit its degradation upon auxin treatment would have in-frame insertion of the targeting construct and functional Tir1 activity. The combination of fluorescent reporters with a high-throughput monitoring system like the Incucyte should facilitate clonal screening at earlier stages without the need to harvest individual clones.

The development of higher throughput methods would be advantageous for the generation of AID cell lines because generation of many clones in the same experiment would reduce the effects of clonal variability. In our experience, clonally isolated cell lines often display considerable variation with respect to their morphology, growth rate, and signaling networks. This is a challenge for phosphoproteomics experiments that detect even subtle changes in cell signaling. When studying the phosphorylation signaling networks regulated by a kinase or phosphatase of interest, it is essential to ensure that the observed effects are not the result of clonal variability and are more broadly applicable. Cultured cells are known to experience genetic drift over time, and two cells from the same

parent population may grow into distinct populations owing to the unique set of acquired mutations (Liu et al., 2019; Tang, 2019). This is especially true for cell populations derived from a single cell. To correct this bottleneck effect, it would be ideal to isolate many AID clones for a single gene target and recombine them into a single population, ensuring the engineered cell line resembles the parent population as closely as possible.

Although endogenous targeting offers several benefits for targeted protein degradation, including maintenance of native transcriptional regulatory mechanisms, the drawbacks of this approach seem to outweigh the benefits as generating homozygous knock-ins due to the labor-intensive and time-consuming process of generating homozygous AID knock-ins with CRISPR-Cas9. A significant consideration is the months-long wait times to develop a cell line for a target protein as well as the necessity to screen hundreds of individual colonies. Therefore, the development of a knock-out and replace strategy that does not rely on endogenous tagging to make cell lines would be a significant improvement to the workflow. One possible approach would be knocking in an AID-tagged version of the protein of interest to a safe-harbor locus, such as the hRosa26 locus, while simultaneously transfecting sgRNAs to knock out the endogenous gene, which could be accomplished in a single transfection experiment. An efficient knockout and replace strategy would reduce the time needed to generate a cell line and cut down on issues with clonal variability.

p21-Activated Kinase 1 (PAK1)

To gain a deeper understanding of the PAK1-dependent phosphoproteome, we generated AID-PAK1 cell lines in 293s to analyze the effects of acute PAK1 degradation and compared the results to inhibition by a selective inhibitor of the group 1 PAKs, NVS-PAK1-1. Our initial PAK1 degradation experiments suggested that basal PAK1 activity is relatively low because we were unable to identify PAK1-dependent phosphosites that conformed to the previously characterized PAK1 phosphorylation motif. Experiments in SU.86.86, a pancreatic cancer cell line that has been reported to have high PAK1 and PAK2 expression and activity, also revealed that NVS-PAK1-1, at concentrations that inhibit PAK1 but not PAK2, did not cause identifiable changes to the phosphoproteome. However, we consistently observed that inhibition of PAK1 and PAK2 with higher concentrations of NVS-PAK1-1 resulted in significant decrease of hundreds of

phosphosites, indicating that signaling pathways regulated by group 1 PAKs are active in these cell lines. We hypothesized that either PAK2 is responsible for phosphorylation signaling of group 1 PAK-dependent phosphosites, or that PAK1 and PAK2 have overlapping or redundant functions in the cell.

To hyperactive PAK1 signaling, we expressed constitutively active Cdc42 or stimulated the EGFR pathway with EGF, but we were unable to consistently identify downstream activation of PAK1 or PAK2. The results of these hyperactivation experiments were surprising and contradict reports in the literature, which routinely define roles for PAK1 as a Cdc42 effector and as an important node in the EGF and KRAS signaling pathways. Despite validation by western blot of the induction of constitutively active Cdc42 at levels comparable to endogenous, proteomics experiments did not reveal abundant changes to the phosphoproteome. It is possible that this is the result of carrying out these experiments in 293 cells, which are semi-adherent. If other key regulators of cytoskeletal remodeling are either missing or inactive in this cell line, it could have prevented a strong activation by induced Cdc42. To test this theory, it would be necessary to generate inducible Cdc42 lines in other adherent cell types, such as HeLa, U2OS, or SU.86.86, and analyze effects on the proteome and phosphoproteome in response to Cdc42 induction. This would confirm if our observations were the result of performing these experiments in semi-adherent 293s or if constitutively active Cdc42 is not sufficient to activate PAK1 and PAK2 signaling in broader contexts. The results of stimulation with EGF are equally surprising given the number of studies demonstrating downstream PAK1 activation in this pathway. Despite strong evidence of EGFR pathway activation in HeLa, 293, and SU.86.86, we never observed PAK1 or PAK2 activation in response to EGF stimulation. Taken together, our attempts to hyperactive PAK1 using Cdc42 or EGF demonstrate that PAK1 does not have a universal involvement in these pathways and that its activity is likely to be more context dependent than previously suspected.

Overall, the results of the PAK1-focused experiments presented in this thesis demonstrate a need to reevaluate the relationship between PAK1 and PAK2. A deeper understanding of the signaling networks regulated by these kinases will help determine the extent of redundancy between the two, as well as their contributions to oncogenesis. It is possible that PAK2 plays more of a role as a small GTPase effector kinase than PAK1 and that interest in developing therapeutic inhibitors should be shifted towards PAK2.

Alternatively, it is possible that PAK1 and PAK2 serve redundant roles in common signaling pathways, and that depletion of the activity of one is not sufficient to block these pathways.

To study PAK1 and PAK2 redundancy, CRISPR knockout lines for both kinases could be generated in multiple cell types. This approach would isolate PAK1 and PAK2 to individual cell lines, allowing for the interrogation of one kinase in the absence of the other. Inhibition with group 1 PAK inhibitors would reveal all of the phosphorylation sites that can potentially be phosphorylated by either PAK1 or PAK2, providing insight into the extent of redundancy between these two kinases or revealing substrates and pathways that are specific to PAK1 or PAK2. Performing these experiments in multiple cell types would highlight how universal group 1 PAK signaling is and how PAK1 and PAK2 may compensate for each other in different cell types and signaling contexts.

An alternative method to investigate PAK1 and PAK2 signaling would be to identify cell lines that are dependent on PAK1 or PAK2 expression, and more likely to have high group 1 PAK signaling. For example, CRISPR knockout experiments that have been reported on the cancer DepMap portal reveal that two esophagogastric adenocarcinoma cell lines seem to be dependent on PAK1 expression and there are multiple ovarian and breast cancer cell lines that are dependent on PAK2 expression. It would be interesting to develop AID-PAK1 and AID-PAK2 lines in a variety of these cell types that are dependent on PAK1 and PAK2 and investigate the effects of acute group 1 PAK depletion on the phosphoproteome. Considering our difficulties with studying PAK signaling using traditional cell culture models, it appears necessary to identify specific cell types and cell states where these kinases are likely to be active in order to gain deeper insight into the pathways that these kinases regulate. However, using these approaches to develop a deeper understanding of the PAK1/PAK2 relationship, as well as how these kinases fit into signaling pathways that are implicated in cell motility and metastasis will be essential for informing the next generation of PAK-specific therapeutics.

Aurora Kinase B

We presented data showing the development and validation of an Aurora B-AID cell line in HeLa cells and used this cell line to obtain Aurora B-dependent phosphorylation sites in cells arrested with S-trityl-L-cysteine (STLC). Importantly, there is a high

correlation in the change in abundance of phosphorylation sites after the addition of auxin or the Aurora B inhibitor AZD1152, indicating that the Aurora B degradation and inhibition cause similar perturbations to the Aurora B-dependent phosphoproteome. However, we identified a subset of phosphosites that are downregulated with AZD1152 and MLN8054, but not with auxin, highlighting the potential for off-target effects with small molecule inhibitors and underscoring the selectivity of targeted protein degradation. Additionally, there is a subset of phosphopeptides that are significantly decreased with auxin, AZD1152, and MLN8054. This suggests that some phosphorylation sites may be regulated by Aurora A and Aurora B, which is an aspect of phosphorylation signaling in mitosis that has not been previously characterized. However, it is still not possible to rule out the effects of off-target inhibition by MLN8054 on Aurora B. The interpretation of these results will be greatly aided by phosphoproteomics experiments analyzing the effects of Aurora A degradation and a comparison of phosphorylation sites that are significantly downregulated after degradation of either Aurora A or Aurora B. Phosphoproteomics experiments analyzing the effects of Aurora A degradation in mitotically arrested cells are currently ongoing. Targeted degradation of either Aurora A or Aurora B will definitively determine if there are shared substrates of Aurora A and Aurora B, particularly at kinetochores, which would provide fascinating insight into how the Aurora kinases coordinate to regulate kinetochore-microtubule attachments.

Phosphoproteomics experiments showing the effects of Aurora B degradation or inhibition were conducted in cells arrested with STLC, an inhibitor of the kinesin Eg5. This was necessary to prevent mitotic escape after Aurora B inhibition or degradation, as was observed after mitotic arrest with taxol and nocodazole. Eg5 inhibition results in a monopolar spindle and attachment of chromosomes to a single centrosome. As a result, we would expect an absence of tension at kinetochore-microtubule attachment points and high activity of the spindle assembly checkpoint (SAC) and error correction checkpoint (EC). It would be interesting to compare the results from STLC arrest to a variety of other arrest conditions to analyze how Aurora B signaling changes through the cell cycle. To test this, we developed an inducible, non-degradable Cyclin B2 (ndCyclinB2) Aurora B-AID cell line. Induction of ndCyclinB2 is sufficient to induce mitotic arrest at metaphase because the persistent activity of Cdk1/Cyclin B prevents the activation of the phosphatases PP2A and PP1 that drive mitotic progression through anaphase. We would expect that, in ndCyclinB2-induced arrest, kinetochore-microtubule attachments would

form and stabilize, applying tension and resulting in low SAC and EC signaling. This arrest condition could be combined with taxol, which stabilizes microtubules, to create a tension-low and SAC/EC-high environment. Then, analysis by phosphoproteomics would reveal how Aurora B signaling evolves as tension is established.

Aurora B changes localization from centromeres to the central spindle at the onset of anaphase to regulate a host of sites related to the faithful resolution of mitosis and cytokinesis. Mitotic release experiments with our Aurora B-AID cell lines could be used to analyze the Aurora B substrates from the beginning of anaphase to the end of cytokinesis. One option to accomplish this would be to include an AID tag on ndCyclinB2 and arrest cells with ndCyclinB2 induction. Treatment with auxin would induce degradation of both Aurora B and ndCyclinB2, releasing the arrested cells into anaphase while simultaneously depleting Aurora B activity. A comparison between Aurora B depletion and control would reveal Aurora B substrates in later stages of mitosis. Furthermore, TMT multiplexing, which allows up to 18 conditions in a single experiment, could be used to track the change in Aurora B substrates with high temporal resolution, precisely tracking changes in Aurora B signaling in the later stages of mitosis.

A surprising finding to come out of this project is the existence of a second, truncated Aurora B isoform that has not been previously characterized. We identified this isoform after degradation of N-terminal AID-Aurora B failed to result in any identifiable changes to the phosphoproteome in mitotically arrested cells. Strangely, the Aurora B truncation appears to compensate for the loss of full-length Aurora B as prolonged degradation of AID-Aurora B in N-terminally tagged cells did not result in mitotic defects. Moreover, our initial Flag immunoprecipitation experiments for both full-length and truncated Aurora B isoforms did not reveal significant differences in the interactome. This poses an interesting question as to the utility of having two redundant Aurora B isoforms. Recently, it was shown that translational isoforms of Cdc20, a regulator of APC/C activity in mitosis, coordinate to regulate the duration of mitotic arrest (Tsang & Cheeseman, 2023). Considering that there is a degradation motif in the N-terminus of Aurora B that is missing in the truncated version, it is possible that a similar mechanism exists for Aurora B. Additionally, it is possible that the different Aurora B isoforms play slightly different roles in response to perturbations of mitosis. Both of these hypotheses could be tested by creating cell lines to specifically knock out one of the Aurora B isoforms and examining changes to the duration of mitotic arrest or responses to perturbations in mitosis. These

knockout cell lines could also be used in genome wide synthetic lethality screens to identify subtle differences in pathways regulated by the Aurora B isoforms. The existence of a second Aurora B isoform is an exciting finding but much more work is required to determine the significance of this isoform.

Another observation that should be investigated in future projects is the cross-regulation of Aurora A and Aurora B. These two kinases are not known to interact during mitosis, and it is thought that one does not contribute to the activation of the other. However, we have repeatedly observed that degradation of Aurora B leads to a decrease in phosphorylation of the Aurora A T loop, and vice versa. This effect is rapid, occurring within 30 minutes of degradation, and it has been observed in multiple mitotic arrest conditions. It is possible that this is an early sign of mitotic exit that occurs before Cyclin B degradation but given the rapidity and consistency of dephosphorylation in response to degradation, follow-up experiments are needed.

References

Adam, L., Vadlamudi, R., Mandal, M., Chernoff, J., & Kumar, R. (2000). Regulation of microfilament reorganization and invasiveness of breast cancer cells by kinase dead p21-activated kinase-1. *Journal of Biological Chemistry*, *275*(16), 12041-12050. https://doi.org/10.1074/jbc.275.16.12041

Aebersold, R., Agar, J. N., Amster, I. J., Baker, M. S., Bertozzi, C. R., Boja, E. S., Costello, C. E., Cravatt, B. F., Fenselau, C., Garcia, B. A., Ge, Y., Gunawardena, J., Hendrickson, R. C., Hergenrother, P. J., Huber, C. G., Ivanov, A. R., Jensen, O. N., Jewett, M. C., Kelleher, N. L., . . . Zhang, B. (2018). How many human proteoforms are there? *Nat Chem Biol*, *14*(3), 206-214. https://doi.org/10.1038/nchembio.2576

Aebersold, R., & Mann, M. (2003). Mass spectrometry-based proteomics. *Nature*, *422*(6928), 198-207. https://doi.org/10.1038/nature01511

Alexander, J., Lim, D., Joughin, B. A., Hegemann, B., Hutchins, J. R. A. A., Ehrenberger, T., Ivins, F. J., Sessa, F., Hudecz, O., Nigg, E. A., Fry, A. M., Musacchio, A., Stukenberg, P. T., Mechtler, K., Peters, J.-M. M., Smerdon, S. J., & Yaffe, M. B. (2011). Spatial Exclusivity Combined with Positive and Negative Selection of Phosphorylation Motifs Is the Basis for Context-Dependent Mitotic Signaling. *Science Signaling*, *4*(179), ra42-ra42. https://doi.org/10.1126/scisignal.2001796

Ando, K., Ozaki, T., Yamamoto, H., Furuya, K., Hosoda, M., Hayashi, S., Fukuzawa, M., & Nakagawara, A. (2004). Polo-like kinase 1 (Plk1) inhibits p53 function by physical interaction and phosphorylation. *J Biol Chem*, *279*(24), 25549-25561. https://doi.org/10.1074/jbc.M314182200

Aquino Perez, C., Palek, M., Stolarova, L., von Morgen, P., & Macurek, L. (2020). Phosphorylation of PLK3 Is Controlled by Protein Phosphatase 6. *Cells*, *9*(6). https://doi.org/10.3390/cells9061506

Archambault, V., & Carmena, M. (2012). Polo-like kinase-activating kinases: Aurora A, Aurora B and what else? *Cell Cycle*, *11*(8), 1490-1495. https://doi.org/10.4161/cc.19724

Archambault, V., & Glover, D. M. (2009). Polo-like kinases: Conservation and divergence in their functions and regulation. In *Nature Reviews Molecular Cell Biology* (Vol. 10, pp. 265-275): Nature Publishing Group.

Archambault, V., Lépine, G., & Kachaner, D. (2015). Understanding the Polo Kinase machine. In *Oncogene* (Vol. 34, pp. 4799-4807): Nature Publishing Group.

Ardito, F., Giuliani, M., Perrone, D., Troiano, G., & Lo Muzio, L. (2017). The crucial role of protein phosphorylation in cell signaling and its use as targeted therapy (Review). *Int J Mol Med*, *40*(2), 271-280. https://doi.org/10.3892/ijmm.2017.3036

Asteriti, I. A., De Mattia, F., & Guarguaglini, G. (2015). Cross-Talk between AURKA and Plk1 in Mitotic Entry and Spindle Assembly. *Front Oncol*, *5*, 283. https://doi.org/10.3389/fonc.2015.00283

Attwood, M. M., Fabbro, D., Sokolov, A. V., Knapp, S., & Schioth, H. B. (2021). Trends in kinase drug discovery: targets, indications and inhibitor design. *Nat Rev Drug Discov*, *20*(11), 839-861. https://doi.org/10.1038/s41573-021-00252-y

Bahassi el, M., Conn, C. W., Myer, D. L., Hennigan, R. F., McGowan, C. H., Sanchez, Y., & Stambrook, P. J. (2002). Mammalian Polo-like kinase 3 (Plk3) is a multifunctional protein involved in stress response pathways. *Oncogene*, *21*(43), 6633-6640. https://doi.org/10.1038/sj.onc.1205850

Bahassi el, M., Hennigan, R. F., Myer, D. L., & Stambrook, P. J. (2004). Cdc25C phosphorylation on serine 191 by Plk3 promotes its nuclear translocation. *Oncogene*, *23*(15), 2658-2663. https://doi.org/10.1038/sj.onc.1207425

Bahassi, E. M., Myer, D. L., McKenney, R. J., Hennigan, R. F., & Stambrook, P. J. (2006). Priming phosphorylation of Chk2 by polo-like kinase 3 (Plk3) mediates its full activation by ATM and a downstream checkpoint in response to DNA damage. *Mutation Research - Fundamental and Molecular Mechanisms of Mutagenesis*, *596*(1-2 SPEC. ISS.), 166-176. https://doi.org/10.1016/j.mrfmmm.2005.12.002

Bard, J. A. M., Goodall, E. A., Greene, E. R., Jonsson, E., Dong, K. C., & Martin, A. (2018). Structure and Function of the 26S Proteasome. *Annu Rev Biochem*, *87*, 697-724. https://doi.org/10.1146/annurev-biochem-062917-011931

Barr, A. R., & Gergely, F. (2007). Aurora-A: the maker and breaker of spindle poles. *J Cell Sci*, *120*(Pt 17), 2987-2996. https://doi.org/10.1242/jcs.013136

Bayliss, R., Sardon, T., Vernos, I., & Conti, E. (2003). Structural basis of Aurora-A activation by TPX2 at the mitotic spindle. *Mol Cell*, *12*(4), 851-862. https://doi.org/10.1016/s1097-2765(03)00392-7

Best, M., Gale, M. E., & Wells, C. M. (2022). PAK-dependent regulation of actin dynamics in breast cancer cells. *Int J Biochem Cell Biol*, *146*, 106207. https://doi.org/10.1016/j.biocel.2022.106207

Biondi, R. M., & Nebreda, A. R. (2003). Signalling specificity of Ser/Thr protein kinases through docking-site-mediated interactions. *Biochem J*, *372*(Pt 1), 1-13. https://doi.org/10.1042/BJ20021641

Bird, A. W., & Hyman, A. A. (2008). Building a spindle of the correct length in human cells requires the interaction between TPX2 and Aurora A. *J Cell Biol*, *182*(2), 289-300. https://doi.org/10.1083/jcb.200802005

Bishop, A. C., Ubersax, J. A., Pøtsch, D. T., Matheos, D. P., Gray, N. S., Blethrow, J., Shimizu, E., Tsien, J. Z., Schultz, P. G., Rose, M. D., Wood, J. L., Morgan, D. O., & Shokat, K. M. (2000). A chemical switch for inhibitor-sensitive alleles of any protein kinase. *Nature*, *407*(6802), 395-401. https://doi.org/10.1038/35030148

Blethrow, J. D., Glavy, J. S., Morgan, D. O., & Shokat, K. M. (2008). Covalent capture of kinase-specific phosphopeptides reveals Cdk1-cyclin B substrates. *Proceedings of the National Academy of Sciences of the United States of America*, *105*(5), 1442-1447. https://doi.org/10.1073/pnas.0708966105

Bodenmiller, B., Mueller, L. N., Mueller, M., Domon, B., & Aebersold, R. (2007). Reproducible isolation of distinct, overlapping segments of the phosphoproteome. *Nat Methods*, *4*(3), 231-237. https://doi.org/10.1038/nmeth1005

Boersema, P. J., Foong, L. Y., Ding, V. M., Lemeer, S., van Breukelen, B., Philp, R., Boekhorst, J., Snel, B., den Hertog, J., Choo, A. B., & Heck, A. J. (2010). In-depth qualitative and quantitative profiling of tyrosine phosphorylation using a combination of phosphopeptide immunoaffinity purification and stable isotope dimethyl labeling. *Mol Cell Proteomics*, *9*(1), 84-99. https://doi.org/10.1074/mcp.M900291-MCP200

Boersema, P. J., Raijmakers, R., Lemeer, S., Mohammed, S., & Heck, A. J. (2009). Multiplex peptide stable isotope dimethyl labeling for quantitative proteomics. *Nat Protoc*, *4*(4), 484-494. https://doi.org/10.1038/nprot.2009.21

Bokoch, G. M. (2003). Biology of the p21-Activated Kinases. *Annual Review of Biochemistry*, *72*(1), 743-781. https://doi.org/10.1146/annurev.biochem.72.121801.161742

Bondeson, D. P., Mullin-Bernstein, Z., Oliver, S., Skipper, T. A., Atack, T. C., Bick, N., Ching, M., Guirguis, A. A., Kwon, J., Langan, C., Millson, D., Paolella, B. R., Tran, K., Wie, S. J., Vazquez, F., Tothova, Z., Golub, T. R., Sellers, W. R., & Ianari, A. (2022). Systematic profiling of conditional degron tag technologies for target validation studies. *Nat Commun*, *13*(1), 5495. https://doi.org/10.1038/s41467-022-33246-4

Bondeson, D. P., Smith, B. E., Burslem, G. M., Buhimschi, A. D., Hines, J., Jaime-Figueroa, S., Wang, J., Hamman, B. D., Ishchenko, A., & Crews, C. M. (2018). Lessons in PROTAC Design from Selective Degradation with a Promiscuous Warhead. *Cell Chemical Biology*, *25*(1), 78-87.e75. https://doi.org/10.1016/j.chembiol.2017.09.010

Brautigan, D. L., & Shenolikar, S. (2018). Protein Serine/Threonine Phosphatases: Keys to Unlocking Regulators and Substrates. *Annu Rev Biochem*, *87*, 921-964. https://doi.org/10.1146/annurev-biochem-062917-012332

Brown, N. R., Noble, M. E. M., Endicott, J. A., & Johnson, L. N. (1999). The structural basis for specificity of substrate and recruitment peptides for cyclin-dependent kinases. *NATURE CELL BIOLOGY*, *1*(7), 438-443. https://doi.org/10.1038/15674

Buckley, D. L., Raina, K., Darricarrere, N., Hines, J., Gustafson, J. L., Smith, I. E., Miah, A. H., Harling, J. D., & Crews, C. M. (2015). HaloPROTACS: Use of Small Molecule PROTACs to Induce Degradation of HaloTag Fusion Proteins. *ACS Chemical Biology*, *10*(8), 1831-1837. https://doi.org/10.1021/acschembio.5b00442

Buehler, E., Khan, A. A., Marine, S., Rajaram, M., Bahl, A., Burchard, J., & Ferrer, M. (2012). siRNA off-target effects in genome-wide screens identify signaling pathway members. *Sci Rep*, *2*, 428. https://doi.org/10.1038/srep00428

Burgess, S. G., Peset, I., Joseph, N., Cavazza, T., Vernos, I., Pfuhl, M., Gergely, F., & Bayliss, R. (2015). Aurora-A-Dependent Control of TACC3 Influences the Rate of Mitotic Spindle Assembly. *PLoS Genet*, *11*(7), e1005345. https://doi.org/10.1371/journal.pgen.1005345

Burslem, G. M., & Crews, C. M. (2020). Proteolysis-Targeting Chimeras as Therapeutics and Tools for Biological Discovery. In *Cell* (Vol. 181, pp. 102-114): Cell Press.

Burslem, G. M., Schultz, A. R., Bondeson, D. P., Eide, C. A., Stevens, S. L. S., Druker, B. J., & Crews, C. M. (2019). Targeting BCR-ABL1 in chronic myeloid leukemia by

PROTAC-mediated targeted protein degradation. *Cancer Research*, *79*(18), 4744-4753. https://doi.org/10.1158/0008-5472.CAN-19-1236

Burslem, G. M., Smith, B. E., Lai, A. C., Jaime-Figueroa, S., McQuaid, D. C., Bondeson, D. P., Toure, M., Dong, H., Qian, Y., Wang, J., Crew, A. P., Hines, J., & Crews, C. M. (2018). The Advantages of Targeted Protein Degradation Over Inhibition: An RTK Case Study. *Cell Chemical Biology*, *25*(1), 67-77.e63. https://doi.org/10.1016/j.chembiol.2017.09.009

Bylund, D. B., & Krebs, E. G. (1975). *Effect of Denaturation on the Susceptibility of Proteins to Enzymic Phosphorylation** (Journal of Biological Chemistry, Issue.

Carlson, S. M., Chouinard, C. R., Labadorf, A., Lam, C. J., Schmelzle, K., Fraenkel, E., & White, F. M. (2011). Large-scale discovery of ERK2 substrates identifies ERK-mediated transcriptional regulation by ETV3. *Sci Signal*, *4*(196), rs11. https://doi.org/10.1126/scisignal.2002010

Carmena, M., Pinson, X., Platani, M., Salloum, Z., Xu, Z., Clark, A., Macisaac, F., Ogawa, H., Eggert, U., Glover, D. M., Archambault, V., & Earnshaw, W. C. (2012). The chromosomal passenger complex activates Polo kinase at centromeres. *PLoS Biol*, *10*(1), e1001250. https://doi.org/10.1371/journal.pbio.1001250

Carmena, M., Ruchaud, S., & Earnshaw, W. C. (2009). Making the Auroras glow: regulation of Aurora A and B kinase function by interacting proteins. *Curr Opin Cell Biol*, *21*(6), 796-805. https://doi.org/10.1016/j.ceb.2009.09.008

Carmena, M., Wheelock, M., Funabiki, H., & Earnshaw, W. C. (2012). The chromosomal passenger complex (CPC): from easy rider to the godfather of mitosis. *Nat Rev Mol Cell Biol*, *13*(12), 789-803. https://doi.org/10.1038/nrm3474

Cheeseman, I. M., Chappie, J. S., Wilson-Kubalek, E. M., & Desai, A. (2006). The conserved KMN network constitutes the core microtubule-binding site of the kinetochore. *Cell*, *127*(5), 983-997. https://doi.org/10.1016/j.cell.2006.09.039

Choudhary, C., & Mann, M. (2010). Decoding signalling networks by mass spectrometry-based proteomics. *Nat Rev Mol Cell Biol*, *11*(6), 427-439. https://doi.org/10.1038/nrm2900

Chow, H. Y., Jubb, A. M., Koch, J. N., Jaffer, Z. M., Stepanova, D., Campbell, D. A., Duron, S. G., O'Farrell, M., Cai, K. Q., Klein-Szanto, A. J. P., Gutkind, J. S., Hoeflich, K. P., & Chernoff, J. (2012). P21-Activated Kinase 1 Is Required for Efficient Tumor Formation and Progression in a Ras-Mediated Skin Cancer

Model. *Cancer Research*, *72*(22), 5966-5975. https://doi.org/10.1158/0008-5472.CAN-12-2246

Cohen, P. (1992). Signal integration at the level of protein kinases, protein phosphatases and their substrates. *Trends Biochem Sci*, *17*(10), 408-413. https://doi.org/10.1016/0968-0004(92)90010-7

Cohen, P. (2000). The regulation of protein function by multisite phosphorylation--a 25 year update. *Trends Biochem Sci*, *25*(12), 596-601. https://doi.org/10.1016/s0968-0004(00)01712-6

Cohen, P. (2002a). The origins of protein phosphorylation. *Nat Cell Biol*, *4*(5), E127-130. https://doi.org/10.1038/ncb0502-e127

Cohen, P. (2002b). Protein kinases--the major drug targets of the twenty-first century? *Nat Rev Drug Discov*, *1*(4), 309-315. https://doi.org/10.1038/nrd773

Cohen, P., Cross, D., & Janne, P. A. (2021). Kinase drug discovery 20 years after imatinib: progress and future directions. *Nat Rev Drug Discov*, *20*(7), 551-569. https://doi.org/10.1038/s41573-021-00195-4

Cromm, P. M., & Crews, C. M. (2017). Targeted Protein Degradation: from Chemical Biology to Drug Discovery. In *Cell Chemical Biology* (Vol. 24, pp. 1181-1190): Elsevier Ltd.

Dai, W., Li, Y., Ouyang, B., Pan, H., Reissmann, P., Li, J., Wiest, J., Stambrook, P., Gluckman, J. L., Noffsinger, A., & Bejarano, P. (2000). PRK, a cell cycle gene localized to 8p21, is downregulated in head and neck cancer. *Genes Chromosomes Cancer*, *27*(3), 332-336. https://doi.org/10.1002/(sici)1098-2264(200003)27:3<332::aid-gcc15>3.0.co;2-k

Daile, P., Carnegie, P. R., & Young, J. D. (1975). Synthetic substrate for cyclic AMP-dependent protein kinase. *Nature*, *257*(5525), 416-418. https://doi.org/10.1038/257416a0

Daub, H., Gevaert, K., Vandekerckhove, J., Sobel, A., & Hall, A. (2001). Rac/Cdc42 and p65PAK regulate the microtubule-destabilizing protein stathmin through phosphorylation at serine 16. *J Biol Chem*, *276*(3), 1677-1680. https://doi.org/10.1074/jbc.C000635200

Davis, F. P. (2011). Phosphorylation at the interface. *Structure*, *19*(12), 1726-1727. https://doi.org/10.1016/j.str.2011.11.006

de Cárcer, G. (2019). The mitotic cancer target polo-like kinase 1: Oncogene or tumor suppressor? In *Genes* (Vol. 10): MDPI AG.

De Luca, M., Lavia, P., & Guarguaglini, G. (2006). A functional interplay between Aurora-A, Plk1 and TPX2 at spindle poles: Plk1 controls centrosomal localization of Aurora-A and TPX2 spindle association. *Cell Cycle*, *5*(3), 296-303. https://doi.org/10.4161/cc.5.3.2392

de Oliveira, P. S. L., Ferraz, F. A. N., Pena, D. A., Pramio, D. T., Morais, F. A., & Schechtman, D. (2016). Revisiting protein kinase-substrate interactions: Toward therapeutic development. *Science Signaling*, *9*(420). https://doi.org/10.1126/scisignal.aad4016

DeLuca, K. F., Meppelink, A., Broad, A. J., Mick, J. E., Peersen, O. B., Pektas, S., Lens, S. M. A., & DeLuca, J. G. (2018). Aurora A kinase phosphorylates Hec1 to regulate metaphase kinetochore-microtubule dynamics. *J Cell Biol*, *217*(1), 163-177. https://doi.org/10.1083/jcb.201707160

Deribe, Y. L., Pawson, T., & Dikic, I. (2010). Post-translational modifications in signal integration. *Nat Struct Mol Biol*, *17*(6), 666-672. https://doi.org/10.1038/nsmb.1842

Dharmasiri, N., Dharmasiri, S., & Estelle, M. (2005). The F-box protein TIR1 is an auxin receptor. *Nature*, *435*(7041), 441-445. https://doi.org/10.1038/nature03543

Ditchfield, C., Johnson, V. L., Tighe, A., Ellston, R., Haworth, C., Johnson, T., Mortlock, A., Keen, N., & Taylor, S. S. (2003). Aurora B couples chromosome alignment with anaphase by targeting BubR1, Mad2, and Cenp-E to kinetochores. *J Cell Biol*, *161*(2), 267-280. https://doi.org/10.1083/jcb.200208091

Doench, J. G., Fusi, N., Sullender, M., Hegde, M., Vaimberg, E. W., Donovan, K. F., Smith, I., Tothova, Z., Wilen, C., Orchard, R., Virgin, H. W., Listgarten, J., & Root, D. E. (2016). Optimized sgRNA design to maximize activity and minimize off-target effects of CRISPR-Cas9. *Nat Biotechnol*, *34*(2), 184-191. https://doi.org/10.1038/nbt.3437

Dohmen, R. J., & Varshavsky, A. (2005). Heat-inducible degron and the making of conditional mutants. In *Methods in Enzymology* (Vol. 399, pp. 799-822): Academic Press.

Dohmen, R. J., Wu, P., & Varshavsky, A. (1994). Heat-inducible degron: a method for constructing temperature-sensitive mutants. *Science*, *263*(5151), 1273-1276. https://doi.org/10.1126/science.8122109

Donohue, P. J., Alberts, G. F., Guo, Y., & Winkles, J. A. (1995). Identification by targeted differential display of an immediate early gene encoding a putative

serine/threonine kinase. *J Biol Chem*, *270*(17), 10351-10357. https://doi.org/10.1074/jbc.270.17.10351

Draviam, V. M., Orrechia, S., Lowe, M., Pardi, R., & Pines, J. (2001). The localization of human cyclins B1 and B2 determines CDK1 substrate specificity and neither enzyme requires MEK to disassemble the Golgi apparatus. *J Cell Biol*, *152*(5), 945-958. https://doi.org/10.1083/jcb.152.5.945

Eckerdt, F., Yuan, J., & Strebhardt, K. (2005). Polo-like kinases and oncogenesis. In *Oncogene* (Vol. 24, pp. 267-276).

Edwards, D. C., Sanders, L. C., Bokoch, G. M., & Gill, G. N. (1999). Activation of LIM-kinase by Pak1 couples Rac/Cdc42 GTPase signalling to actin cytoskeletal dynamics. *NATURE CELL BIOLOGY*, *1*(5), 253-259. https://doi.org/10.1038/12963

Elia, A. E., Cantley, L. C., & Yaffe, M. B. (2003). Proteomic screen finds pSer/pThr-binding domain localizing Plk1 to mitotic substrates. *Science*, *299*(5610), 1228-1231. https://doi.org/10.1126/science.1079079

Elia, A. E., Rellos, P., Haire, L. F., Chao, J. W., Ivins, F. J., Hoepker, K., Mohammad, D., Cantley, L. C., Smerdon, S. J., & Yaffe, M. B. (2003). The molecular basis for phosphodependent substrate targeting and regulation of Plks by the Polo-box domain. *Cell*, *115*(1), 83-95. https://doi.org/10.1016/s0092-8674(03)00725-6

Eyers, P. A., Erikson, E., Chen, L. G., & Maller, J. L. (2003). A novel mechanism for activation of the protein kinase Aurora A. *Curr Biol*, *13*(8), 691-697. https://doi.org/10.1016/s0960-9822(03)00166-0

Ficarro, S. B., McCleland, M. L., Stukenberg, P. T., Burke, D. J., Ross, M. M., Shabanowitz, J., Hunt, D. F., & White, F. M. (2002). Phosphoproteome analysis by mass spectrometry and its application to Saccharomyces cerevisiae. *Nat Biotechnol*, *20*(3), 301-305. https://doi.org/10.1038/nbt0302-301

Fuller, B. G., Lampson, M. A., Foley, E. A., Rosasco-Nitcher, S., Le, K. V., Tobelmann, P., Brautigan, D. L., Stukenberg, P. T., & Kapoor, T. M. (2008). Midzone activation of aurora B in anaphase produces an intracellular phosphorylation gradient. *Nature*, *453*(7198), 1132-1136. https://doi.org/10.1038/nature06923

Ghandi, M., Huang, F. W., Jane-Valbuena, J., Kryukov, G. V., Lo, C. C., McDonald, E. R., 3rd, Barretina, J., Gelfand, E. T., Bielski, C. M., Li, H., Hu, K., Andreev-Drakhlin, A. Y., Kim, J., Hess, J. M., Haas, B. J., Aguet, F., Weir, B. A., Rothberg, M. V., Paolella, B. R., . . . Sellers, W. R. (2019). Next-generation characterization of the

Cancer Cell Line Encyclopedia. *Nature*, *569*(7757), 503-508. https://doi.org/10.1038/s41586-019-1186-3

Ghenoiu, C., Wheelock, M. S., & Funabiki, H. (2013). Autoinhibition and Polo-dependent multisite phosphorylation restrict activity of the histone H3 kinase Haspin to mitosis. *Mol Cell*, *52*(5), 734-745. https://doi.org/10.1016/j.molcel.2013.10.002

Giet, R., Uzbekov, R., Cubizolles, F., Le Guellec, K., & Prigent, C. (1999). The Xenopus laevis aurora-related protein kinase pEg2 associates with and phosphorylates the kinesin-related protein XlEg5. *J Biol Chem*, *274*(21), 15005-15013. https://doi.org/10.1074/jbc.274.21.15005

Goroshchuk, O., Kolosenko, I., Vidarsdottir, L., Azimi, A., & Palm-Apergi, C. (2019). Polo-like kinases and acute leukemia. In *Oncogene* (Vol. 38): Nature Publishing Group.

Grassetti, A. V., Hards, R., & Gerber, S. A. (2017). Offline pentafluorophenyl (PFP)-RP prefractionation as an alternative to high-pH RP for comprehensive LC-MS/MS proteomics and phosphoproteomics. *Analytical and Bioanalytical Chemistry*, *409*(19), 4615-4625. https://doi.org/10.1007/s00216-017-0407-6

Grosstessner-Hain, K., Hegemann, B., Novatchkova, M., Rameseder, J., Joughin, B. A., Hudecz, O., Roitinger, E., Pichler, P., Kraut, N., Yaffe, M. B., Peters, J. M., & Mechtler, K. (2011). Quantitative phospho-proteomics to investigate the polo-like kinase 1-dependent phospho-proteome. *Molecular and Cellular Proteomics*, *10*(11), M111.008540-M008111.008540. https://doi.org/10.1074/mcp.M111.008540

Hadders, M. A., & Lens, S. M. A. (2022). Changing places: Chromosomal Passenger Complex relocation in early anaphase. *Trends Cell Biol*, *32*(2), 165-176. https://doi.org/10.1016/j.tcb.2021.09.008

Hanahan, D., & Weinberg, R. A. (2011). Hallmarks of cancer: The next generation. In *Cell*.

Hanzl, A., & Winter, G. E. (2020). Targeted protein degradation: current and future challenges. *Current Opinion in Chemical Biology*, *56*. https://doi.org/10.1016/j.cbpa.2019.11.012

Hards, R., Howarth, C. L., Wiredu, K., LaCroix, I., Valle, J. M. d., Adamo, M., Kettenbach, A. N., Holland, A. J., & Gerber, S. A. (2021). Development and validation of inducible protein degradation and quantitative phosphoproteomics to

identify kinase-substrate relationships. *bioRxiv*, 2021.2012.2008.471812. https://doi.org/10.1101/2021.12.08.471812

Hauf, S., Cole, R. W., LaTerra, S., Zimmer, C., Schnapp, G., Walter, R., Heckel, A., van Meel, J., Rieder, C. L., & Peters, J. M. (2003). The small molecule Hesperadin reveals a role for Aurora B in correcting kinetochore-microtubule attachment and in maintaining the spindle assembly checkpoint. *J Cell Biol*, *161*(2), 281-294. https://doi.org/10.1083/jcb.200208092

Helmke, C., Becker, S., & Strebhardt, K. (2016). The role of Plk3 in oncogenesis. In *Oncogene* (Vol. 35, pp. 135-147): Nature Publishing Group.

Heroes, E., Lesage, B., Gornemann, J., Beullens, M., Van Meervelt, L., & Bollen, M. (2013). The PP1 binding code: a molecular-lego strategy that governs specificity. *FEBS J*, *280*(2), 584-595. https://doi.org/10.1111/j.1742-4658.2012.08547.x

Hindriksen, S., Lens, S. M. A., & Hadders, M. A. (2017). The Ins and Outs of Aurora B Inner Centromere Localization. *Front Cell Dev Biol*, *5*, 112. https://doi.org/10.3389/fcell.2017.00112

Hirota, T., Kunitoku, N., Sasayama, T., Marumoto, T., Zhang, D., Nitta, M., Hatakeyama, K., & Saya, H. (2003). Aurora-A and an interacting activator, the LIM protein Ajuba, are required for mitotic commitment in human cells. *Cell*, *114*(5), 585-598. https://doi.org/10.1016/s0092-8674(03)00642-1

Hochegger, H., Hegarat, N., & Pereira-Leal, J. B. (2013). Aurora at the pole and equator: overlapping functions of Aurora kinases in the mitotic spindle. *Open Biol*, *3*(3), 120185. https://doi.org/10.1098/rsob.120185

Holder, J., Mohammed, S., & Barr, F. A. (2020). Ordered dephosphorylation initiated by the selective proteolysis of cyclin B drives mitotic exit. *eLife*, *9*. https://doi.org/10.7554/eLife.59885

Holland, A. J., Fachinetti, D., Han, J. S., & Cleveland, D. W. (2012). Inducible, reversible system for the rapid and complete degradation of proteins in mammalian cells. *Proceedings of the National Academy of Sciences of the United States of America*, *109*(49), E3350-E3357. https://doi.org/10.1073/pnas.1216880109

Hoppe, A. D., & Swanson, J. A. (2004). Cdc42, Rac1, and Rac2 display distinct patterns of activation during phagocytosis. *Mol Biol Cell*, *15*(8), 3509-3519. https://doi.org/10.1091/mbc.e03-11-0847

Hornbeck, P. V., Kornhauser, J. M., Latham, V., Murray, B., Nandhikonda, V., Nord, A., Skrzypek, E., Wheeler, T., Zhang, B., & Gnad, F. (2019). 15 years of

PhosphoSitePlus(R): integrating post-translationally modified sites, disease variants and isoforms. *Nucleic Acids Res*, *47*(D1), D433-D441. https://doi.org/10.1093/nar/gky1159

Horowitz, N. H. (1950). Biochemical Genetics of Neurospora. *Advances in Genetics*, *3*(C), 33-71. https://doi.org/10.1016/S0065-2660(08)60082-6

Hsieh, E. J., Hoopmann, M. R., MacLean, B., & MacCoss, M. J. (2010). Comparison of database search strategies for high precursor mass accuracy MS/MS data. *J Proteome Res*, *9*(2), 1138-1143. https://doi.org/10.1021/pr900816a

Hsu, J. L., Huang, S. Y., Chow, N. H., & Chen, S. H. (2003). Stable-isotope dimethyl labeling for quantitative proteomics. *Anal Chem*, *75*(24), 6843-6852. https://doi.org/10.1021/ac0348625

Huang, H. T., Dobrovolsky, D., Paulk, J., Yang, G., Weisberg, E. L., Doctor, Z. M., Buckley, D. L., Cho, J. H., Ko, E., Jang, J., Shi, K., Choi, H. G., Griffin, J. D., Li, Y., Treon, S. P., Fischer, E. S., Bradner, J. E., Tan, L., & Gray, N. S. (2018). A Chemoproteomic Approach to Query the Degradable Kinome Using a Multi-kinase Degrader. *Cell Chemical Biology*, *25*(1), 88-99.e86. https://doi.org/10.1016/j.chembiol.2017.10.005

Hughes, C. S., Moggridge, S., Muller, T., Sorensen, P. H., Morin, G. B., & Krijgsveld, J. (2019). Single-pot, solid-phase-enhanced sample preparation for proteomics experiments. *Nat Protoc*, *14*(1), 68-85. https://doi.org/10.1038/s41596-018-0082-x

Humphrey, S. J., James, D. E., & Mann, M. (2015). Protein Phosphorylation: A Major Switch Mechanism for Metabolic Regulation. *Trends Endocrinol Metab*, *26*(12), 676-687. https://doi.org/10.1016/j.tem.2015.09.013

Hunter, T. (2000). Signaling--2000 and beyond. *Cell*, *100*(1). https://doi.org/10.1016/s0092-8674(00)81688-8

Hutti, J. E., Jarrell, E. T., Chang, J. D., Storz, P., Toker, A., Cantley, L. C., Turk, B. E., Abbott, D. W., Storz, P., Toker, A., Cantley, L. C., Turk, B. E., Abbott, D. W., Storz, P., Toker, A., Cantley, L. C., & Turk, B. E. (2004). A rapid method for determining protein kinase phosphorylation specificity. *Nature Methods*, *1*(1), 27-29. https://doi.org/10.1038/nmeth708

Huttlin, E. L., Bruckner, R. J., Navarrete-Perea, J., Cannon, J. R., Baltier, K., Gebreab, F., Gygi, M. P., Thornock, A., Zarraga, G., Tam, S., Szpyt, J., Gassaway, B. M., Panov, A., Parzen, H., Fu, S., Golbazi, A., Maenpaa, E., Stricker, K., Guha

Thakurta, S., . . . Gygi, S. P. (2021). Dual proteome-scale networks reveal cell-specific remodeling of the human interactome. *Cell*, *184*(11), 3022-3040 e3028. https://doi.org/10.1016/j.cell.2021.04.011

Inoue, D., & Sagata, N. (2005). The Polo-like kinase Plx1 interacts with and inhibits Myt1 after fertilization of Xenopus eggs. *EMBO J*, *24*(5), 1057-1067. https://doi.org/10.1038/sj.emboj.7600567

Jackson, A. L., Burchard, J., Schelter, J., Chau, B. N., Cleary, M., Lim, L., & Linsley, P. S. (2006). Widespread siRNA "off-target" transcript silencing mediated by seed region sequence complementarity. *RNA*, *12*(7), 1179-1187. https://doi.org/10.1261/rna.25706

Jensen, O. N. (2006). Interpreting the protein language using proteomics. *Nat Rev Mol Cell Biol*, *7*(6), 391-403. https://doi.org/10.1038/nrm1939

Johnson, E. F., Stewart, K. D., Woods, K. W., Giranda, V. L., & Luo, Y. (2007). Pharmacological and functional comparison of the polo-like kinase family: Insight into inhibitor and substrate specificity. *Biochemistry*, *46*(33), 9551-9563. https://doi.org/10.1021/bi7008745

Johnson, J. L., Yaron, T. M., Huntsman, E. M., Kerelsky, A., Song, J., Regev, A., Lin, T. Y., Liberatore, K., Cizin, D. M., Cohen, B. M., Vasan, N., Ma, Y., Krismer, K., Robles, J. T., van de Kooij, B., van Vlimmeren, A. E., Andree-Busch, N., Kaufer, N. F., Dorovkov, M. V., . . . Cantley, L. C. (2023). An atlas of substrate specificities for the human serine/threonine kinome. *Nature*, *613*(7945), 759-766. https://doi.org/10.1038/s41586-022-05575-3

Johnson, L. N. (2011). Substrates of mitotic kinases. In *Science Signaling* (Vol. 4, pp. pe31-pe31): American Association for the Advancement of Science.

Joukov, V., & De Nicolo, A. (2018). Aurora-PLK1 cascades as key signaling modules in the regulation of mitosis. *Sci Signal*, *11*(543). https://doi.org/10.1126/scisignal.aar4195

Joukov, V., Walter, J. C., & De Nicolo, A. (2014). The Cep192-organized aurora A-Plk1 cascade is essential for centrosome cycle and bipolar spindle assembly. *Mol Cell*, *55*(4), 578-591. https://doi.org/10.1016/j.molcel.2014.06.016

Kanemaki, M. T. (2022). Ligand-induced degrons for studying nuclear functions. *Curr Opin Cell Biol*, *74*, 29-36. https://doi.org/10.1016/j.ceb.2021.12.006

Karpov, A. S., Amiri, P., Bellamacina, C., Bellance, M.-H., Breitenstein, W., Daniel, D., Denay, R., Fabbro, D., Fernández, C., Galuba, I., Guerro-Lagasse, S., Gutmann,

S., Hinh, L., Jahnke, W., Klopp, J., Lai, A., Lindvall, M., Ma, S., Möbitz, H., . . . Marzinzik, A. (2015). Optimization of a Dibenzodiazepine Hit to a Potent and Selective Allosteric PAK1 Inhibitor. *ACS Medicinal Chemistry Letters*, *6*(7). https://doi.org/10.1021/acsmedchemlett.5b00102

Kelly, A. E., Ghenoiu, C., Xue, J. Z., Zierhut, C., Kimura, H., & Funabiki, H. (2010). Survivin reads phosphorylated histone H3 threonine 3 to activate the mitotic kinase Aurora B. *Science*, *330*(6001), 235-239. https://doi.org/10.1126/science.1189505

Kemp, B. E., Bylund, D. B., Huang, T.-S., & Krebs, E. G. (1975). Substrate specificity of the cyclic AMP-dependent protein kinase. *Proceedings of the National Academy of Sciences of the United States of America*, *72*(9). https://doi.org/10.1073/pnas.72.9.3448

Kepinski, S. (2007). The anatomy of auxin perception. *BioEssays*, *29*(10), 953-956. https://doi.org/10.1002/bies.20657

Kepinski, S., & Leyser, O. (2004). Auxin-induced SCFTIR1-Aux/IAA interaction involves stable modification of the SCFTIR1 complex. *Proceedings of the National Academy of Sciences of the United States of America*, *101*(33), 12381-12386. https://doi.org/10.1073/pnas.0402868101

Kepinski, S., & Leyser, O. (2005). The Arabidopsis F-box protein TIR1 is an auxin receptor. *Nature*, *435*(7041), 446-451. https://doi.org/10.1038/nature03542

Kettenbach, A. N., & Gerber, S. A. (2011). Rapid and reproducible single-stage phosphopeptide enrichment of complex peptide mixtures: application to general and phosphotyrosine-specific phosphoproteomics experiments. *Anal Chem*, *83*(20), 7635-7644. https://doi.org/10.1021/ac201894j

Kettenbach, A. N., Schweppe, D. K., Faherty, B. K., Pechenick, D., Pletnev, A. A., & Gerber, S. A. (2011). Quantitative Phosphoproteomics Identifies Substrates and Functional Modules of Aurora and Polo-Like Kinase Activities in Mitotic Cells. *Science Signaling*, *4*(179), rs5-rs5. https://doi.org/10.1126/scisignal.2001497

Kim, Y. B., Shin, Y. J., Roy, A., & Kim, J. H. (2015). The Role of the Pleckstrin Homology Domain-containing Protein CKIP-1 in Activation of p21-activated Kinase 1 (PAK1). *J Biol Chem*, *290*(34), 21076-21085. https://doi.org/10.1074/jbc.M115.675124

Koch, A., Krug, K., Pengelley, S., Macek, B., & Hauf, S. (2011). Mitotic substrates of the kinase aurora with roles in chromatin regulation identified through quantitative

phosphoproteomics of fission yeast. *Science Signaling*, *4*(179), rs6-rs6. https://doi.org/10.1126/scisignal.2001588

Kubota, T., Nishimura, K., Kanemaki, M. T., & Donaldson, A. D. (2013). The Elg1 Replication Factor C-like Complex Functions in PCNA Unloading during DNA Replication. *Molecular Cell*, *50*(2), 273-280. https://doi.org/10.1016/j.molcel.2013.02.012

Kufer, T. A., Sillje, H. H., Korner, R., Gruss, O. J., Meraldi, P., & Nigg, E. A. (2002). Human TPX2 is required for targeting Aurora-A kinase to the spindle. *J Cell Biol*, *158*(4), 617-623. https://doi.org/10.1083/jcb.200204155

Kumar, R., Gururaj, A. E., & Barnes, C. J. (2006). p21-activated kinases in cancer. In *Nature Reviews Cancer*.

Kumar, R., & Li, D. Q. (2016). PAKs in Human Cancer Progression: From Inception to Cancer Therapeutic to Future Oncobiology. *Advances in Cancer Research*, *130*. https://doi.org/10.1016/bs.acr.2016.01.002

Kumar, R., Sanawar, R., Li, X., & Li, F. (2017). Structure, biochemistry, and biology of PAK kinases. In *Gene*.

Lambrus, B. G., Moyer, T. C., & Holland, A. J. (2018). Applying the auxin-inducible degradation system for rapid protein depletion in mammalian cells. *Methods in Cell Biology*, *144*. https://doi.org/10.1016/bs.mcb.2018.03.004

Landry, J. J., Pyl, P. T., Rausch, T., Zichner, T., Tekkedil, M. M., Stutz, A. M., Jauch, A., Aiyar, R. S., Pau, G., Delhomme, N., Gagneur, J., Korbel, J. O., Huber, W., & Steinmetz, L. M. (2013). The genomic and transcriptomic landscape of a HeLa cell line. *G3 (Bethesda)*, *3*(8), 1213-1224. https://doi.org/10.1534/g3.113.005777

Lemmon, M. A., & Schlessinger, J. (2010). Cell signaling by receptor tyrosine kinases. *Cell*, *141*(7), 1117-1134. https://doi.org/10.1016/j.cell.2010.06.011

Leyser, O. (2018). Auxin signaling. In *Plant Physiology* (Vol. 176, pp. 465-479): American Society of Plant Biologists.

Li, B., Ouyang, B., Pan, H., Reissmann, P. T., Slamon, D. J., Arceci, R., Lu, L., & Dai, W. (1996). Prk, a cytokine-inducible human protein serine/threonine kinase whose expression appears to be down-regulated in lung carcinomas. *J Biol Chem*, *271*(32), 19402-19408. https://doi.org/10.1074/jbc.271.32.19402

Li, J., Cai, Z., Bomgarden, R. D., Pike, I., Kuhn, K., Rogers, J. C., Roberts, T. M., Gygi, S. P., & Paulo, J. A. (2021). TMTpro-18plex: The Expanded and Complete Set of

TMTpro Reagents for Sample Multiplexing. *J Proteome Res*, *20*(5), 2964-2972. https://doi.org/10.1021/acs.jproteome.1c00168

Li, J., Van Vranken, J. G., Pontano Vaites, L., Schweppe, D. K., Huttlin, E. L., Etienne, C., Nandhikonda, P., Viner, R., Robitaille, A. M., Thompson, A. H., Kuhn, K., Pike, I., Bomgarden, R. D., Rogers, J. C., Gygi, S. P., & Paulo, J. A. (2020). TMTpro reagents: a set of isobaric labeling mass tags enables simultaneous proteome-wide measurements across 16 samples. *Nat Methods*, *17*(4), 399-404. https://doi.org/10.1038/s41592-020-0781-4

Li, K., & Crews, C. M. (2022). PROTACs: past, present and future. *Chem Soc Rev*, *51*(12), 5214-5236. https://doi.org/10.1039/d2cs00193d

Li, S., Prasanna, X., Salo, V. T., Vattulainen, I., & Ikonen, E. (2019). An efficient auxin-inducible degron system with low basal degradation in human cells. *Nature Methods*, *16*(9), 866-869. https://doi.org/10.1038/s41592-019-0512-x

Li, Z., Niu, J., Uwagawa, T., Peng, B., & Chiao, P. J. (2005). Function of polo-like kinase 3 in NF-κB-mediated proapoptotic response. *Journal of Biological Chemistry*, *280*(17), 16843-16850. https://doi.org/10.1074/jbc.M410119200

Lin, D. W., Chung, B. P., Huang, J. W., Wang, X., Huang, L., & Kaiser, P. (2019). Microhomology-based CRISPR tagging tools for protein tracking, purification, and depletion. *Journal of Biological Chemistry*, *294*(28), 10877-10885. https://doi.org/10.1074/jbc.RA119.008422

Lin, Y. C., Boone, M., Meuris, L., Lemmens, I., Van Roy, N., Soete, A., Reumers, J., Moisse, M., Plaisance, S., Drmanac, R., Chen, J., Speleman, F., Lambrechts, D., Van de Peer, Y., Tavernier, J., & Callewaert, N. (2014). Genome dynamics of the human embryonic kidney 293 lineage in response to cell biology manipulations. *Nat Commun*, *5*, 4767. https://doi.org/10.1038/ncomms5767

Lindqvist, A., Rodriguez-Bravo, V., & Medema, R. H. (2009). The decision to enter mitosis: feedback and redundancy in the mitotic entry network. *J Cell Biol*, *185*(2), 193-202. https://doi.org/10.1083/jcb.200812045

Liu, B. P., & Burridge, K. (2000). Vav2 Activates Rac1, Cdc42, and RhoA Downstream from Growth Factor Receptors but Not β1 Integrins. *Molecular and Cellular Biology*, *20*(19), 7160-7169. https://doi.org/10.1128/mcb.20.19.7160-7169.2000

Liu, D., Davydenko, O., & Lampson, M. A. (2012). Polo-like kinase-1 regulates kinetochore-microtubule dynamics and spindle checkpoint silencing. *J Cell Biol*, *198*(4), 491-499. https://doi.org/10.1083/jcb.201205090

Liu, D., Vader, G., Vromans, M. J., Lampson, M. A., & Lens, S. M. (2009). Sensing chromosome bi-orientation by spatial separation of aurora B kinase from kinetochore substrates. *Science*, *323*(5919), 1350-1353. https://doi.org/10.1126/science.1167000

Liu, Y., Mi, Y., Mueller, T., Kreibich, S., Williams, E. G., Van Drogen, A., Borel, C., Frank, M., Germain, P. L., Bludau, I., Mehnert, M., Seifert, M., Emmenlauer, M., Sorg, I., Bezrukov, F., Bena, F. S., Zhou, H., Dehio, C., Testa, G., . . . Aebersold, R. (2019). Multi-omic measurements of heterogeneity in HeLa cells across laboratories. *Nat Biotechnol*, *37*(3), 314-322. https://doi.org/10.1038/s41587-019-0037-y

Lowe, E. D., Noble, M. E. M., Skamnaki, V. T., Oikonomakos, N. G., Owen, D. J., & Johnson, L. N. (1997). The crystal structure of a phosphorylase kinase peptide substrate complex: Kinase substrate recognition. *EMBO Journal*, *16*(22), 6646-6658. https://doi.org/10.1093/emboj/16.22.6646

Ma, H. T., & Poon, R. Y. (2011). How protein kinases co-ordinate mitosis in animal cells. *Biochem J*, *435*(1), 17-31. https://doi.org/10.1042/BJ20100284

Macdonald, L., Taylor, G. C., Brisbane, J. M., Christodoulou, E., Scott, L., von Kriegsheim, A., Rossant, J., Gu, B., & Wood, A. J. (2022). Rapid and specific degradation of endogenous proteins in mouse models using auxin-inducible degrons. *eLife*, *11*. https://doi.org/10.7554/eLife.77987

Macurek, L., Lindqvist, A., Lim, D., Lampson, M. A., Klompmaker, R., Freire, R., Clouin, C., Taylor, S. S., Yaffe, M. B., & Medema, R. H. (2008). Polo-like kinase-1 is activated by aurora A to promote checkpoint recovery. *Nature*, *455*(7209), 119-123. https://doi.org/10.1038/nature07185

Mali, P., Yang, L., Esvelt, K. M., Aach, J., Guell, M., DiCarlo, J. E., Norville, J. E., & Church, G. M. (2013). RNA-guided human genome engineering via Cas9. *Science*, *339*(6121), 823-826. https://doi.org/10.1126/science.1232033

Mann, M., & Jensen, O. N. (2003). Proteomic analysis of post-translational modifications. *Nat Biotechnol*, *21*(3), 255-261. https://doi.org/10.1038/nbt0303-255

Manning, G., Plowman, G. D., Hunter, T., & Sudarsanam, S. (2002). Evolution of protein kinase signaling from yeast to man. *Trends Biochem Sci*, *27*(10), 514-520. https://doi.org/10.1016/s0968-0004(02)02179-5

Manning, G., Whyte, D. B., Martinez, R., Hunter, T., & Sudarsanam, S. (2002). The Protein Kinase Complement of the Human Genome. *Science*, *298*(5600). https://doi.org/10.1126/science.1075762

Maroto, B., Ye, M. B., Von Lohneysen, K., Schnelzer, A., & Knaus, U. G. (2008). P21-activated kinase is required for mitotic progression and regulates Plk1. *Oncogene*, *27*(36), 4900-4908. https://doi.org/10.1038/onc.2008.131

McAlister, G. C., Huttlin, E. L., Haas, W., Ting, L., Jedrychowski, M. P., Rogers, J. C., Kuhn, K., Pike, I., Grothe, R. A., Blethrow, J. D., & Gygi, S. P. (2012). Increasing the multiplexing capacity of TMTs using reporter ion isotopologues with isobaric masses. *Anal Chem*, *84*(17), 7469-7478. https://doi.org/10.1021/ac301572t

McIntosh, J. R. (2016). Mitosis. *Cold Spring Harb Perspect Biol*, *8*(9). https://doi.org/10.1101/cshperspect.a023218

McLachlin, D. T., & Chait, B. T. (2001). Analysis of phosphorylated proteins and peptides by mass spectrometry. *Curr Opin Chem Biol*, *5*(5), 591-602. https://doi.org/10.1016/s1367-5931(00)00250-7

Mertins, P., Mani, D. R., Ruggles, K. V., Gillette, M. A., Clauser, K. R., Wang, P., Wang, X., Qiao, J. W., Cao, S., Petralia, F., Kawaler, E., Mundt, F., Krug, K., Tu, Z., Lei, J. T., Gatza, M. L., Wilkerson, M., Perou, C. M., Yellapantula, V., . . . Carr, S. A. (2016). Proteogenomics connects somatic mutations to signalling in breast cancer. *Nature*, *534*(7605), 55-62. https://doi.org/10.1038/nature18003

Minoshima, Y., Kawashima, T., Hirose, K., Tonozuka, Y., Kawajiri, A., Bao, Y. C., Deng, X., Tatsuka, M., Narumiya, S., May, W. S., Jr., Nosaka, T., Semba, K., Inoue, T., Satoh, T., Inagaki, M., & Kitamura, T. (2003). Phosphorylation by aurora B converts MgcRacGAP to a RhoGAP during cytokinesis. *Dev Cell*, *4*(4), 549-560. https://doi.org/10.1016/s1534-5807(03)00089-3

Mishima, M., Kaitna, S., & Glotzer, M. (2002). Central spindle assembly and cytokinesis require a kinesin-like protein/RhoGAP complex with microtubule bundling activity. *Dev Cell*, *2*(1), 41-54. https://doi.org/10.1016/s1534-5807(01)00110-1

Moret, N., Liu, C., Gyori, B. M., Bachman, J. A., Steppi, A., Taujale, R., Huang, L. C., Hug, C., Berginski, M., Gomez, S., Kannan, N., & Sorger, P. K. (2020). Exploring the understudied human kinome for research and therapeutic opportunities. In *bioRxiv* (pp. 2020.2004.2002.022277-022020.022204.022202.022277): bioRxiv.

Müller, M. P., & Rauh, D. (2018). Try Me: Promiscuous Inhibitors Still Allow for Selective Targeted Protein Degradation. In *Cell Chemical Biology* (Vol. 25, pp. 4-6): Elsevier Ltd.

Musacchio, A. (2010). Molecular biology. Surfing chromosomes (and Survivin). *Science*, *330*(6001), 183-184. https://doi.org/10.1126/science.1197261

Musacchio, A., & Salmon, E. D. (2007). The spindle-assembly checkpoint in space and time. *Nat Rev Mol Cell Biol*, *8*(5), 379-393. https://doi.org/10.1038/nrm2163

Myer, D. L., Bahassi, E. M., & Stambrook, P. J. (2005). The Plk3-Cdc25 circuit. In *Oncogene* (Vol. 24, pp. 299-305).

Nabet, B., Ferguson, F. M., Seong, B. K. A., Kuljanin, M., Leggett, A. L., Mohardt, M. L., Robichaud, A., Conway, A. S., Buckley, D. L., Mancias, J. D., Bradner, J. E., Stegmaier, K., & Gray, N. S. (2020). Rapid and direct control of target protein levels with VHL-recruiting dTAG molecules. *Nat Commun*, *11*(1), 4687. https://doi.org/10.1038/s41467-020-18377-w

Nabet, B., Roberts, J. M., Buckley, D. L., Paulk, J., Dastjerdi, S., Yang, A., Leggett, A. L., Erb, M. A., Lawlor, M. A., Souza, A., Scott, T. G., Vittori, S., Perry, J. A., Qi, J., Winter, G. E., Wong, K. K., Gray, N. S., & Bradner, J. E. (2018). The dTAG system for immediate and target-specific protein degradation. *Nature Chemical Biology*, *14*(5), 431-441. https://doi.org/10.1038/s41589-018-0021-8

Nagashima, R., Hibino, K., Ashwin, S. S., Babokhov, M., Fujishiro, S., Imai, R., Nozaki, T., Tamura, S., Tani, T., Kimura, H., Shribak, M., Kanemaki, M. T., Sasai, M., & Maeshima, K. (2019). Single nucleosome imaging reveals loose genome chromatin networks via active RNA polymerase II. *Journal of Cell Biology*, *218*(5), 1511-1530. https://doi.org/10.1083/jcb.201811090

Nakade, S., Tsubota, T., Sakane, Y., Kume, S., Sakamoto, N., Obara, M., Daimon, T., Sezutsu, H., Yamamoto, T., Sakuma, T., & Suzuki, K. I. T. (2014). Microhomology-mediated end-joining-dependent integration of donor DNA in cells and animals using TALENs and CRISPR/Cas9. *Nature Communications*, *5*. https://doi.org/10.1038/ncomms6560

Natsume, T., & Kanemaki, M. T. (2017). Conditional Degrons for Controlling Protein Expression at the Protein Level. *Annual Review of Genetics*, *51*(1), 83-102. https://doi.org/10.1146/annurev-genet-120116-024656

Natsume, T., Kiyomitsu, T., Saga, Y., & Kanemaki, M. T. (2016). Rapid Protein Depletion in Human Cells by Auxin-Inducible Degron Tagging with Short Homology Donors. *Cell Reports*, *15*(1), 210-218. https://doi.org/10.1016/j.celrep.2016.03.001

Nayal, A., Webb, D. J., Brown, C. M., Schaefer, E. M., Vicente-Manzanares, M., & Horwitz, A. R. (2006). Paxillin phosphorylation at Ser273 localizes a GIT1-PIX-PAK complex and regulates adhesion and protrusion dynamics. *Journal of Cell Biology*, *173*(4), 587-599. https://doi.org/10.1083/jcb.200509075

Ndubaku, C. O., Crawford, J. J., Drobnick, J., Aliagas, I., Campbell, D., Dong, P., Dornan, L. M., Duron, S., Epler, J., Gazzard, L., Heise, C. E., Hoeflich, K. P., Jakubiak, D., La, H., Lee, W., Lin, B., Lyssikatos, J. P., Maksimoska, J., Marmorstein, R., . . . Rudolph, J. (2015). Design of Selective PAK1 Inhibitor G-5555: Improving Properties by Employing an Unorthodox Low-pKa Polar Moiety. *ACS Medicinal Chemistry Letters*, *6*(12), 1241-1246. https://doi.org/10.1021/acsmedchemlett.5b00398

Neklesa, T. K., Tae, H. S., Schneekloth, A. R., Stulberg, M. J., Corson, T. W., Sundberg, T. B., Raina, K., Holley, S. A., & Crews, C. M. (2011). Small-molecule hydrophobic tagging-induced degradation of HaloTag fusion proteins. *Nature Chemical Biology*, *7*(8), 538-543. https://doi.org/10.1038/nchembio.597

Nekrasova, T., & Minden, A. (2011). PAK4 is required for regulation of the cell-cycle regulatory protein p21, and for control of cell-cycle progression. *J Cell Biochem*, *112*(7), 1795-1806. https://doi.org/10.1002/jcb.23092

Nezi, L., & Musacchio, A. (2009). Sister chromatid tension and the spindle assembly checkpoint. *Curr Opin Cell Biol*, *21*(6), 785-795. https://doi.org/10.1016/j.ceb.2009.09.007

Nguyen, H., & Kettenbach, A. N. (2023). Substrate and phosphorylation site selection by phosphoprotein phosphatases. *Trends Biochem Sci*. https://doi.org/10.1016/j.tibs.2023.04.004

Nicholson, J. M., & Cimini, D. (2013). Cancer karyotypes: survival of the fittest. *Front Oncol*, *3*, 148. https://doi.org/10.3389/fonc.2013.00148

Nicklas, R. B. (1997). How cells get the right chromosomes. *Science*, *275*(5300), 632-637. https://doi.org/10.1126/science.275.5300.632

Nigg, E. A. (1995). Cyclin-dependent protein kinases: key regulators of the eukaryotic cell cycle. *BioEssays*, *17*(6), 471-480. https://doi.org/10.1002/bies.950170603

Nigg, E. A. (2001). Mitotic kinases as regulators of cell division and its checkpoints. *Nat Rev Mol Cell Biol*, *2*(1), 21-32. https://doi.org/10.1038/35048096

Nishi, H., Hashimoto, K., & Panchenko, A. R. (2011). Phosphorylation in protein-protein binding: effect on stability and function. *Structure*, *19*(12), 1807-1815. https://doi.org/10.1016/j.str.2011.09.021

Nishimura, K., Fukagawa, T., Takisawa, H., Kakimoto, T., & Kanemaki, M. (2009). An auxin-based degron system for the rapid depletion of proteins in nonplant cells. *Nature Methods*, *6*(12), 917-922. https://doi.org/10.1038/nmeth.1401

Nishimura, K., Yamada, R., Hagihara, S., Iwasaki, R., Uchida, N., Kamura, T., Takahashi, K., Torii, K. U., & Fukagawa, T. (2020). A super-sensitive auxin-inducible degron system with an engineered auxin-TIR1 pair. *Nucleic Acids Research*, *48*(18). https://doi.org/10.1093/nar/gkaa748

Nuche-Berenguer, B., & Jensen, R. T. (2015). Gastrointestinal hormones/neurotransmitters and growth factors can activate P21 activated kinase 2 in pancreatic acinar cells by novel mechanisms. *Biochim Biophys Acta*, *1853*(10 Pt A), 2371-2382. https://doi.org/10.1016/j.bbamcr.2015.05.011

Nusinow, D. P., Szpyt, J., Ghandi, M., Rose, C. M., McDonald, E. R., Kalocsay, M., Jané-Valbuena, J., Gelfand, E., Schweppe, D. K., Jedrychowski, M., Golji, J., Porter, D. A., Rejtar, T., Wang, Y. K., Kryukov, G. V., Stegmeier, F., Erickson, B. K., Garraway, L. A., Sellers, W. R., & Gygi, S. P. (2020). Quantitative Proteomics of the Cancer Cell Line Encyclopedia. *Cell*, *180*(2), 387-402.e316. https://doi.org/10.1016/j.cell.2019.12.023

Ochoa, D., Jarnuczak, A. F., Vieitez, C., Gehre, M., Soucheray, M., Mateus, A., Kleefeldt, A. A., Hill, A., Garcia-Alonso, L., Stein, F., Krogan, N. J., Savitski, M. M., Swaney, D. L., Vizcaino, J. A., Noh, K. M., & Beltrao, P. (2020). The functional landscape of the human phosphoproteome. *Nat Biotechnol*, *38*(3), 365-373. https://doi.org/10.1038/s41587-019-0344-3

Olivieri, M., & Durocher, D. (2021). Genome-scale chemogenomic CRISPR screens in human cells using the TKOv3 library. *STAR Protoc*, *2*(1), 100321. https://doi.org/10.1016/j.xpro.2021.100321

Olsen, J. V., Blagoev, B., Gnad, F., Macek, B., Kumar, C., Mortensen, P., & Mann, M. (2006). Global, in vivo, and site-specific phosphorylation dynamics in signaling networks. *Cell*, *127*(3), 635-648. https://doi.org/10.1016/j.cell.2006.09.026

Olsen, J. V., & Mann, M. (2013). Status of large-scale analysis of post-translational modifications by mass spectrometry. *Mol Cell Proteomics*, *12*(12), 3444-3452. https://doi.org/10.1074/mcp.O113.034181

Olsen, J. V., Vermeulen, M., Santamaria, A., Kumar, C., Miller, M. L., Jensen, L. J., Gnad, F., Cox, J., Jensen, T. S., Nigg, E. A., Brunak, S., & Mann, M. (2010). Quantitative phosphoproteomics reveals widespread full phosphorylation site occupancy during mitosis. *Sci Signal*, *3*(104), ra3. https://doi.org/10.1126/scisignal.2000475

Ong, C. C., Gierke, S., Pitt, C., Sagolla, M., Cheng, C. K., Zhou, W., Jubb, A. M., Strickland, L., Schmidt, M., Duron, S. G., Campbell, D. A., Zheng, W., Dehdashti, S., Shen, M., Yang, N., Behnke, M. L., Huang, W., McKew, J. C., Chernoff, J., . . . Hoeflich, K. P. (2015). Small molecule inhibition of group I p21-activated kinases in breast cancer induces apoptosis and potentiates the activity of microtubule stabilizing agents. *Breast Cancer Research*, *17*(1), 59-59. https://doi.org/10.1186/s13058-015-0564-5

Ong, C. C., Jubb, A. M., Zhou, W., Haverty, P. M., Harris, A. L., Belvin, M., Friedman, L. S., Koeppen, H., & Hoeflich, K. P. (2011). P21-activated kinase 1: PAK'ed with potential. *Oncotarget*, *2*(6), 491-496. https://doi.org/10.18632/oncotarget.271

Ong, S. E., Blagoev, B., Kratchmarova, I., Kristensen, D. B., Steen, H., Pandey, A., & Mann, M. (2002). Stable isotope labeling by amino acids in cell culture, SILAC, as a simple and accurate approach to expression proteomics. *Mol Cell Proteomics*, *1*(5), 376-386. https://doi.org/10.1074/mcp.m200025-mcp200

Ong, S. E., & Mann, M. (2006). A practical recipe for stable isotope labeling by amino acids in cell culture (SILAC). *Nat Protoc*, *1*(6), 2650-2660. https://doi.org/10.1038/nprot.2006.427

Ota, T., Suzuki, Y., Nishikawa, T., Otsuki, T., Sugiyama, T., Irie, R., Wakamatsu, A., Hayashi, K., Sato, H., Nagai, K., Kimura, K., Makita, H., Sekine, M., Obayashi, M., Nishi, T., Shibahara, T., Tanaka, T., Ishii, S., Yamamoto, J., . . . Sugano, S. (2004). Complete sequencing and characterization of 21,243 full-length human cDNAs. *Nat Genet*, *36*(1), 40-45. https://doi.org/10.1038/ng1285

Pandey, A., & Mann, M. (2000). Proteomics to study genes and genomes. *Nature*, *405*(6788), 837-846. https://doi.org/10.1038/35015709

Papini, D., Levasseur, M. D., & Higgins, J. M. G. (2021). The Aurora B gradient sustains kinetochore stability in anaphase. *Cell Rep*, *37*(6), 109818. https://doi.org/10.1016/j.celrep.2021.109818

Patterson, S. D., & Aebersold, R. H. (2003). Proteomics: the first decade and beyond. *Nat Genet*, *33 Suppl*, 311-323. https://doi.org/10.1038/ng1106

Paweletz, N. (2001). Walther Flemming: pioneer of mitosis research. *Nat Rev Mol Cell Biol*, *2*(1), 72-75. https://doi.org/10.1038/35048077

Pawson, T., & Scott, J. D. (1997). Signaling through scaffold, anchoring, and adaptor proteins. *Science*, *278*(5346), 2075-2080. https://doi.org/10.1126/science.278.5346.2075

Petsalaki, E., & Zachos, G. (2019). Building bridges between chromosomes: novel insights into the abscission checkpoint. *Cell Mol Life Sci*, *76*(21), 4291-4307. https://doi.org/10.1007/s00018-019-03224-z

Pettersson, M., & Crews, C. M. (2019). PROteolysis TArgeting Chimeras (PROTACs) - Past, present and future. *Drug Discovery Today: Technologies*, *31*, 15-27. https://doi.org/10.1016/j.ddtec.2019.01.002

Pinilla-Macua, I., Grassart, A., Duvvuri, U., Watkins, S. C., & Sorkin, A. (2017). EGF receptor signaling, phosphorylation, ubiquitylation and endocytosis in tumors in vivo. *eLife*, *6*. https://doi.org/10.7554/eLife.31993

Porath, J., Carlsson, J., Olsson, I., & Belfrage, G. (1975). Metal chelate affinity chromatography, a new approach to protein fractionation. *Nature*, *258*(5536), 598-599. https://doi.org/10.1038/258598a0

Prozzillo, Y., Fattorini, G., Santopietro, M. V., Suglia, L., Ruggiero, A., Ferreri, D., & Messina, G. (2020). Targeted Protein Degradation Tools: Overview and Future Perspectives. *Biology (Basel)*, *9*(12). https://doi.org/10.3390/biology9120421

Qiu, W., Evans, C. A., Landels, A., Pham, T. K., & Wright, P. C. (2020). Phosphopeptide enrichment for phosphoproteomic analysis - A tutorial and review of novel materials. *Anal Chim Acta*, *1129*, 158-180. https://doi.org/10.1016/j.aca.2020.04.053

Radu, M., Semenova, G., Kosoff, R., & Chernoff, J. (2014). PAK signalling during the development and progression of cancer. *Nature Reviews Cancer*, *14*(1), 13-25. https://doi.org/10.1038/nrc3645

Rajakulendran, T., & Sicheri, F. (2010). Allosteric protein kinase regulation by pseudokinases: insights from STRAD. *Sci Signal*, *3*(111), pe8. https://doi.org/10.1126/scisignal.3111pe8

Rane, C. K., & Minden, A. (2019). P21 activated kinase signaling in cancer. *Seminars in Cancer Biology*, *54*, 40-49. https://doi.org/10.1016/J.SEMCANCER.2018.01.006

Rappsilber, J., Ishihama, Y., & Mann, M. (2003). Stop and go extraction tips for matrix-assisted laser desorption/ionization, nanoelectrospray, and LC/MS sample pretreatment in proteomics. *Anal Chem*, *75*(3), 663-670. https://doi.org/10.1021/ac026117i

Rauniyar, N., & Yates, J. R. (2014). Isobaric labeling-based relative quantification in shotgun proteomics. In *Journal of Proteome Research* (Vol. 13, pp. 5293-5309): American Chemical Society.

Reinders, J., & Sickmann, A. (2005). State-of-the-art in phosphoproteomics. *Proteomics*, *5*(16), 4052-4061. https://doi.org/10.1002/pmic.200401289

Rennefahrt, U., Deacon, S. W., Parker, S. A., Devarajan, K., Beeser, A., Chernoff, J., Knapp, S., Turk, B. E., & Peterson, J. R. (2007). Specificity profiling of Pak kinases allows identification of novel phosphorylation sites. *Journal of Biological Chemistry*, *282*(21). https://doi.org/10.1074/jbc.m700253200

Riley, N. M., & Coon, J. J. (2016). Phosphoproteomics in the Age of Rapid and Deep Proteome Profiling. *Anal Chem*, *88*(1), 74-94. https://doi.org/10.1021/acs.analchem.5b04123

Rix, U., & Superti-Furga, G. (2009). Target profiling of small molecules by chemical proteomics. *Nat Chem Biol*, *5*(9), 616-624. https://doi.org/10.1038/nchembio.216

Roskoski, R. (2019). Properties of FDA-approved small molecule protein kinase inhibitors. In *Pharmacological Research* (Vol. 144, pp. 19-50): Academic Press.

Roskoski, R. (2020). Properties of FDA-approved small molecule protein kinase inhibitors: A 2020 update. In *Pharmacological Research* (Vol. 152, pp. 104609-104609): Academic Press.

Roy, B., Han, S. J. Y., Fontan, A. N., Jema, S., & Joglekar, A. P. (2022). Aurora B phosphorylates Bub1 to promote spindle assembly checkpoint signaling. *Curr Biol*, *32*(1), 237-247 e236. https://doi.org/10.1016/j.cub.2021.10.049

Rudolph, D., Steegmaier, M., Hoffmann, M., Grauert, M., Baum, A., Quant, J., Haslinger, C., Garin-Chesa, P., & Adolf, G. R. (2009). BI 6727, a polo-like kinase inhibitor with improved pharmacokinetic profile and broad antitumor activity. *Clinical*

Cancer Research, *15*(9), 3094-3102. https://doi.org/10.1158/1078-0432.CCR-08-2445

Rudolph, J., Murray, L. J., Ndubaku, C. O., O'Brien, T., Blackwood, E., Wang, W., Aliagas, I., Gazzard, L., Crawford, J. J., Drobnick, J., Lee, W., Zhao, X., Hoeflich, K. P., Favor, D. A., Dong, P., Zhang, H., Heise, C. E., Oh, A., Ong, C. C., . . . Zhong, Y. (2016). Chemically Diverse Group i p21-Activated Kinase (PAK) Inhibitors Impart Acute Cardiovascular Toxicity with a Narrow Therapeutic Window. *Journal of Medicinal Chemistry*, *59*(11), 5520-5541. https://doi.org/10.1021/acs.jmedchem.6b00638

Rush, J., Moritz, A., Lee, K. A., Guo, A., Goss, V. L., Spek, E. J., Zhang, H., Zha, X. M., Polakiewicz, R. D., & Comb, M. J. (2005). Immunoaffinity profiling of tyrosine phosphorylation in cancer cells. *Nat Biotechnol*, *23*(1), 94-101. https://doi.org/10.1038/nbt1046

Sackton, K. L., Dimova, N., Zeng, X., Tian, W., Zhang, M., Sackton, T. B., Meaders, J., Pfaff, K. L., Sigoillot, F., Yu, H., Luo, X., & King, R. W. (2014). Synergistic blockade of mitotic exit by two chemical inhibitors of the APC/C. *Nature*, *514*(7524), 646-649. https://doi.org/10.1038/nature13660

Sadelain, M., Papapetrou, E. P., & Bushman, F. D. (2012). Safe harbours for the integration of new DNA in the human genome. In *Nature Reviews Cancer* (Vol. 12, pp. 51-58): Nature Publishing Group.

Saito, Y., & Kanemaki, M. T. (2021). Targeted Protein Depletion Using the Auxin-Inducible Degron 2 (AID2) System. *Curr Protoc*, *1*(8), e219. https://doi.org/10.1002/cpz1.219

Sakuma, T., Nakade, S., Sakane, Y., Suzuki, K. I. T., & Yamamoto, T. (2016). MMEJ-Assisted gene knock-in using TALENs and CRISPR-Cas9 with the PITCh systems. *Nature Protocols*, *11*(1), 118-133. https://doi.org/10.1038/nprot.2015.140

Samejima, K., Platani, M., Wolny, M., Ogawa, H., Vargiu, G., Knight, P. J., Peckham, M., & Earnshaw, W. C. (2015). The Inner Centromere Protein (INCENP) Coil Is a Single alpha-Helix (SAH) Domain That Binds Directly to Microtubules and Is Important for Chromosome Passenger Complex (CPC) Localization and Function in Mitosis. *J Biol Chem*, *290*(35), 21460-21472. https://doi.org/10.1074/jbc.M115.645317

Sanson, K. R., Hanna, R. E., Hegde, M., Donovan, K. F., Strand, C., Sullender, M. E., Vaimberg, E. W., Goodale, A., Root, D. E., Piccioni, F., & Doench, J. G. (2018). Optimized libraries for CRISPR-Cas9 genetic screens with multiple modalities. *Nat Commun*, *9*(1), 5416. https://doi.org/10.1038/s41467-018-07901-8

Santamaria, A., Wang, B., Elowe, S., Malik, R., Zhang, F., Bauer, M., Schmidt, A., Sillje, H. H., Korner, R., & Nigg, E. A. (2011). The Plk1-dependent phosphoproteome of the early mitotic spindle. *Mol Cell Proteomics*, *10*(1), M110 004457. https://doi.org/10.1074/mcp.M110.004457

Schiller, M. R. (2006). Coupling receptor tyrosine kinases to Rho GTPases-GEFs what's the link. *Cellular Signalling*, *18*(11), 1834-1843. https://doi.org/10.1016/j.cellsig.2006.01.022

Schwartz, P. A., & Murray, B. W. (2011). Protein kinase biochemistry and drug discovery. In *Bioorganic Chemistry* (Vol. 39, pp. 192-210): Academic Press.

Sdelci, S., Schutz, M., Pinyol, R., Bertran, M. T., Regue, L., Caelles, C., Vernos, I., & Roig, J. (2012). Nek9 phosphorylation of NEDD1/GCP-WD contributes to Plk1 control of gamma-tubulin recruitment to the mitotic centrosome. *Curr Biol*, *22*(16), 1516-1523. https://doi.org/10.1016/j.cub.2012.06.027

Semenova, G., & Chernoff, J. (2017). Targeting PAK1. In *Biochemical Society Transactions* (Vol. 45, pp. 79-88): Portland Press Ltd.

Sfeir, A., & Symington, L. S. (2015). Microhomology-Mediated End Joining: A Back-up Survival Mechanism or Dedicated Pathway? In *Trends in Biochemical Sciences* (Vol. 40, pp. 701-714): Elsevier Ltd.

Shah, K., & Shokat, K. M. (2003). A chemical genetic approach for the identification of direct substrates of protein kinases. *Methods of Molecular Biology*, *233*. https://doi.org/10.1385/1-59259-397-6:253

Shalem, O., Sanjana, N. E., Hartenian, E., Shi, X., Scott, D. A., Mikkelson, T., Heckl, D., Ebert, B. L., Root, D. E., Doench, J. G., & Zhang, F. (2014). Genome-scale CRISPR-Cas9 knockout screening in human cells. *Science*, *343*(6166), 84-87. https://doi.org/10.1126/science.1247005

Sharma, K., D'Souza, R. C., Tyanova, S., Schaab, C., Wisniewski, J. R., Cox, J., & Mann, M. (2014). Ultradeep human phosphoproteome reveals a distinct regulatory nature of Tyr and Ser/Thr-based signaling. *Cell Rep*, *8*(5), 1583-1594. https://doi.org/10.1016/j.celrep.2014.07.036

Shrestha, Y., Schafer, E. J., Boehm, J. S., Thomas, S. R., He, F., Du, J., Wang, S., Barretina, J., Weir, B. A., Zhao, J. J., Polyak, K., Golub, T. R., Beroukhim, R., & Hahn, W. C. (2012). PAK1 is a breast cancer oncogene that coordinately activates MAPK and MET signaling. *Oncogene*, *31*(29), 3397-3408. https://doi.org/10.1038/onc.2011.515

Singhal, R., & Kandel, E. S. (2012). The response to PAK1 inhibitor IPA3 distinguishes between cancer cells with mutations in BRAF and Ras oncogenes. *Oncotarget*, *3*(7), 700-708. https://doi.org/10.18632/oncotarget.587

Skoufias, D. A., DeBonis, S., Saoudi, Y., Lebeau, L., Crevel, I., Cross, R., Wade, R. H., Hackney, D., & Kozielski, F. (2006). S-trityl-L-cysteine is a reversible, tight binding inhibitor of the human kinesin Eg5 that specifically blocks mitotic progression. *J Biol Chem*, *281*(26), 17559-17569. https://doi.org/10.1074/jbc.M511735200

Smits, V. A., Klompmaker, R., Arnaud, L., Rijksen, G., Nigg, E. A., & Medema, R. H. (2000). Polo-like kinase-1 is a target of the DNA damage checkpoint. *Nat Cell Biol*, *2*(9), 672-676. https://doi.org/10.1038/35023629

Sobajima, T., Kowalczyk, K. M., Skylakakis, S., Hayward, D., Fulcher, L. J., Neary, C., Batley, C., Kurlekar, S., Roberts, E., Gruneberg, U., & Barr, F. A. (2023). PP6 regulation of Aurora A-TPX2 limits NDC80 phosphorylation and mitotic spindle size. *J Cell Biol*, *222*(5). https://doi.org/10.1083/jcb.202205117

Songyang, Z., Blechner, S., Hoagland, N., Hoekstra, M. F., Piwnica-Worms, H., & Cantley, L. C. (1994). Use of an oriented peptide library to determine the optimal substrates of protein kinases. *Current Biology*, *4*(11), 973-982. https://doi.org/10.1016/S0960-9822(00)00221-9

Songyang, Z., Lu, K. P., Kwon, Y. T., Tsai, L.-H. H., Filhol, O., Cochet, C., Brickey, D. A., Soderling, T. R., Bartleson, C., Graves, D. J., DeMaggio, A. J., Hoekstra, M. F., Blenis, J., Hunter, T., & Cantley, L. C. (1996). A structural basis for substrate specificities of protein Ser/Thr kinases: primary sequence preference of casein kinases I and II, NIMA, phosphorylase kinase, calmodulin-dependent kinase II, CDK5, and Erk1. *Molecular and Cellular Biology*, *16*(11), 6486-6493. https://doi.org/10.1128/mcb.16.11.6486

Steegmaier, M., Hoffmann, M., Baum, A., Lenart, P., Petronczki, M., Krssak, M., Gurtler, U., Garin-Chesa, P., Lieb, S., Quant, J., Grauert, M., Adolf, G. R., Kraut, N., Peters, J. M., & Rettig, W. J. (2007). BI 2536, a potent and selective inhibitor of

polo-like kinase 1, inhibits tumor growth in vivo. *Curr Biol*, *17*(4), 316-322. https://doi.org/10.1016/j.cub.2006.12.037

Steen, H., & Mann, M. (2004). The ABC's (and XYZ's) of peptide sequencing. *Nat Rev Mol Cell Biol*, *5*(9), 699-711. https://doi.org/10.1038/nrm1468

Strebhardt, K. (2010). Multifaceted polo-like kinases: Drug targets and antitargets for cancer therapy. In *Nature Reviews Drug Discovery* (Vol. 9, pp. 643-660).

Sugiyama, N., & Ishihama, Y. (2016). Large-scale profiling of protein kinases for cellular signaling studies by mass spectrometry and other techniques. *Journal of Pharmaceutical and Biomedical Analysis*, *130*. https://doi.org/10.1016/j.jpba.2016.05.046

Tae, H. S., Sundberg, T. B., Neklesa, T. K., Noblin, D. J., Gustafson, J. L., Roth, A. G., Raina, K., & Crews, C. M. (2012). Identification of hydrophobic tags for the degradation of stabilized proteins. *Chembiochem*, *13*(4), 538-541. https://doi.org/10.1002/cbic.201100793

Takagi, M., Natsume, T., Kanemaki, M. T., & Imamoto, N. (2016). Perichromosomal protein Ki67 supports mitotic chromosome architecture. *Genes to Cells*, *21*(10), 1113-1124. https://doi.org/10.1111/gtc.12420

Tan, X., Calderon-Villalobos, L. I. A., Sharon, M., Zheng, C., Robinson, C. V., Estelle, M., & Zheng, N. (2007). Mechanism of auxin perception by the TIR1 ubiquitin ligase. *Nature*, *446*(7136), 640-645. https://doi.org/10.1038/nature05731

Tang, L. (2019). Investigating heterogeneity in HeLa cells. *Nat Methods*, *16*(4), 281. https://doi.org/10.1038/s41592-019-0375-1

Taus, T., Kocher, T., Pichler, P., Paschke, C., Schmidt, A., Henrich, C., & Mechtler, K. (2011). Universal and confident phosphorylation site localization using phosphoRS. *J Proteome Res*, *10*(12), 5354-5362. https://doi.org/10.1021/pr200611n

Thompson, A., Schafer, J., Kuhn, K., Kienle, S., Schwarz, J., Schmidt, G., Neumann, T., Johnstone, R., Mohammed, A. K., & Hamon, C. (2003). Tandem mass tags: a novel quantification strategy for comparative analysis of complex protein mixtures by MS/MS. *Anal Chem*, *75*(8), 1895-1904. https://doi.org/10.1021/ac0262560

Thompson, A., Wolmer, N., Koncarevic, S., Selzer, S., Bohm, G., Legner, H., Schmid, P., Kienle, S., Penning, P., Hohle, C., Berfelde, A., Martinez-Pinna, R., Farztdinov, V., Jung, S., Kuhn, K., & Pike, I. (2019). TMTpro: Design, Synthesis, and Initial

Evaluation of a Proline-Based Isobaric 16-Plex Tandem Mass Tag Reagent Set. *Anal Chem*, *91*(24), 15941-15950. https://doi.org/10.1021/acs.analchem.9b04474

Tsang, M. J., & Cheeseman, I. M. (2023). Alternative CDC20 translational isoforms tune mitotic arrest duration. *Nature*, *617*(7959), 154-161. https://doi.org/10.1038/s41586-023-05943-7

Tsherniak, A., Vazquez, F., Montgomery, P. G., Weir, B. A., Kryukov, G., Cowley, G. S., Gill, S., Harrington, W. F., Pantel, S., Krill-Burger, J. M., Meyers, R. M., Ali, L., Goodale, A., Lee, Y., Jiang, G., Hsiao, J., Gerath, W. F. J., Howell, S., Merkel, E., . . . Hahn, W. C. (2017). Defining a Cancer Dependency Map. *Cell*, *170*(3), 564-576.e516. https://doi.org/10.1016/j.cell.2017.06.010

Tu, S., Wu, W. J., Wang, J., & Cerione, R. A. (2003). Epidermal Growth Factor-dependent Regulation of Cdc42 Is Mediated by the Src Tyrosine Kinase *. *278*(49), 49293-49300. https://doi.org/10.1074/jbc.M307021200

Tyers, M., & Mann, M. (2003). From genomics to proteomics. *Nature*, *422*(6928), 193-197. https://doi.org/10.1038/nature01510

Ubersax, J. A., & Ferrell, J. E. (2007). Mechanisms of specificity in protein phosphorylation. *Nature Reviews Molecular Cell Biology*, *8*(7), 530-541. https://doi.org/10.1038/nrm2203

Uchida, N., Takahashi, K., Iwasaki, R., Yamada, R., Yoshimura, M., Endo, T. A., Kimura, S., Zhang, H., Nomoto, M., Tada, Y., Kinoshita, T., Itami, K., Hagihara, S., & Torii, K. U. (2018). Chemical hijacking of auxin signaling with an engineered auxin-TIR1 pair. *Nature Chemical Biology*, *14*(3), 299-305. https://doi.org/10.1038/nchembio.2555

Urban, J. (2022). A review on recent trends in the phosphoproteomics workflow. From sample preparation to data analysis. *Anal Chim Acta*, *1199*, 338857. https://doi.org/10.1016/j.aca.2021.338857

van de Weerdt, B. C., & Medema, R. H. (2006). Polo-like kinases: a team in control of the division. *Cell Cycle*, *5*(8), 853-864. https://doi.org/10.4161/cc.5.8.2692

van Vugt, M. A., Bras, A., & Medema, R. H. (2004). Polo-like kinase-1 controls recovery from a G2 DNA damage-induced arrest in mammalian cells. *Mol Cell*, *15*(5), 799-811. https://doi.org/10.1016/j.molcel.2004.07.015

van Vugt, M. A., & Medema, R. H. (2005). Getting in and out of mitosis with Polo-like kinase-1. *Oncogene*, *24*(17), 2844-2859. https://doi.org/10.1038/sj.onc.1208617

Vazquez, F., & Sellers, W. R. (2021). Are CRISPR Screens Providing the Next Generation of Therapeutic Targets? *Cancer Res*, *81*(23), 5806-5809. https://doi.org/10.1158/0008-5472.CAN-21-1784

Verma, R., Mohl, D., & Deshaies, R. J. (2020). Harnessing the Power of Proteolysis for Targeted Protein Inactivation. *Molecular Cell*, *77*(3). https://doi.org/10.1016/j.molcel.2020.01.010

Verma, R., Peters, N. R., D'Onofrio, M., Tochtrop, G. P., Sakamoto, K. M., Varadan, R., Zhang, M., Coffino, P., Fushman, D., Deshaies, R. J., & King, R. W. (2004). Ubistatins inhibit proteasome-dependent degradation by binding the ubiquitin chain. *Science*, *306*(5693), 117-120. https://doi.org/10.1126/science.1100946

Villen, J., & Gygi, S. P. (2008). The SCX/IMAC enrichment approach for global phosphorylation analysis by mass spectrometry. *Nat Protoc*, *3*(10), 1630-1638. https://doi.org/10.1038/nprot.2008.150

Vit, G., Duro, J., Rajendraprasad, G., Hertz, E. P. T., Holland, L. K. K., Weisser, M. B., McEwan, B. C., Lopez-Mendez, B., Sotelo-Parrilla, P., Jeyaprakash, A. A., Montoya, G., Mailand, N., Maeda, K., Kettenbach, A., Barisic, M., & Nilsson, J. (2022). Chemogenetic profiling reveals PP2A-independent cytotoxicity of proposed PP2A activators iHAP1 and DT-061. *EMBO J*, *41*(14), e110611. https://doi.org/10.15252/embj.2022110611

Wadsworth, P. (2005). Cytokinesis: Rho marks the spot. *Curr Biol*, *15*(21), R871-874. https://doi.org/10.1016/j.cub.2005.10.021

Wang, F., Dai, J., Daum, J. R., Niedzialkowska, E., Banerjee, B., Stukenberg, P. T., Gorbsky, G. J., & Higgins, J. M. (2010). Histone H3 Thr-3 phosphorylation by Haspin positions Aurora B at centromeres in mitosis. *Science*, *330*(6001), 231-235. https://doi.org/10.1126/science.1189435

Wang, R. A., Zhang, H., Balasenthil, S., Medina, D., & Kumar, R. (2006). PAK1 hyperactivation is sufficient for mammary gland tumor formation. *Oncogene*, *25*(20), 2931-2936. https://doi.org/10.1038/sj.onc.1209309

Wang, T., Wei, J. J., Sabatini, D. M., & Lander, E. S. (2014). Genetic screens in human cells using the CRISPR-Cas9 system. *Science*, *343*(6166), 80-84. https://doi.org/10.1126/science.1246981

Watanabe, N., Arai, H., Nishihara, Y., Taniguchi, M., Watanabe, N., Hunter, T., & Osada, H. (2004). M-phase kinases induce phospho-dependent ubiquitination of somatic

Wee1 by SCFbeta-TrCP. *Proc Natl Acad Sci U S A*, *101*(13), 4419-4424. https://doi.org/10.1073/pnas.0307700101

Waters, K. M., Liu, T., Quesenberry, R. D., Willse, A. R., Bandyopadhyay, S., Kathmann, L. E., Weber, T. J., Smith, R. D., Wiley, H. S., & Thrall, B. D. (2012). Network analysis of epidermal growth factor signaling using integrated genomic, proteomic and phosphorylation data. *PLoS ONE*, *7*(3), e34515. https://doi.org/10.1371/journal.pone.0034515

Wee, P., & Wang, Z. (2017). Epidermal Growth Factor Receptor Cell Proliferation Signaling Pathways. *Cancers (Basel)*, *9*(5). https://doi.org/10.3390/cancers9050052

Werner, T., Becher, I., Sweetman, G., Doce, C., Savitski, M. M., & Bantscheff, M. (2012). High-resolution enabled TMT 8-plexing. *Anal Chem*, *84*(16), 7188-7194. https://doi.org/10.1021/ac301553x

Willems, E., Dedobbeleer, M., Digregorio, M., Lombard, A., Lumapat, P. N., & Rogister, B. (2018). The functional diversity of Aurora kinases: a comprehensive review. *Cell Div*, *13*, 7. https://doi.org/10.1186/s13008-018-0040-6

Williams, K. C., Cepeda, M. A., Javed, S., Searle, K., Parkins, K. M., Makela, A. V., Hamilton, A. M., Soukhtehzari, S., Kim, Y., Tuck, A. B., Ronald, J. A., Foster, P. J., Chambers, A. F., & Leong, H. S. (2019). Invadopodia are chemosensing protrusions that guide cancer cell extravasation to promote brain tropism in metastasis. *Oncogene*, *38*(19), 3598-3615. https://doi.org/10.1038/s41388-018-0667-4

Winkles, J. A., & Alberts, G. F. (2005). Differential regulation of polo-like kinase 1, 2, 3, and 4 gene expression in mammalian cells and tissues. *Oncogene*, *24*(2), 260-266. https://doi.org/10.1038/sj.onc.1208219

Wittmann, T., Bokoch, G. M., & Waterman-Storer, C. M. (2004). Regulation of microtubule destabilizing activity of Op18/stathmin downstream of Rac1. *J Biol Chem*, *279*(7), 6196-6203. https://doi.org/10.1074/jbc.M307261200

Wu, T., Yoon, H., Xiong, Y., Dixon-Clarke, S. E., Nowak, R. P., & Fischer, E. S. (2020). Targeted protein degradation as a powerful research tool in basic biology and drug target discovery. *Nature Structural & Molecular Biology*, *27*(7). https://doi.org/10.1038/s41594-020-0438-0

Xiao, M., Zhao, J., Wang, Q., Liu, J., & Ma, L. (2022). Recent Advances of Degradation Technologies Based on PROTAC Mechanism. *Biomolecules*, *12*(9). https://doi.org/10.3390/biom12091257

Xie, S., Wang, Q., Wu, H., Cogswell, J., Lu, L., Jhanwar-Uniyal, M., & Dai, W. (2001). Reactive Oxygen Species-induced Phosphorylation of p53 on Serine 20 Is Mediated in Part by Polo-like Kinase-3. *Journal of Biological Chemistry*, *276*(39), 36194-36199. https://doi.org/10.1074/jbc.M104157200

Xie, S., Wu, H., Wang, Q., Cogswell, J. P., Husain, I., Conn, C., Stambrook, P., Jhanwar-Uniyal, M., & Dai, W. (2001). Plk3 Functionally Links DNA Damage to Cell Cycle Arrest and Apoptosis at Least in Part via the p53 Pathway. *Journal of Biological Chemistry*, *276*(46), 43305-43312. https://doi.org/10.1074/jbc.M106050200

Xie, S., Wu, H., Wang, Q., Kunicki, J., Thomas, R. O., Hollingsworth, R. E., Cogswell, J., & Dai, W. (2002). Genotoxic stress-induced activation of Plk3 is partly mediated by Chk2. In *Cell cycle (Georgetown, Tex.)* (Vol. 1, pp. 424-429).

Xu, D., Yao, Y., Lu, L., Costa, M., & Dai, W. (2010). Plk3 functions as an essential component of the hypoxia regulatory pathway by direct phosphorylation of HIF-1α. *Journal of Biological Chemistry*, *285*(50), 38944-38950. https://doi.org/10.1074/jbc.M110.160325

Yamagishi, Y., Honda, T., Tanno, Y., & Watanabe, Y. (2010). Two histone marks establish the inner centromere and chromosome bi-orientation. *Science*, *330*(6001), 239-243. https://doi.org/10.1126/science.1194498

Yanagida, M. (2014). The role of model organisms in the history of mitosis research. *Cold Spring Harb Perspect Biol*, *6*(9), a015768. https://doi.org/10.1101/cshperspect.a015768

Yang, N., Higuchi, O., Ohashi, K., Nagata, K., Wada, A., Kangawa, K., Nishida, E., & Mizuno, K. (1998). Cofflin phosphorylation by LIM-kinase 1 and its role in Rac-mediated actin reorganization. *Nature*, *393*(6687), 809-812. https://doi.org/10.1038/31735

Yang, Y., Bai, J., Shen, R., Brown, S. A. N., Komissarova, E., Huang, Y., Jiang, N., Alberts, G. F., Costa, M., Lu, L., Winkles, J. A., & Dai, W. (2008). Polo-like kinase 3 functions as a tumor suppressor and is a negative regulator of hypoxia-inducible factor-1α under hypoxic conditions. *Cancer Research*, *68*(11), 4077-4085. https://doi.org/10.1158/0008-5472.CAN-07-6182

Yang, Y., Du, J., Hu, Z., Liu, J., Tian, Y., Zhu, Y., Wang, L., & Gu, L. (2011). Activation of Rac1-PI3K/Akt is required for epidermal growth factor-induced PAK1 activation and cell migration in MDA-MB-231 breast cancer cells. *J Biomed Res*, *25*(4), 237-245. https://doi.org/10.1016/S1674-8301(11)60032-8

Yates, J. R., 3rd. (2019). Recent technical advances in proteomics. *F1000Res*, *8*. https://doi.org/10.12688/f1000research.16987.1

Yesbolatova, A., & Kanemaki, M. T. (2018). TAGing for destruction news-and-views. In *Nature Chemical Biology* (Vol. 14, pp. 414-415): Nature Publishing Group.

Yesbolatova, A., Natsume, T., Hayashi, K. i., & Kanemaki, M. T. (2019). Generation of conditional auxin-inducible degron (AID) cells and tight control of degron-fused proteins using the degradation inhibitor auxinole. *Methods*, *164-165*, 73-80. https://doi.org/10.1016/j.ymeth.2019.04.010

Yesbolatova, A., Saito, Y., & Kanemaki, M. T. (2020). Constructing auxin-inducible degron mutants using an all-in-one vector. *Pharmaceuticals*, *13*(5), 103-103. https://doi.org/10.3390/ph13050103

Yesbolatova, A., Saito, Y., Kitamoto, N., Makino-Itou, H., Ajima, R., Nakano, R., Nakaoka, H., Fukui, K., Gamo, K., Tominari, Y., Takeuchi, H., Saga, Y., Hayashi, K. i., & Kanemaki, M. T. (2020). The auxin-inducible degron 2 technology provides sharp degradation control in yeast, mammalian cells, and mice. *Nature Communications*, *11*(1), 1-13. https://doi.org/10.1038/s41467-020-19532-z

Yesbolatova, A., Tominari, Y., & Kanemaki, M. T. (2019). Ligand-induced genetic degradation as a tool for target validation. *Drug Discovery Today: Technologies*, *31*, 91-98. https://doi.org/10.1016/j.ddtec.2018.11.001

Zeng, K., Bastos, R. N., Barr, F. A., & Gruneberg, U. (2010). Protein phosphatase 6 regulates mitotic spindle formation by controlling the T-loop phosphorylation state of Aurora A bound to its activator TPX2. *J Cell Biol*, *191*(7), 1315-1332. https://doi.org/10.1083/jcb.201008106

Zeng, X., & King, R. W. (2012). An APC/C inhibitor stabilizes cyclin B1 by prematurely terminating ubiquitination. *Nat Chem Biol*, *8*(4), 383-392. https://doi.org/10.1038/nchembio.801

Zeng, X., Sigoillot, F., Gaur, S., Choi, S., Pfaff, K. L., Oh, D. C., Hathaway, N., Dimova, N., Cuny, G. D., & King, R. W. (2010). Pharmacologic inhibition of the anaphase-promoting complex induces a spindle checkpoint-dependent mitotic arrest in the

absence of spindle damage. *Cancer Cell*, *18*(4), 382-395. https://doi.org/10.1016/j.ccr.2010.08.010

Zhang, J., Yang, P. L., & Gray, N. S. (2009). Targeting cancer with small molecule kinase inhibitors. *Nat Rev Cancer*, *9*(1), 28-39. https://doi.org/10.1038/nrc2559

Zhang, T., Fassl, A., Vaites, L. P., Fu, S., Sicinski, P., Paulo, J. A., & Gygi, S. P. (2022). Interrogating Kinase-Substrate Relationships with Proximity Labeling and Phosphorylation Enrichment. *J Proteome Res*, *21*(2), 494-506. https://doi.org/10.1021/acs.jproteome.1c00865

Zhang, Y., Fonslow, B. R., Shan, B., Baek, M. C., & Yates, J. R., 3rd. (2013). Protein analysis by shotgun/bottom-up proteomics. *Chem Rev*, *113*(4), 2343-2394. https://doi.org/10.1021/cr3003533

Zhao, Z.-s., Lim, J. P., Ng, Y.-W., Lim, L., Lim, L., & Manser, E. (2005). The GIT-Associated Kinase PAK Targets to the Centrosome and Regulates Aurora-A. *Molecular Cell*, *20*(2). https://doi.org/10.1016/j.molcel.2005.08.035

Zhao, Z. S., Lim, J. P., Ng, Y. W., Lim, L., & Manser, E. (2005). The GIT-Associated Kinase PAK Targets to the Centrosome and Regulates Aurora-A. *Molecular Cell*, *20*(2), 237-249. https://doi.org/10.1016/J.MOLCEL.2005.08.035

Zhou, H., Watts, J. D., & Aebersold, R. (2001). A systematic approach to the analysis of protein phosphorylation. *Nat Biotechnol*, *19*(4), 375-378. https://doi.org/10.1038/86777

Zhou, L., Tian, X., Zhu, C., Wang, F., & Higgins, J. M. (2014). Polo-like kinase-1 triggers histone phosphorylation by Haspin in mitosis. *EMBO Rep*, *15*(3), 273-281. https://doi.org/10.1002/embr.201338080

Zimmerman, W. C., & Erikson, R. L. (2007a). Finding Plk3. In *Cell Cycle* (Vol. 6, pp. 1314-1318): Taylor and Francis Inc.

Zimmerman, W. C., & Erikson, R. L. (2007b). *Polo-like kinase 3 is required for entry into S phase*. www.pnas.orgcgidoi10.1073pnas.0610856104

Zimmermann, M., Murina, O., Reijns, M. A. M., Agathanggelou, A., Challis, R., Tarnauskaite, Z., Muir, M., Fluteau, A., Aregger, M., McEwan, A., Yuan, W., Clarke, M., Lambros, M. B., Paneesha, S., Moss, P., Chandrashekhar, M., Angers, S., Moffat, J., Brunton, V. G., . . . Durocher, D. (2018). CRISPR screens identify genomic ribonucleotides as a source of PARP-trapping lesions. *Nature*, *559*(7713), 285-289. https://doi.org/10.1038/s41586-018-0291-z

Zitouni, S., Nabais, C., Jana, S. C., Guerrero, A., & Bettencourt-Dias, M. (2014). Polo-like kinases: Structural variations lead to multiple functions. In *Nature Reviews Molecular Cell Biology* (Vol. 15, pp. 433-452): Nature Publishing Group.